The evolution of macrotexture on asphalt pavements using non-contact field techniques

Victoria Edmondson

Ph.D.

2021

The evolution of macrotexture on asphalt pavements using non-contact field techniques

Victoria Edmondson

A thesis submitted in partial fulfilment of the requirement of the University of Northumbria at Newcastle for the degree of Doctor of Philosophy

Research undertaken in the Faculty of Engineering and the Environment

December 2021

ABSTRACT

Adequate skid resistance is required to ensure vehicle safety on pavements in wet conditions and depends upon road surface characteristics, particularly texture. Texture is composed of a range of different scales each of which contributes differently to the generation of adequate friction at the tyre-road interface. Macrotexture acts to disperse water, under wet conditions, through the gaps in between road aggregates, and influences the way skid resistance reduces with increasing speed in wet conditions. Increasingly, correlations between macrotexture measurements captured using non-contact techniques and tyre-pavement contact friction are being investigated. There is a notable scarcity of research into the respective accuracy of the non-contact measurement techniques at these scales. This thesis compares three non-contact techniques: a laser profile scanner, Structure from Motion photogrammetry (SfM) and Terrestrial Laser Scanning (TLS). Spectral analysis, areal surface texture parameters and 2D cross-correlation analysis are used to evaluate the suitability of each approach for characterising and monitoring pavement macrotexture. The results show that SfM can produce successful measures of the areal root mean square height (*Sq*), which represents pavement texture depth and is positively correlated with skid resistance. Significant noise in the TLS data prevented agreement with the laser profiler but new filtering procedures result in improved values for the peak density (*Spd*) and the arithmetic peak mean curvature (*Spc*), which together define the shape and distribution of pavement aggregates forming macrotexture. However, filtering the TLS data results in a trade-off with vertical accuracy, thus altering the reliability of *Sq*. The work undertaken reveals that the functional areal parameters *Spd* and *Spc* are sensitive to sample size. This means that pavement specimen size of 150 mm x 150 mm or smaller, when used in laboratory or field observations, are inadequate to capture the true value of areal surface texture parameters. Therefore, the deployment of wider scale approaches such as SfM are required in order to successfully capture the functional areal parameters (*Spc* and *Spd*) for road surfaces.

This thesis also provides the first meaningful analysis of a long-term study of legacy texture data obtained using TRACS (TRAffic Speed Condition Survey). A new data analysis approach utilising time series data with spectral analysis and spatial filtering procedures is presented, to determine long term rates of change in road surface macrotexture and compared with meteorological and traffic datasets. The results reveal for hot rolled asphalt (HRA) surfaces that changes to Sensor Measured Texture Depth (SMTD) follow a linearly increasing trend with time. The ‘rate of change’ is influenced by the order of magnitude of annual average daily traffic (AADT), when factored for the percentage of heavy goods vehicles. This linear trend is disrupted by environmental parameters such as rainfall events and seasonal

conditioning. In the summer this signal is evident as a transient peak in the 'rate of change' of texture greater than 0.04 mm, and in the winter as a reduction. The transient changes in texture corresponded to above average rainfall occurring in the week prior to SMTD measurement. The signal observed demonstrates an inverse pattern to the classically understood seasonal variation of skid resistance in the UK, where values are low in the summer and high in the winter. The findings demonstrate for the first time that texture measurements experience a seasonal signal, and provide compelling evidence pointing toward surface processes (such as polishing and the wetting and drying of surface contaminants) causing changes to texture that are affecting seasonal variation in skid resistance. Furthermore, results expose a systematic periodicity occurring each year within the SMTD data studied, corresponding to longitudinal oscillations with wavelengths between 33 m to 62 m. The time-invariant periodicity of these oscillations suggests that it is 'imprinted' in the early life of the pavement. 'Imprinting' may theoretically arise with cyclic tyre loading applied by the suspension systems of heavy vehicles or during road construction.

Finally, this thesis contributes to understanding of the role of the different scales of texture on the development of skid resistance. A signal processing technique termed Empirical Mode Decomposition was used to decompose the texture measurements into a set of component profiles of different wavelengths. The Dynamic Friction Model, a computational friction model already validated on real road surfaces, was then used to determine the relative effect of partially recomposed profiles with their components on skid resistance. The results demonstrate the importance of not only "small-scale" and "large-scale" textures but also their spatial arrangement and shape. Indeed, on wet road surfaces, "small-scale-texture" was found to be key to achieving good skid resistance at low speeds, whilst "large-scale-texture" was found to be crucial to maintaining it with increasing speed. The distribution of the summits of the large-scale-textures was established as being able to compensate for a lack of small-scale-texture. Conversely, the reverse was established as also being true, with the small sharp local summits of small-scale-texture being found to compensate for a lack of large-scale-texture.

The work undertaken in this PhD scrutinises the measurement of pavement macrotexture using non-contact techniques and defines new approaches to analyse legacy data sets to visualise spatially macrotexture evolution. Significantly, the work provides compelling evidence of a 'seasonal signal' in texture data, linked to environmental conditions, particularly precipitation. These results place a new emphasis on the future need to quantify the contribution of pavement surface processes to the phenomenon of seasonal variation of skid resistance, to improve texture evolution assessment and frictional measurement on road networks.

TABLE OF CONTENTS

List of figures……. VII
List of tables……... XI
Abbreviations……. XII
Acknowledgements…… XIV
Declaration……. XV

Chapter 1
INTRODUCTION…… 1
1.1 Introduction and project rationale…… 1
1.2 Research aims and objectives…… 4
1.3 Thesis structure…… 7
1.4 Published papers……... 14

Chapter 2
LITERATURE REVIEW…… 15
2.1 Definition of road surface texture……. 15
2.2 Characterisation of road macrotexture for field measurements……. 16
2.3 Non-contact field method for measuring road macrotexture……. 27
2.3.1 Static contactless spot techniques……. 27
2.3.2 Wide-scale contactless techniques for macrotexture field measurement….. 38
2.4 Use of road surface texture measurement in pavement maintenance regimes…. 50
2.5 Evolution of macrotexture on road networks……. 52
2.6 Correlating skid resistance and road texture…… 55
2.7 The contribution of road surface processes to the phenomenon of seasonal variation in skid resistance ……... 60
2.8 Summary……... 63

Chapter 3
PUBLISHED PAPER 1 – IMPROVED NON-CONTACT 3D FIELD PROCESSING TECHNIQUES TO ACHIEVE MACROTEXTURE CHARACTERISATION OF PAVEMENT……... 65
3.1 Abstract……. 65
3.2 Introduction……... 65

3.3 Methods…… 68
3.3.1 Remote sensing technology…….. 68
3.3.1.1 Terrestrial Laser Scanning……... 68
3.3.1.2 Structure from Motion photogrammetry…….. 68
3.3.2 Test location…… 73
3.3.3 Deriving macrotexture parameters from non-contact survey techniques….. 73
3.3.4 Deriving 2D wavenumber amplitude spectra from non-contact techniques and filtering…….. 73
3.4 Results and discussion…….. 76
3.4.1 Unfiltered areal parameters…….. 78
3.4.2 2D correlation analysis…… 80
3.4.3 Filtered areal parameters…….. 82
3.4.4 Spectral analysis……... 82
3.4.5 Spatial variability…… 85
3.5 Conclusion…… 90

Chapter 4

PUBLISHED PAPER 2 – QUANTIFYING LONG-TERM RATE OF TEXTURE CHANGE ON ROAD NETWORKS…….. 92

4.1 Abstract…… 92
4.2 Introduction……... 92
4.3 Selecting the site and legacy data…….. 95
4.4 Data processing method…… 97
4.5 Validating results and discussion…….. 99
4.5.1 Filtered road texture time series data…… 99
4.5.2 Road texture change data…… 103
4.5.3 Road spectra analysis data…… 107
4.6 Conclusion…… 111

Chapter 5

PUBLISHED PAPER 3 – SEASONAL SIGNALS OBSERVED IN NON-CONTACT LONG-TERM ROAD TEXTURE MEASUREMENTS……... 112

5.1 Abstract…… 112
5.2 Introduction……... 112
5.3 Methods…… 115

5.3.1 Selecting the sites and legacy data…… 115
5.3.2 Data processing of the SMTD data…….. 117
5.3.3 Comparison of SMTD with Traffic Flow…… 117
5.3.4 Seasonal analysis……. 117
5.4 Results……... 120
5.4.1 Change in road texture……. 120
5.4.2. Seasonal trends in road texture…… 121
5.5 Discussion……. 128
5.6 Conclusion…… 132

Chapter 6

PUBLISHED PAPER 4 – SKID RESISTANCE: UNDERSTANDING THE ROLE OF ROAD TEXTURE SCALES USING A SEASONAL DECOMPOSITION SIGNAL TECHNIQUE AND A FRICTION MODEL….. 134

6.1 Abstract……. 134
6.2 Introduction……... 134
6.3 Revisiting the DFM……... 137
6.4 Selecting the tested surfaces…….. 140
6.5 Capturing texture and skid resistance of the tested surface…….. 140
6.6 Decomposing the surface profiles and creating the new profiles……... 143
6.6.1 Texture decomposition……. 143
6.6.2 Creation of the new profiles……. 146
6.7 Analysis procedure…… 146
6.8 Results and discussion…….. 149
6.8.1 Analytical surface…… 149
6.8.2 Analysis of the test-tract surface……... 153
6.8.2.1 The asphalt concrete……. 153
6.8.2.2 The painted flexible asphalt and the smooth epoxy resin…… 156
6.8.2.3 The calcined bauxite colgrip…… 156
6.9 Conclusion…… 159
6.10 Paper 4 - Appendix ……. 160

Chapter 7

DISCUSSION…… 163

7.1 Introduction……... 163

7.2 Measuring the surface macrotexture of asphalt pavements using non-contact techniques……. 163
7.3 Methods to determine the evolution of asphalt pavement macrotexture…….. 166
7.4 The influence of environmental parameters on asphalt pavement macrotexture... 168
7.5 The role of asphalt texture scales on the development of skid resistance……... 171
7.6 Summary……... 171

Chapter 8

CONCLUSION……. 174

8.1 Introduction……... 174
8.2 Main findings…… 174
8.3 Limitations of this research……... 177
8.4 Suggestions for further work……. 177

REFERENCES……. 179

List of Figures

Chapter 2: Literature review

Figure 2.1a. Illustration of the term ‘texture depth’ on a macrotexture road surface… 17

Figure 2.1b. Scales of road texture…… 17

Figure 2.2. Illustration of the terms ‘baseline’, ‘average level’, ‘peak level’, ‘profile depth’ and ‘MPD’……. 18

Figure 2.3a. General limitations of profile measurements…… 20

Figure 2.3b. Positive and negative texture……..... 20

Figure 2.4. Topography of a honed surface with form, waviness and roughness……. 24

Figure 2.5. Discrete Fourier Transform – Digitally sampled functions of a finite length…… 26

Figure 2.6. (a) Analog profile representation of section of US road. (b) Profile power spectral density. (c) Amplitude and frequency distribution (AFD) tabulation for section of US road……..... 28

Figure 2.7. Circular Texture Meter: (a) Front view and (b) Bottom view. (c) In use on the highway (d) Measurement segments…… 29

Figure 2.8. Outflow Meter……..... 31

Figure 2.9. Schematics for stereovision……..... 33

Figure 2.10a. Three light source stereovision equipment……. 35

Figure 2.10b. The zenith angle for taking picture in the photometric stereo system…. 35

Figure 2.11. The matching of varying intensity using (a) SIFT (b) SURF and (c) ORB…….. 37

Figure 2.12. Laser triangulation…… 39

Figure 2.13a. Phased Signal Range Measurement…… 42

Figure 2.13b. Typical vertical and horizontal coverage of a terrestrial laser scanner..... 42

Figure 2.14. The influence of laser pulse rate on scanner range for pulsed ‘Laser imaging, Detection and Ranging’ (LiDAR) systems…… 44

Figure 2.15. The influence of resolution on terrestrial laser scan data. Performance data is based on a FARO Focus 3D X phase-based scanner……. 46

Figure 2.16. Illustration of the decay in point count density with distance from a terrestrial laser scanner set-up position…… 47

Figure 2.17. Example of ‘specular flare’ or noise in a terrestrial laser scanner point cloud data caused by the reflectivity of a light surface……. 49

Figure 2.18a. Early-life macrotexture trends for straight and curved road sections…. 53

Figure 2.18b. GripTester Number (GN) and MPD versus the cumulative traffic…… 53
Figure 2.19a. Factors affecting available pavement……. 56
Figure 2.19b. Hysteresis and adhesion components of tyre/road friction…… 56
Figure 2.20. Variation of friction coefficient with speed for various macrotexture and microtexture types……. 58
Figure 2.21a. Seasonal variation in skid resistance. Results are obtained at two-weekly intervals using the pendulum skid resistance test…… 61
Figure 2.21b. Average rainfall for East and North East England……. 61
Figure 2.21c. Average summer skid resistance on roads in East and North East England……... 61

Chapter 3.0: Published Paper 1 – Improved non-contact 3D field processing techniques to achieve macrotexture characterisation of pavements

Figure 3.1. Equipment set-up…….. 69
Figure 3.2. Workflow for programming both the Faro Focus 3D X Series Terrestrial Laser Scanner's onboard computer and the LMI Technologies Gocator 2350 3D Smart Laser Profile Sensor prior to completing a scan…… 70
Figure 3.3. Key Stages of construction of a scaled point cloud reconstruction from digital images. The surface modelled is a Hot Rolled Asphalt with 20mm red chipping…… 72
Figure 3.4. Field site……. 74
Figure. 3.5. Surface height plots derived from the unfiltered point cloud data for a 150mm x 150mm sample area of each surfacing material…… 79
Figure. 3.6. 150mm x 150mm 2D normalised cross-correlation plots for the unfiltered point cloud data……..... 81
Figure. 3.7. Surface height plots derived from the 0.1 wavenumber filtered point cloud data for a 150mm x 150mm sample area of each surfacing material…….. 83
Figure 3.8. 2D wavenumber (mm-1) spectral analysis of the unfiltered point cloud data…… 84
Figure. 3.9. Digital image of the 1.8m x 0.9m area of Hot Rolled Asphalt considered in the spatial variance study…….. 86
Figure. 3.10. Spatial variance of *Sq*, *Ssk*, *Sp*, *Sv*, *Spd*, *Spc* over a 1.8m x 0.9m area of Hot Rolled Asphalt surfacing for 150 mm x 150 mm and 300 mm samples, data captured with Structure from Motion…… 87

Figure. 3.11. The influence of upscaling sample size on areal parameters *Sq*, *Ssk*, *Sp*, *Sv*, *Spd*, *Spc* for an area of Hot Rolled Asphalt surfacing captured using Structure from Motion…….. 89

Chapter 4: Published Paper 2 – Quantifying long-term rates of texture change on road networks

Figure 4.1. Field Site Location and Equipment……. 96
Figure 4.2. Raw Data……. 100
Figure 4.3. 0.1 m-1 Wavenumber Filtered Time Series Sensor Measured Texture Data Lane 1……... 101
Figure 4.4. 0.1 m-1 Wavenumber Filtered Time Series Sensor Measured Texture Data for Lane 2…….. 102
Figure 4.5. Lane 1 Rate of Change of Road Texture with Time……. 104
Figure 4.6. Lane 2 Rate of Change of Road Texture with Time……. 105
Figure 4.7. Spectra Analysis and Band Pass Filtered Data……. 108
Figure 4.8. Comparison of Spectra Analysis Data for Section 2 of Lane 1 and Lane 2 110

Chapter 5.0: Published Paper 3 – Seasonal signals observed in non-contact long-term road texture measurements

Figure 5.1. Location of the study sites on the A1 in the United Kingdom……. 116
Figure 5.2. (a) Filtered mean Sensor Measured Texture Depth (SMTD) data for the northern sites on the A1. (b) Normalized mean SMTD data for the northern sites on the A1…… 118
Figure 5.3. Normalized mean Sensor Measured Texture Depth (SMTD) data for the southern sites on the A1……. 119
Figure 5.4. (a) Rate of change in mean Sensor Measured Texture Depth (SMTD) data compared with annual average daily traffic flow (AADT). (b) Rate of change in mean SMTD compared with heavy good vehicle (HGV) AADT…… 122
Figure 5.5. Mean Sensor Measured Texture Depth (SMTD) data compared with a 7th order polynomial best fit line for Site 3 on the A1…….. 124
Figure 5.6. The graph plots the seasonal timing of the deviation in ‘peaks’ and ‘troughs’ from the 7th order polynomial trend for the northern sites of the A1…….. 125
Figure 5.7. The graph plots change from mean monthly rainfall for the period 17th August 1999 to 17th July 2016, against the ‘peaks’ and ‘troughs’ in the deviation of mean SMTD for the northern sites on the A1……. 126

Figure 5.8. The graph plots change from mean monthly rainfall, against the 'peaks' and 'troughs' in the deviation of mean SMTD for the southern sites on the A1……. 127
Figure 5.9. The governing trends of long-term change to pavement texture on Hot Rolled Asphalt (HRA) pavement surface…….. 129

Chapter 6.0 : Published Paper 4 – Skid resistance: understanding the role of road texture scales using a signal decomposition technique and a friction model

Figure 6.1. Forces acting in the contact point between a rubber element and a road profile…… 138
Figure 6.2. Analytical Surface and test track surfaces……... 141
Figure 6.3. Side (Up) and bottom (Down) views of the DFT (Left) and the CTM (Right)……... 142
Figure 6.4. Original profile of the analytical surface captured using the CTM…….. 144
Figure 6.5. The nine embedded Intrinsic Mode Functions (IMF) of the Analytical Surface…….. 145
Figure 6.6. The nine embedded Intrinsic Mode Functions (IMF) of the Analytical Surface…….. 147
Figure 6.7. The overall analysis procedure followed for each surface……... 148
Figure 6.8. The Analytical Surface – DFM and DFT friction coefficients of Profiles 0, 1 and 2 versus speed……... 151
Figure 6.9. The Profiles 0 and 1 derived from the Analytical Surface (on the left) and their height distributions (on the right)…….. 152
Figure 6.10. The Profiles 1 and 2 derived from the Analytical Surface (on the left) and their height distributions (on the right)…… 154
Figure 6.11. The Very Thin Asphalt Concrete Surface…….. 155
Figure 6.12. The Epoxy Resin (smooth) Surface……... 157
Figure 6.13. The Calcined Bauxite Colgrip Surface……. 158
Figure 6.14. The Very Porous Asphalt Surface……. 160
Figure 6.15. The Dense Asphalt Concrete Surface…… 161
Figure 6.16. The Painted Flexible Asphalt Surface……... 162

List of Tables

Chapter 2: Literature Review

Table 2.1. Areal surface texture parameters used to characterise macrotexture……. 22

Chapter 3.0: Published Paper 1 – Improved non-contact 3D field processing techniques to achieve macrotexture characterisation of pavements

Table 3.1. Areal surface texture parameters used to characterise macrotexture……. 75

Table 3.2. Unfiltered and filtered results – point density, Nyquist length and areal surface texture parameters for the surfaces…… 77

Chapter 6.0 : Published Paper 4 – Skid resistance: understanding the role of road texture scales using a signal decomposition technique and a friction model

Table 6.1. The DFM input parameters……... 150

ABBREVIATIONS

AADT	Annual Average Daily Traffic
AFD	Amplitude and Frequency Distribution
ASTM	American Society of Testing and Materials
BIMF	Basic Intrinsic Mode Functions
CCD	Charged Coupled Device
CRP	Close Range Photogrammetry
CTM	Circular Texture Meter
DAC	Dense Asphalt Concrete
DBM	Dense Bitumen Macadam
DFM	Dynamic Friction Model
DFT	Dynamic Friction Tester
EIFOV	Effective Instantaneous Field of View
EMD	Empirical Mode Decomposition
ER	Epoxy Resin
FFT	Fast Fourier Transform
GPS	Global Positioning System
HAPMS	Highways England Pavement Management System
HGV	Heavy Good Vehicle
HRA	Hot Rolled Asphalt
IRI	International Roughness Index
IMFs	Intrinsic Mode Functions
LiDAR	Laser imaging, Detection and Ranging
LST	Large-Scale-Texture
MPD	Mean Profile Depth
MSP	Machine Survey Pre-processor
MTD	Mean Texture Depth
OFT	Outflow Time
ORB	Oriented FAST and Rotated Brief
PA	Porous Asphalt
PSD	Power Spectral Density
SCANNER	Surface Condition Assessment for National Network of Roads
SCRIM	Sideway-force Coefficient Routine Investigation Machine
SD	Surface Dressing

SIFT	Scale Invariant Feature Transform
SfM	Structure from Motion
SLR	Single Lens Reflex
SMTD	Sensor Measured Texture Data
SST	Small-Scale-Texture
S_p	Areal measurement maximum peak height
S_{pc}	Areal measurement arithmetic peak mean curvature
S_{pd}	Areal measurement peak density
S_q	Areal measurement root mean square height
S_{sk}	Areal measurement skewness
S_v	Areal measurement maximum pit height
SURF	Speed Up Robust Feature’
TRACS	TRAffic Speed Condition Survey
TLS	Terrestrial Laser Scanning
UK	United Kingdom
VTAC	Very Thin Asphalt Concrete

ACKNOWLEDGEMENTS

The front page of this thesis only shows one name, but many people have contributed to this work, through their inspiration, discussion and encouragement.

First of all, I would like to express my appreciation and thanks to my principal supervisor, Professor John Woodward, for all of his advice, knowledge and encouragement. I would also like to thank my other supervisors; Professor Michael Lim, Professor James Martin and Professor Malal Kane (Université Gustave Eiffel).

I am grateful for the support of National Highways who provided access to legacy pavement texture data sets, and in particular to Owen Ardill, former Senior Advisor – Pavement Policy, Safety, Engineering and Standards.

I am thankful for the enthusiasm of the technician team within the Faculty of Engineering and Environment and at Université Gustave Eiffel's test track in Nantes. Particular, thanks are expressed to Leon Amess, for his company and support during field trips.

I thank my family for their support and endless patience as this work was completed. Finally, I thank my grandfather who many years ago inspired me to pursue engineering.

DECLARATION

I declare that the work contained in this thesis has not been submitted for any other award and that it is all my own work. I also confirm that this work fully acknowledges opinions, ideas and contributions from the work of others.

Any ethical clearance for the research presented in this thesis has been approved. Approval has been sought and granted through the Researcher's submission to Northumbria University's Ethics Online System.

I declare that the word count of this thesis is 45,577 words

Name: Victoria Jane Edmondson

Date 20.12.2021

Chapter 1: Introduction

1.1 Introduction and project rationale

The provision of a safe, energy-efficient and environmentally friendly transportation system is important to every nation. Road pavements, as an integral part of a transportation system, must contribute towards meeting this requirement. Pavements need to be designed to be safe through the grip they provide with a tyre, comfortable through the minimisation of rolling noise, and environmentally friendly by lessening rolling resistance to reduce fuel consumption.

All of these desired pavement performances are directly related to the surface texture, which is of great importance. Road texture is defined as the deviation of a pavement surface from a true planar surface (Smith et al., 2009). Texture is characterised as being composed of the three increasing wavelength scales: microtexture, macrotexture and megatexture (International Standards Organisation, 2009), introduced in Chapter 2. Each of these wavelengths plays an essential role in pavement performance. This thesis primarily examines macrotexture, which represents the texture components with wavelengths from 0.5 mm to 50 mm and amplitude of 0.1 mm to 20 mm, formed by the shape, size and gradation of road aggregates on a pavement surface. Macrotexture has been shown to contribute to tyre and road noise (Ejsmont et al., 2017; Gardziejczyk, 2014), and to the amount of splash and spray experienced by vehicles (PIARC, 1987). Macrotexture acts to disperse water, under wet conditions, through the gaps in between road aggregates (Dunford and Leach, 2013). Thus, macrotexture has been shown to influence the way skid resistance reduces with increasing speed in wet conditions (Flintsch et al., 2013). With equal microtexture, pavement surfaces with higher macrotexture offer more friction resistance as speed increases than pavements with lower macrotexture under the same contact conditions (Rado and Kane, 2014; Roe and Hartshorne, 1998). Thereby, to ensure suitable pavement friction the maintenance of adequate macrotexture is important to road agencies.

Friction at the tyre/road interface, represents the grip developed by a tyre on a road surface. The coefficient of friction is a measure of the ratio of the tyre load (the force applied in the vertical direction) to the tyre traction (the force resisting movement in the horizontal direction). Friction is a phenomenon collectively influenced by microtexture and macrotexture; as well as temperature, presence of contaminants, speed and tyre tread thickness (Kane and Edmondson, 2018). The principal components of pavement friction are hysteresis and adhesion. Adhesion friction arises through the small-scale bonding or interlocking of the

rubber of a tyre with microtexture, and is correlated to the asperities on the surface of coarse road aggregates (Klüppel and Heinrich, 2001; Moore, 1975; Persson, 2001). Adhesion is therefore a function of the tyre interface shear strength and contact area (Hall et al., 2009). Adhesion works in dry conditions in a complex combination with hysteresis friction. Hysteresis arises as a consequence of the viscoelasticity of a tyre, which means that when a tyre compresses on a road surface the energy to deform the tyre is greater than the energy to reform (Do and Cerezo, 2015). The difference in energy is dissipated as heat, and the loss generates a net frictional force resisting forward movement. Hysteresis considers processes happening with the rubber material of the tyre and adhesion processes at the tyre contact patch. In this way both are considering energy dissipation, but at different scales; this was recognised by Kummer, (1966) who proved that hysteresis and adhesion are actually the same phenomenon. In wet conditions, adhesion is reduced, by the phenomenon of viscoplaning (Do and Cerezo, 2015), where a degree of tyre contact is lost with the pavement due to the presence of a thin water film (in the order of a tenth of a millimetre or less) immediately in front of the tyre. Skid resistance describes the contribution that the wet road pavement makes to tyre/road friction. The mechanics of friction have been extensively researched, with several authors recently providing useful state of the art reviews for those interested (Guo et al., 2021; Kogbara et al., 2016; Yu et al., 2020) A detailed review of skid resistance and friction theory is not covered here. This thesis will consider skid resistance, only in so far as it is influenced by texture.

The preservation of adequate pavement texture is achieved by a regime of monitoring and maintenance undertaken by road agencies; national practices vary, but data are typically collected at least annually (Design Manual for Road and Bridges, 2020; European Collaborative Project, 2014). Macrotexture is monitored at traffic speed, normally as part of two different types of road condition survey. Network level visual condition surveys are undertake using non-contact laser profile sensor techniques and video cameras mounted on specialist survey vehicles (Meegoda and Gao, 2015b). This type of survey examines the shape and texture of a highway pavement checking longitudinal and transverse profiles, and characterising areas of cracking, rutting and edge deterioration. As part of this survey macrotexture is usually measured across a tyre width, at approximately 1mm intervals, within the nearside wheel track of a highway lane (Department for Transport, 2019). The measurement of macrotexture is therefore confined to a small proportion of the lane width. This width whilst strategically chosen to consider the position in a highway lane most likely to experience the lowest skid resistance, suffers the disadvantage that it is still possible that other areas of the lane might also have low skid resistance. Thereby a technique which enables macrotexture to be measured in the field across a full lane width is desirous.

The contribution of macrotexture to skid resistance is also measured simultaneously with that of microtexture using frictional contact techniques. At the road network scale these contact techniques frequently use a fixed or variable slip rate test wheel, which measures the frictional contact at traffic speed made with the wheel and a wetted pavement. Measurement within a lane, is again limited to the width where the wheel makes contact with the texture. Kogbara et al. (2016) provide a useful full summary of contact devices and their operating principles. Contact devices are known to be susceptible to seasonal variation (Bijsterveld and Val, 2016). This phenomenon has been attributed to a number of factors: the sensitivity of rubber resilience to temperature change (Hosking and Woodford, 1976); changes induced by temperature in the viscosity of the test water of a device (Khasawneh and Laing, 2012) ; and differential polishing of the aggregate microtexture throughout the year (Smith, 2008). Survey results obtained from these devices require statistical interpretation (Design Manual for Roads and Bridges, 2015; Plati et al., 2014) with individual devices requiring harmonisation with the rest of a fleet (Sanders et al., 2015). Friction measurements from rubber contact base devices are also known to be susceptible to changes in travel speed (Dunford, 2008). Direct comparison between different devices adopted in particular countries is also difficult, as measurements are influenced by machine operating conditions such as the load, speed, slip ratio and the composition of the rubber.

The problems associated with contact measurement techniques, make a reliable and standalone non-contact technique for measuring macrotexture in the field desirable. As accurate non-contact macrotexture measurement is one step towards the estimation of pavement friction values via analytical modelling (Kane et al., 2019; Kane and Cerezo, 2015a; Ueckermann et al., 2015). The spatial characterisation of macrotexture across a full lane width is fundamental to not missing areas of textural change, which might contribute to loss of skid resistance. Recent research suggests that skid resistance is sensitive to the density, shape and curvature of peaks within macrotexture (Kogbara et al., 2018), which is not readily captured with discrete profile lane measurement. Spatial characterisation also facilitates the potential to use areal parameters introduced in Chapter 2 of this thesis (Dunford and Leach, 2013), which define three-dimensional information about a pavement surface. Moreover, it is considered that spatial measurement of macrotexture should be explored in the field, in order to isolate and define the contribution of macrotexture to the phenomenon of seasonal variation in skid resistance. Measurement in the field also enables any environmental affects that influence processes on macrotexture to be determined.

Thus, this thesis provides the first spatial consideration of the characterisation of measurement techniques for macrotexture in the field. The work undertaken also considers the evolution of macrotexture to assist with addressing a fundamental challenge facing road agencies: the identification of locations on a large road network requiring investigation, and characterisation of deterioration to facilitate timely, appropriate and effective maintenance approaches (Edmondson et al., 2020).

Road condition survey data is commonly used in pavement management systems to inform pavement condition and performance indices that support decision making processes (FSV-Austrian Transport Research Association, 2008). For pavement texture there are a number of accepted pavement condition indices utilised across the world, these are introduced in Chapter 2. A limitation of the pavement condition indices reviewed, is the sensitivity of the techniques to evaluation length (Transport Research Laboratory, 2006) i.e. the length over which indices are reported. Evaluation lengths typically vary from 10 m to 1600 m, and their selection defines the granularity of the texture data available in pavement management systems for decisions. This can be illustrated by a simple assessment of texture level against a minimum acceptable threshold. In a case where pavement texture is averaged over a long length which contains sections of localised texture variability, the averaged result will smooth the texture data, potentially masking the true condition of shorter lengths. Stakeholders evaluating road texture for maintenance, require confidence in the deployment of follow-up resources for visual inspection and condition assessment. A preferred approach is to augment pavement condition indices with a method to track and understand the rate of change of texture condition at every location on a real road network. This would support the identification of deteriorating sections of the road network; but to date, estimating reliably the rate of change of pavement texture at discrete locations on a real road network has proved difficult (Rainsford and Parkman, n.d.). Today, access to 'big data' in the format of pavement management systems containing historic pavement geometries, and advances in data processing techniques means that data can now be analysed in new ways (De Mauro et al., 2016). Therefore, this thesis also explores new methods to analyse legacy macrotexture data to produce a rare long-term evaluation of the evolution or 'rate of change' of texture on real road networks.

1.2 Research aims and objectives

The overall aim of this PhD project is to assess:

The evolution of macrotexture on asphalt pavements using non-contact field techniques.

In order to fulfil this aim, a number of research objective have been identified.

Objective 1: **Measure the surface macrotexture of asphalt pavements using non-contact techniques.**

The suitability of three non-contact measurement techniques: a 3D smart laser profile scanner, Structure from Motion (SfM) photogrammetry and Terrestrial Laser Scanning (TLS) for characterising and monitoring pavement macrotexture in the field will be evaluated. The TLS data will be collected using a Faro Focus 3D X Series phase-based laser scanner on a levelled tripod mounted inverted 1m above a pavement surface. Overlapping static digital images (5478 x 3648 pixels) captured using a digital single-lens reflex camera with 50 mm fixed focal length, mounted on a camera tripod and dolly will be reconstructed using Agisoft Photoscan version 1.3.4.5067 to produce SfM data. An LMI Technologies Gocator 2350 mounted on a trolley will be used to collect 3D smart laser profile scanner data. Three standard types of pavement surface will be measured a close graded dense bitumen macadam (DBM), and a gap graded hot rolled asphalt (HRA), as well as surface dressing (SD). Point cloud data will be obtained from each technique and aligned to facilitate direct comparison. MountainsMap Premium version 7.4 will be used to calculate areal parameters. Image datasets will be transformed to the wavenumber domain and 2D Kx-Ky wavenumber spectral analysis of macrotexture samples will be calculated in MATLAB. A 2D wavenumber filter to attenuate high wavenumber noise from the macrotexture signal will be applied. Normalised 2D autocorrelation and cross correlation plots of the filtered surface data will be prepared to measure spatial similarity. The results will provide a scarce comparison of the respective accuracy of these wider scale techniques, when used to spatially measure macrotexture with areal parameters. The findings will consider the sensitivity of functional areal parameters to both sample size and filtering.

Objective 2: **Develop an analysis method to determine the evolution of asphalt pavement macrotexture.**

Legacy Sensor Measured Texture Data (SMTD) collected using TRACS (TRAffic Speed Condition Survey) annually over a 2 km stretch of motorway in the UK from 1995 to 2019 will be analysed. SMTD is used in the UK for macrotexture reporting and has been previously found to be related by Viner et al. 2006 to mean profiled depth used internationally (International Standards Organisation, 2009). A new approach will be developed to enable this previously discounted data (Viner et al., 2006) to be used to determine long term rates of change in road macrotexture. The SMTD will be plotted longitudinally in timeseries and a low pass zero-phase $0.1m^{-1}$ wavenumber filter (Gubbins, 2004) applied using MATLAB. Filtered profiles will be presented as chainage-time areal plots with differencing techniques applied (Williams, 2012), to reveal change in road condition with time. Long-term change in

SMTD will be characterised using linear regression and wavenumber amplitude spectra used to characterise the dominating wavenumber in the data. Findings will unlock the potential for annually collected SMTD, to inform road maintenance programmes by extrapolation.

Objective 3: **Determine the influence of environmental parameters on asphalt pavement macrotexture.**

Nineteen years of SMTD survey data for fourteen sites located along a north to south transect spanning the A1(M), the longest highway in the UK will be analysed. Sites will be selected at locations with traffic counters on the southbound heavily trafficked nearside lane. Sites will have a Hot Rolled Asphalt (HRA) pavement; a dense gap graded asphalt with bitumen coated 20 mm aggregate rolled into the surface (UK Government, 2019). A low 0.1 m^{-1} wavenumber filter will be applied (Gubbins, 2004) to the SMTD data. The filtered mean SMTD will be calculated for the overall lane chainage for each measurement date and plotted with a 7^{th} order polynomial best fit line applied to illustrate the long-term evolution trend. The long-term evolution will be compared with Annual Average Daily Traffic (AADT) flow and HGV AADT flow determined from the WebTRIS Highways England Traffic database (Highways England, 2020). Signals in filtered mean SMTD data, defined as peaks and troughs above the 7^{th} order polynomial best fit line, will be investigated for seasonal and meteorological timing. Findings will indicate if macrotexture experiences a seasonal signal arising from surface processes (such as polishing and wetting and drying of surface contaminants) with the potential to influence the phenomenon of seasonal variation of skid resistance.

Objective 4: **Determine the role of asphalt textures scales on the development of skid resistance.**

Friction and texture measurements will be undertaken in the field, on seven surfaces ranging from macrorough-microsmooth through to microsmooth-macrorough at the French Institute of Science and Technology for Transport test track. Measurement will be made using a Circular Texture Meter (CTM) (ASTM International, 2019) and a Dynamic Friction Tester (DFT) device (ASTM International, 2019). In the same manner an artificial surface fabricated by sticking rounded and sandblasted aggregates onto a plate will be measured. A signal processing technique termed Empirical Mode Decomposition (Kane et al., 2015) will be used to decompose the collected texture measurements into a set of component profiles of different wavelengths. These different profiles will be partially recomposed to derive a profile consisting of 'small-scale-texture' (SST) and 'large-scale-texture' (LST), a profile without SST, and a third profile where LST is smoothed even further. The friction on these three recomposed surfaces will be calculated using the Dynamic Friction Model (Kane and Cerezo, 2015b). Findings will demonstrate the importance of 'small-scale' and 'large-scale' texture

on the development of friction. The observations will support skidding prevention and the future safer design of pavement surfaces.

1.3 Thesis structure

The structure of this thesis is summarised below:

CHAPTER 1: This chapter introduces the work described in this thesis. An introduction and project rationale are given by way of a justification for the work undertaken, before specific research aims, and objectives are presented. The structure of the overall thesis is described including the rigour, originality and significance of the four published papers presented. Details of the contribution of each author to the four publications associated with this thesis are provided. Finally, details of four further papers published by the candidate are listed.

CHAPTER 2: This chapter encompasses the literature review for this thesis. Methods for the characterisation of road surface texture and the use of these geometrical specifications in pavement asset management regimes are evaluated. Non-contact approaches to measure road texture in the field are examined. Research undertaken to evaluate the evolution of texture is considered. Finally, previous work undertaken to correlate road texture with skid resistance is analysed, including the influence of road surface processes on the phenomenon of seasonal variation in skid resistance.

The core results of the thesis are then presented as four papers published during the registration period of the PhD.

CHAPTER 3: This chapter contains **Paper 1 - Improved non-contact 3D field processing techniques to achieve macrotexture characterisation of pavements**.

Edmondson, V., Woodward, J., Lim, M., Kane, M., Martin, J., Shyha, I., 2019. Improved non-contact 3D field and processing techniques to achieve macrotexture characterisation of pavements. *Construction and Building Materials* 227, 116693. https://doi.org/10.1016/j.conbuildmat.2019.116693

This paper was authored by Vikki Edmondson (V.E.), John Woodward (J.W.), Michael Lim (M.L.), Malal Kane (M.K.), James Martin (J.M.) and Islam Shyha (I.S.). The individual contributions of these authors were as follows:

V.E., J.W. and M.L. designed the project. V.E., J.W. and M.L. devised the conceptual idea of validating areal surface parameters and the non-contact measurement techniques. V.E., J.W. and M.L, specified the laser technology and designed the experimental rig for the laser profile scanner. V.E. collected surface texture measurements in the field. I.S. provided field assistance. V.E., J.W., and M.L. perfected a method to capture predominantly flat highway surfaces using SfM. V.E. and M.L. extracted and post-processed data to point cloud format. V.E., M.L. and J.M. derived the computational workflow. I.S. and V.E. were involved with the application of areal characterisation methods. V.E., J.W., M.L. and J.M. analysed the data. J.W., M.L, J.M. and M.K. assisted with data interpretation, manuscript structure and editing. V.E. and M.K. reviewed relevant literature. V.E. wrote the manuscript. J.W., M.L., M.K. and J.M. supervised the project. All authors discussed the results and commented on the manuscript.

The rigour, originality and significance of Paper 1 are:

Rigour:

- Three non-contact measurement techniques have been used to capture pavement macrotexture for three pavement surface materials: dense bitumen macadam, hot rolled asphalt and surface dressing. An industry standard laser profile scanner was used to assess the effectiveness of Structure from Motion photogrammetry (SfM) and Terrestrial Laser Scanning (TLS) data to characterise and monitor pavement macrotexture. Areal surface texture parameters and 2D cross-correlation analysis are used to evaluate the suitability of each approach.
- Filtering improved the vertical accuracy of SfM and the laser profile scanner data but reduced that of the TLS data, altering the reliability of *Sq* measurements.

Originality:

- Skid resistance positively correlated by other researchers with areal root mean square height (S_q), has for the first time been measured using SfM photogrammetry.
- New filtering procedures are introduced to improve the areal parameters typically used to define the shape and distribution of pavement aggregates: peak density (S_{pd}) and arithmetic peak mean curvature (S_{pc}).
- Novel spectral analysis has been used to evaluate the suitability of each approach for characterising and monitoring pavement macrotexture. Image data sets were transformed in MATLAB to the wavenumber domain, and a 2D Kx-Ky wavenumber spectral analysis, utilising a cosine Tukey window

to prevent spectral leakage cause by edge discontinuities, was applied to characterise the three non-contact methods.

Significance:

- The 150 mm x 150 mm sample size typically used in laboratory or field observation, is inadequate to precisely characterise hot rolled asphalt surface texture using areal peak density (S_{pd}) and arithmetic peak mean curvature (S_{pc}) parameters; the parameters were found to be sensitive to sample size.
- The areal parameter root mean square of surface departures (S_q), as the standard deviation of peak height from an average plane, has been shown to be spatially equivalent to mean profile depth, used to monitor the adequacy of pavement texture levels for vehicle safety.

CHAPTER 4: This chapter contains **Paper 2 - Quantifying long-term rates of texture change on road networks.**

Edmondson, V., Ardill, O., Martin, J., Lim, M., Kane, M., Woodward, J., 2020. Quantifying long-term rates of texture change on road networks. *International Journal of Pavement Engineering* 0, 1–13. https://doi.org/10.1080/10298436.2020.1830283

This paper was authored by Vikki Edmondson (V.E.), Owen Ardill (O.A.), James Martin (J.M.), Michael Lim (M.L.), Malal Kane (M.K.) and John Woodward (J.W.). The individual contributions of these authors were as follows:

V.E., J.W. M.L., and J.M. designed the project. V.E., J.W., M.L., and J.M. devised the conceptual idea of filtering legacy SMTD data. A.O provided the legacy data. V.E. extracted SMTD data from the Highway Agency Pavement Management System (HAPMS). A.O assisted with extracting data from HAPMS. V.E. and J.M. derived the computational spatial filters, timeseries and spectral workflow. V.E., J.M. and M.L. analysed the data. A.O. and M.K. provided discussions that were helpful to data interpretation. V.E., J.W., M.L. and J.M. assisted with data interpretation, manuscript structure and editing. V.E. reviewed relevant literature. V.E. wrote the manuscript. J.W., M.L., and J.M. supervised the project. All authors discussed the results and commented on the manuscript.

The rigour, originality and significance of Paper 2 are:

Rigour:

- Laser profile Sensor Measured Texture Depth (SMTD) data were collected annually, using TRAffic Speed Condition Survey (TRACS), over a 2 km stretch of motorway from 1995 to 2019.
- SMTD data were plotted in time series and a low pass zero-phase 0.1 m^{-1} wavenumber filter applied to remove noise. Differencing techniques were applied to filtered SMTD to reveal change in road surface condition with time. Long-term rate of change in SMTD where characterised by linear regression. Wavenumber amplitude 1D spectra were calculated using a Fast Fourier Transform to characterise dominating wavenumber. A band-pass wave number filter was applied to attenuate high and low frequency wavenumber signals.

Originality:

- A novel data analysis approach utilising time series data with spectral analysis and spatial filtering procedures is presented.
- The approach enables SMTD data to be used to visually observe discrete segments of a road surface which are changing with time. The long-term rate of change in SMTD is quantified.
- Results exposed for the first time a systematic periodicity occurring each year within the SMTD data, corresponding to longitudinal oscillations with wavelengths between 33 m to 62 m.

Significance:

- This paper provides the first meaningful analysis of a long-term study of texture data obtained using TRACS at a site in the UK. Legacy TRACS laser profile SMTD data were used to determine long term rates of change in road surface macrotexture. The technique unlocked the potential for SMTD data collected annually for 7000 km of the Strategic Road Network in the UK, to inform road maintenance programmes by extrapolation.
- The time-invariant periodicity discovered for the first time in SMTD data suggests that it is ‘imprinted’ in the early life of the pavement. ‘Imprinting’ may theoretically arise with cyclic tyre loading applied by the suspension systems of heavy vehicles or during road construction.

CHAPTER 5: This chapter contains **Paper 3 - Seasonal signals observed in non-contact long-term road texture measurements.**

Edmondson, V., Martin, J., Ardill, O., Lim, M., Kane, M., Woodward, J., 2021. Seasonal Signals Observed in Non-Contact Long-Term Road Texture Measurements. *Coatings* 11, 735. https://doi.org/10.3390/coatings11060735

This paper was authored by Vikki Edmondson (V.E.), James Martin (J.M.), Owen Ardill (O.A.), Michael Lim (M.L.), Malal Kane (M.K.) and John Woodward (J.W.). The individual contributions of these authors were as follows:

V.E, J.W., M.L., and J.M. designed the study. A.O. provided the legacy data. V.E. extracted SMTD data from the HAPMS. A.O assisted with extracting data from HAPMS . V.E. extracted AADT and precipitation data from traffic and meteorological databases. V.E., J.W., M.L., and J.M. derived the computational models and analysis. V.E and J.M. analysed the data. A.O and M.K. provided discussions that were helpful to data interpretation. A.O. commented on seasonal variation in skid resistance. J.W., J.M., M.L., and V.E. assisted with data interpretation, article structure and editing. V.E reviewed the literature. V.E. wrote the manuscript. J.W., M.L., J.M. and M.K. supervised the project. All authors discussed the results and commented on the manuscript.

The rigour, originality and significance of Paper 3 are:

Rigour:

- 19 years of Sensor Measured Texture Depth (SMTD) data collected using TRAffic Speed Condition Survey (TRACS), from fourteen sites, with a persistent hot rolled asphalt (HRA) surface have been analysed. Sites with HRA were selected for comparison in the North and South of England, to allow the greatest potential differences in traffic flow and meteorological conditions.
- SMTD data was filtered with a 0.1 m^{-1} low pass wavenumber filter and a 7^{th} order polynomial best fit used to model the long-term evolution of mean SMTD. 'Troughs' were defined as negative deviations and 'peaks' positive deviations greater than 0.04mm from the long-term trend; and plotted against day number to characterise seasonality. The timing of the 'troughs' and 'peaks' where compared with site precipitation data.

- Rate of change in mean SMTD was compared with annual average daily traffic flow (AADT) adjusted for the percentage of heavy good vehicles (HGV).

Originality:

- This paper provides a unique analysis of long-term SMTD data obtained for HRA using TRACS data, located along a north to south transect spanning, the longest highway in the UK the A1.
- Findings demonstrate for the first time that the otherwise long-term linear trend of SMTD for HRA is disrupted by environmental parameters such as rainfall events and seasonal conditioning. In the summer this 'seasonal-signal' is evident as a transient peak in the 'rate of change' of texture greater than 0.04 mm, and in the winter as a reduction.

Significance:

- On HRA surfaces changes to SMTD follow a linearly increasing trend directly related to the order magnitude of AADT, when factored for the percentage of HGVs. This substantiates that the heavier axle loading and tyre types associated with commercial vehicles cause more impact on macrotexture polishing than other types of road vehicle.
- Texture measurements experience a 'seasonal-signal'. The transient changes in texture corresponded to above average rainfall occurring in the week prior to SMTD measurement. This provides compelling evidence pointing toward surface processes (such as polishing, washing, and the wetting and drying of surface contaminants) causing changes to texture. The 'seasonal-signal' observed demonstrates an inverse pattern to the classically understood seasonal variation of skid resistance in the UK, where values are low in the summer and high in the winter. As skid resistance is measured as a frictional response to pavement texture, this suggest that processes on pavement surfaces are an influence on seasonal variation in skid resistance, along with other recognised parameter such as speed, temperature, tire tread thickness and viscoelastic deformation.

CHAPTER 6: This chapter contains **Paper 4 - Skid resistance: understanding the role of road texture scales using a signal decomposition technique and a friction model**.

Kane, M., Edmondson, V., 2020. Skid resistance: understanding the role of road texture scales using a signal decomposition technique and a friction model. *International Journal of Pavement Engineering* 0, 1–15. https://doi.org/10.1080/10298436.2020.1757669

This paper was authored by Malal Kane (M.K.) and Vikki Edmondson (V.E.). The individual contributions of these authors were as follows:

V.E and M.K conceived and planned the project. M.K. performed the CTM measurements. M.K. compiled the EMD and DFM model. M.K deconstructed the surface profiles and recomposed them to derive the SST and LST. M.K. and V.E. contributed to the analysis of the results. M.K. and V.E. interpretated the data and planned the structure of the manuscript. M.K and V.E reviewed the relevant literature. M.K and V.E wrote and edited the manuscript.

The rigour, originality and significance of Paper 4 are:

Rigour:

- The surface profiles of seven pavement materials a very thin asphalt concrete, a porous asphalt, a dense asphalt concrete, a painted flexible asphalt, a calcined bauxite surface dressing, a smooth epoxy resin and an analytical reference surface are captured using a Circular Track Meter (CTM).
- Empirical Mode Decomposition (EMD), a signal processing technique is used to decompose the collected road surface textures into a set of nine component profiles of different wavelengths. These profiles where recombined to produce a set of new profiles of different levels of 'Small-Scale-Texture' (SST) and 'Large-Scale-Texture' (LST). LST equating to natural inherent texture wavelengths and amplitudes equivalent to the size of road surface aggregate, and SST to the roughness present on the surface of these aggregates.
- The Dynamic Friction Model (DFM), a computational friction model already validated on real road surfaces, is then used to determine the relative effect of partially recomposed profiles with their components on skid resistance.

Originality:

- The distribution of the summits of LST was established as being able to compensate for a lack of SST. Conversely, the reverse was established as also being true, with the small sharp local summits of SST being found to compensate for a lack of LST.

Significance:

- On wet road surfaces, SST was found to be key to achieving good skid resistance at low speeds, whilst LST was found to be crucial to maintaining it with increasing speed.

CHAPTER 7: This chapter contains the discussion for this thesis. The findings from Chapter 3, 4, 5 and 6 are discussed in the context of the research aim and objectives posed at the outset.

CHAPTER 8: This chapter comprises the conclusion for this thesis. The key findings for the work undertaken are summarised and recommendations are made for future work.

1.4 Published Papers

Below for completeness are details of four further papers that the candidate has also published during the PhD registration period. These papers are not part of this submission for degree of Doctor of Philosophy as they fall outside of the scope of the thesis, being primarily related to the modelling of skid resistance.

i. Kane, M., Edmondson, V., 2018. Modelling the bitumen scour effect: enhancement of a dynamic friction model to predict the skid resistance of rubber upon asphalt pavement surfaces subjected to wear by traffic polishing. *Wear* 400-401, 100-110. https://doi.org/10.1016/j.wear.2017.12.013
ii. Kane, M., Edmondson, V., 2020. Long-term skid resistance of asphalt surfacings and aggregates' mineralogical composition: generalisation to pavements made of difference aggregate types. *Wear* 454-455, 203339. https://doi.org/10.1016/j.wear.2020.203339
iii. Kane, M., Edmondson, V., 2020. Tire/road friction prediction: introduction a simplified numerical tool based on contact modelling. *Vehicle Systems Dynamic*. https://doi.org/10.1080/00423114.2020.1832696
iv. Kane, M., Edmondson, V., 2020. Aggregate mineralogical composition dataset to estimate the averaged hardness parameter to predict the long-term skid resistance of pavements. *Data in Brief*. 31, 1-3 https://doi.org/10.1016/j.dib.2020.105849

Chapter 2: Literature Review

2.1 Definition of road surface texture

Road pavement texture is defined as the deviation of the pavement surface from a true planar surface (Smith et al., 2009). The plane is given to be the size of the tyre pavement interface, and to pass through the three highest peaks within the contact area (refer to Figure 2.1a) . Texture depth is the difference between the plane and an arbitrary sample point on the pavement surface (International Standards Organisation, 2019), and is sensitive to the size of the tyre pavement interface, positioning of the plane as well as the sampling point location.

Texture depth has been classically characterised at three different scales according to the wavelengths of the deviations (refer to Figure 2.1b) (PIARC, 1987) as follows:

i. *Microtexture* suspected to induce tyre adhesion, represents the texture components with wavelengths of less than 0.5 mm and peak amplitudes from 0.001 to 0.5 mm (International Standards Organisation, 2009). Microtexture correlates to the asperities upon the surface of coarse road aggregates (Dunford, 2013), and also to the fine particles present in the mixture constituting the wearing course of the pavement. Microtexture is therefore typically a function of road aggregate mineralogy and petrology; and is affected by climate/weather effects and traffic action.

ii. *Macrotexture* suspected to induce hysteresis response in the viscoelastic tyre, represents the texture components with wavelengths from 0.5 mm to 50 mm and amplitude of 0.1 mm to 20 mm (formed by the shape, size and gradation of road aggregates on a pavement surface) (International Standards Organisation, 2009). Macrotexture acts also to disperse water, under wet conditions, through the gaps in between the road aggregates (Dunford and Leach, 2013). Thus, macrotexture, has been shown to influence the way skid resistance reduces with increasing speed in wet conditions (Flintsch et al., 2013). Generally, with equal microtexture, pavement surfaces with higher macrotexture offer more friction resistance as speed increases than pavements with lower macrotexture under the same contact conditions.

iii. *Megatexture* strongly linked to low frequency rumbling noise (in and outside a vehicle) and rolling resistance, represents the texture components with wavelengths 50 to 500 mm and amplitude of 1 to 50 mm (International Standards Organisation, 2009) . Examples of megatexture include rutting, potholes, spalling joints and cracks.

Megatexture, has dimensions larger than those which directly affect skid resistance but might have some influence on tyre/road contact.

Wavelengths greater than 0.5 m are considered to be above texture and are referred to as *unevenness.* Unevenness represents texture components with wavelengths 0.5 m to 50 m (International Standards Organisation, 2009). Longitudinal unevenness is normally caused by irregularities in laying and compacting pavements. Longitudinal unevenness is given to influence ride comfort and the road holding of vehicles. Transverse unevenness can arise from the presence of ruts and affects vehicle safety causing lateral instability and the accumulation of water on pavement surfaces.

2.2 Characterisation of road macrotexture for field measurements

Conventionally, road agencies around the world used mean texture depth (MTD), mean profile depth (MPD), and specific to the UK, sensor measured texture depth (SMTD) to characterise road surface macrotexture in the field. MTD is a discrete representation of a small patch of macrotexture determined using the volumetric patch technique (American Society for Testing and Materials, 2015; British Standard Institute, 2010), often by highway operatives seeking an immediate *in situ* macrotexture measurement, for example to confirm the quality of newly laid asphalt. The technique involves spreading a known quantity of sand in a circle onto a pavement surface and recording the diameter of the area covered. MTD is then calculated using the following equation:

$$MTD = \frac{4V}{\pi d^2} \qquad \text{Equation 2.1}$$

Where V is the volume of sand spread onto the surface and d is the average diameter of the circular area covered by the material. Due to the method of collection MTD measurements can lack consistency particularly where applied to porous or deeply grooved surfaces. Mean texture depth is recognised as providing an incomplete assessment of particle shape, size and distribution (British Standard Institute, 2010). This has implications for using MTD to model friction as both positive and negative macrotexture can produce similar MTD measurements but their friction properties are completely different (Guo et al., 2021) . Conversely, it is possible for pavements with different MTD readings to have similar friction values.

Profile depth is the height between a 2D macrotexture road profile and the highest peak (refer to Figure 2.2). MPD is calculated over a baseline of 100 mm. This baseline is split in half and

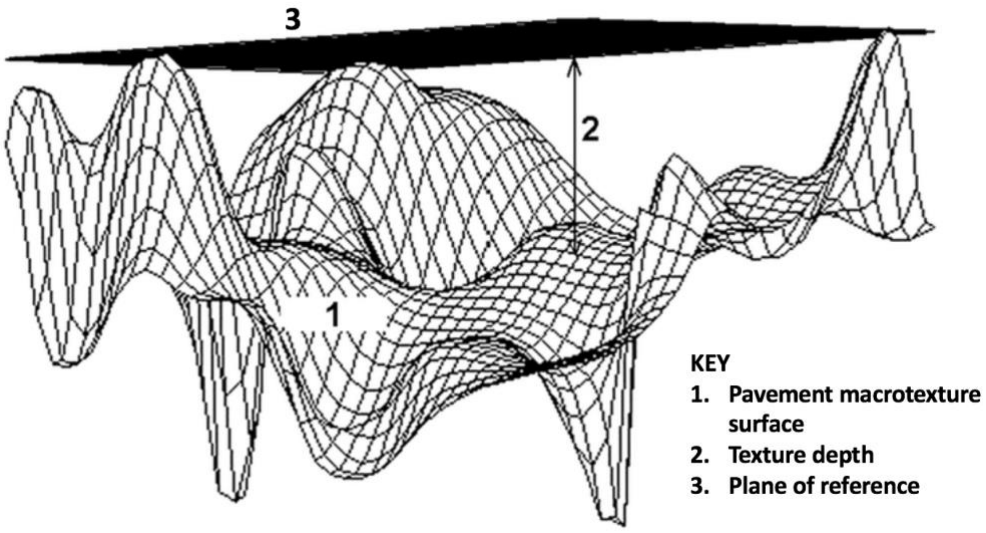

Figure 2.1a. Illustration of the term 'texture depth' on a macrotexture road surface (International Standards Organisation, 2019)

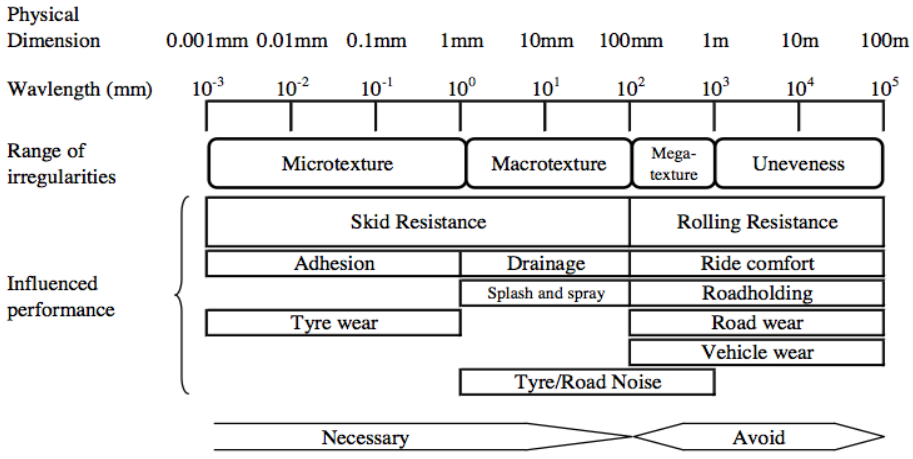

Figure 2.1b. Scales of road texture (Viner and Dunford, 2006).

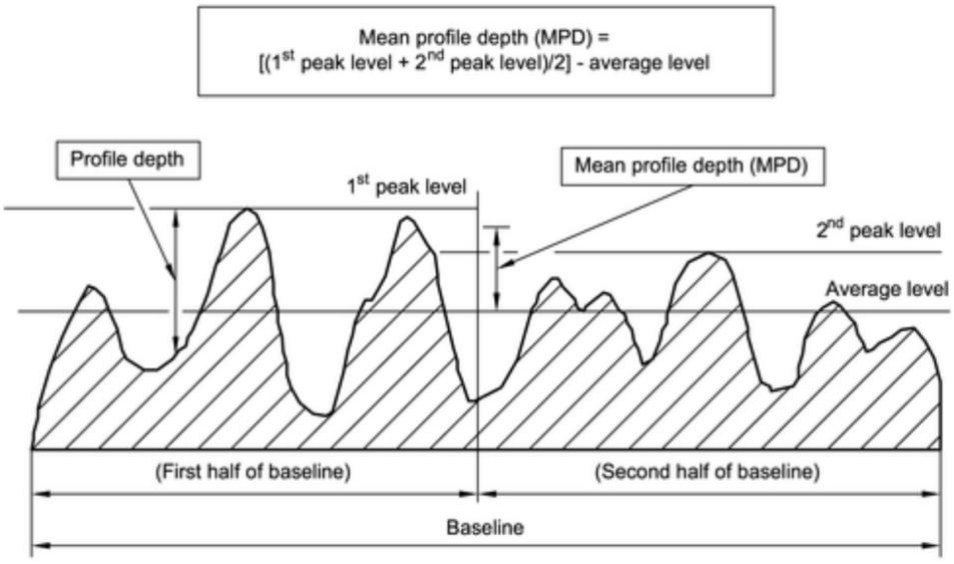

Figure 2.2. Illustration of the terms 'baseline', 'average level', 'peak level', 'profile depth' and 'MPD'. (International Standards Organisation, 2019)

and the profile depth found for each segment. MPD can then be found from the arithmetic mean of the 1st peak level and the 2nd peak level minus the average profile depth over the full 100 mm baseline as shown in Figure 2.2 (International Standards Organisation, 2019). To facilitate calculations MPD data are filtered or a least square fit is subtracted, to remove wavelengths above 100 mm, slope, and to bring the mean level of the profile to zero. Similarly, to MTD, MPD will change if a different baseline is considered.

SMTD is essentially the root mean square height of a 2D road texture profile above and below a mean level. Data for SMTD are collected in the UK using 'TRAffic Speed Condition Survey' (TRACS) (Department for Transport, 2019) and 'Surface Condition Assessment for National Network of Roads' (SCANNER) (Roads UK Road Board, 2009). Measurements are made at 1 mm intervals for an evaluation length of 300 mm, equivalent to the width of the nearside wheel track of a road. SMTD is averaged over a 10 m length for reporting and is calculated using the following equation:

$$SMTD = \frac{n\sum y^2 - (\sum y)^2 - \{12(\sum xy)^2 + P\} - (n^2 - 1)}{n^2} \qquad \text{Equation 2.2}$$

$$\text{for } P = \frac{5\{(n^2-1)\sum y - 12\sum x^2 y\}^2}{4(n^2-4)}$$

Where y is the height measurement made by the laser, n (which is always forced to be odd) represents the number of measurements made in the 300 mm evaluation, and x is the nominal scaled distance used for sampling heights ranging from $-½(n-1)$ to $½(n-1)$ over the length. The specification of x follows the principles of Nyquist theorem (D Gubbins, 2004), effectively facilitating sampling at the lower bound rate of twice the measurement interval.

Dunford (2013) recognised that SMTD, MTD and MPD do not consistently characterise macrotexture in the same way and may fail to give a full representation of a road surface. A general limitation of profile measurements like MPD or SMTD, are that they do not give a full indication of the peak density or the shape of macrotexture. Forster (1989) found peak density and shape descriptors together with depth to be important, demonstrating that shape provided the closest link to friction. To illustrate the limitations of using profile measurements to characterise macrotexture shape, consider the two profiles taken through 'Surface A' and 'Surface B' shown on Figure 2.3a. The profiles give an indication of the width and height of the raised elements on the surfaces, but the circular shape of 'Surface A' or the elongation of 'Surface B' are not discernible. The specific algorithms use for SMTD, MTD and MPD can

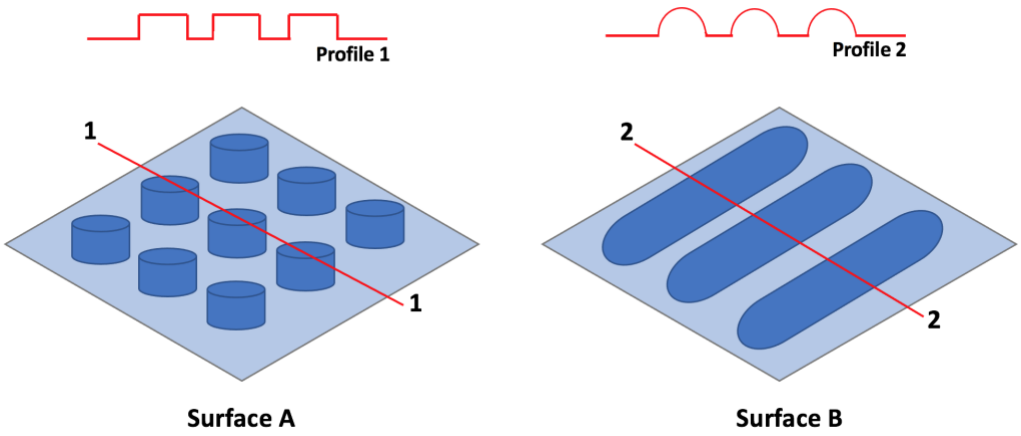

Figure 2.3a. General limitations of profile measurements.

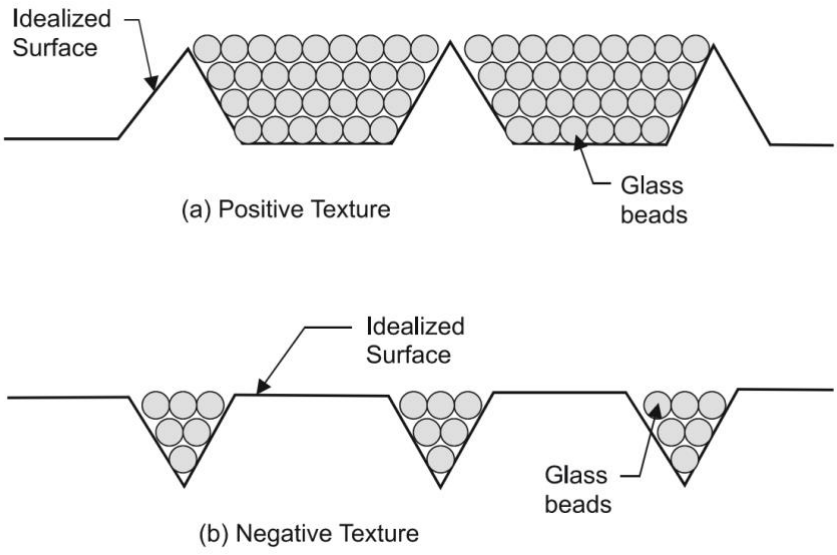

Figure 2.3b. Positive and negative texture (McGhee and Flintsch, 2003)

also provide different results. This has been illustrated previously by McGhee and Flintsch (2003), using the mirror image idealised road texture diagram replicated in Figure 2.3b. McGhee and Flintsch (2003) explained that whilst SMTD would remain the same for both types of texture, the value of MPD and MTD would be much higher for the positive texture on account of the greater volume between the peaks as depicted by the glass beads.

Some of the limitations of conventional SMTD, MPD and MTD used for macrotexture field characterisation can be addressed by exploring spatial methods. Within the field of metrology, the spatial characterisation of surfaces is regularly practiced. This field does not adopt the PIARC (1987) classification of texture, instead defining two scales of texture: short wavelengths called 'roughness' and long wavelengths called 'waviness'. Furthermore, there is no distinct wavelength boundary between these classifications, with the selection of 'roughness' and 'waviness' instead being associated with the surface being measured (Dunford, 2013). Spatial roughness and waviness are captured using the 3D Cartesian co-ordinate system, where the '*x*' and '*y*' represent the real surface, and the '*z*' axis the outward direction of the material from the surface. Spatial roughness and waviness are characterised using areal parameters. which were first defined as part of a European project led by Ken Stout from the University of Birmingham, who proposed the 'Birmingham-14' parameters (Thomas, 2009). A further project 'SURFSTAND' considered the practical application of these parameters and tightened up their definition (Blunt et al., 2008). Work to standardise areal surface texture measurement methods internationally was started in 2002 with the establishment of a working group WG16 for ISO 25178 (International Organisation of Standardisation, 2012; Leach, 2013). Part 2 of ISO 25178 covering terms, definitions and parameters was published in 2012; some of the commonly used parameters are described in Table 2.1. S_q the root mean square of surface departures, and the linked parameters S_p and S_v (maximum peak and pit height) are equivalent to MTD. S_{pd} represents the density of the peaks formed chiefly by the road aggregate of the pavement macrotexture and S_{pc} is a measure of the principal curvature of the peaks, characterising the shape and size of the road aggregates.

Being relatively new, limited research has been undertaken in the use of areal parameters in the field. Kogbara et al (2008) completed a small study using close range photogrammetry to reconstruct the surface of a dense graded asphalt concrete with gabbro aggregate. They considered just twelve samples from the outer wheel path of a 900 m length of road. Surface rippling was removed from the images of the area of interest using a 2nd order polynomial filter, and a Robust Gaussian (Leach, 2013) filter operation was used to separate high wavenumber microroughness from the low wavenumber macroroughness of the surface. MountainsMap Premium version 7.4 was then used to calculate the surface texture parameters

Parameter Symbol	Parameter Name	Description	Calculation Equation
Sq	Root mean square height	Root mean square value of the surface departures within the sampling area.	$S_q = \sqrt{\frac{1}{A}\iint_A z^2\,(x,y)\,dx\,dy}$
Ssk	Skewness	Defines the shape of topography height distribution as a measure of symmetry about the mean line.	$S_{sk} = \frac{1}{S_q^{\,3}}\left[\frac{1}{A}\iint_A z^3(x,y)\,dx\,dy\right]$
Sp	Maximum peak height	Largest peak height within a definition area A.	S_p
Sv	Maximum pit height	Smallest pit height value within a definition area.	S_v
Spd	Peak density	The number of peaks per unit area.	$S_{pd} = \frac{N}{A}$
Spc	Arithmetic mean peak curvature	Measure of the principal curvature of the peaks.	$S_{pc} = -\frac{1}{2}\frac{1}{n}\sum_{k=1}^{n}\left(\frac{\partial^2 z(x,y)}{\partial x^2} + \frac{\partial^2 z(x,y)}{\partial y^2}\right)$

Table 2.1. Areal surface texture parameters used to characterise macrotexture.

S_q, S_a, S_{pd}, and S_{pc} following the principles of ISO 25178-2 (International Organisation of Standardisation, 2012). The study indicated that frictional resistance is sensitive to the density of the peaks within the macrotexture surface of a highway (S_{pc}) and to the pointiness or arithmetic curvature of the same peaks (S_{pc}), characterising the shape and size of road aggregate. The authors suggest this is because sharp edges in the pavement surface assist in breaking through the lubricating water film between the tyre and the pavement surface.

The Kogbara et al. (2008) study presents just one application of areal parameters being used to characterise macrotexture in the field for a sole non-contact technique. The study has some limitations, it does not provide a clear justification of the size of area sampled. S_{pd} for example represents the number of peaks in a unit area, on a random road surface the area of interest selected for sampling needs to be of a sufficient size to be spatially representative of the overall road surface. This was not considered in the paper presented by Kogbara et al. (2008). Moreover, the resolution which can be thought of for point clouds arising from close range photogrammetry as the point-to-point physical distance between data points, potentially impacts on the calculation of areal parameters and was not discussed. Finally, filtering requires the consideration of scale and a choice of method to separate the measured data into different scales of interest. The Kogbara et al. (2008) study considered the relationship of the filtered data with skid resistance but did not specifically consider the sensitivity of area parameters to filtering. Further research is needed to understand the sensitivity of areal parameters to resolution, sample size and filters.

The International Standard ISO 27158 Part 2 (International Organisation of Standardisation, 2012), for metrology defined three types of filter:

- an *S-filter* where short-wavelength surface deviations are eliminated by a low pass filter.

- an *L-filter* where long-wavelength surface deviations are removed using a high pass filter. The long-wave surface deviations are typically components of form deviation or waviness (refer to Figure 2.4 for further explanation).

- an *F-filter* removes the nominal form from a surface dataset, typically by a least square fit operation on the priori nominal form.

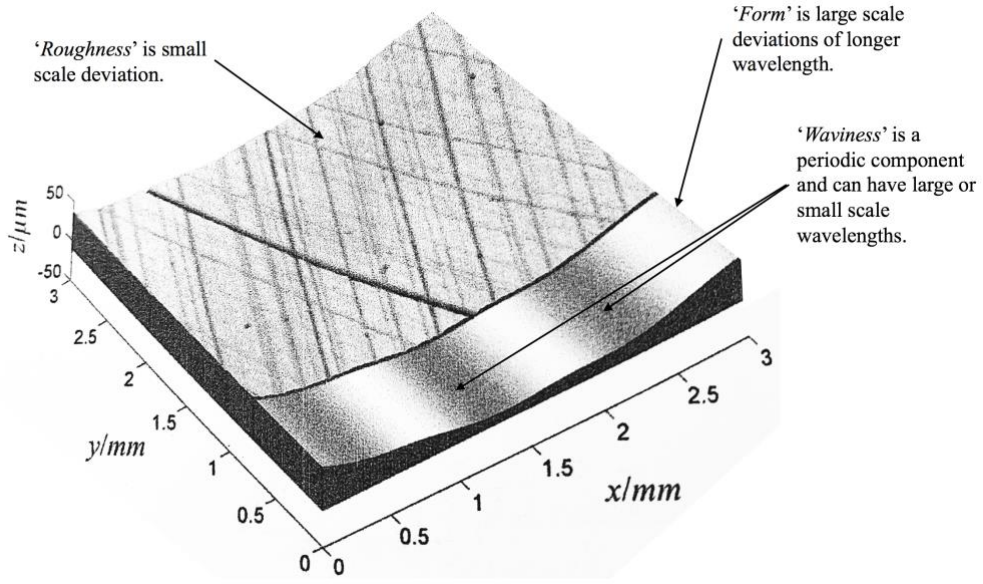

Figure 2.4. Topography of a honed surface with form, waviness and roughness (modified from Leach, 2013)

There are many different types of filter method: linear, Gaussian, spline, Fourier, planar, cylindrical etc. A full review of these is beyond the scope of this thesis, but Leach (2013) provides a useful summary.

Another analytical approach to show the extent to which various wavelengths contribute to a surface of profile is the power spectrum. If a surface profile can be represented by a function *f(x)* in the spatial domain. Then a discrete Fourier transform *F(k)* can be used to break down a spatial function into its different constituent sinusoidal spatial wavenumbers (spatial frequencies) to provide wavenumber amplitude and phase spectra. The square of each of the spectral amplitude components yields the power spectrum density, with the energy per unit spatial frequency interval being proportional to $|F(k)|^2$. Peaks in the power spectrum occur where there is a dominant wavenumber (the corresponding wavelength = 1/wavenumber) or wavelength (refer to Figure 2.5).

Pidwerbesky et al. (2008), used the power density spectrum to find flushing and stripping defects in surface dressing. Flushing is a fault leading to the excessive embedment of chippings into an asphalt binder, whilst stripping refers to the loss of chippings from the surface dressing; both lead to the macrotexture being smoothed. Pidwerbesky et al. (2008), recognised that high contrast in the illuminance of pixelated digital images occurred at the edges of a chipping. This was caused by the increased light reflecting of the exposed chipping compared to the black asphaltic binder. Accordingly, they realised they could use lack of contrast, in the pixelated images to search for areas where chippings were missing or embedded. They used a 2D Fast Fourier Transform (FFT) to determine the frequency spectrum of 256 grey-scale bitmap digital images of the surface dressing. A bandpass filter (Bose and Meyer, 2003) was applied to eliminate noise from the images. The images were then parsed into rectangular frequency bands to determine the power spectrum, which was graphed and compared using regression models with MTD. The power spectrum proved effective in finding smooth areas of macrotexture or locations with embedded/lost chippings for single racked surface dressing. The research team found that the technique struggled to deal with surface dressing containing multiple sized chippings. Later, Specht et al. (2013) used the same technique successfully in comparison with MTD readings for 26 pavements of varying texture from fine (0.15 mm to 0.22 mm) and coarse (1.2 mm to 4.97 mm). They found that the technique proved to be efficient in the correlation of frequency distribution of the FFT bands and MTD determined from the volumetric patch test.

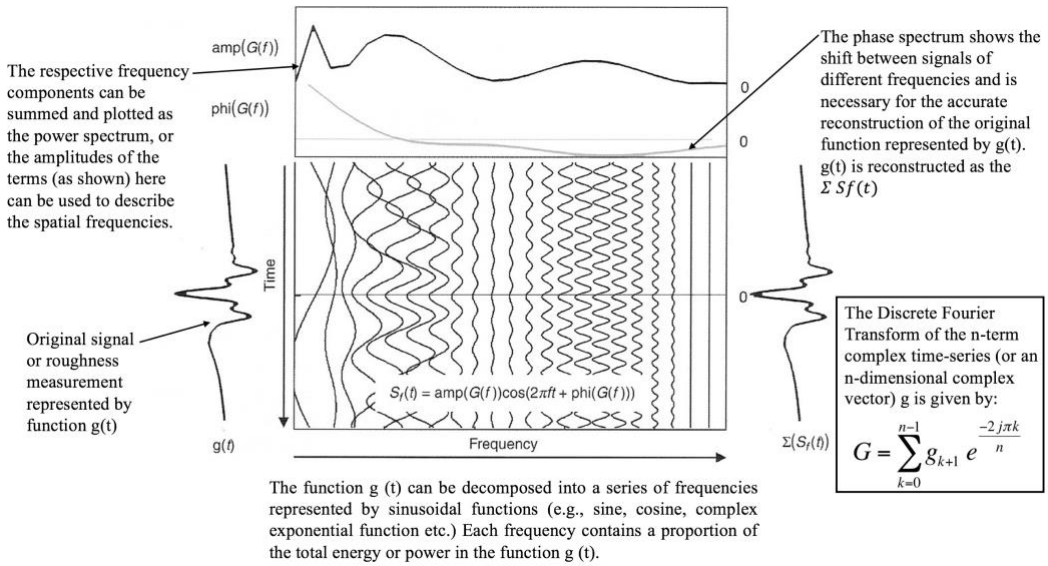

Figure 2.5. Discrete Fourier Transform – Digitally sampled functions of a finite length (modified from David Gubbins, 2004).

Cigada et al. (2010) also made use of the power spectrum when developing a method to determine 'real-time' micro and macrotexture texture measurements at medium and high speed. To facilitate 'real-time' measurement from a vehicle it is necessary to know the instantaneous vehicle speed to correctly find the relationship between time signal and spatial signal for a laser mounted on a measurement vehicle. Cigada et al. (2010) use two industrial laser triangulation displacement transducers and cross-correlated the respective signals '*x*' and '*y'* from the two sensors. The cross-correlated maximum facilitated an indication of the time delay between the signals *x(t)* and *y(t)* of the two displacement transducers. As the mounting distance between the two displacement transducers was known it was possible to calculate vehicle speed. Cigada et al. (2010) used the power spectrum density to compare the reliability of repeat measurements made using the dual sensor technique on the same section of road. Whilst their approach was not fully explained, the results obtained for the measuring technique were found to be similar each time. A limitation of the power spectrum was recognised by Wambold as early as 1979 (Wambold, 1979). The power spectrum as a summation effectively indicates only the average signal amplitude at a particular frequency. This means a large power spectrum value can be produced by either a few cycles of large amplitude or a large number of small amplitudes. For this reason, Wambold (1979) proposed representing macrotexture roughness as a '*combined amplitude and frequency distribution' (AFD)* in a tabular format (refer to Figure 2.6).

2.3 Non-contact field methods for measuring road macrotexture

2.3.1 Static contactless spot techniques

The simplest non-contact method to measure road macrotexture in the field is the volumetric patch test (American Society for Testing and Materials, 2015; British Standard Institute, 2010) previously explained in Section 2.2. Other more sophisticated proprietary *in situ* contactless spot techniques are available which offer an alternative to the straightforward patch test. The Circular Texture Meter (CT Meter) was first introduced in 1998 (ASTM, 2015), and uses a charged coupled device (CCD) laser displacement sensor (Emerald Insight, 1998) mounted on a rotating arm 80 mm above the road macrotexture surface (refer to Figure 2.7). The arm is driven at 6 m a minute in a counterclockwise direction, and 1024 samples are taken. Profile measurement of macrotexture are made at 0.87 mm on a radius of 142 mm or a circumference of 892 mm. The circumferential measurement is divided into eight 111.5 mm arcs (refer to Figure 2.7d) and the MPD reported for each. The laser has a spot size of 70 μm over a range of 65 to 90 mm, and a vertical resolution of 3 μm. The CT Meter is given to operate to a

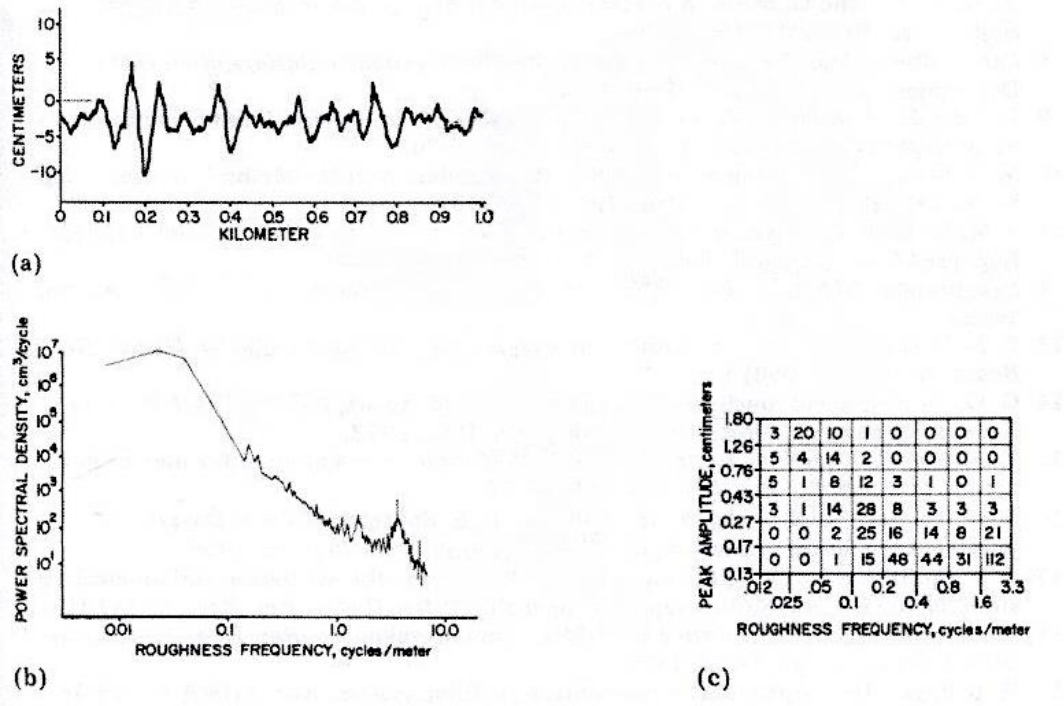

Figure 2.6. (a) Analog profile representation of section of US road. (b) Profile power spectral density. (c) Amplitude and frequency distribution (AFD) tabulation for section of US road. (Wambold, 1979)

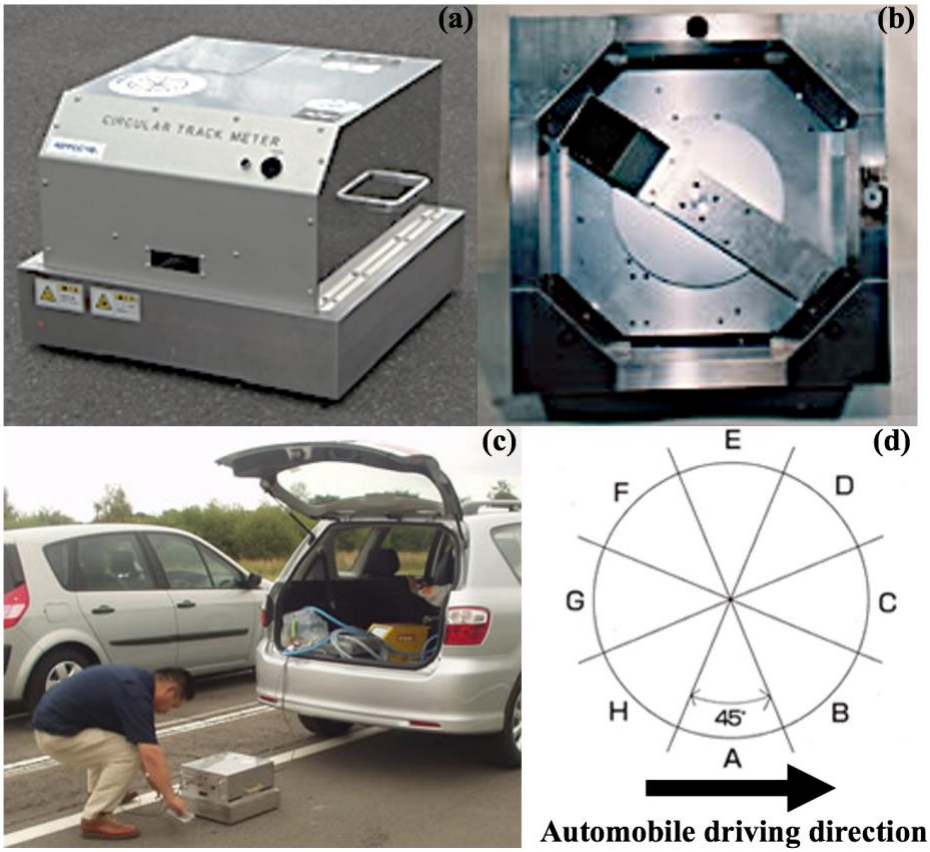

Figure 2.7. Circular Texture Meter: (a) Front view and (b) Bottom view. (c) In use on the highway (d) Measurement segments. (Nippo Sangyo Co. Ltd, n.d)

precision of a standard deviation of 0.03 mm for eight measurements. The CT Meter is one of a number of circumferential macrotexture profile measurement meters which operate on these principles, for example the ELAtextur (IWS Messtechnik, n.d.) would be another such device. The results of the CT Meter are equated to MTD derived for the volumetric patch test using Equation 2.3 (ASTM, 2015)

$$MTD = 0.947\,MPD + 0.069 \qquad \text{Equation 2.3}$$

Prowell and Hanson (2005) compared CT Meter measurements with MTD obtained from a volumetric patch test for 46 different flexible pavement surfaces, and found that when open-graded asphalt mixes where excluded results of a best fit line were statistically significant, ranging from R^2 equal to 0.93 to 1.01. Abe et al. (2001) also established strong correlations between the CT Meter and MTD, but similarly for highly porous surfaces the correlation was weaker as sand tended to flow into pores. Arguably, as a consequence for open-graded asphalts, results from a CT Meter are more reliable.

Abe et al. (2001) also considered the relationship between MTD and readings derived from an Outflow Meter. An Outflow Meter (ASTM International, 2019) is an in situ contactless spot technique that makes use of a glass cylinder (refer to Figure 2.8). The cylinder disperses a known volume of water under head between the gaps in macrotexture and a circular rubber annulus (which simulates a tyre) in contact with a road surface. The method does not measure texture directly, rather the time it takes for the water to fall by a fixed amount in the cylinder is recorded as the outflow time (OFT) in seconds. OFT readings are less accurate on porous surfaces where water can be lost into pores. The method has greater application to low texture road surfaces, rather than coarse texture surfacing where water can be lost too quickly from the macrotexture matrix to make the technique practical. Completing a comparative study of the volumetric patch test with the Outflow Meter on 23 macrotexture test sections Aktaş et al., (2011) found the instrument to be effective for macrotexture depths less than 1.29 mm, while the patch test performed better on higher macrotexture depths above 0.79 mm. The Outflow Meter method is often used to determine how a road pavement will perform with a water film when investigating hydroplaning. A quick OFT indicates that the film of water will be lower, and more grip will be available at the tyre/road contact.

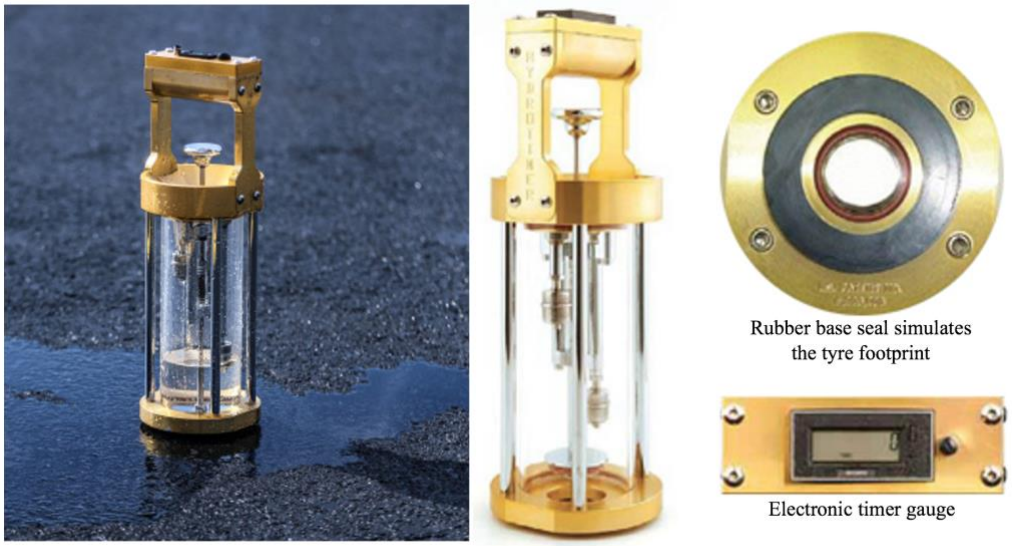

(a) Outflow meter in use **(b) Principal elements of the equipment**

Figure 2.8. Outflow Meter (KPR, n.d)

To calculate MTD from an OFT the following relationship is used (Aktaş et al., 2011):

$$MTD = 3.114/OFT + 0.636 \quad \text{Equation 2.4}$$

Abe et al. (2001) found the relationship between MTD and readings derived from an Outflow Meter, finding results to be highly correlated

Another less common non-contact *in situ* spot technique is stereo photogrammetry or stereovision. The principles of stereovision where first explained by Sabey and Luton as early as 1967 (Sabey and Luton, 1967). The approach involves taking two images of the same object from positions separated by a known small distance. Sabey and Luton (1967) used as the object a pencil, photographed from above at point *A* and point *A'* with a separating distance of *b* (refer to Figure 2.9). The two photographs obtain slightly different views of the pencil and when superimposed on top of each other are slightly displaced. The top *T* and bottom *B* of the pencil with the camera lens position directly above at *A*, superimpose at position *M* on the camera sensor array. Similarly, if the camera lens is moved to position *A'* the top and bottom of the pencil will appear at *T'* and *B'* respectively on the camera sensor array. The displacement of the camera to the right, is the equivalent of the displacement of the pencil the same distance to the left. If the pencil had been moved to the left, then the image of the pencil would appear at *T''* and *B''* on the camera sensor array as indicated by the dashed lines on Figure 2.9. When the first image is superimposed on the second the displacement is termed the parallax and is represented by p . The parallax can be found by:

$$\frac{p}{b} = \frac{f}{h} \quad \text{Equation 2.5}$$

$$\Delta p = -\frac{bf}{h^2}\Delta h \quad \text{Equation 2.6}$$

Where b = distance between the two camera lens positions, f is the distance between the lens and the camera sensor array, h is the vertical distance between the lens and the object. Thus, applying these equations for multiple images it is possible for software comparing the respective shift between photographs to calculate a 3D surface. Flintsch et al. (2008) used the approach to develop a two-camera system, encapsulated in a lightweight housing to control external environmental lighting factors. Their proof-of-concept tests compared the technique with conventional texture measurements for different surfaces and found the technique to be

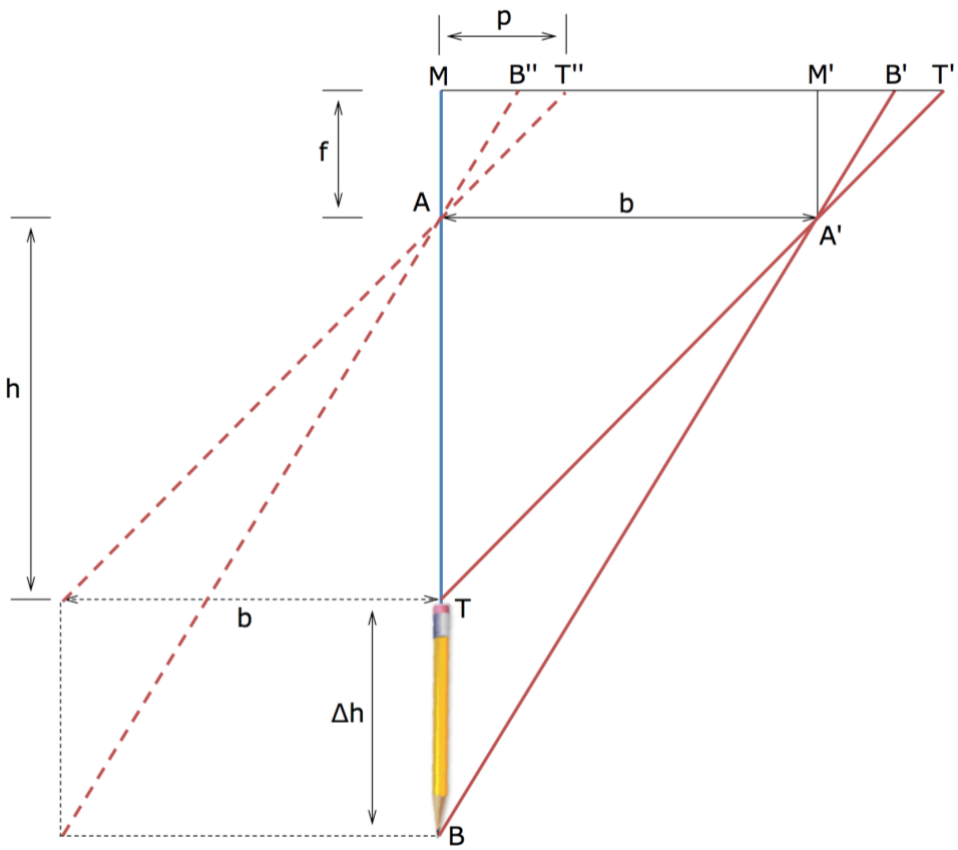

Figure 2.9. Schematics for stereovision (Sabey and Luton, 1967)

accurate and a beneficial area-based method to record macrotexture. Do (2005) developed a three-source photometric system using a high-resolution camera with 3000 x 2000 pixels surrounded by three light sources (refer to Figure 2.10a). The approach used the Lambertian model (Herbert et al., 2007) to extract the relief of the pavement, which facilitated the removal of the problems of interreflection between aggregate facets, shadowing and masking which can occur on a surface with high macrotexture. Gendy and Shalaby (2007) used a four light photometric system, including one unit as redundancy to help detect and remove specular and shadowing effects. They found that with a three-light system, specular effects manifesting as spikes in reflective intensity occur when a point on the surface is orientated in the same direction as one of the three lights sources. The system called 'PhotoTexture' was mounted and clad in a 0.6 m x 0.6 m x 0.6 m box to reduce image noise arising from light from the ambient environment. A fibre optic 50 W light source adjustable between 400 mm and 900 mm at 50 mm increments was used to ensure optimum scene exposure. PhotoTexture captured the pavement macrotexture for an area of 160 mm x 160 mm. The camera captured four images of the pavement under four illuminated angles $\frac{\pi}{2}$, π, $\frac{3\pi}{2}$, and 2π radians. In later work Alamdarlo and Hesami, (2018) sought to optimise this four light photo source system by experimenting with different zenith angles (refer to Figure 2.10b) between the camera and light sources for different texture depths. The study recommended a zenith angle of $\frac{\pi}{5}$ radians for a surface with a texture of 0.5 mm, reducing to an angle of $\frac{7\pi}{50}$ radians for a 1.5 mm to 2 mm. The study concluded that the quality of a reconstructed surface could also be influenced by the type and effect of light intensity, as well as the distance of the camera and light source from a surface but did not directly investigate these variables. The quality of a stereovision image depends on image set up, the camera lens optics and the elimination of any camera shake which is why most systems are mounted on a fixed frame (Kogbara et al., 2016).

A general limitation of all stereovision techniques for macrotexture measurement is that they create a 3D reconstruction of a surface similar in size to the volumetric sand patch. In recent years some researchers have experimented with the use of close-range photogrammetry (CRP)(James and Robson, 2012a; Micheletti et al., 2015), which offers a low-cost method utilising digital images, typically captured with an single-lens reflex (SLR) camera fitted with a fixed lens to generate a 3D dense point cloud data for surfaces. The technique is slightly different from the fixed metric approach of stereovision, relying on the acquisition of multiple overlapping images. Features across the image sets are identified and matched up using proprietary software running operators like 'Scale Invariant Feature Transform' (SIFT) (Lowe, 2004),

Figure 2.10a. Three light source stereovision equipment.

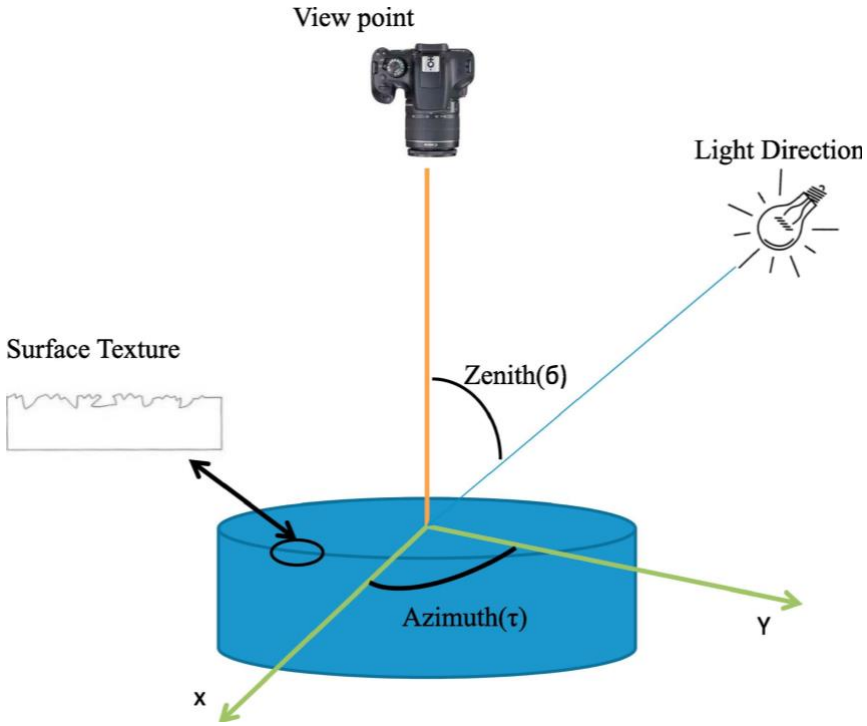

Figure 2.10b. The zenith angle for taking picture in the photometric stereo system. (Alamdarlo and Hesami, 2018)

'Speed Up Robust Feature' (SURF) (Bay et al., 2008) or 'Oriented FAST and Rotated Brief' (ORB) (Rublee et al., 2011) to establish 3D co-ordinates and generate a sparse point cloud. SURF which is an approximation of SIFT was developed to perform faster without reducing the number of detection points; whilst ORB was developed in 2011 as an alternative to SIFT and SURF. A full review of the processing principles of the these image matching techniques is beyond the scope of this thesis, but a useful detailed evaluation is provided by Karami et al., (2015). Karami et al, (2015) tested the sensitivity of the three techniques to image intensity, rotation, scaling, fish-eye distortion and noise. They compared the efficiency of the techniques' matching feature where there was a varying intensity or colour composition between two images (refer to Figure 2.11). In this instance SIFT was found to be most effective 76.7% of the available features compared with SURF at 72.6%, and finally ORB at 63.6%. However, the higher match rate of SIFT came at the cost of processing time, which was found to be 3.25 times slower than SURF. The overall conclusion of the study was that ORB was the fastest operator algorithm but tended to focus on features primarily just in the centre of an image (refer to Figure 2.11). SIFT generally outperformed the other two techniques in most scenarios apart from when images where noisy.

The strength of CRP approaches such as 'Structure-from-Motion' (SfM) (Ullman, 1979), is that they enable a large volume of images to be automatically processed. This means there is the potential for CRP to be applied over wider areas. Interestingly, whilst CRP has been adopted in other disciplines such as geoscience for expansive surfaces (James and Robson, 2012b) to date in the discipline of highways application has been largely limited to the reconstruction of spot surfaces, for comparison with the volumetric patch test or frictional measurement techniques (Millar and Woodward, 2011; Woodward et al., 2014). McQuaid et al. (2015) use CRP to assess pothole growth, and Millar et al., (2009) to support laboratory assessment of accelerated wear on asphalt concrete samples. Hence the technique has not been used to reconstruct from digital images taken in the field, large areas of highway surface.

A recognised problem with endeavours to capture expansive flat surfaces with CRP is the potential for 'doming' effects to occur in the generated point clouds if predominately parallel images and self-calibrated camera locations are used (James and Robson, 2012b). Doming effects are reduced with variability of camera pointing direction and height above a surface (James and Robson, 2014). Moreover images need to have appropriate overlap; a minimum of 60% forward overlap and 30% sideways overlap between photographs being recommended by Kogbara et al., (2018). A lack of overlap means there will be insufficient features for matching, and usually leads to voids occurring in the reconstructed surfaces. Similarly,

(a)

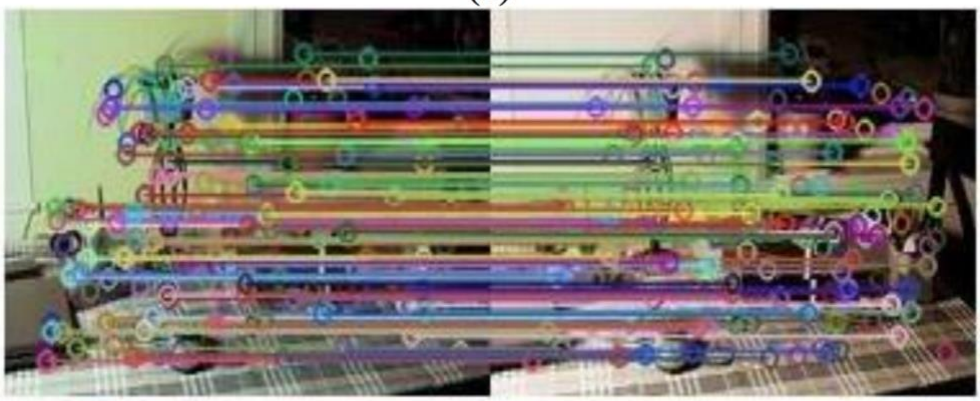

(b)

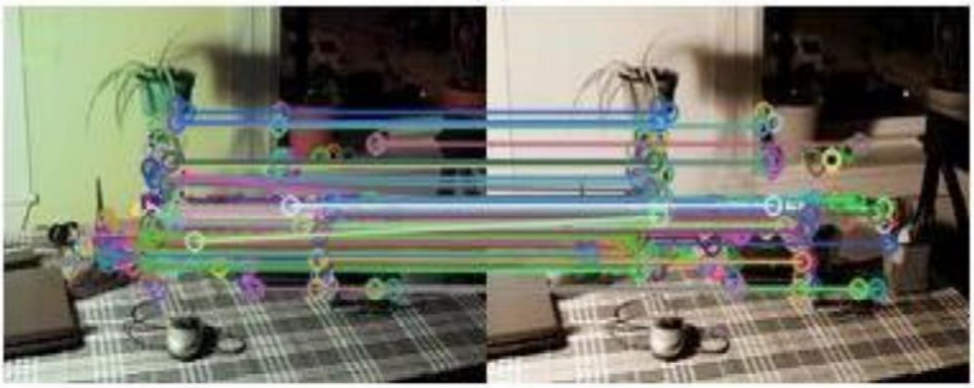

(c)

Table 1: Results of comparing images with varying intensity and colour composition values (left to right).

Image matching technique	Overall processing time to complete matching (sec)	Matches achieved	Match rate as a percentage of available features for matching (%)
SIFT	0.13	183	76.7
SURF	0.04	119	72.6
ORB	0.03	168	63.6

Figure 2.11. The matching of varying intensity using (a) SIFT (b) SURF and (c) ORB. (adapted from Karami et al, 2015)

surfaces with few features or limited texture are by the 'matching' nature of the technique also difficult to reconstruct. Typically, although the SIFT, SURF and ORB operators are largely tolerant to changes in photo intensity it is better to capture images in diffuse conditions such as during bright but overcast days. This practically tends to limit strong shadows or specular effects such as glints off wet surfaces appearing in the collected image data sets (James and Robson, 2012b).

Finally, recent experimental research has focused on the development of a prototype test rig (Wang et al., 2011) adopting a laser range finder, that uses triangulation, to measure texture in the field for a localised area comparable to that of a sand patch test. The minimum texture profile height measured by the rig was limited to 0.032 mm, with a spatial sampling frequency of about 4 mm^{-1}, thus meeting only part of the range needed for macrotexture. 3D handheld scanners (Creaform, n.d.; Z Corporation, 2007) using triangulation principles, have also been deployed to capture macrotexture in-situ (Hu et al., 2016). These scanners are designed for metrology applications, have a limited field of view, and lack scalability.

2.3.2 Wide-scale contactless techniques for macrotexture field measurement.

For large scale measurements at traffic speed on road networks laser profile sensors are used to measure macrotexture, ultimately reporting results as SMTD or MPD. These lasers employ triangulation in order to measure distance (refer to Figure 2.12). A solid-state laser light source projects a spot onto the object to be measured. The peak value of reflected light falls incident onto the receiving CCD sensor at a varying angle, contingent upon the distance from the pavement surface. From the position of the light source on the receiving sensor, as well as the fixed distance between the laser diode and the CCD, the distance to the object is calculated. For road surveys a 'profile beam' consisting of a number of triangulating lasers is often mounted on a vehicle. A servo system is usually installed in the measuring device to maintain the laser at a known distance above the highway, enabling small changes in distance caused by pavement surface asperities to be accommodated. The laser beam is most often the width of the nearside wheel path but might also accommodate a central path or in advanced cases the full lane width. In the UK for example, HARRIS1 (Viner et al., 2006) measures the nearside and central path, with profile lasers operating at 64 kHz and is capable of collecting measurements at 1 mm intervals at a survey speed of 100 kmh^{-1}. In France, a similar system RUGO (Gothie et al., 2004), with profile lasers operate at 32 to 64 kHz, collects measurements at 0.5 mm to 1 mm at 60 kmh^{-1}. Recently in Holland, the technology has been advanced and developed to measure the whole lane width (Kiwa, nd). The accuracy of

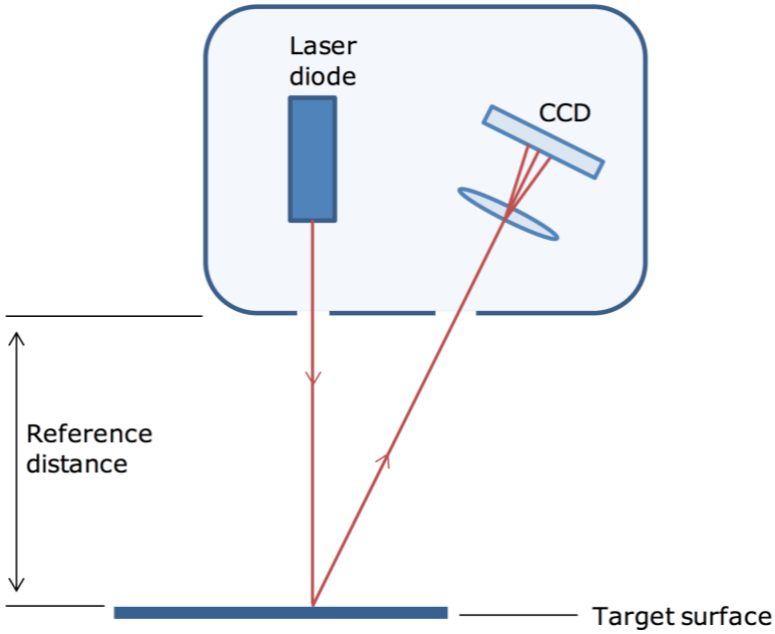

Figure 2.12. Laser triangulation (Source: Dunford, 2013)

these laser measurements is assessed against standards set by ISO 13473-1:2009 (International Organisation for Standardisation, 2019), with a ten percent drop-out constraint governing the quality of measured data acceptable for post processing and inclusion into a pavement management system. Similarly, in the United State, ASTM E1845 (ASTM International, 2015) governs the standards for laser spot size, sampling resolution, sampling spacing and sampling frequency for macrotexture. The laser spot is required to be no bigger than 1 mm; a vertical resolution of 0.05 mm or better is specified, and a sample spacing of no more than 1 mm is desired. In practice a laser travels at the same speed as the vehicle, so the effective frequency of sampling is governed by the relationship (Serway and Jewett, 2006) :

$$f = \frac{v}{\lambda} \qquad \text{Equation 2.7}$$

Where v is velocity, λ is the wavelength and f is frequency measured in units of Hz. Sampling macrotexture at 1 mm (two times the minimum wave length to comply with Nyquist sampling theorem (Gubbins, 2004)) means that theoretically at 50 kmh^{-1} a minimum laser frequency of 13.88 kHz is required to measure macrotexture. In reality, macrotexture on a pavement surface in the field consists of an assortment of wavelengths, and Li et al. (2010) found that with a 62.4 kHz laser the effects of vehicle speed at 80.5 kmh^{-1} (the normal survey speed) went unnoticed, but for 1 kHz they observed washout for sunlight. This is possibly why lasers on commercial traffic survey equipment typically operate at 32 kHz and above.

Several studies explore the potential to duplicate the volumetric sand patch test (British Standard Institute, 2010) using hand held 3D lasers operating on triangulation principles for spot tests of macrotexture. Sengoz et al. (2012) operated a laser with a lateral and vertical resolution of 15 μm and 10 μm respectively, and an accuracy of 0.04 mm. The laser automatically adjusted power output based on field condition e.g. pavement reflectivity and bitumen colour. They calculate MPD from profiles acquired for 31 different asphalt surfaces reconstructed from point clouds, achieving a strong correlation with MTD (R^2 = 0.97). Čelko et al. (2016) undertook similar work and also achieved a strong correlation between MPD and MTD (R^2 = 0.94). Xin et al. (2017) took another approach seeking to extend MTD measurement, by developing a new volume of parts parameter ω equal to the ratio of the volume of the macrotexture model at different depths V and the cutting depth H. The reconstructed macrotexture surface was sliced into consecutive layers from the nadir base layer, and similar trends for plots of ω against depth identified for 4 asphalt surfaces. Results were compared collectively and whilst accuracy was claimed, the study is largely limited with no real comment on laser resolution, reliability of scan or used of an independent control surface. Others have used handheld triangulating 3D scanner to make comparison with static (Hu et al., 2016) and dynamic (Čelko et al., 2016) friction measurements (refer to Section 2.6

for further details), but again these studies presented limited information on the suitability or reliability of the scanning techniques.

There is now also the potential to capture macrotexture over larger areas using Terrestrial Laser Scanning (TLS), which offers rapid 3D high resolution reconstruction of a highway surface as a point cloud (Serway and Jewett, 2006). Terrestrial laser scanners can be broadly defined as phased-based or time-of-flight. Phase-based laser measurements utilise the frequency, amplitude and phase of a continuous beam of radiation with a sinusoidal wave pattern. The wavelength of laser radiation is characteristically short, around 0.001 mm (Shan and Toth, 2009). As this accuracy is typically greater than required for topographic measurement, manufacturers of laser equipment often modulate the signal. A measuring wave pattern with a defined return period 'Tm' and wavelength 'λm' is superimposed onto the signal emitted from the laser transmitter. Measurement of a distance 'R' is achieved by determining the phase shift between the emitted signal (refer to 'Point A' on Figure 2.13a) and a received signal reflected from the surface of interest (refer to 'Point B' on Figure 2.13a). Phase is generally measured using a digital pulse counting technique. Phased-based scanners are usually short-ranged having a maximum scan range of typically 120 m (Faro, 2011). The scanners often adopt panoramic technology using a rotating mirror and head to achieve 360-degree horizontal coverage and 305 degrees vertical coverage (refer to Figure 2.13b). The laser then makes use of a digital encoder to measure the angles of the mirror rotation and laser head rotation. This information is used in conjunction with phase difference distance measurements described above to calculate *x*, *y*, *z* coordinates.

The determination of *x*, *y*, *z* coordinates for time-of-fight laser scanners uses similar horizontal and vertical rotating mirrors, but the laser operates on different principles. Time-of-flight terrestrial laser scanners offer greater range than phased-based systems, typically completing scans at distances of 120 m to 300 m, but with capacity to scan much greater distances (Heritage and Large, 2009). Time-of-flight scanners operate by firing a laser pulse at an object, and using an in built photodiode-based sensor to sense its reflection (Wehr and Lohr, 1999). The distance to the object is determined from the time-of-flight of the pulse, measured by a clock in the laser instrument. The distance to the object is calculated from:

$$R = \frac{ct}{2} \qquad \text{Equation 2.8}$$

Where R is the range in metres, c is the speed of light 299,792,458 ms^{-1} and t is the time-of-flight to the object and back to the instrument (Baltsavias, 1999). As time-of-flight scanners

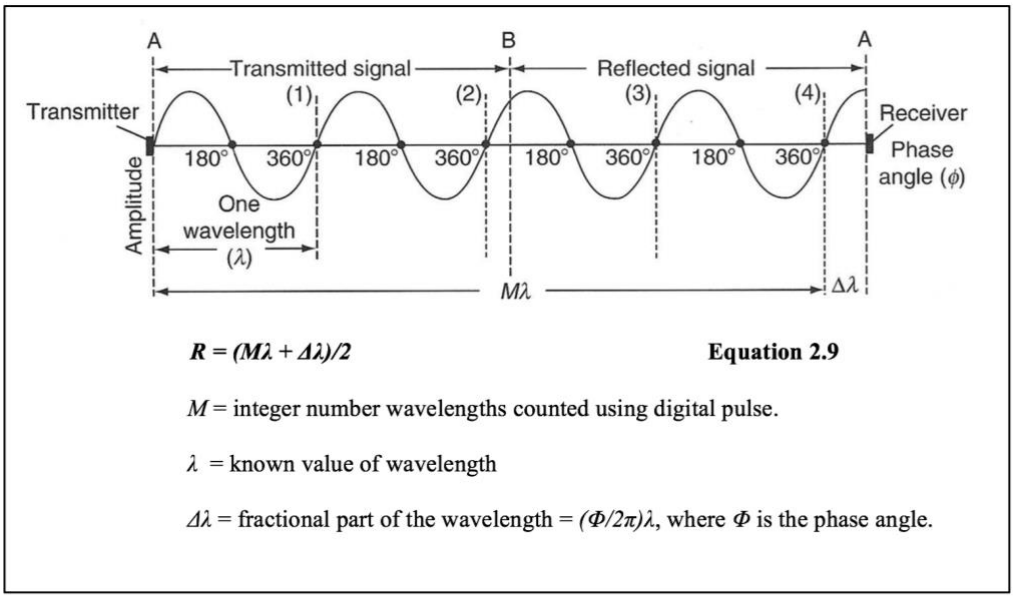

$$R = (M\lambda + \Delta\lambda)/2 \qquad \textbf{Equation 2.9}$$

M = integer number wavelengths counted using digital pulse.

λ = known value of wavelength

$\Delta\lambda$ = fractional part of the wavelength = $(\Phi/2\pi)\lambda$, where Φ is the phase angle.

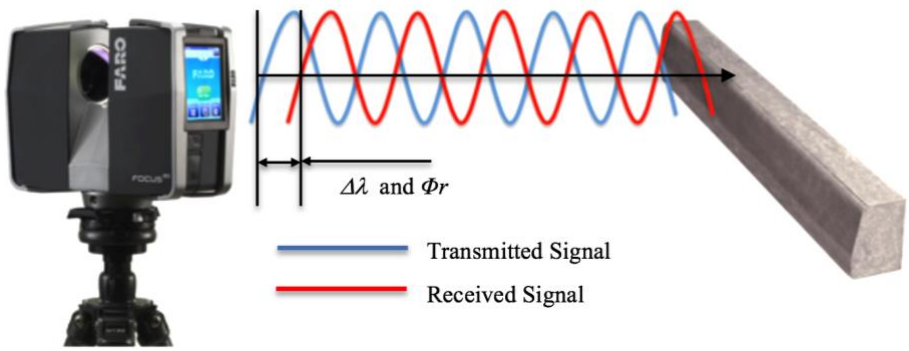

Figure 2.13a. Phased Signal Range Measurement (Source: Shan and Toth, 2009)

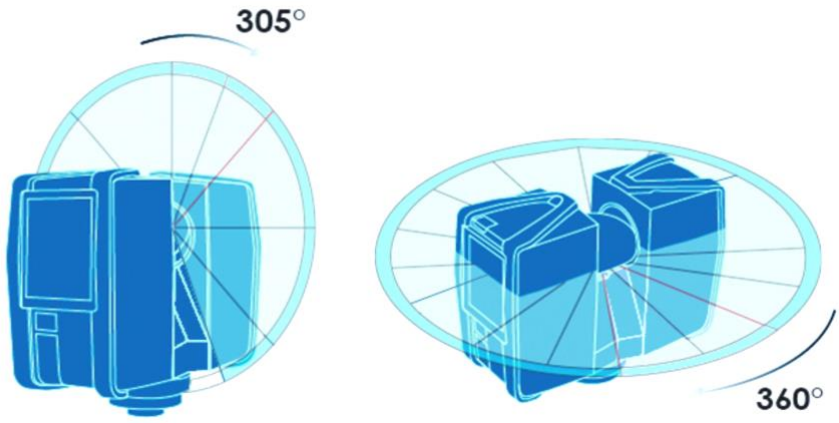

Figure 2.13b. Typical vertical and horizontal coverage of a terrestrial laser scanner (Source: Faro, 2011)

emit discrete pulses of laser light, the range is therefore effectively limited by the emission to return time. This limitation arises because where a pulse returns after the next pulse has been emitted by an instrument it is not registered (refer to Figure 2.14) (Heritage and Large, 2009). This means that at greater range the energy of the emission pulse, and the sensitivity of the sensor measuring the reflective pulse becomes increasingly important. This matters as the decline in energy of a pulse is inversely proportional to the square of the distance travelled, and at increasing range more powerful instruments are thereby desired (Heritage and Large, 2009). The acquisition of data at longer distances with time-of-flight laser technology is generally at the expense of speed of acquisition and accuracy. Boehler et al. (2003) endeavoured to quantify the respective range accuracy of a dozen instruments by measuring known short range (less than 10 m) and far range (over 50 m) distances. They determine that range measurement variance is instrument specific and might vary from 1 mm to several millimetres as distances extend. Boehler et al. (2003) found that for range up to 100 m the accuracy was about the same for any distance and thereby systematic. Range accuracy had a greater influence on time-of-flight laser scan surveys when the distances being measured were in excess of 100 m. Reshetyuk, (2006) investigating pulse TLS asserts that ranging errors are proportionate with distance.

Phase-based TLS systems by comparison typically offer 'faster' image acquisition rates, utilising motorised mirrors, but have similar accuracy decay with increasing distance and resolution. For example, the Faro Focus3D X scanner (FARO, 2021), a phase-based instrument records at 10 m, likely ranging noise of 0.6 mm at 90% reflectivity and 1.2 mm at 10% reflectivity. This range noise increases with distance to 0.95 mm and 2.2 mm respectively at 2 5m. With both phased-based and time-of-flight terrestrial laser measurements there is the potential for other errors in the captured point cloud data. Comprehensive work completed at the start of the millennium (Baltsavias, 1999; Balzani et al., 2001; Lichti et al., 2000) to characterise laser scanner accuracy, identified potential sources of errors during 3D point cloud capture as follows:

- *Angular Accuracy* – the head unit of terrestrial laser scanner adopts the use of an arrangement of horizontal and vertical spinning mirrors to propagate a panoramic array of laser beams onto an object of interest. Errors in the digital encoder, the angular reading device controlling these mirrors, may result in errors in distance measurement perpendicular to the laser beam.

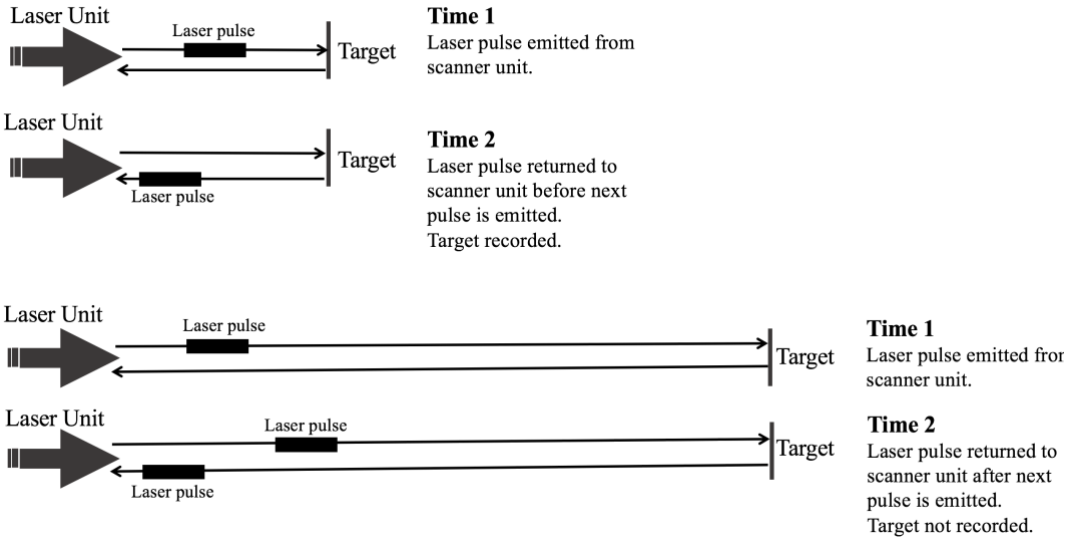

Figure 2.14. The influence of laser pulse rate on scanner range for pulsed 'Laser imaging, Detection and Ranging' (LiDAR) systems. (Heritage and Large, 2009)

- *Resolution accuracy* – the output from a TLS is a grid of points referred to as a cloud. The distance between the points is influenced by angular resolution and the distance of the TLS instrument from the highway surface, or range resolution. Resolution governs the level of identifiable detail in a point cloud. Lichti and Jamtsho, (2006) proposed an 'effective instantaneous field of view' EIFOV to model resolution for TLS, affirming the importance of both angular sampling resolution and band width. Angular sampling resolution is governed by the increment of angle between two successive points, and bandwidth the size of the laser spot itself upon the object of interest. In practice, TLS instruments usually have touch screen control settings enabling resolution and quality to be adjusted. 'Quality' in this context is a 'user-friendly' term describing the suppression of ranging noise; with an increase in 'quality' leading to a reduction in noise. Similarly, 'resolution' on an TLS instrument's touch screen control is proxy for 'angular resolution' and is expressed as the smallest distance between laser points. When 'resolution' setting is decreased, 'angular resolution' or the increment angle increases and the distance between scanned points increases. (FARO, 2021) This behaviour is clearly illustrated in Figure 2.15 for a sample of road pavement, with the table at the bottom of the figure indicates how the choice of scan resolution influences point distance, quantity and scan time for the Faro Focus 3D X scanner (FARO, 2021). TLS operators need to be mindful that demand for greater resolution will lead to longer scan times. Furthermore, if distance from the highway surface increases and resolution settings remains unchanged on an instrument, then the distance between data points also increases. This decay in resolution is illustrated in Figure 2.16, with the spacing between points widening with distance from the TLS laser instruments set-up position. This widening arises as a consequence of simple trigonometry, with angular projection leading to greater point spacing with range. As a result of these factors, the selected resolution (angular and range) of a TLS instrument must be calibrated to the detail and scale of the features to be captured, in order to achieve appropriate point cloud data. The Nyquist-Shannon (Shannon, 1998) sampling theorem is a useful rule, to apply to point cloud resolution. It states that the minimum size of the features should be twice that of the sampling interval.

- *Edge Effects* – occur when a laser spot hits the edge of an object, only part of the spot will be reflected back to the scanner. The remaining part of the spot may be reflected from another surface either adjacent to, or behind the object being considered, or

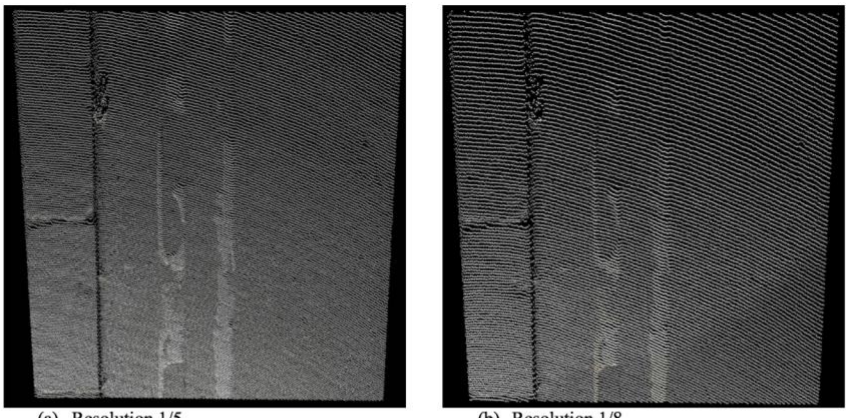

(a) Resolution 1/5

(b) Resolution 1/8

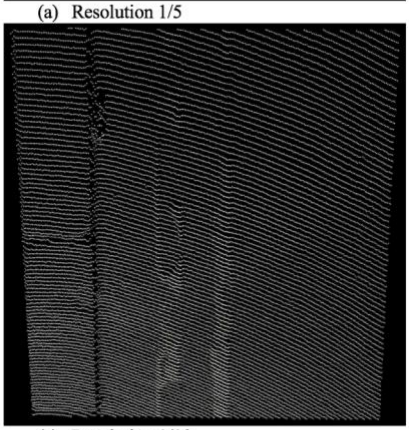

(c) Resolution 1/10

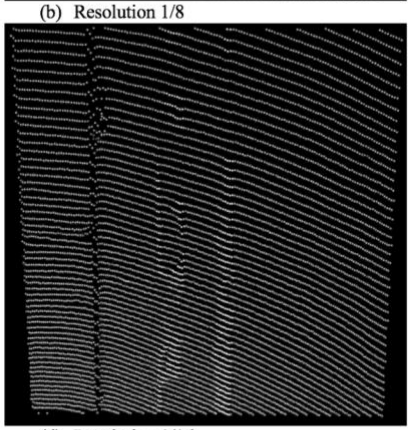

(d) Resolution 1/16

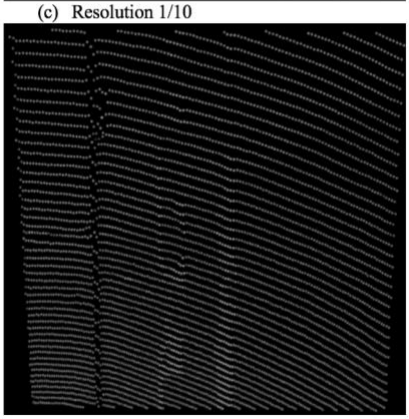

(e) Resolution 1/20

Resolution	Quality	Scan Time in Minutes	Number of points in millions	Point Distance in mm/10m distance
1/20	4x	2:14	1,7	30,680
1/16	4x	2:23	2,7	24,544
1/10	4x	3:05	7,0	15,340
1/8	4x	3:44	10,9	12,272
1/5	4x	6:31	28,0	7,670

Figure 2.15. The influence of resolution on terrestrial laser scan data. Performance data is based on a FARO Focus 3D X phase-based scanner. (Source (FARO, 2021)

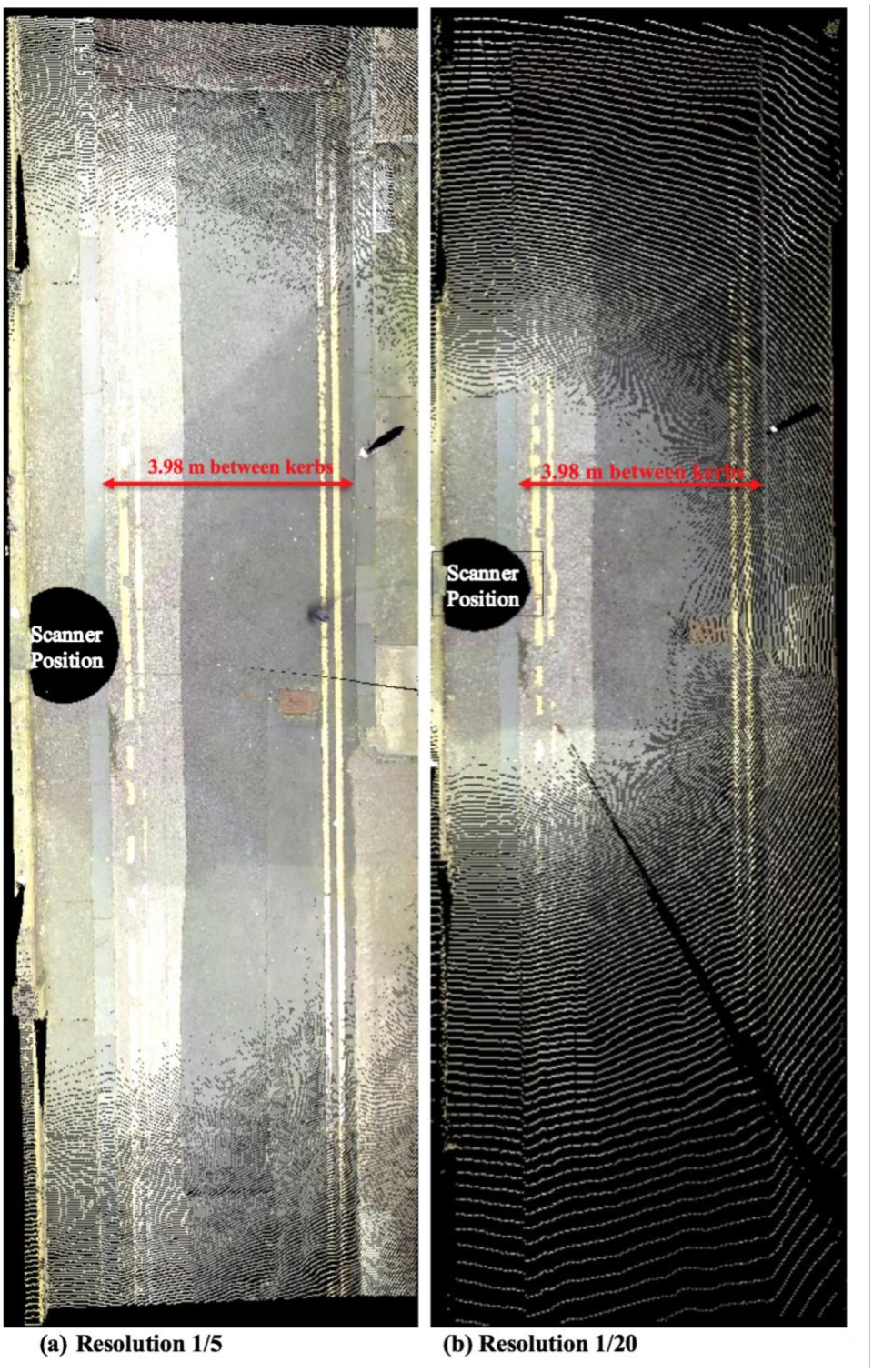

Figure 2.16. Illustration of the decay in point count density with distance from a terrestrial laser scanner set-up position.

simply lost and not reflected back at all to the scanner. Boehler et al. (2003) note that because the object the laser point hits will be recorded by the scanner at the angular position of the centre of the laser beam, even though it was in fact hit at the edge, the overall object may appear closer than reality in the point cloud. These effects can lead to inaccuracies, artefacts, and phantom points occurring in the vicinity of edges.

- *Influence of Surface Reflectivity* – Bolehler and Marbs (2002) observed error in range arising from the reflectivity of different coloured surfaces. The albedo of a surface influences the strength of the return signal reflected back to a laser scanner. Black surfaces such as asphalt typically have lower reflectivity compared to white surfaces, which generally yield a strong reflected signal. Hence white spherical targets are often selected for use with a scanner, and scanning road surfaces requires a powerful laser or the instrument to be position at an appropriate range. On surfaces which are shiny or where there is a differing reflectivity from one area to another, it is possible to get 'specular flares' or noise. An example of a specular flare is shown in Figure 2.17, a common source on road surfaces are white lines which are design to be highly reflective being made from a thermoplastic resin mixed with titanium dioxide pigment and tiny glass beads (Matthews, n.d).

- *Environmental Conditions* – a terrestrial laser scanner is designed to operate within a given range of temperature. If the internal mechanism of the scanner falls outside of the recommended temperature range, then deviations in range measurements are likely. Certain atmospheric conditions can also influence results, e.g. presence of dust, mist, strong sunlight or variations in temperature and pressure. Strong sunlight can 'wash out' the lasers signal influencing the performance of the receiver, whilst the other atmospheric conditions all have the potential to alter the propagation speed of light.

Of the sources of inaccuracy identified the principal factors that are likely to influence validity during data collection for road macrotexture are considered to be edge effects, a scanner's resolution and the reflectivity of the highway surface. In addition to these sources of errors, there remains the potential for inaccuracies to be introduced during the registration of the point cloud data in scanning software, and as a consequence of poor control arising perhaps from limited or badly placed laser targets. Fan et al. (2015) and Becerik-Gerber et al. (2011) provide a review of these problems.

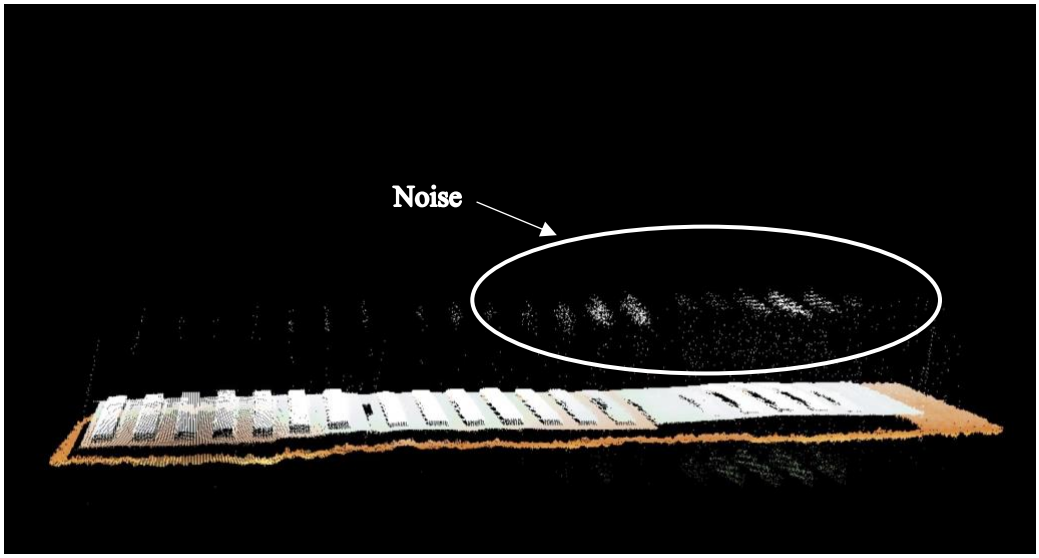

Figure 2.17. Example of 'specular flare' or noise in a terrestrial laser scanner point cloud data caused by the reflectivity of a light surface.

In conclusion, to date limited research has been undertaken to characterise road macrotexture using TLS instruments adopting phased-based or time-of-flight technology. Most work focuses on spot tests representing the size of the volumetric sand patch using handheld 3D lasers operating on triangulation principles, and larger full lane width studies are not considered. The optimisation of the scanning techniques in terms of appropriate angular and range resolution for different types of pavement surface has also not been rigorously investigated.

2.4 Use of road surface texture measurement in pavement maintenance regimes

The preservation of adequate texture on road networks is required to prevent skidding. Roe et al. (1991) related macrotexture depth directly to accidents in the UK and found the risk of accidents to be greater for roads with an average SMTD below 0.7 mm. On new UK pavement surfaces a minimum macrotexture level of 1.0 mm is set for roads with a design speed limit of between 80.5 kmh^{-1} to 96.56 kmh^{-1} based upon a volumetric patch test (National Highways, 2021). In other parts of the world the accepted minimum macrotexture level for roads is slightly higher, for example in Australia 1.2 mm is required (VicRoads, 2002). When setting minimum macrotexture depths, a balance is required between the level selected as appropriate for preventing skidding, and the requirement to optimise rolling resistance in terms of managing tyre wear, road noise, surface water spray and fuel efficiencies (Ejsmont et al., 2017). Overall, the purpose of macrotexture on a pavement surface is to break the film of any lying surface water so that a tyre can come into contact with the road. This is achieved as a component of the macrotexture depth, and also the microtexture of the road surface aggregate.

In order to maintain adequate macrotexture on road networks monitoring is undertaken at traffic speed using laser profile sensors to report SMTD and MPD levels (refer to Section 2.3.2). These macrotexture measurements are usually interpreted to report texture longitudinally along a road. Furthermore, as microtexture also contributes to the prevention of skidding, particularly at low speeds, most countries principally monitor networks for adequate skid resistance (refer to Section 2.6). Direct measurement of frictional resistance is achieved through a rubber pad (British Standard Institute, 2011) or test wheel making contact with a wetted pavement (British Standard Institute, 2006, 2000). The operating principles of these devices is beyond the scope of this literature review, but Kogbara et al. (2016) provide a useful summary. The ‘response’ to macrotexture is thereby indirectly monitored in conjunction with microtexture, and where skid resistance is found to be below an acceptable advisory level visual inspections of road texture is completed by a road manager (Design Manual for Roads and Bridges, 2015).

The frictional and pavement geometry data obtained from road surveys is commonly held in a pavement management system (Meegoda and Goa, 2015) and made available to government authorities, road agencies, asset managers, engineers, and suppliers to enable them to reach decisions on road pavement maintenance priorities and programming. The aim is to provide the road user with a reliable level of service and ride safety (Transport Research Board, 2016). Maintenance planning presents to the stakeholders two key fundamental challenges: the identification of locations on a large road network requiring investigation, and the characterisation of deterioration at these locations to facilitate timely, appropriate and effective maintenance approaches. Furthermore, characterising suitable intervention engenders the additional challenge of judging when preventative maintenance is required, which typically offers lower cost repair options to extend pavement life, and when full resurfacing is needed.

Pavement condition and performance indices that support the decision-making process are based on analysis of the survey data held within the pavement management system (FSV-Austrian Transport Research Association 2008). For longitudinal pavement texture there are a number of accepted pavement condition indices utilised across the world. The International Roughness Index (IRI) models the virtual response of a 'golden car' travelling at 80 km/hr on a road profile (Sayer et al., 1986; ASTM International, 2015, European Committee for Standardisation, 2017). The 'golden car' is a simulated system utilising standardised values for the damping, springs and masses relating to a portion (or a quarter) of a car supported upon one wheel, often termed the quarter-car. The IRI represents the dimensionless ratio, of the accumulated vertical motion of the 'golden' quarter-car's suspension, divided by the distance travelled; known as the evaluation or segment length. Acceptable IRI threshold values are specified on a country-by-country basis for new, reconstructed or rehabilitated roads. Depending upon the country of application, these IRI thresholds are reported either as a constant value for an evaluation length, the average value of a series of segments within an evaluation length, or as a percentile. The evaluation or segment lengths typically vary from 10 m to 1600 m. Furthermore, the IRI thresholds can be specified by a country as a function of the road surface type, category (e.g. motorway or minor road), speed limit or traffic flow. Mucka (2017) provides a full summary of the IRI specifications used around the world. Another approach to the characterisation of longitudinal road profiles is presented in ISO 8608 (International Organization for Standardization, 2016). The ISO 8608 standard provides a description and classification of synthetic road profiles for use in computational modelling, based upon vertical displacement power spectral density (PSD). PSD is represented on a logarithmic scale and is defined by two parameters of a straight line: an unevenness index and waviness. The road classifications presented in ISO 8608 are primarily used for vibration

modelling and are not directly linked to real road categories, although some research has been completed to derive validation (Mucka, 2018). Within the UK, texture threshold values are adopted to define minimum advisory road texture levels in relation to both longitudinal profile (with an evaluation length of 100 m) (Design Manual for Roads and Bridges, 2008) and also skid resistance (Design Manual for Roads and Bridges, 2015).

A limitation of the pavement condition indices reviewed, is the sensitivity of the techniques to the evaluation length (Transport Research Laboratory 2006). The selection of evaluation length defines the granularity of the texture data. This can be illustrated by a simple assessment of texture level against a minimum threshold. In such a case where pavement texture is averaged over a long length, which contains sections of localised texture variability, the averaged result will smooth the texture data potentially masking the true condition of shorter lengths. Stakeholders evaluating road texture for maintenance, require confidence in the deployment of follow-up resources for visual inspection and condition assessment. A preferred approach would be to augment pavement condition indices with a method to track and understand the rate of change of texture condition at every location on a real road network. This would support the identification of deteriorating sections of the road network; but to date the rate of change for pavement texture at discrete locations on a real road network has been difficult to estimate reliably (Rainsford and Parkman, ND).

2.5 Evolution of macrotexture on road networks

This section reviews the evolution of pavement macrotexture as it has been characterised in the field, using data collected on live road networks. Whilst much experimental work has been completed in the laboratory using the Wehner Schulze machine (European Standards, 2014) and other techniques to simulate the evolution of pavement texture with polishing (Do et al., 2009; Ech et al., 2012, 2009, 2007; Edjeou et al., 2020; Kane et al., 2013), limited discrete long-term field studies of macrotexture evolution have been undertaken. Pavement macrotexture changes over time, these variations were characterised into ‘long-term variations’ and ‘short-term variations’ by Vaiana et al. (2012). ‘Short-term variations’ have been hypothesized to arise due to seasonal and meteorological conditions such as temperature and rainfall (Masad et al., 2009); this is discussed further in Section 2.7.

Vaiana et al. (2012) completed a two-year study of four newly laid dense graded friction courses (refer to Figure 2.18a) situated on both curved and straight sections of a two-way single carriageway. Friction and macrotexture measurements were taken in the wheel track using the British Pendulum Tester (ASTM International, 2018), volumetric sand patch test

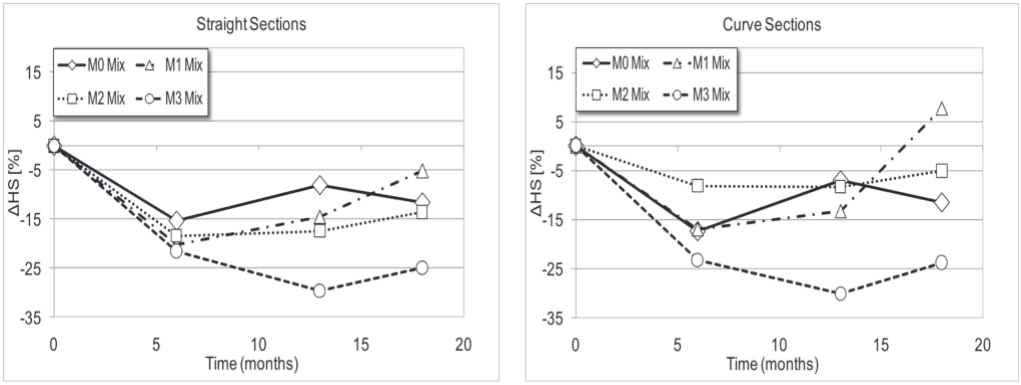

- M0 Mix: 100 % limestone aggregate
- M1 Mix: 85 % limestone aggregate, 15 % basaltic aggregate (aggregate size > 5mm)
- M2 Mix: 70 % limestone aggregate, 30 % basaltic aggregate (aggregate size > 5 mm)
- M3 Mix: 82 % limestone aggregate, 8 % expanded clay(aggregate size 3 – 11mm)

Binder content was 5.5 % the weight of the asphalt mix, with the exception of M3 which was 8.8%.

Figure 2.18a. Early-life macrotexture trends for straight and curved road sections (Source: Vaiana et al., 2012). The parameter ΔHS represents the percentage difference in MTD measured using the volumetric sand patch test from the initial survey.

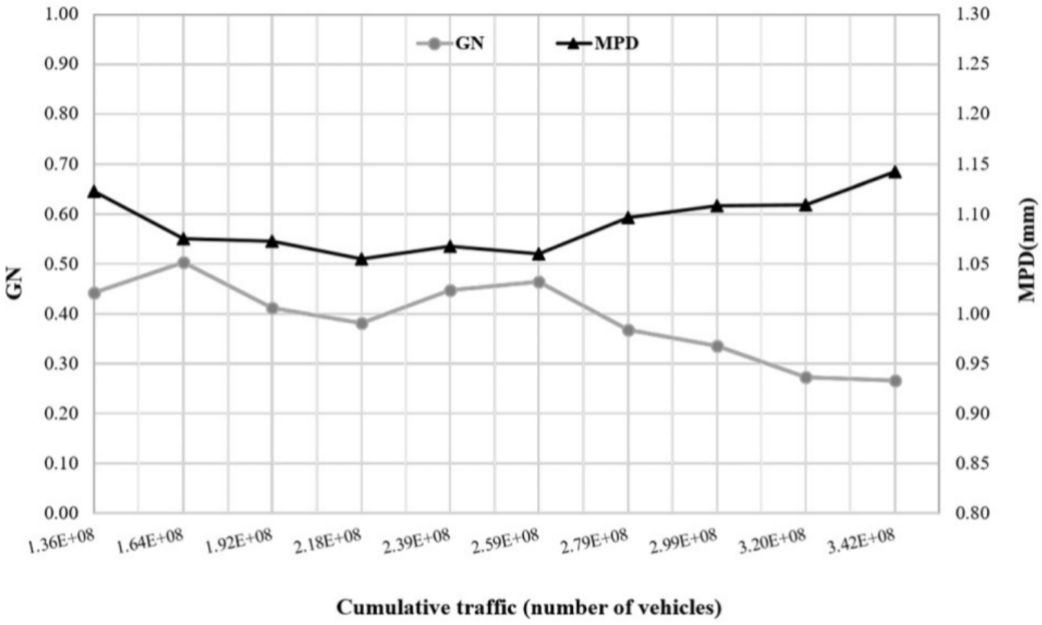

Figure 2.18b. GripTester Number (GN) and MPD versus the cumulative traffic (Source: Plati and Pomoni, 2019). The threshold cumulative traffic was achieved at 2.59E+0.8 vehicles.

(British Standard Institute, 2010) and a laser profilometer every six months. Macrotexture was found to decrease in the early life of the pavement (refer to Figure 2.18a), usually within the first 6 months, and then to slowly increase again. The initial decrease was attributed to two processes firstly, the smearing or migration of the bitumen binder from road surface aggregates under the action of traffic. Secondly, the post-construction compaction and embedment of aggregates into the asphalt pavement. The subsequent increase in macrotexture was connected with gradual removal of the bitumen film associated with newly laid roads and 'repositioning' of aggregates in softened binder under traffic action in the summer. It has been determined in several studies (Woodward et al., 2008, 2003), that during the early life of a pavement when polymer modified bitumen binder are used in asphalt mixtures, road aggregates remain coated for a longer period of time than unmodified binders. Similarly, Vaiana et al. (2012) found that for the 'M3 mix' with higher bitumen binder at 8.8%, the increase in macrotexture was delayed to around 13 months. Thus, the 'early-life' evolution of macrotexture was established to be linked to the composition of the asphalt mix, particularly the specification of binder. The work of Vaiana et al. (2012) also considered road geometry; macrotexture degrades more quickly around bends due to centrifugal forces, or with proximity to junctions where vehicle breaking forces transmit greater stresses to the road surface. Vaiana et al. (2012) completed tests on road curves, and results were found to largely correspond to those for the straight road sections (refer to Figure 2.18a), with greater variability in fact linked to the type of asphalt mix. This means that at least in the early life of a pavement, road geometry has limited impact. Road geometry might have greater bearing on the long-term evolution of macrotexture, but more investigations are required to establish if this is the case.

Later work by Zou et al. (2021) seems to contradict the work of Vaiana et al. (2012). Completing a study over 3 years on a newly laid dense grade asphalt pavement Zou et al. (2021) found that the surface peaks of macrotexture decrease. These data were collected yearly for 42 locations, and trends were averaged, a limitation in result reporting that may have led to an early increase in texture being disguised in the results. Certainly Zou et al. (2021) include photographic evidence and reported qualitatively that bitumen film covered the macrotexture in 2018; the macrotexture aggregate was exposed in 2019 and visually appeared more polished in 2020. The work of Zou et al. (2021) highlights the requirement to visualise macrotexture deterioration spatially through time at discrete locations along the section of a highway.

'Long-term variations' in macrotexture are given to be predominantly due to traffic actions (Vaiana et al., 2012). Traffic flow has a significant influence on the evolution of pavement texture (Plati and Pomoni, 2019) and as a result maintenance planning. Pavement texture deterioration has been shown to be influenced particularly by the percentage of heavy goods

vehicles in a trafficked lane (O'Brien and Haddock, 2009, Ragland et al., 2010, Khasawneh et al., 2016). The cumulative damage to a pavement due to commercial vehicle traffic flow for a given time period can be characterised as equivalent standard axles, with a 'standard axle' given to exert a force of 80 kN (Design Manual for Road and Bridges, 2020). Recently, an inverse evolution trend between skid resistance and pavement macrotexture deterioration has been identified, associated with a minimum cumulative traffic threshold (Plati and Pomoni, 2019). Plati and Pomoni (2019) considered eleven years of data for six, 5 to 10 km section of a live road network. The pavement surfaces were comprised of hot mixed asphalt concrete surfaced with an antiskid wearing course in accordance with ASTM D3515 standard (ASTM International, 2001). They analysed macrotexture depth obtained with a triangulating profile laser operating at traffic speed (ASTM International, 2015), and friction data were obtained using a GripTester (Findlay Irvine, 2002). They discovered that traffic effects are not a constant factor during the operational service life of a road. They identified two zones for a pavement's life governed by cumulative trafficking. In 'Zone 1' macrotexture exhibited a slow decrease with some fluctuations attributed to short-term variation effects (refer to Figure 2.18b), and there was no correlation with skid resistance readings obtained from the GripTester. In 'Zone 2', after a minimum cumulative traffic threshold, macrotexture evolution was found generally to increase and skid resistance to reduce with further trafficking. In 'Zone 2' a clear correlation between the GripTester number (representing skid resistance) and MPD was discernible in the data. The threshold was theorised to mark the point where sufficient polishing of fine aggregates had occurred, resulting in the coarse aggregates dominating skid resistance. The collective work of Vaiana et al. (2012), Plati and Pomoni (2019) and Zou et al. (2010) was limited to short discrete road sections and collectively encompassed the early to mid-service life of road assets. As road service-life typically extends to around twenty-five years (BituChem, n.d.), longer term studies of macrotexture representative of the full lifespan of a pavement are required to understand the full evolution of macrotexture . It would be helpful if these studies could compare and contrast macrotexture evolution for extended stretches of a major arterial highway route so that the influence of traffic, materials, environment and other factors might be studied over a wider geographical area. Furthermore, the granularity of macrotexture data means that there is really a requirement to visualise macrotexture evolution spatially through time at discrete locations along the section of a road.

2.6 Correlating skid resistance and road texture

Skid resistance, or the friction available at tyre/road interface can be influenced by many factors as illustrated in Figure 2.19a. The critical factors include temperature, presence of contaminants, speed, tyre tread thickness, pavement macrotexture and microtexture (Kane and Edmondson, 2018). The principal components of pavement friction are hysteresis and

Pavement Surface Characteristics	Vehicle Operating Parameters	Tire Properties	Environment
• **Micro-texture** • **Macro-texture** • Mega-texture/ unevenness • **Material properties** • Temperature	• **Slip speed** ➢ Vehicle speed ➢ Braking action • Driving maneuver ➢ Turning ➢ Overtaking	• Foot Print • **Tread design and condition** • Rubber composition and hardness • **Inflation pressure** • Load • Temperature	• Climate ➢ Wind ➢ **Temperature** ➢ **Water (rainfall, condensation)** ➢ **Snow and Ice** • **Contaminants** ➢ Anti-skid material (salt, sand) ➢ Dirt, mud, debris

Note: Critical factors are shown in bold.

Figure 2.19a. Factors affecting available pavement (Source: Hall et al., 2009).

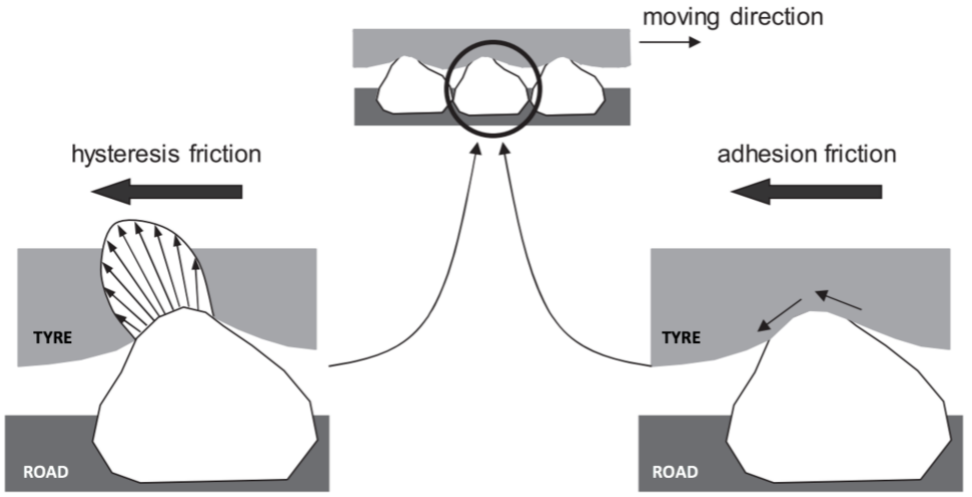

Figure 2.19b. Hysteresis and adhesion components of tyre/road friction (Source: Do and Cerezo, 2015).

adhesion. Adhesion friction arises through the small-scale bonding or interlocking of vehicle tyre rubber with microtexture (refer to Figure 2.19b). Adhesion (F_A) can be considered as the sum of forces between individual points of contact so that:

$$F_A = \sum_i n_i j_i \qquad \text{Equation 2.9}$$

where n_i is the number of molecular contacts between the pavement surface at location i and j_i is the bond strength, so the more points of contact the greater adhesion. Adhesion is therefore a function of the tyre interface shear strength and contact area (Hall et al., 2009). Adhesion works in dry conditions in a complex combination with hysteresis friction. Hysteresis arises as a consequence of the viscoelasticity of a tyre, which means that when a tyre compresses on a road surface the energy to deform the tyre is greater than the energy to reform (Do and Cerezo, 2015). The difference in energy is dissipated as heat, and the loss generates a net frictional force resisting forward movement (refer to Figure 2.19b). In summary, hysteresis considers processes happening with the rubber material of the tyre and adhesion processes at the tyre contact patch. In this way both are considering energy dissipation but at different scales; this was recognised by Kummer, (1966) who proved that hysteresis and adhesion are actually the same phenomenon.

In wet conditions, adhesion is reduced, by the phenomenon of viscoplaning (Do and Cerezo, 2015), where a degree of tyre contact is lost with the pavement due to the presence of a thin water film (in the order of a tenth of a millimetre or less) immediately in front of the tyre. Previous tests have shown that as little as a 0.05 mm film of water on a pavement can reduce friction by 20 to 30 percent (Harwood et al., 1987). Under wet conditions macrotexture predominantly governs skid resistance above 90 km/hr (Kogbara et al., 2016). Macrotexture, is understood to act to disperse water, through the gaps in between the road aggregates (Leach, 2013), and thus influences the depth of water film in front of the tyre contact area (Dunford, 2013). Macrotexture, has been shown to influence the way skid resistance reduces with increasing speed in wet conditions (Flintsch et al., 2013), impacting on the gradient of friction-speed plots for pavement surfaces (Smith et al., 2009). Generally, pavement surfaces with higher macrotexture offer more friction resistance as speed increases than pavements with lower macrotexture under the same conditions, refer to Figure 2.20 (Flintsch et al., 2013). Moreover, as illustrated by Figure 2.20 microtexture tends to govern the peak value of friction coefficient, and macrotexture the rate of decrease with increasing speed. The lower the macrotexture the steeper the decrease in friction, and generally a higher macrotexture can improve skid resistance over a range of speeds (Ueckermann et al., 2015). Work has been completed by Rado and Kane (2014) considering

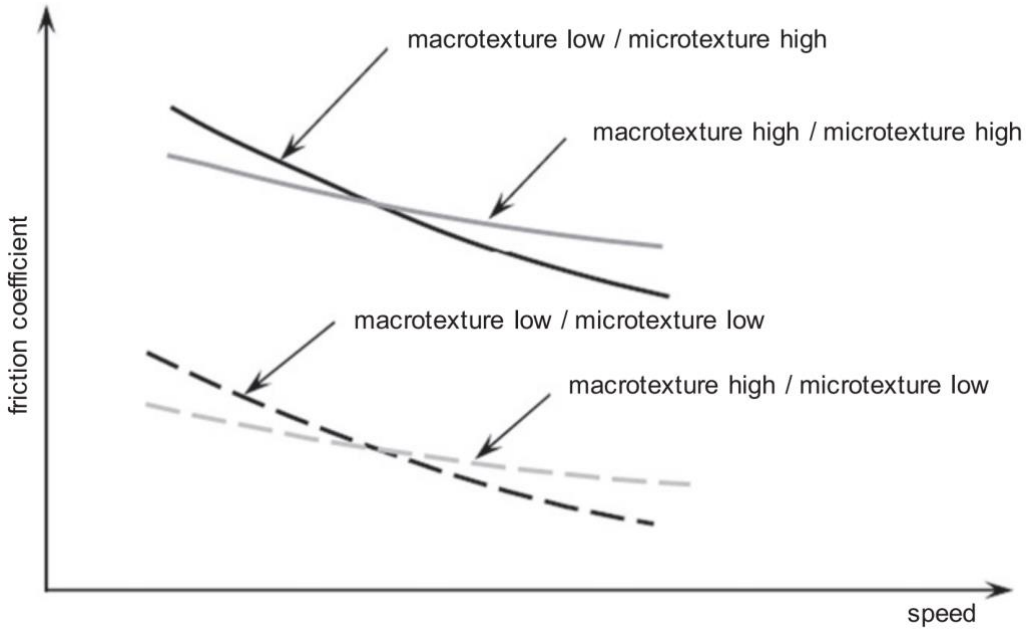

Figure 2.20. Variation of friction coefficient with speed for various macrotexture and microtexture types (Source: Do and Cerezo, 2015).

the contribution of wavenumber and amplitude to frictional skid resistance. Rado and Kane (2014), used the Huang-Hilbert Transformation (Huang and Pan, 2006) to decompose texture measurements obtained from a Circular Texture Meter into a set of ten basic profiles termed 'Intrinsic Mode Functions' (IMFs). The combination of these IMFs into 'Basic Intrinsic Mode Functions' (BIMF) were then explored, with the aim of determining the best wavenumber and amplitude model to characterise friction. Four new functions or BIMFs were characterised, which when tested with frictional results obtained from a Dynamic Friction Tester displayed a statistically linear relationship. The work of Rado and Kane (2014) presents a method to consider the respective contribution of microtexture and macrotexture wavelengths and amplitudes on frictional skid resistance.

Many models consider the relationship between frictional skid resistance measurements and speed. Vaiana et al. (2012), provide a useful review of frictional models. Less common are models predicting friction directly from microtexture or macrotexture. Approaches largely involve determining empirical statistical relationships between texture and friction measurements obtained using contact devices (Deng et al., 2021; Du et al., 2021; Hu et al., 2016; Kogbara et al., 2018). Ergun et al. (2005) completed work examining texture using image analysis techniques and proposed as an empirical model:

$$F(S) = (0.37 + 0.11/MPD_{mac} + 0.15/La_{mic}) \; x \; exp - \left(\frac{S}{149+81\,Log\,(MPD_{mac}) + 80\,Log\,(Rq_{\,mic})} \right) \quad \text{Equation 2.10}$$

where $F(S)$ is the friction coefficient at slip speed, MPD_{mac} is the mean profile depth of the macrotexture, La_{mic} is the average wavelength of the microtexture and Rq_{mic} is the root mean square deviation of microtexture. Ergun et al. (2005) tested the sensitivity of the different parameters of the model and found that as Rq_{mic} increased the friction coefficient increases, confirming the importance of the harshness of macrotexture. As La_{mic} increased the friction coefficient was observed to decrease, demonstrating that fewer asperities or points of contact on course road aggregates per unit length leads to a reduction in friction. Finally, it was determined that with an increase in macrotexture, the friction coefficient decreased at low speed and increased at high speed. The work of Eugun et al. (2005) shows that microtexture and macrotexture can describe the friction coefficient of a road surface and further work to consider the respective microtexture and macrotexture wavelengths and amplitudes would be useful.

2.7 The contribution of road surface processes to the phenomenon of seasonal variation in skid resistance.

The phenomenon of seasonal variation refers to a pattern observed in frictional measurements of skid resistance. Readings have been found to vary throughout the year, with values being lowest in the summer months and highest in winter (Guo et al., 2021). The pattern, which was first noticed in 1936 (Bird and Scott, 1936), is classically illustrated by Hosking and Woodford (1976) as a sinusoidal wave in results from an eleven year study undertaken from 1958 to 1968 in the UK (refer to Figure 2.21a). It was discovered that the lowest values of skid resistance were obtained in hot fine years such as 1959 ('Year 2' with reference to Figure 2.20). Similarly, if an autumn was warm and dry the value of skid resistance would not rise as quickly as in cooler wetter conditions (Hosking and Woodford, 1976).

The sinusoidal seasonal variation pattern observed by Hosking and Woodford (1976) is generally consistent with comparable studies completed in other parts of the world (Ahammed and Tighe, 2009a; Ahammed and Tighe, 2010; Bijsterveld and Val, 2016a; Oliver et al., 1988; Runkle and Mahone, 1980), although specific months vary according to the influence of a study's specific location in the northern and southern hemispheres. For instance, Oliver et al. (1988) undertaking a study in Victoria, Australia, established skid resistance is lower in the months December to February representing the Australian summer. Moreover, some researchers have observed comparable trends between seasonal variation of skid resistance and meteorological conditions. Dunford (2013), demonstrated comparable trends between monthly average rainfall (refer to Figure 2.21b), and average skid resistance measurements taken in the North East of England using SCRIM (British Standard Institute, 2006) over a period of ten years between 2000 and 2009 (refer to Figure 2.21c). Bijsterveld and Val (2016) detected that accumulative rainfall in the week prior to a frictional measurement seemed to have some influence on SCRIM measurements. The accumulative rainfall was calculated as the precipitation falling up to the day before the SCRIM measurement. Bijsterveld and Val (2016) demonstrated a weak linear trend ($R^2 = 0.2469$) of increasing accumulative rainfall with increasing frictional values. Jayawickrama and Thomas, (1998) also detected strong indication that frictional measurements obtained from a locked wheel trailer device, varied in response to temperature and precipitation. Sabey (in unpublished research reported by Hosking and Woodford, (1976)) conducted tests at midday and at night on seven types of surface (concrete and bituminous) using a portable skid tester to investigate the influence of air temperature on skid resistance. Sabey calculated that skid resistance varies by 0.26 units per degree Celsius , over a range of 7 °C and 35 °C. Sabey concluded that air temperature appeared to account for just one quarter of the overall change in skid resistance arising from seasonal variation, occurring midsummer to midwinter. Flintsch et al. (2008) investigated

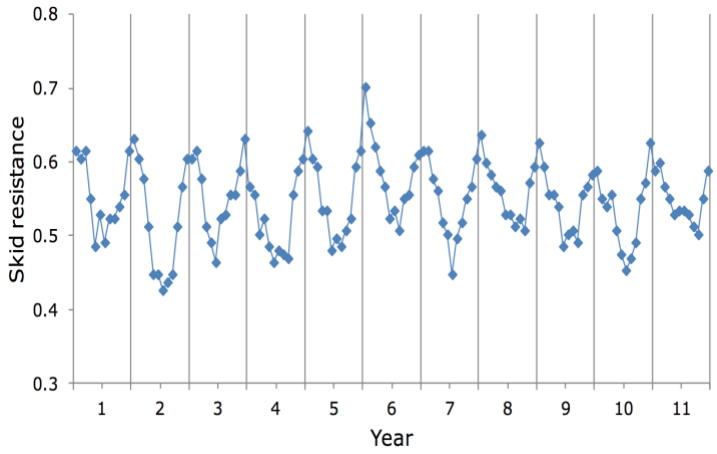

Figure 2.21a. Seasonal variation in skid resistance. Results are obtained at two-weekly intervals using the pendulum skid resistance test. (Source: Hosking and Woodford, 1976)

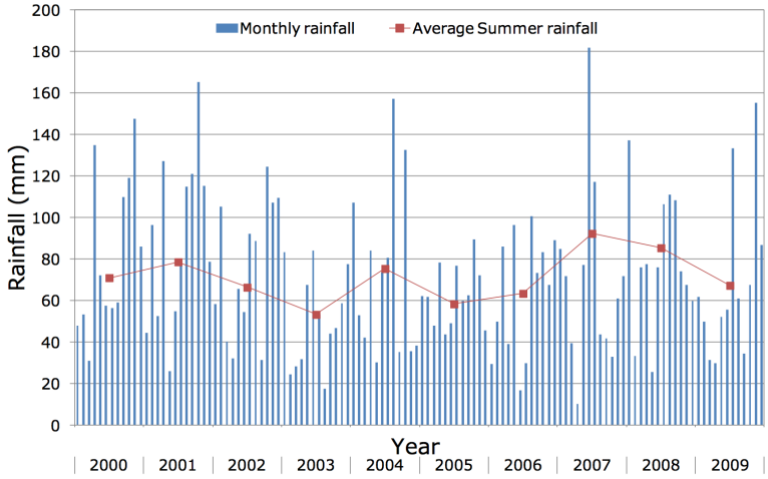

Figure 2.21b. Average rainfall for East and North East England. (Source: Dunford 2013)

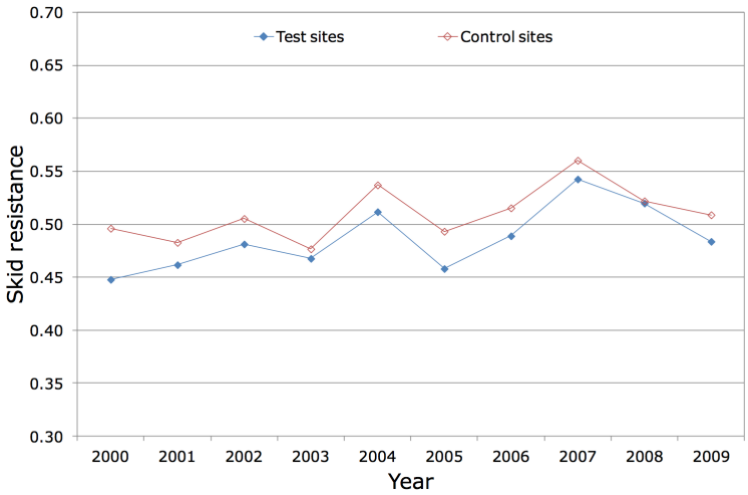

Figure 2.21c. Average summer skid resistance on roads in East and North East England. (Source: Dunford 2013)

seven fine wearing surfaces using a skid trailer and thermocouples embedded in the surface course of live roads. They concluded that pavement temperature has a significant effect on pavement frictional measurements and the sensitivity of frictional measurements to test speed. At low-speed pavement friction tends to decrease with increasing pavement temperature and the reverse was found to be true at high temperature. Bazlamit and Reza, (2005) completed laboratory tests on briquettes made from newly laid roads determined that the hysteresis component of friction decreases with temperature and that adhesion is more sensitive to road surface temperature effects. Hysteresis was found to account for the larger part of the total friction force.

Seasonal variation means that frictional measurements are usually taken in the summer, which in the UK for example is the start of May through to the end of October (Design Manual for Roads and Bridges, 2021). In the UK, during these months tyre temperature is not often outside the range of 20 °C and 57 °C (corresponding to a range of 8 °C to 45 °C for air/road temperature) and friction measurements obtained from SCRIM have been determined to vary by around 7.5 % (Hosking and Woodford, 1976). Frictional results are often statistically interpreted between years (Plati et al., 2014), and individual friction devices usually require harmonisation once a year at the start of the measuring season with the rest of a country's fleet (Sanders et al., 2016). It is worth noting, although beyond the detailed review of this thesis, that direct comparison between different frictional devices adopted in particular countries is also difficult, as measurements are influenced by machine operating conditions such as the load, speed, slip ratio and the composition of the rubber (Dunford, 2013).

In addition, to the trends observed with meteorological conditions (typically air/road temperature and precipitation) discussed above, the phenomenon of seasonal variation of skid resistance has been attributed to a number of other factors: the sensitivity of rubber resilience to temperature change (Hosking and Woodford, 1976); changes induced by temperature in the viscosity of the test water of a device (Khasawneh and Laing, 2012); differential polishing of road aggregate throughout the year (Smith, 2008); and presences of contaminants on the road surface (Green, 1973). The latter two points will be reviewed here, as the focus of this thesis is non-contact measurement techniques for characterisation macrotexture in the field. There has been for some time a hypothesis that processes occurring on the road surface influence seasonal variation in skid resistance. Green (1973) observed regular 'black deposits' or contaminates appearing on motorway surfaces during long dry periods. These deposits where established to consist of oil, rubber and mineral matter and dispersed with heavy rain. The presence of black deposits was found to cause a reduction in SCRIM measurements in the order of 0.1 units. Differential polishing of pavement surfaces as a consequence of the

presence of such deposits is one theory presented as contributing to seasonal variation in skid resistance (Ahammed and Tighe, 2009b; Bijsterveld and Val, 2016b; Jayawickrama and Thomas, 1998; Oh et al., 2010; Pomoni et al., 2020; Wang et al., 2018). In dry weather during the summer months, fine dust and debris builds up on the roads, which is continually ground up under the action of tyres and polishes the surface. This polishing effect combined with the accumulation of contaminants such as oils and rubber particles, is believed to lead to loss of microtexture and macrotexture, smoothing road surfaces and reducing skid resistance values. Conversely, in the winter fine dust is more easily expurgated from the pavement texture with rainfall events, resulting in coarse debris dominating the surfaces (Wilson, 2013). The presence of primarily coarse debris leads to pavement surfaces becoming rougher, resulting in higher skid resistance readings. The work of West and Ross (1962) showed that the size of grit effects the polishing rate of road aggregates. Reflecting on all the work undertaken to understand the phenomenon of seasonal variation, most researchers have focused upon the influence on frictional measurement of skid resistance. It would be useful to characterise if a seasonal signal is evident in non-contact road texture measurements. The observation of 'seasonal conditioning' in texture measurement will address the hypothesis that processes occurring on the surface of pavement are contributing to seasonal variation.

2.8 Summary

This literature review has highlighted that limited research has been undertaken to characterise road macrotexture using terrestrial laser scanning instruments adopting phased-based or time-of-flight technology. Previous work has largely focused on spot tests to characterise macrotexture representing the size of the volumetric sand patch test, and with few full lane width studies undertaken. The optimisation of scanning approaches for different types of pavement surface, selecting for example appropriate angular and range resolution, has also not been rigorously investigated by others. This thesis will consider in *Chapter 4* the application of non-contact techniques such as terrestrial laser scanning and close-range photogrammetry to 'areas-of-interest' bigger than the size of a conventional sand patch test. Work will explore the sensitivity of areal parameters (spatial methods to characterise pavement texture) which are relatively novel to highway field applications, to resolution, sample size and filtering.

The literature has identified that long term studies of macrotexture representative of the service lifespan of a pavement are rare, and particularly, further work would be helpful to understand the evolution of macrotexture beyond the early and mid-service life of a pavement. In *Chapter 5* techniques to determine long term rates of change in road macrotexture and to visualise macrotexture evolution spatially through time at discrete locations along a road

section will be investigated. Moreover, previous work undertaken to understand the phenomenon of seasonal variation, has tended to focus predominately upon the influence on frictional measurement of skid resistance. It is important to further knowledge of the phenomenon, by characterising if a seasonal signal is evident in non-contact macrotexture measurements. The observation of 'seasonal conditioning' in macrotexture measurements will address a long-established hypothesis that processes occurring on the surface of pavement are contributing to seasonal variation. This thesis will in *Chapter 6* compare and contrast macrotexture evolution for extended stretches of a major arterial highway route so that the influence of traffic, materials, environment and other factors might be studied over a wide geographical area.

Finally, initial work has been undertaken by Rado and Kane (2014) into decomposed pavement texture into different profiles of wavelengths and amplitude, or 'bands'. In *Chapter 7*, an investigation advances this work considers the contribution of 'small-scale' and 'large-scale' wavelengths and amplitudes, decomposed from microtexture and macrotexture on frictional skid resistance.

Chapter 3.0: Published Paper 1 - Improved non-contact 3D field processing techniques to achieve macrotexture characterisation of pavements.

3.1. Abstract

Macrotexture is required on pavements to provide skid resistance for vehicle safety in wet conditions. Increasingly, correlations between macrotexture measurements captured using non-contact techniques and tyre-pavement contact friction are being investigated in order to enable more robust and widescale measurement and monitoring of skid resistance. There is a notable scarcity of research into the respective accuracy of the non-contact measurement techniques at these scales. This paper compares three techniques: a laser profile scanner, Structure from Motion photogrammetry and Terrestrial Laser Scanning (TLS). We use spectral analysis, areal surface texture parameters and 2D cross-correlation analysis to evaluate the suitability of each approach for characterising and monitoring pavement macrotexture. The results show that SfM can produce successful measures of the areal root mean square height (S_q), which represents pavement texture depth and is positively correlated with skid resistance. Significant noise in the TLS data prevented agreement with the laser profiler but we show that new filtering procedures result in significantly improved values for the peak density (S_{pd}) and the arithmetic peak mean curvature (S_{pc}), which together define the shape and distribution of pavement aggregates forming macrotexture. However, filtering the TLS data results in a trade-off with vertical accuracy, thus altering the reliability of S_q. Finally, we show the functional areal parameters S_{pd} and S_{pc} are sensitive to sample size. This means that pavement specimen size of 150 mm x 150 mm or smaller, when used in laboratory or field observations, are inadequate to capture the true value of areal surface texture parameters. The deployment of wider scale approaches such as SfM and spectrally filtered TLS are required in order to successfully capture the functional areal parameters (S_{pc} and S_{pd}) for road surfaces.

3.2 Introduction

Adequate texture on the surface of a pavement is required to provide skid resistance or friction at the tyre/road interface for vehicle safety in wet conditions (Design Manual for Roads and Bridges, 2015; Klüppel and Heinrich, 2001; Moore, 1975; Persson, 2001). Skid resistance is also influenced by temperature, presence of contaminants, speed and tyre tread thickness (Kane and Edmondson, 2018). Friction forces generated from the contact of the tyre with texture are a consequence of the viscoelastic deformation of the tyre, and increase in dry conditions with adhesion (Do and Cerezo, 2015). Pavement texture is defined as the deviation

of the pavement surface from a true planar surface (Smith et al., 2009) and has been characterised at different scales according to the wavelengths of the deviations (PIARC, 1987). Microtexture suspected to induce adhesion, represents the texture components with wavelengths from less than 0.5mm and peak amplitude from 0.001 to 0.5mm. Microtexture correlates to the asperities upon the surface of coarse road aggregates (Dunford, 2013), and also to the fine particles present in the mixture constituting the wearing course of the pavement. In wet conditions, adhesion is reduced by the phenomenon of viscoplaning (Do and Cerezo, 2015), where a degree of tyre contact is lost with the pavement due to the presence of a thin water film (in the order of a tenth of a millimetre or less). Macrotexture, suspected to induce hysteresis response in the viscoelastic tyre, represents the texture components with wavelengths from 0.5 mm to 50 mm and amplitude of 0.1 mm to 20mm (formed by the shape, size and gradation of road aggregates on a pavement surface). Macrotexture acts also to disperse water, under wet conditions, through the gaps in between the road aggregates (Dunford and Leach, 2013). Thus, macrotexture, has been shown to influence the way skid resistance reduces with increasing speed in wet conditions (Flintsch et al., 2013). Generally, with equal microtexture, pavement surfaces with higher macrotexture offer more friction resistance as speed increases than pavements with lower macrotexture under the same contact conditions (Rado and Kane, 2014; Roe and Hartshorne, 1998).

Thus, the preservation of adequate skid resistance requires the monitoring of macrotexture (Design Manual for Roads and Bridges, 2015) to ensure sufficient texture remains on the pavement to prevent skidding. Standard monitoring techniques involve either a sand patch test (British Standard Institute, 2010) or a direct measurement of the frictional resistance through a rubber pad (British Standard Institute, 2011) or test wheel making contact with a wetted pavement (British Standard Institute, 2006, 2000). Kogbara et al. (2016) provide a full summary of devices and their operating principles. These contact devices are known to be susceptible to seasonal variation (Bijsterveld and Val, 2016). This phenomenon has been attributed to a number of factors: the sensitivity of rubber resilience to temperature change (Hosking and Woodford, 1976); changes induced by temperature in the viscosity of the test water of a device (Khasawneh and Laing, 2012); and differential polishing of the aggregate microtexture throughout the year (Smith, 2008). Survey results obtained from these devices require statistical interpretation (Design Manual for Roads and Bridges, 2015; Plati et al., 2014) with individual devices requiring harmonisation with the rest of a fleet (Sanders et al., 2015). Friction measurements from rubber contact base devices are also known to be susceptible to changes in travel speed (Dunford, 2008). Direct comparison between different devices adopted in particular countries is also difficult, as measurements are influenced by machine operating conditions such as the load, speed, slip ratio and the composition of the

rubber.

The problems associated with contact measurement techniques, make a reliable non-contact technique desirable. Accurate non-contact macrotexture measurement is one step towards the estimation of pavement friction values via analytical modelling (Kane et al., 2019; Kane and Cerezo, 2015; Kane and Edmondson, 2018; Ueckermann et al., 2015). Researchers have successfully deployed contactless techniques under laboratory conditions to measure texture; typically to a size of 100 x 100 mm (Araujo et al., 2015; Zhang et al., 2014). At present, there are also a number of in-situ proprietary spot contactless techniques available for use in the field, including the Circular Texture Meter (Prowell and Hanson, 2005), the Model 9300 laser texture scanner (Li et al., 2012) and close-range stereo photogrammetry (Alamdarlo and Hesami, 2018; Kogbara et al., 2016; Shalaby and El Gendy, 2010), which requires a minimum of three images taken from different perspectives to reconstruct a 3D pavement surface. These techniques offer an alternative to the simple sand patch test (British Standard Institute, 2010; Gao et al., 2019; Praticò and Astolfi, 2017), where a measured volume of fine material is spread in a circular motion into a road's surface depressions to find the mean texture depth, for in-situ localised pavement texture assessment. Recent research, focused on the development of a prototype test rig (Wang et al., 2011) adopting a laser range finder, that uses triangulation, to measure texture in the field or to detect defect on pavements (Zhang et al., 2018), but is still restricted to a localised area comparable to that of a sand patch test. The minimum texture profile height measured by the rig was limited to 0.032 mm, with a spatial sampling frequency of about 4 mm^{-1}, thus meeting only part of the range needed for macrotexture. 3D handheld scanners (Creaform, n.d.; Z Corporation, 2007), using triangulation principles, have also been deployed to capture macrotexture in-situ (Hu et al., 2016). These scanners are designed for metrology applications, and having a limited field of view, lack scalability. Advances in 'off-the-shelf' laser and photogrammetry technology and point cloud post-processing applications means there is now the potential to capture macrotexture over larger areas, potentially more representative areas using contactless techniques. Terrestrial Laser Scanning (TLS) offers rapid, full 3D high resolution reconstruction of a highway surface as a point cloud (Abellán et al., 2009) and Structure from Motion (SfM) photogrammetry (James and Robson, 2012; Micheletti et al., 2015) offers a low-cost method utilising digital images to generate a 3D dense point cloud data of surfaces.

This paper introduces a method to characterise macrotexture using TLS and SfM over a typical full lane width. Recent research (Kogbara et al., 2018) suggests that frictional resistance is sensitive to certain areal parameters (Boscaino and Praticò, 2001; Leach, 2013) (Table 3.1). Particularly, to the density of peaks within the macrotexture of a highway surface, S_{pd}, and to

the pointiness or arithmetic mean of the principal curvature of the same peaks S_{pc}; which together characterise the shape and size of the road aggregates. Furthermore, the areal parameters root mean square of surface departures, S_q, as the standard deviation of peak height from an average plane, is spatially equivalent to mean profile depth (International Organisation for Standardisation, 2019). Mean profile depth represents the averaged values over an overall 2D profile length, of the difference within a lateral distance (typically in the order of a tyre/pavement contact) between the profile and a horizontal line through the top of the highest peak. This paper explores the accuracy of the scalable TLS and SFM approaches to determining these measurements in comparison to measurements achieved using a 3D Smart Laser Profile Sensor (LMI Technologies, n.d.). The 3D Smart Laser Profile Sensor was selected as an accurate well-constrained controlled dataset of 2D profile macrotexture measurements from which to formulate a 3D surface, as such laser profile sensors are well-understood have been deployed widely previously to capture 2D profile measurements of macrotexture (International Organisation for Standardisation, 1996; International Organisation of Standardisation, 2012; Yaacob et al., 2014). This paper will first introduce the methods applied to capture point cloud data in the field using the three techniques, before rigorously considering the accuracy of results obtained through the application of spectral analysis, areal parameters and 2D cross-correlation.

3.3 Methods

3.3.1 Remote sensing technology

3.3.1.1 Terrestrial Laser Scanning

The TLS data were collected using the Faro Focus 3D X Series phase-based laser scanner on a tripod mounted inverted as shown in Figure 3.1.a. The static scanner was set-up at a height of 1 m above the pavement surface on a levelled tripod, and the desired scanning parameters were entered on the instrument's home screen. Figure 3.2 details the workflow for programming the scanner's settings prior to completing a scan. To retain a practical completion time for the survey, a resolution of 1/5 and quality of 6x was adopted, providing a scan time of 22.38 minutes. The scanner stores data on a SD memory card, and this was post processed using Faro Scene 7.1 software to extract, register and align the point cloud.

3.3.1.2 Structure from Motion photogrammetry

Static digital images (5472 x 3648 pixels) were captured at the test location using a digital single-lens reflex camera with 50 mm fixed focal length, mounted on a camera tripod and dolly (refer to Figure 3.1b). Following the method of (Kogbara et al., 2018) a minimum of

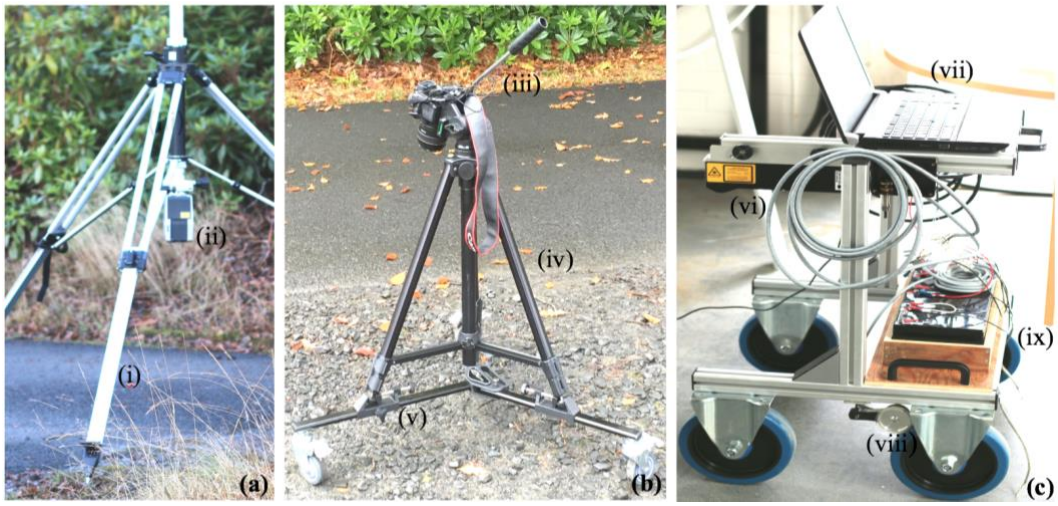

Figure 3.1. Equipment set-up for: (a) Terrestrial Laser Scanner. The Faro Focus 3D X Series scanner is fitted onto a tripod stand (i) using an invert head fitting (ii). (b) Structure from Motion. A digital single-lens reflex camera with 50mm fixed focal lens (iii), is mounted on a standard Leica camera tripod (iv) and dolly (v). (c) 3D Smart Laser Profile Sensor. LMI Technologies Gocator 2350 laser profile sensor (vi) is fixed at a height of 500mm to the trolley frame and operated using Gocator Emulator version 4.6.7.17 software installed on a standard laptop (vii). A quadrature digital encoder fitted to a 200mm measuring wheel (viii) enables images to be captured at variable speed up to a maximum of 10km/h. The system is powered by a 60-volt battery (ix).

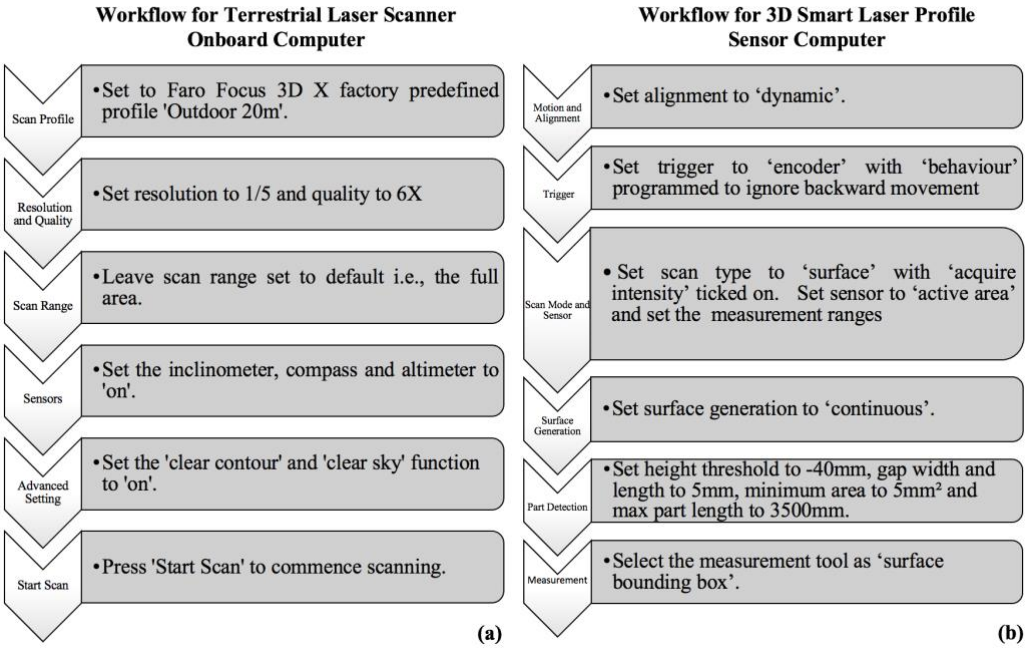

Figure 3.2. Workflow for programming both the Faro Focus 3D X Series Terrestrial Laser Scanner's onboard computer and the LMI Technologies Gocator 2350 3D Smart Laser Profile Sensor prior to completing a scan. The Faro Focus 3D X Series Terrestrial Laser Scanner's onboard computer is accessed via the scanner's main touch screen display, housed within the head of the instrument. Key settings are accessed by selecting the 'Parameters' button on the 'Home' screen. Key setting requirements illustrated by the vertical arrows (left of figure) were adjusted in accordance with the instruction presented in the grey box (right of figure). The LMI Technologies Gocator 2350 3D Smart Laser Profile sensor computer is programmed using Gocator Emulator version 4.6.7.17 software, installed on a conventional laptop. Key settings are accessed by selecting the 'Manage' or 'Scan' buttons from the software's top toolbar. Key setting requirements illustrated by the vertical arrows (left of figure) were adjusted in accordance with the instruction presented in the grey box (right of figure).

60% forward overlap and 30% sideways overlap between photographs was maintained. Previous research (James and Robson, 2012) has demonstrated that capturing flat surfaces using SfM with predominantly parallel images and adopting self-calibration of camera locations can cause deformation of the point cloud typified by 'doming' effects. To prevent these affects, over lapping photographs, were captured at three heights (500 mm, 600 mm and 750 mm) above the pavement surface, across the width of the highway (Figure 3.1a).

Agisoft Photoscan version 1.3.4.5067 software 6 was used to post process the images enabling reconstruction of the overlapping photographs into a 3D point cloud. The software determines the position and orientation of cameras automatically using a scale invariant feature transform (SIFT) (Micheletti et al., 2015). The SIFT matches up identified features across the image set, to establish their 3D co-ordinates and generate a sparse cloud. The sparse cloud is then densified into a dense point cloud by the software using Multi View Stereo techniques (Furukawa and Ponce, 2010). Figure 3.3 illustrates the key stages of the construction of a point cloud from the camera images. Using this approach, an area equivalent to the width of a standard road lane (3.65 m) was successfully reconstructed without deformation.

3.3.1.3 Smart Laser Profiling

The 3D Smart Laser Profile Sensor, an LMI Technologies Gocator 2350, was mounted upon a trolley at a height of 500 mm (Figure 3.1c) and powered by a 60-volt battery. One trolley wheel made contact with a digital quadrature encoder fitted to a 200 mm circumference measuring wheel. The digital encoder was wired to provide a pulse signal to the 3D Smart Sensor, being programmed to produce 40,000 pulses per rotation of the measuring wheel. Each pulse equates to a travel distance of 0.005 mm and this information is used to enable 3D surface profiles to be captured at variable speed. The 3D Smart Laser Profile Sensor's settings where programme using Gocator Emulator version 4.6.7.17 software, installed on a conventional laptop. Figure 3.1b details the workflow for programming the 3D Smart Laser Profile Sensor's settings prior to completing a scan. The data were collected at walking speed every 201 pulses or 1.005 mm over a 3 m section, with the 3D Smart Laser Profile Sensor operating at a typical field of view width of 300 mm. The 3D Smart Laser Profile Sensor, is equipped with the capacity to view the laser points forming the profile line on the highway surface in 'real-time'. This facilitates adjustment of the laser exposure level and active measurement area to accommodate ambient light levels, stray light and variability of highway surface reflectivity. The surface profiles extracted from the 3D Smart Laser Profile Sensor were post processed using Gocator_Emulator version 4.6.7.17 and kCSvConveter software to an ASCII xyz file format suitable for point cloud post processing (LMI Technologies, 2021).

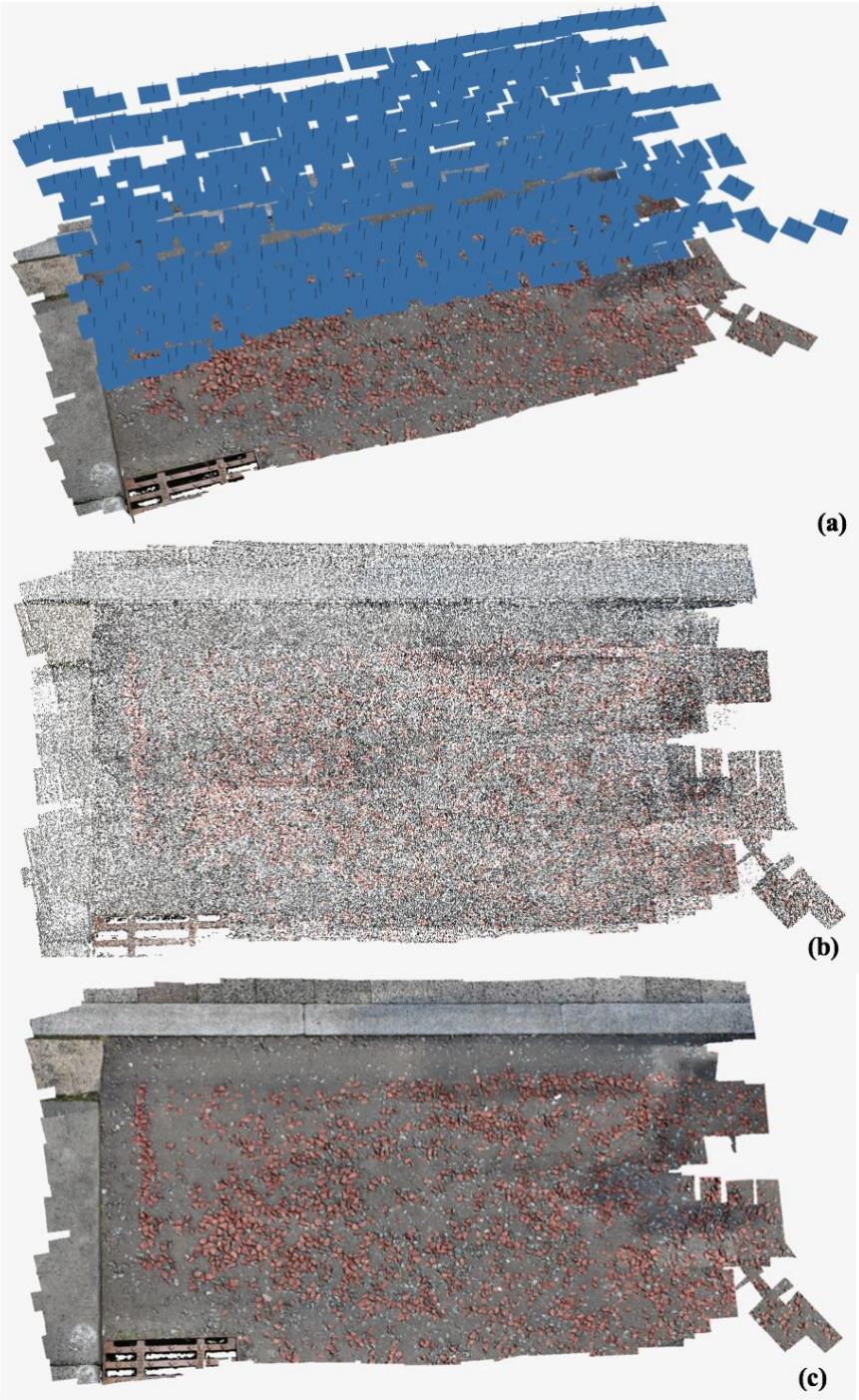

Figure 3.3. Key Stages of construction of a scaled point cloud reconstruction from digital images. The surface modelled is a Hot Rolled Asphalt with 20mm red chipping. (a) The camera position for each photograph image, (indicatively represented in the figure by the blue rectangles (i.e., not to scale)) are calculated in Agisoft Photoshop. The camera images are captured in the field at three independent heights, typically 500mm, 600mm and 750mm, with a minimum of 60 percent forward overlap and 30 percent sideways overlap between images. (b) 3D co-ordinates for key features across the aligned photograph image set are determined and used to construct points in a sparse point cloud. (c) The sparse point cloud is used to generate a dense point cloud in Agisoft Photoshop. The final dense cloud is scaled using known ground control points measurements established in the field.

3.3.2 Test location

To test the three techniques a field site was selected that contained three standard types of pavement surface within close proximity (Figure 3.4), allowing for the same ambient conditions to be assumed over the surfaces. The site included a close graded dense bitumen macadam (DBM), and a gap graded hot rolled asphalt (HRA), as well as surface dressing (SD). Test were undertaken on the dry pavement surfaces with permanent ground control points being installed to demarcate each surface using 16 mm survey nails.

3.3.3 Deriving macrotexture parameters from non-contact survey techniques

The 3D point cloud data for the DBM, HRA and SD surfaces were captured consecutively on the same day using the three different techniques. The point clouds obtained from each technique were then aligned utilising the installed reference ground control points in Cloud Compare v 2.10 software (Girardeau-Montaut, n.d.), to facilitate direct comparison between the surfaces. Subsequently, 150 mm x 150 mm sample areas (representing a typical laboratory specimen size) were clipped for each surface from the aligned point clouds for analysis. These clipped point clouds were then loaded into MountainsMap Premium version 7.4 (Digital Surf, n.d.) and the software used to remove any transverse or longitudinal slope by method of least squares, and to calculate the standard areal parameters as listed in Table 3.1, to characterise the macrotexture. Areal parameters were adopted, in contrast to 2D profile parameters (Gubbins, 2004), as these are recognised as providing a more complete description of a surface (Leach, 2013), capturing height with respect to both the 'x' and 'y' direction to characterise functional aspects such as texture, shape and direction. In sampling the point cloud data to make successful areal measurements it is important that Nyquist values be smaller than the smallest desired surface macrotexture requiring characterisation. Nyquist sampling theorem states that the shortest wavelength that can be defined from a digital dataset is two digital sample intervals long. Therefore, the wavelength or sample length available to characterise pavement texture areal parameters, is defined by the relationship between point cloud density and sample size.

3.3.4 Deriving 2D wavenumber amplitude spectra from non-contact techniques and filtering

Image datasets can be analysed by MATLAB software to transform them to the wavenumber domain, allowing images to be characterised by spatial frequency. Accordingly, 2D Kx-Ky wavenumber spectral analyses of the samples (Gubbins, 2004) were calculated in MATLAB to determine the areal wavenumber characteristics of the surfaces captured using the different techniques. To prevent spectral leakage caused by discontinuities at the edges of each measured sample area, the amplitude of the signal at the outer edges was attenuated using a

Figure 3.4. Field site: The field site was located adjacent to St James Church on Northumberland Road, Newcastle Upon Tyne, UK Grid Reference NZ 25112 64814. (a) Conventional photograph of the field site. (b) Point cloud panorama of the site captured using the Faro Focus 3D X Series phased-based laser scanner. The three surfacing materials studied are (i) surface dressing, (ii) dense bitumen macadam, and (iii) hot rolled asphalt.

Parameter Symbol	Parameter Name	Description	Calculation Equation
Sq	Root mean square height	Root mean square value of the surface departures within the sampling area.	$S_q = \sqrt{\frac{1}{A}\iint_A z^2(x,y)\,dx\,dy}$
Ssk	Skewness	Defines the shape of topography height distribution as a measure of symmetry about the mean line.	$S_{sk} = \frac{1}{S_q^3}\left[\frac{1}{A}\iint_A z^3(x,y)\,dx\,dy\right]$
Sp	Maximum peak height	Largest peak height within a definition area A.	S_p
Sv	Maximum pit height	Smallest pit height value within a definition area.	S_v
Spd	Peak density	The number of peaks per unit area.	$S_{pd} = \frac{N}{A}$
Spc	Arithmetic mean peak curvature	Measure of the principal curvature of the peaks.	$S_{pc} = -\frac{1}{2}\frac{1}{n}\sum_{k=1}^{n}\left(\frac{\partial^2 z(x,y)}{\partial x^2} + \frac{\partial^2 z(x,y)}{\partial y^2}\right)$

Table 3.1. Areal surface texture parameters used to characterise macrotexture. Parameters are defined by ISO 25178 (International Organisation of Standardisation, 2012). S_q the root mean square of surface departures, and the linked parameters S_p and S_v (maximum peak and pit height) are equivalent to mean texture depth used at present to evaluate macrotexture, principally by means of the volumetric patch techniques. S_{pd} represents the density of the peaks of the road aggregate on the pavement surface and S_{pc} is a measure of the principal curvature of the peaks, characterising the shape and size of the road aggregates.

cosine taper Tukey window that extended for 10% from the extreme edges of the sample line (International Organisation of Standardisation, 1997). The resulting 2D wavenumber spectra enabled the wavenumber content of the data to be determined, which facilitated the selection of an appropriate 2D wavenumber filter to attenuate high wavenumber noise from the macrotexture signal.

Examining the spectra for each non-contact technique the 3D Smart Laser Profile Sensor was the lowest resolution technique, containing wavenumbers not greater than 0.1 mm^{-1}. Consequently, to achieve conformity of the wavelengths for areal parameter analysis across techniques a wavenumber filter of 0.1 mm^{-1} was applied to the SfM and TLS data. A low pass zero phase Butterworth wavenumber filter (International Organisation of Standardisation, 1997) was then designed to remove high wavenumber noise components from the data, up to the Nyquist wavenumber (Bloomfield, 2004). The filter was applied in a two-pass process, firstly for every trace in the x-direction and then the y-direction, thus creating a 2D filtered data set. Normalised 2D autocorrelations and cross-correlation plots of the filtered surface data were then prepared as a means of measuring image spatial similarity (as the macro-texture scale pushes the limit of conventional differencing techniques adopted for identifying similarity and change in point cloud analysis (Gubbins, 2004).

3.4. Results and discussion

Nyquist values are given in Table 3.2, the 3D Smart Laser Profile Sensor minimum Nyquist wavelengths mean that the technique is unable to measure a small part of the lower range of macrotexture wavelengths between 0.5 and 1 mm. The SfM and TLS Nyquist wavelengths mean the techniques can measure the full range of macrotexture wavelengths and have the potential to also measure some part of microtexture below 0.5 mm, this capability should be explored as part of a further research study. The Nyquist wavelengths vary between samples, possibly because the techniques are sensitive to pavement surface albedo, environmental conditions, and edge effects. Given technique sensitivity, oversampling to ensure a sufficiently fine Nyquist wavelength is beneficial and, in this regard, adopting a higher resolution technique such as TLS is advantageous. The Nyquist wavelength for a TLS, will increase with distance from the laser source, because of the elongation of the beam, as the angle of incidence with a surface increases. Therefore, the optimal location to acquire TLS data with an ‘off-the-shelf scanner’, is within a narrow cone of incidence directly in line with the laser source, with data captured using an inverted head tripod set-up.

	Parameter		Point Density (mm^{-2})	Nyquist Wavelength (mm)	Sq (mm)	Ssk	Sp (mm)	Sv (mm)	Spd (mm^{-2})	Spc (mm^{-1})
UNFILTERED	Dense Bitumen Macadam	Smart Sensor	0.97	x= 1.02 y= 1.02	**0.951**	-0.321	**2.21**	**3.37**	0.00354	0.1360
		SfM	35.80	x= 0.167 y= 0.167	**0.949**	-0.711	**1.80**	**3.91**	0.01110	0.7720
		TLS	83.59	x= 0.091 y= 0.131	1.090	-0.124	4.99	5.25	0.14100	27.8000
	Hot Rolled Asphalt	Smart Sensor	4.19	x= 0.489 y= 0.489	**1.280**	-1.040	**2.93**	**5.75**	0.00185	0.2020
		SfM	26.47	x= 0.184 y= 0.206	**1.370**	-0.901	**3.13**	**5.76**	0.00273	0.6550
		TLS	163.84	x= 0.073 y= 0.083	1.560	-0.215	6.18	6.37	0.25000	76.8000
	Surface Dressing	Smart Sensor	3.39	x= 0.547 y= 0.539	**0.544**	-0.680	**1.58**	**3.19**	0.01110	0.4000
		SfM	31.19	x= 0.145 y= 0.222	**0.557**	-0.743	**1.76**	**2.80**	0.01140	0.5670
		TLS	63.27	x= 0.142 y= 0.111	0.938	-0.267	3.89	4.49	0.14000	17.9000
FILTERED	Dense Bitumen Macadam	Smart Sensor	0.66	x= 1.23 y= 1.23	3.940	-0.565	9.78	15.30	0.00166	0.3480
		SfM	24.37	x= 0.202 y= 0.204	3.660	-0.947	9.30	16.50	0.00253	0.3610
		TLS	55.67	x= 0.120 y= 0.150	0.738	-0.654	2.24	2.89	0.00225	0.0748
	Hot Rolled Asphalt	Smart Sensor	3.74	x= 0.519 y= 0.515	12.600	-0.972	30.30	56.30	0.00223	2.4100
		SfM	23.95	x= 0.194 y= 0.215	13.300	-0.937	30.10	57.50	0.01640	17.4000
		TLS	148.19	x= 0.078 y= 0.087	3.200	-0.233	7.45	9.38	0.01970	5.0900
	Surface Dressing	Smart Sensor	2.31	x= 0.664 y= 0.652	2.000	-0.801	4.91	12.60	0.00196	0.2070
		SfM	20.61	x= 0.194 y= 0.250	2.390	-0.947	5.98	13.50	0.00240	0.2740
		TLS	42.63	x= 0.165 y= 0.142	0.607	-0.741	1.50	2.75	0.00250	0.7190

Table 3.2. Unfiltered and filtered results - point density, Nyquist length and areal surface texture parameters for the surfaces. The parameters are obtained from the raw point cloud data captured using the Faro Focus 3D X Series Phased-Based Laser Scanner, Structure from Motion and LMI Technologies Gocator 2350 Smart Laser Profile Sensor. Unfiltered results (top of table) demonstrate closer agreement between the Smart Laser Profile Sensor and Structure from Motion for S_q, and the linked parameters S_p and S_v (shown in bold). The spatial areal functions S_{pd} and S_{pc} representing the density and curvature of peak, (shown by previous researchers to have a positive correlation with skid resistance), are dissimilar and being sensitive to resolution, increase in magnitude with point density. The filtered results (bottom of table in grey) demonstrate increased agreement between S_{pd} and S_{pc} for the techniques, but the Smart Laser Profile Sensor and Structure from Motion techniques experience magnification of vertical measurements S_q, S_p and S_v in comparison to the unfiltered data.

Surface height plots for each surface scanning technique are illustrated in Figure 3.5. For the DBM greater similarity is evident between Figure 3.5(a) and Figure 3.5(b) as the 3D Smart Laser Profile Sensor and SfM techniques have similar resolution. The higher resolution of the TLS is evident in the finer granularity of plot Figure 3.5(c). All the techniques are able to capture the voids between aggregates (e.g. i) and aggregate features (e.g. ii) on the DBM surface at the same locations. Equally, for the HRA surface there is greater similarity between Figure 3.5(e) and Figure 3.5(f), the data captured with the 3D Smart Laser Profile Sensor and SfM techniques. The higher resolution of the TLS is evident again in the finer granularity of the edges of the red chipping aggregate (Figure 3.5g). Finally, although the SD aggregate chippings are the smallest for the three surfaces, all the techniques have still collectively identified areas of void between aggregates in blue Figure 3.5(J) to (l)(e.g. vi) and areas of elevated macrotexture in orange located to the right and left edge of each plot. Again, there is greater similarity between Figure 3.5(j) and Figure 3.5(k), the data capture with the 3D Smart Laser Profile Sensor and SfM technique. The higher resolution of the TLS is evident in the finer granularity of plot (l). The degree of similarity between the techniques has been characterised using areal parameters and 2D correlation analysis discussed in Section 4.4.1 and 4.4.2 respectively.

3.4.1 Unfiltered areal parameters

The areal parameters derived for each technique are given in Table 3.2. Sq is spatially equivalent to the mean profile depth that is used at present to evaluate macrotexture. Table 3.2 shows that S_q, for the 3D Smart Laser Profile Sensor and SfM are within 0.002 mm agreement for the DBM, 0.013 mm for the SD and 0.09 mm for the HRA. This presents the 3D Smart Laser Profile Sensor and SfM, as an alternative method to capture texture depth. The TLS obtained results for S_q are very different, with differences in comparison with the 3D Smart Laser Profile Sensor value ranging from 0.139 mm to 0.394 mm; the largest value being obtained for the SD surface. The value for S_p and S_v, the maximum peak and pit heights, demonstrate greater agreement between the SfM and 3D Smart Laser Profile Sensor results, than the TLS technique. The variance in TLS derived parameters is because of the higher resolution nature of the data. Values for Spd and Spc, which have previously been shown to have positive correlations with skid resistance (Kogbara et al., 2016), are typically different by an order of magnitude for all the techniques and surfaces considered. The variability of S_{pd} and S_{pc} suggests the parameters are also sensitive to resolution and limits the potential to adopt unfiltered data in 'universal' across technique parametric comparison studies with friction. For S_{sk}, the parameter defining skewness (thus indicating whether texture is positive or negative), all three unfiltered techniques were able to identify the positive texture of the

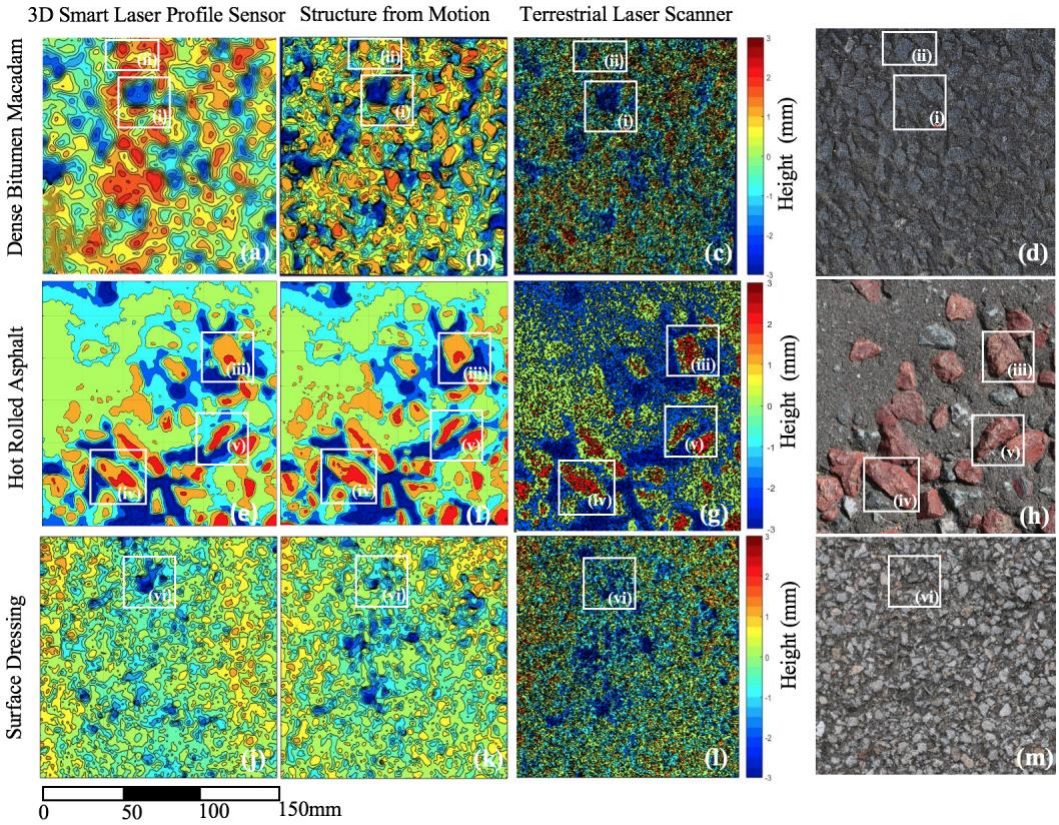

Figure. 3.5. Surface height plots derived from the unfiltered point cloud data for a 150mm x 150mm sample area of each surfacing material. (a) Dense Bitumen Macadam captured with 3D Smart Laser Profile Sensor (b) Dense Bitumen Macadam captured with Structure from Motion (c) Dense Bitumen Macadam capture with the Terrestrial Laser Scanner (d) Digital image of the Dense Bitumen Macadam surface. Greater similarity is evident between (a) and (b) as the 3D Smart Laser Profile Sensor and Structure from Motion techniques have similar resolution. The higher resolution of the Terrestrial Laser Scanner is evident in the finer granularity of plot (c). All the techniques are able to capture voids between aggregate (e.g. i) and aggregate features (e.g. ii) on the Dense Bitumen Macadam surface at the same locations. (e) Hot Rolled Asphalt captured with the 3D Smart Laser Profile Sensor (f) Hot Rolled Asphalt captured with Structure from Motion (g) Hot Rolled Asphalt captured with the Terrestrial Laser Scanner (h) Digital image of the Hot Rolled Asphalt surface. All three techniques have clearly captured the red aggregate chippings of the Hot Rolled Asphalt (e.g. iii to v). There is greater similarity between (e) and (f), the data captured with the 3D Smart Laser Profile Sensor and Structure from Motion techniques. The higher resolution of the Terrestrial Laser Scanner is evident in the finer granularity of the edges of the aggregate. (j) Surface Dressing captured with the 3D Smart Laser Profile Sensor (k) Surface Dressing captured with Structure from Motion (l) Surface Dressing Capture with the Terrestrial Laser Scanner. (m) Digital image of the Surface Dressing surface. There is greater similarity between (j) and (k), the data capture with the 3D Smart Laser Profile Sensor and Structure from Motion technique. The higher resolution of the Terrestrial Laser Scanner is evident in the finer granularity of plot (l). The Surfacing Dressing aggregate chippings are the smallest of the three surfaces, but the techniques have still collectively identified areas of void between aggregates in blue (e.g. vi) and areas of elevated macrotexture in orange located to the right and left edge of each plot.

surfaces. The skewness is sensitive to the spatial sampling resolution of the technique, with closer agreement demonstrated between the SfM and 3D Smart Sensor technique.

3.4.2 2D correlation analysis

Areal parameters only characterise discrete functions of surface roughness. Therefore, 2D cross-correlation analysis to measure x-y and z plane similarity between images was completed. Perfect correlation is characterised by a strong central peak with a value of 1. The normalised 2D cross-correlation plots are shown in Figure 3.6. For the DBM surface a central peak is evident of 0.4492 and 0.3515 for similarity between the 3D Smart Laser Profile Sensor and SfM, and 3D Smart Laser Profile Sensor and TLS respectively (Figure 3.6 (a) and Figure 3.6 (d)); defining positive correlation and symmetry (or lack of shift) between the wavelength frequencies. To the left of the central peak there is a dominating positive feature on both plots, depicted as the yellow to red zone (e.g. Figure 3.6 (a)(i)), representing an area of higher macrotexture departure from the surface. For the SD surface, no central peak is evident with elongated bands of positive and negative agreement being visible (Figure 3.6 cii and ciii) for similarity between both the 3D Smart Laser Profile Sensor and SfM, and 3D Smart Laser Profile Sensor and TLS. The bands arise as the macrotexture of the SD surface is dominated by a repeating texture feature.

Overall, the best correlation is achieved between the 3D Smart Laser Profile Sensor and SfM measurement technique for the HRA surface Figure 3.6b. The plot has a clear strong centralised peak of 0.729, demonstrating an alignment or lack of lateral shift between the wavelength frequencies of the two techniques. The rest of the plot is generally blue indicating a general lack of secondary dominating features on the surface. This can be attributed to the parity of resolution between two techniques and the larger wavelength features of the HRA surface. The 2D cross-correlations affirm the areal parameter results with greater agreement between the unfiltered 3D Smart Laser Profile Sensor and SfM surface measurements. The 2D cross-correlation plots comparing similarity between the 3D Smart Laser Profile Sensor and TLS demonstrate less agreement. The normalised cross-correlation peaks are either not present or where present are lower being 0.3515 for the DBM (Figure 3.6(d)). This confirms the influence of the higher resolution shorter wavelengths within the unfiltered data, which cause the reduction in the normalised peak, and reduced agreement. After the application of a 0.1 wavenumber filter the heights of the normalised 2D cross- correlation peaks increase by 16.6 to 25% demonstrating stronger agreement between the 3D Smart Laser Profile Sensor and the other two techniques.

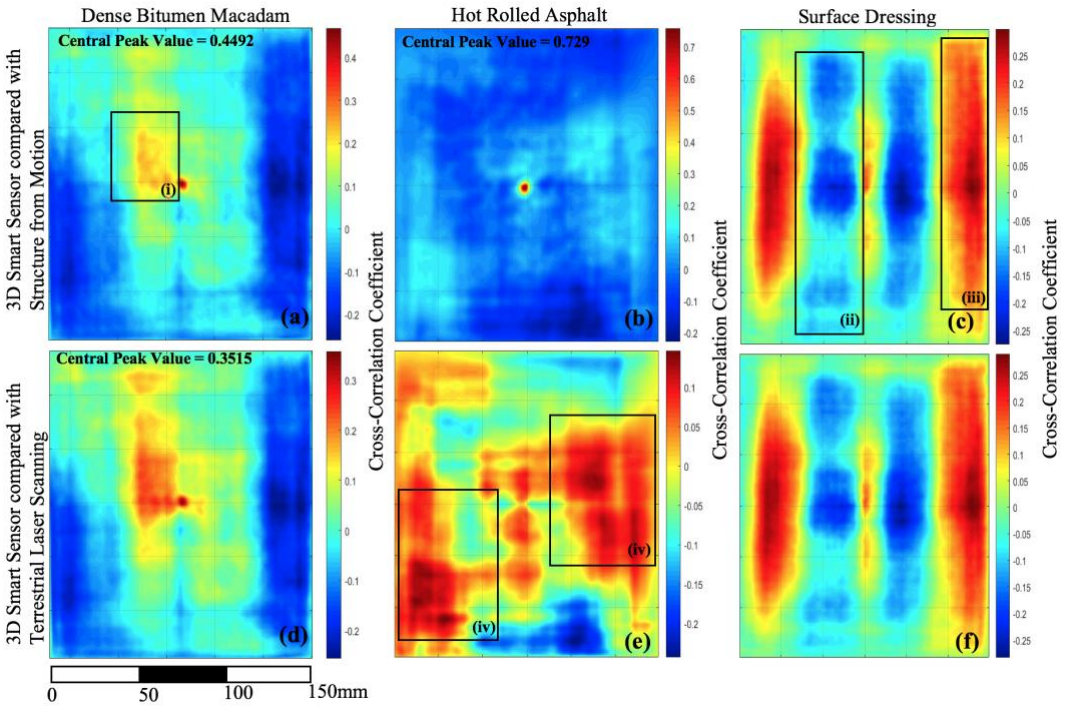

Figure. 3.6. 150mm x 150mm 2D normalised cross-correlation plots for the unfiltered point cloud data. (a) 2D cross-correlation plot, defining the similarity between the point cloud data obtain from the 3D Smart Sensor and Structure from Motion, for the Dense Bitumen Macadam surface. The plot has a clear strong centralised peak of 0.4492, demonstrating an alignment or lack of lateral shift between the wavelength frequencies of the two techniques. On the sidelobes there is a dominating positive feature, depicted as the yellow to red zone (i), representing an area of elevated macrotexture (b) 2D cross-correlation plot defining the similarity between the point cloud data obtain from the 3D Smart Sensor and Structure from Motion for the Hot Rolled Asphalt surface. The plot has a clear strong centralised peak of 0.729, demonstrating an alignment or lack of lateral shift between the wavelength frequencies of the two techniques. The sidelobes of the plot are generally blue indicating a general lack of secondary dominating features on the surface. (c) 2D cross-correlation plot defining the similarity between the point cloud data obtain from the 3D Smart Sensor and Structure from Motion for the Surface Dressing. No central peak is evident with instead elongated bands of positive and negative agreement being visible (ii and iii). The bands arise as the macrotexture of the SD surface is dominated by a repeating feature of bands of increased macrotexture height. (d) 2D cross-correlation plot defining the similarity between the point cloud data obtain from the 3D Smart Sensor and the Terrestrial Laser Scanner for the Dense Bitumen Macadam surface. The plot is similar to (a) having a centralised peak of 0.3515 and a second dominating positive feature on the side lobes. (e) 2D cross-correlation plot defining the similarity between the point cloud data obtain from the 3D Smart Sensor and the Terrestrial Laser Scanner for the Hot Rolled Asphalt surface. No central peak is evident with instead two zones of positive agreement are visible on the sidelobes mirrored about the diagonal (iv and v). These represent the elevated macrotexture of the clustered zones of red aggregate chippings. (f) 2D cross-correlation plot defining the similarity between the point cloud data obtain from the 3D Smart Sensor and the Terrestrial Laser Scanner for the Surface Dressing. The plot is similar to (c).

3.4.3 Filtered areal parameters

Surface height plots for each filtered surface scanning technique are illustrated in Figure 3.7. For all three surfaces after the application of a 0.1 mm^{-1} wavenumber filter there is greater visual similarity between all three techniques. The filter has reduced the resolution of the TLS data, removing the finer granularity, to reveal the macrotexture more clearly. Furthermore, post-filtering increased agreement was achieved for areal parameters S_{pd} and S_{pc}, previously shown to have a positive correlation with skid resistance. The filtered areal parameters are shown in Table 3.2. The filtered S_{pc} (arithmetic mean peak curvature) values, related to the shape of the road aggregates, measured using the 3D Smart Laser Sensor and SfM are within 0.013 mm^{-1} for the DBM and 0.067mm^{-1} for the SD. The filtered values of S_{pc} for the HRA do not demonstrate agreement. The filtered S_{pd} (peak density) values, related to the distribution of road aggregates upon a pavement surface, measured using the 3D Smart Laser Sensor and SfM are within 0.00087mm^{-2} for the DBM, 0.01417 mm^{-2} for the HRA, and 0.00044 mm^{-2} respectively for the SD. The filtered S_{pd} (peak density) values measured using the 3D Smart Laser Sensor and TLS are within 0.00059 mm^{-2} for the DBM, 0.01747 mm^{-2} for the HRA, and 0.00054 mm^{-2} for the SD. The filtered Spd values measured using the SfM and TLS are within 0.00028 mm^{-2} for the DBM, 0.0033 mm^{-2} for the HRA, and 0.0001 mm^{-2} for the SD. Although an increased agreement has been achieved for S_{pd} and S_{pc}, importantly for practical pavement characterisation of surface height departures, for the 3D Smart Laser Profile Sensor and SfM techniques this is at the expense of the accuracy of S_q, which experiences magnification at a range of four to ten times. Therefore, filtering improves spatial agreement, but at the cost of vertical measurement, a factor that should be considered by researchers seeking correlations between non-contact texture measurements and skid resistance. Moreover, the filtered values of S_q obtained from the TLS whilst closer to the original unfiltered 3D Smart Laser Profile Sensor, demonstrate at best ten percent accuracy; being in 0.213 mm agreement for the DBM, 1.928 mm agreement for the HRA and 0.063 mm agreement for the SD. The TLS technique does offer the best balance between the vertical and spatial areal functions post-filtering, fundamentally because it enables oversampling of the surfaces, with correspondingly the shortest Nyquist wavelength. However, the improved resolution of the technique still does not lead to sufficiently accurate measurement of S_q, the vertical departure heights from a pavement surface. Greater technique resolution does not necessarily equate to sufficiently improved accuracy for some measurements

3.4.4 Spectral analysis

The spectra in Figure 3.8 illustrate the areal wavenumber characteristics of the three surface materials in the 'x' and 'y' plane (Girardeau-Montaut, n.d.). As wavenumber is the reciprocal of wavelength, the plots serve to demonstrate differences in macrotexture characteristic

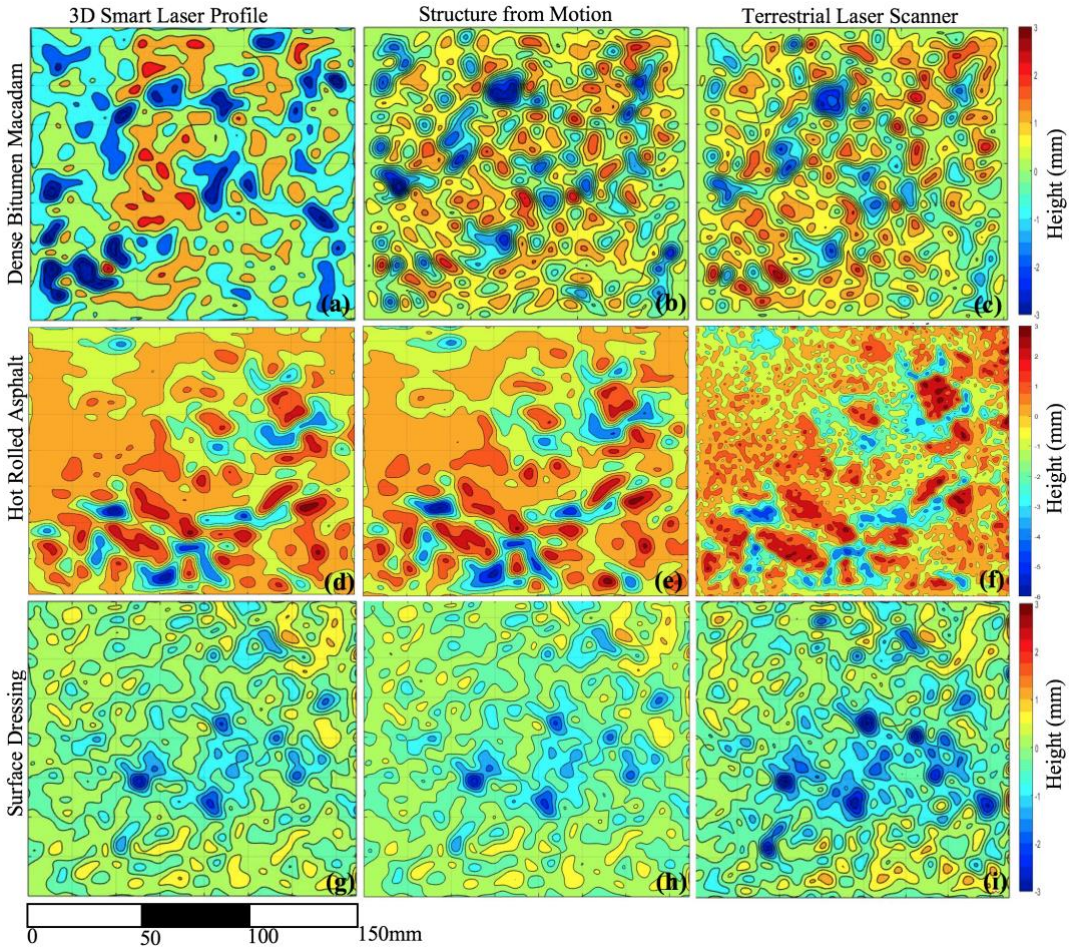

Figure. 3.7. Surface height plots derived from the 0.1 wavenumber filtered point cloud data for a 150mm x 150mm sample area of each surfacing material. (a) Dense Bitumen Macadam captured with 3D Smart Laser Profile Sensor (b) Dense Bitumen Macadam captured with Structure from Motion (c) Dense Bitumen Macadam capture with the Terrestrial Laser Scanner. After the application of a 0.1 wavenumber filter there is greater visual similarity between the Structure from Motion and Terrestrial Laser Scanner data. The filter has reduced the resolution of the Terrestrial Laser Scanner data, removing the finer granularity, to reveal the macrotexture more clearly. (d) Hot Rolled Asphalt captured with the 3D Smart Laser Profile Sensor (e) Hot Rolled Asphalt captured with Structure from Motion (f) Hot Rolled Asphalt captured with the Terrestrial Laser Scanner. After the application of a 0.1 wavenumber filter there is greater visual similarity between all three techniques. The filter has reduced the resolution of the Terrestrial Laser Scanner data, removing some of the finer granularity, to reveal the macrotexture more clearly. (g) Surface Dressing captured with the 3D Smart Laser Profile Sensor (h) Surface Dressing captured with Structure from Motion (i) Surface Dressing Capture with the Terrestrial Laser Scanner. After the application of a 0.1 wavenumber filter there is greater visual similarity between all three techniques. The filter has reduced the resolution of the Terrestrial Laser Scanner data, removing the finer granularity, to reveal the macrotexture more clearly. All techniques have generally identified the same areas as voids between aggregates in blue, and areas of elevated texture in orange.

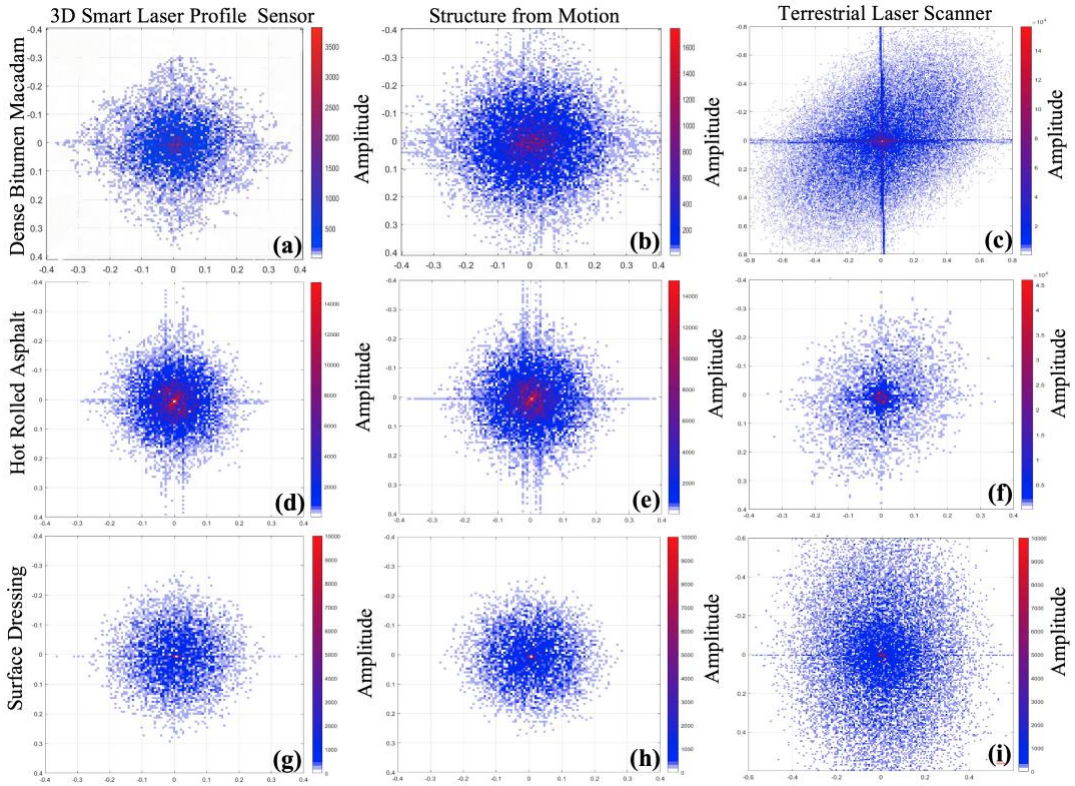

Figure 3.8. 2D wavenumber (mm^{-1}) spectral analysis of the unfiltered point cloud data. (a) Wavenumber spectral analysis for the 3D Smart Laser Profile Sensor scan of the Dense Bitumen Macadam surface. (b) Wavenumber spectral analysis for the Structure from Motion scan of the Dense Bitumen Macadam surface. (c) Wavenumber spectral analysis for the Terrestrial Laser scan of the Dense Bitumen Macadam surface. (d) Wavenumber spectral analysis for the 3D Smart Laser Profile Sensor scan of the Hot Rolled Asphalt surface. (e) Wavenumber spectral analysis for the Structure for Motion scan of the Hot Rolled Asphalt surface. (f) Wavenumber spectral analysis for the 3D Terrestrial Laser scan of the Hot Rolled Asphalt surface. (g) Wavenumber spectral analysis for the 3D Smart Laser Profile Sensor scan of the Surface Dressing. (h) Wavenumber spectral analysis for the Structure from Motion scan of the Surface Dressing. (i) Wavenumber spectral analysis for Terrestrial Laser scan of the Surface Dressing.

between the surfaces. The spectra are sensitive both to the scale of the macrotexture and the technique of measurement. The TLS has the largest spectral cloud of the three techniques for all surfaces, illustrating that it is consistently the highest resolution technique. Considering the SfM spectral plots, it is clear that the HRA surface has the largest wavelength features represented by the brightest spectral cloud centre; whilst the DBM contains the smallest wavelength features represented by the largest cloud. As a high pass filter was not applied to the cloud data, the larger wavelengths in the centre of the spectral plots represent the unevenness of the surfaces. The spectra reveal for the SfM technique that for the HRA the wavelengths features are typically 4 mm or larger; the SD 3.5 mm or larger and DBM 2.6 mm or larger. Finally, greater similarity is generally evident between the unfiltered spectra for the SfM and 3D Smart Laser Profile Sensor, as the techniques have similar resolution and accuracy.

3.4.5 Spatial variability

The spatial variability of S_q, S_{sk}, S_p, S_v, S_{pd} and S_{pc} for seventy-two 150 mm x 150mm samples and eighteen 300 mm x 300 mm samples captured using SfM were considered for a 1.8 m x 0.9 m area of HRA in Figure 3.9 and 3.10. The computed parameters (S_q, S_{sk}, S_p, S_v, S_{pd} and S_{pc}) for each individual sample, were divided into a percentage of the overall maximum for each considered areal parameter, with the discrete colour contrasts representing 20% . Thereby each colour represents a 20th percentile in the overall maximum parameter value, and thus illustrates the variability of the parameters across the 1.8 m x 0.9 m HRA surface . The 150 mm x 150 mm sample size for S_p, maximum peak height, reflects the distribution of red aggregate chippings across the HRA surface. Lower peaks are encountered near the top edge of the sample, where the surface is predominantly bituminous binder. Some discrete squares of increased peak height are shown in dark green, representing the higher texture height of isolated red chippings. Principally, the peak height values S_p are within the percentile range of 1.85 mm to 3.65 mm. The 150 mm x 150 mm sample size for S_v, maximum pit height, demonstrated limited variability between separate sample areas, with 87.5% of the HRA surface being within 4.4 mm to 7.4 mm. This consistency most likely reflects the method of laying HRA, with the precoated red aggregate chippings being scattered across the surface of the previously laid asphalt binder and rolled into the surface at a constant pressure, resulting in more consistent pit heights. For vertical macrotexture characterisation parameters, such as S_v , S_p and S_q spatially equivalent to the mean profile depth used at present to evaluate macrotexture, there is some similarity between the location of darker colour contrast for both the 150 mm x 150 mm and 300 mm x 300 mm sample sizes.

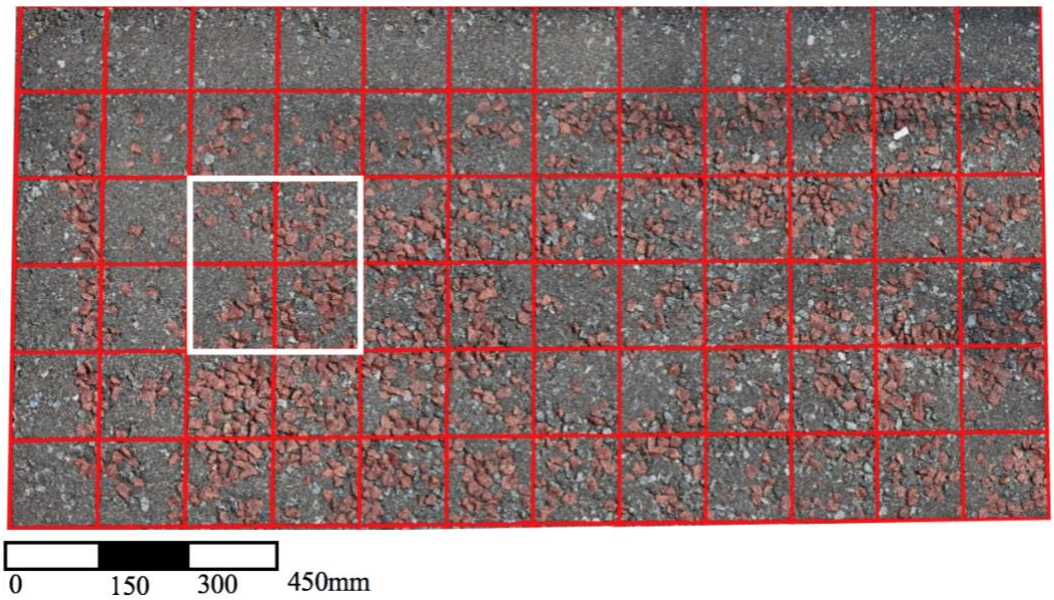

Figure. 3.9. Digital image of the 1.8m x 0.9m area of Hot Rolled Asphalt considered in the spatial variance study. The parameters S_q, S_{sk}, S_p, S_v, S_{pd}, and S_{pc} are computed from raw point cloud data captured using Structure from Motion for the 150 mm x 150 mm samples delineated by the red lines. The parameters parameters S_q, S_{sk}, S_p, S_v, S_{pd}, and S_{pc} were recomputed on the same point cloud data for the 300mm x 300mm samples. The 300mm x 300mm directly overlapped the original 150mm x 150mm samples (as illustrated by the white square).

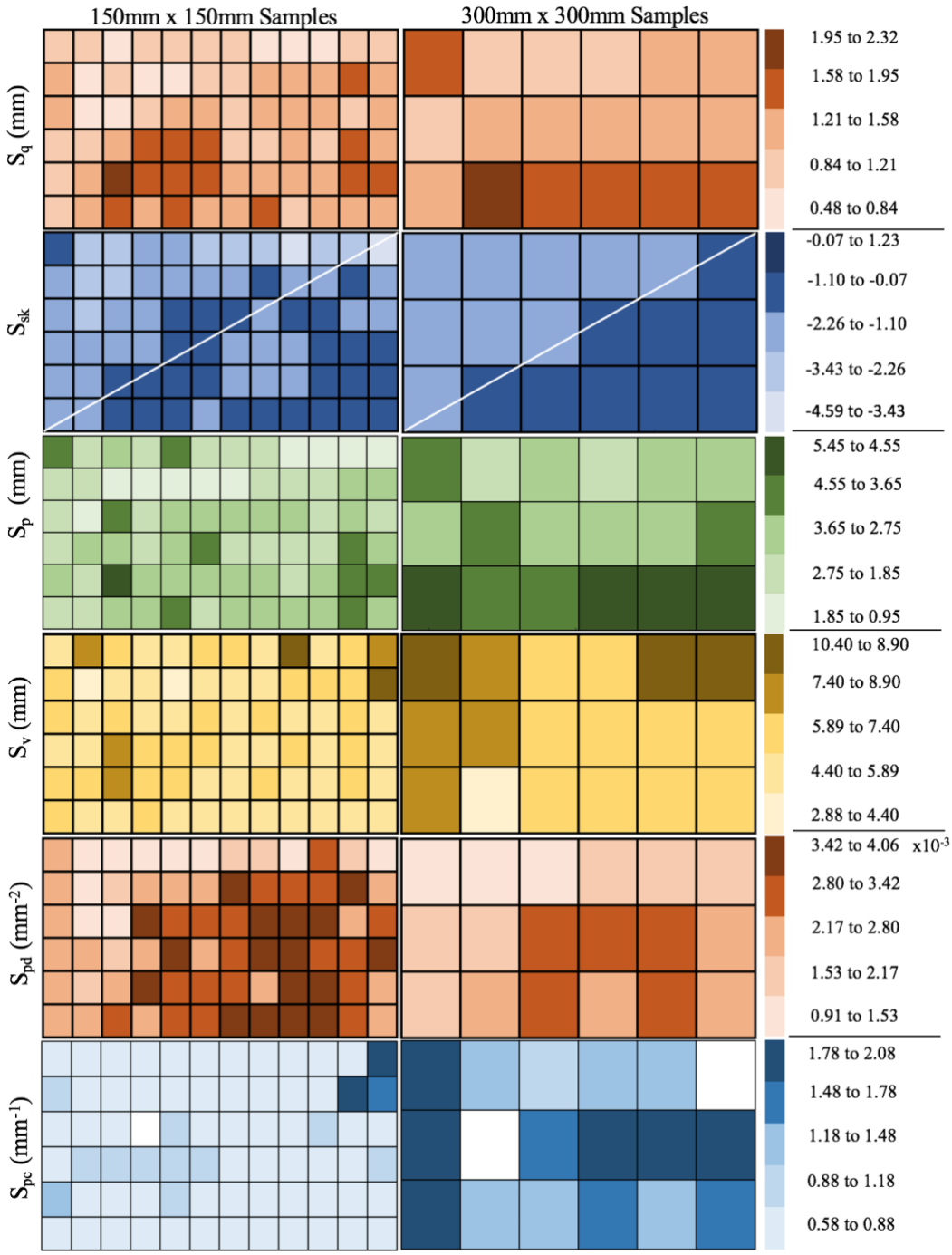

Figure. 3.10. Spatial variance of S_q, S_{sk}, S_p, S_v, S_{pd}, S_{pc} over a 1.8m x 0.9m area of Hot Rolled Asphalt surfacing for 150 mm x 150 mm and 300 mm samples, data captured with Structure from Motion. The computed parameters for each individual sample, were divided into a percentage of the overall maximum for each areal parameter. Each discrete colour contrasts representing a 20-percentile difference in parameter values. The colour tone difference demonstrates the variability of the parameters across the 1.8m x 0.9m hot rolled asphalt surface.

There is a lack of parity between the surface characterised using the 150 mm x 150 mm sample and the 300 mm x 300 mm sample for S_{pd}; with an increase in sample size appearing to 'smooth' the density of peaks removing altogether the highest percentile range 3.42 x 10^{-3} mm^{-2} to 4.06 x 10^{-3} mm^{-2} from the 300 mm x 300 mm plot. The 150 mm x 150 mm samples reflect the distribution of red chippings across the surface, with the lower peak densities recorded near the top and edge of the HRA surface where there is predominantly bituminous binder present. The S_{pd} parameter also demonstrates the greatest variability between different 150 mm x 150 mm samples. S_{pd} has previously been shown as being important to skid resistance, with positive correlation achieved with friction measurements. However, the variability of S_{pd} values, means picking a representative 150 mm x 150 mm sample to characterise the whole surface to correlate with friction is difficult. Spd represents the number of peaks in a unit area and is sensitive to sample size. Figure 3.11 considered the influence of upscaling the sample size for areal parameters (S_q, S_{sk}, S_p, S_v, S_{pd} and S_{pc}) on the HRA surfacing capture using SfM with the point cloud extended to 1.05 m x 1.95m. For S_{pd} the optimum sample size for the HRA surface was found to be 1050 mm x 1050mm. For the vertical macrotexture parameters, the optimum sample size was found to be 750 mm x 750 mm for S_v , 1050 mm x 1200 mm for S_p, and 1050 mm x 1650 mm for S_q.

For S_{pc} mean curvature of peaks, the optimum sample size was discovered to be 450 mm x 450 mm for the HRA surface. S_{pc} was found to have the smallest sample size of all the parameters considered perhaps reflecting its general lack of heterogeneity. The 150 mm x 150 mm sample size demonstrating the least variability across the HRA surface of any of the areal parameters considered by the study; with 80% of the samples falling within the 20% range 0.58 $mm^{-1}$to 0.88 mm^{-1}.

Whilst S_q, S_p, and S_v just capture the overall height and depth of peak and pit surface departures, S_{sk} gives the location (or skewness) above and below the mean plane; consequently, providing an indication of the distribution of texture available to contribute to skid resistance. For S_{sk}, both the 150mm x 150 mm and 300mm x 300 mm sized samples confirm that the HRA has positive texture. The split of the contrasting light and dark blue squares for S_{sk}, is similar for each sample size, with the predominant number of darker squares below the white diagonal line bisecting the 1.8 m x 0.9 m area (refer to Fig 10). However, the location of the mean plane was determined to be sensitive to sample size, with the value of S_{sk} varying. A sample size of 1050 mm x 1200 mm of smaller was found in the upscaling analysis to have a negative texture confirming a positive texture, but above this size S_{sk} was shown to have a positive value indicating a skew to negative texture. The change in S_{sk} can be attributed to the influence of the variability of peak height with changing sample

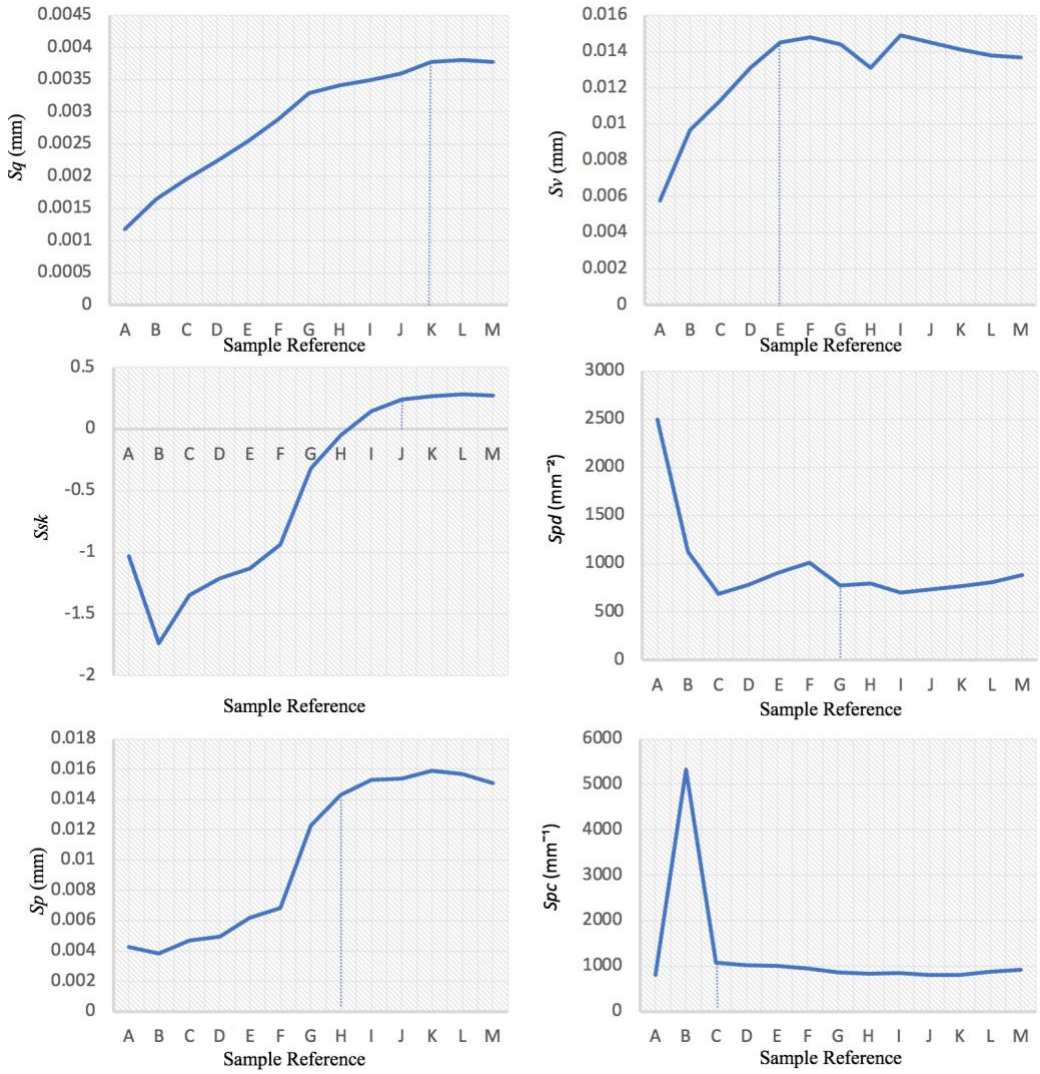

Sample Reference	Size (mm)	Sample Reference	Size (mm)
A	150 x 150	G	1050 x 1050
B	300 x 300	H	1050 x 1200
C	450 x 450	I	1050 x 1350
D	600 x 600	J	1050 x 1500
E	750 x 750	K	1050 x 1650
F	900 x 900		

Figure. 3.11. The influence of upscaling sample size on areal parameters S_q, S_{sk}, S_p, S_v, S_{pd},S_{pc} for an area of Hot Rolled Asphalt surfacing captured using Structure from Motion. The optimum sample size for each parameter is indicated on each graph with a dotted line and occurs where values converge to a stable value.

area, on the location of the mean plane. Overall reviewing individual areal parameters typically used to characterise friction (S_p, S_v, S_{pd} and S_{pc}) optimal sample size, suggests that a suitable sample size of 1050 mm x 1200mm is appropriate to characterise HRA; this being established from the maximum size of the individual parameters.

Further research should be conducted to explore the efficiency of sample sizes for areal parameters for different pavement textures. As contact friction devices are known to be susceptible to seasonal variation and machine operating conditions such as load, speed slip ratio and the composition of rubber, using reliable non-contact areal parameter data to be able to analytically model a relationship with friction is desirable. Moreover, higher resolution does not always equate to greater accuracy. It was found that whilst SfM photogrammetry successfully provides an alternative method to the 3D Smart Laser Profile Sensor to capture vertical pavement measurement S_v, S_p and S_q for mean profile depth estimation and correlation with friction, the higher resolution TLS data contained significant inaccuracies. Furthermore, the values of S_{pd} and S_{pc}, which together define the shape and distribution of pavement aggregates and have previously been proven to have positive correlation with friction (Kogbara et al., 2016), are sensitive to resolution, incurring order of magnitude differences. A 2D low pass wavenumber filter achieved improved agreement with the 3D smart profiler for S_{pd} and S_{pc} parameters. Optimising such filters consistently across a range of non-contact techniques is needed to achieve a 'universal' correlation between these parameters and to model relationships with skid resistance. Further, as the application of such a filter has the potential to impact on vertical accuracy of measurement (S_q, S_p, and S_v) for some high-resolution techniques, findings of this study indicate the filter should be applied only to the S_{pd} and S_{pc} spatial parameters.

3.5 Conclusions

In conclusion, the study has compared the measurement of macrotexture using three different techniques. The study makes a first contribution to the establishment of reliable standardised texture measurements using point cloud derived data to inform analytical prediction methods for tyre-pavement contact friction without the influences of seasonal variation, measuring devices and their operating conditions. Results from the analysis of the data lead to the following conclusions:

- Unfiltered close field SfM photogrammetry provides values of S_p, S_v and S_q, within an acceptable degree of tolerance to those obtained from the 3D Smart Laser Profile Sensor, so as SfM photogrammetry is an effective, readily scalable alternative method to capture mean profile depth for pavement evaluation.

- The parameters S_{pc} and S_{pd}, for which previous studies have established an important correlation with pavement friction, are sensitive to technique resolution and a 2D low pass wavenumber filter needs to be applied to obtain a ‘universal’ measurement for pavement friction assessment.

- A 2D zero-phase wavelength filter of 0.1 mm-1 improves S_{pd}, for the TLS and SfM techniques.

- The Nyquist wavelengths of TLS and SfM techniques mean they have the potential to measure microtexture wavelengths below 0.5mm.

- TLS data are significantly improved for macrostructure surveys after 2D low pass wavenumber filtering.

- Where 150 mm x 150 mm industry sample sizes are used to determine parameters from point clouds data derived from non-contact techniques, these are not sufficient to correctly characterise functional areal parameters to describe the spatial variability of macrotexture upon a pavement. This study suggests a suitable sample size of 1050 mm x 1200mm is appropriate to characterise HRA.

Chapter 4: Published Paper 2 – Quantifying long-term rates of texture change on road networks.

4.1. Abstract

Texture is required on pavements to provide safe and comfortable ride performance for users. This paper provides the first meaningful analysis of a long-term study of texture data obtained using TRACS (TRAffic Speed Condition Survey) at a site in the UK. TRACS data were collected annually, over a 2 km stretch of motorway from 1995 to 2019. A new data analysis approach utilising time series data with spectral analysis and spatial filtering procedures is presented. The results reveal that the approach enables legacy TRACS laser profile Sensor Measured Texture Depth (SMTD) data to be used to determine long term rates of change in road surface macrotexture. Thus, the technique has unlocked the potential for SMTD data collected annually for 7000 km of the Strategic Road Network in the UK, to inform road maintenance programmes by extrapolation. Additionally, results expose a systematic periodicity occurring each year within the SMTD data studied, corresponding to longitudinal oscillations with wavelengths between 33 m to 62 m. The time-invariant periodicity of these oscillations suggests that it is 'imprinted' in the early life of the pavement. 'Imprinting' may theoretically arise with cyclic tyre loading applied by the suspension systems of heavy vehicles or during road construction.

4.2. Introduction

Road surface texture is essential for the safe and effective operation of road networks (Meegoda and Gao, 2015). Texture influences noise and vehicle rolling resistance and by that fuel consumption and carbon monoxide emissions (Ejsmont et al., 2017; Hong et al., 2018). Texture also contributes to wear, with texture measurements taken from road networks helping to inform when maintenance is required (Meegoda and Gao, 2015). The texture components of a highway surface have been characterised at four increasing wavelength scales: megatexture and unevenness, macrotexture and microtexture (International Organization for Standardisation, 2009). Megatexture relates to wavelengths between 63 mm and 500 mm and amplitudes of between 0.1 mm and 50 mm, unevenness is characterised by wavelengths between 0.63 m and 50 m. Highway pavement megatexture and unevenness is known to impact ride quality and driver comfort (Loprencipe, 2019). Microtexture and macrotexture influence skid resistance and the friction available at the interface between the tyre and the road (Moore, 1975; Klüppel and Heinrich, 2001; Persson, 2001). Macrotexture represents the texture with wavelengths between 0.5 mm and 50 mm and amplitudes of between 0.1 mm and 20 mm (formed by the shape, size and gradation of road aggregates on a pavement surface).

Microtexture represents the asperities on the surface of road aggregates and has wavelengths up to 0.5 mm and amplitudes in the range of between 0.001 mm to 0.05 mm. Skid resistance on a pavement surface is essential for vehicle safety and is also affected by temperature, presence of contaminants, speed and tyre tread thickness (Kane and Edmondson, 2018). The preservation of adequate pavement texture is achieved by a regime of monitoring and maintenance undertaken by road agencies; national practices vary, but data are typically collected at least annually (Design Manual for Roads and Bridges, 2008; European Collaborative Project, 2014). Generally, at road network scale unevenness, megatexture and macrotexture are monitored at traffic speed, using laser profile sensor techniques and video cameras mounted on specialist survey vehicles (Meegoda and Gao, 2015). Microtexture which influences skid resistance at low speeds (Cunto and Branco, 2016) and requires contact between a tyre tread and the surface asperities of road aggregates, is monitored using contact techniques. At the road network scale these contact techniques frequently used a fixed or braking test wheel, which measures the frictional contact at traffic speed made with the wheel and a wetted highway pavement. Kogbara et al. (2016) provide a full summary of contact devices and their operating principles.

Road infrastructure assets represent the largest capital assets of most countries (Organization for Economic Co-operation and Development, 2001). The pavement geometry data obtained from surveys is commonly held in a pavement management system (Meegoda and Goa, 2015) and made available to government authorities, road agencies, asset managers, engineers, and suppliers to enable them to reach decisions on road pavement maintenance priorities and programming. The aim is to provide the road user with a reliable level of service and ride safety (Transport Research Board, 2016) . Maintenance planning presents to the stakeholders two key fundamental challenges: the identification of locations on a large road network requiring investigation, and the deterioration characterisation of these locations to facilitate timely, appropriate and effective maintenance approaches. Furthermore, characterising suitable intervention engenders the additional challenge of judging when preventative maintenance is required, which typically offers lower cost repair options to extend pavement life, and when full resurfacing is needed. Pavement texture changes over time, these variations have previously been characterised into ‘long-term variations’ and ‘short-term variations’ (Vaiana et al., 2012). ‘Short-term variations’ have been established to arise due to meteorological conditions such as temperature and rainfall (Masad et al., 2009). ‘Long-term variations’ are given to be predominantly due to traffic actions (Viana et al., 2012). Traffic flow has a significant influence on the evolution of pavement texture (Plati and Pomoni, 2019) and as a result maintenance planning. Pavement texture deterioration has been shown to be influenced particularly by the percentage of heavy goods vehicles in a trafficked lane (O’Brien

and Haddock, 2009; Ragland et al., 2010; Khasawneh et al., 2016). Recently, an inverse trend between skid resistance and pavement macrotexture deterioration has been identified, associated with a minimum cumulative traffic threshold (Plati and Pomoni, 2019). With trafficking, macrotexture evolution was found generally to increase by Plati and Pomoni (2019) and skid resistance to reduce after the minimum cumulative traffic threshold. The threshold was given to mark the point where sufficient polishing of fine aggregates had occurred, resulting in the coarse aggregates dominating skid resistance. Hence, routes with higher volumes of traffic are likely to require prioritisation in maintenance planning. Due to the complexity of the interaction of traffic flow and meteorological conditions with pavement materials, the final decision on intervention is left to the judgement and experience of the road manager after a visual inspection.

Pavement condition and performance indices that support the decision-making process are based on analysis of the survey data held within the pavement management system (FSV-Austrian Transport Research Association, 2008). For longitudinal pavement texture there are a number of accepted pavement condition indices utilised across the world. The International Roughness Index (IRI) models the virtual response of a 'golden car' travelling at 80 km/hr on a road profile (Sayer et al., 1986; ASTM International, 2015; European Committee for Standardisation, 2017). The 'golden car' is a simulated system utilising standardised values for the damping, springs and masses relating to a portion (or a quarter) of a car supported upon one wheel, often termed the quarter-car. IRI represents the dimensionless ratio, of the accumulated vertical motion of the 'golden' quarter-car's suspension, divided by the distance travelled; known as the evaluation or segment length. Acceptable IRI threshold values are specified on a country-by-country basis for new, reconstructed or rehabilitated roads. Depending upon the country of application, these IRI thresholds are reported either as a constant value for an evaluation length, the average value of a series of segments within an evaluation length, or as a percentile. The evaluation or segment lengths typically vary from 10 m to 1600 m. Furthermore, the IRI thresholds can be specified by a country as a function of the road surface type, category (e.g. motorway or minor road), speed limit or traffic flow. Mucka (2017) provides a full summary of the IRI specifications used around the world. Another approach to the characterisation of longitudinal road profiles is presented in ISO 8608 (International Organization for Standardization, 2016). The ISO 8608 standard provides a description and classification of synthetic road profiles for use in computational modelling, based upon vertical displacement power spectral density (PSD). PSD is represented on a logarithmic scale and is defined by two parameters of a straight line: an unevenness index and waviness. The road classifications presented in ISO 8608 are primarily used for vibration modelling and are not directly linked to real road categories, although some research has been

completed to derive validation (Mucka, 2018). Within the UK, texture threshold values are adopted to define minimum advisory road texture levels in relation to both longitudinal profile (with an evaluation length of 100 m) (Design Manual for Roads and Bridges, 2008) and also skid resistance (Design Manual for Roads and Bridges, 2015). The specification of threshold values is based upon road condition and road category, with areas found to be below advisory levels prioritised for visual inspection by a road manager.

A limitation of the pavement condition indices reviewed, is the sensitivity of the techniques to the evaluation length (Transport Research Laboratory, 2006). The selection of evaluation length defines the granularity of the texture data. This can be illustrated by a simple assessment of texture level against a minimum threshold. In such a case where pavement texture is averaged over a long length which contains sections of localised texture variability, the averaged result will smooth the texture data, potentially masking the true condition of shorter lengths. Stakeholders evaluating road texture for maintenance, require confidence in the deployment of follow-up resources for visual inspection and condition assessment. A preferred approach is to augment pavement condition indices with a method to track and understand the rate of change of texture condition at every location on a real road network. This would support the identification of deteriorating sections of the road network; but to date the rate of change for pavement texture at discrete locations on a real road network has been difficult to estimate reliably (Rainsford and Parkman, n.d). Today, access to 'big data' (Mauro, 2016) in the format of pavement management systems containing historic pavement geometries, and advances in data processing techniques means that data can now be analysed in new ways. This paper presents a new method to analyse legacy Sensor Measured Texture Depth (SMTD) (Transport Research Laboratory, 2006) legacy data obtained using the TRAffic Speed Condition Survey (TRACS) system in the UK (Department for Transport, 2019) and stored in the Highways England Pavement Management System (HAPMS) (UK Government, 2019) over twenty-five years for 7000 km of Class A highway. A novel data processing approach utilising time series data with spectral analysis and novel wavenumber filtering procedures is presented, producing a rare long-term evaluation of the rate of texture change on real road networks.

4.3. Selecting the site and legacy data

The study site was a 2 km length of the northbound route of the M6 motorway located within Cumbria, UK, Figure 4.1. The route, a predominantly straight section of rural link motorway is typically at 300 m above Ordnance Datum with some gentle longitudinal undulations. The three northbound lanes climb uphill at a maximum gradient of 3 % between chainages 600 m to 1500 m and are at a downhill incline of a maximum gradient of 3 % between chainages 0

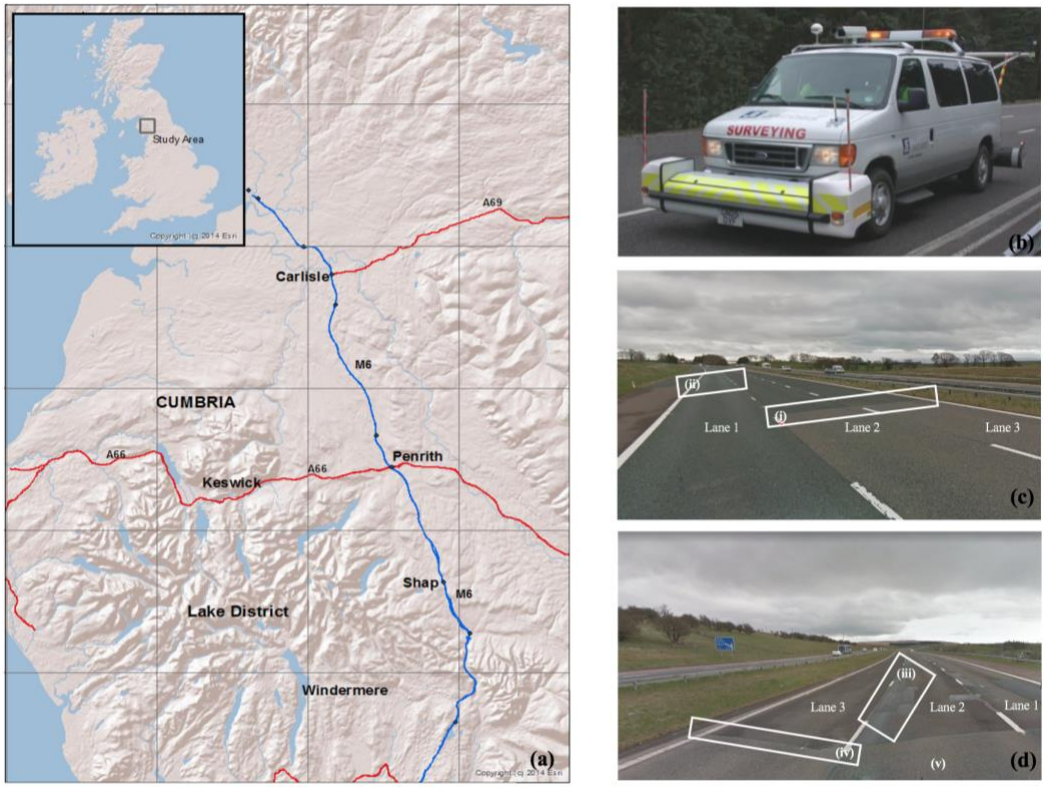

Figure 4.1. Field Site Location and Equipment: (a) The field site. (b) TRACS (TRAffic Speed Condition Survey) road survey equipment. (c) Photograph of the field site at chainage 1480 m looking northwards, clearly depicting the construction joint (e.g. i) in Lane 2 and 3 and the construction joint at 1500 m in Lane 1 (e.g. ii). (d) Photograph of the field site at chainage 600 m looking southwards, showing localised patched repairs (e.g. iii); a construction joint across (e.g. iv) all three lanes and the change to thin surfacing material (e.g. v).

m to 600 m and 1500 m to 2000 m. The nearest traffic counter to the site operated by the country's roads agency, Highways England, held traffic data for a six-year period from 2011 to 2016. These data revealed no significant fluctuation in traffic flow for that period, with an overall mean average 24-hour traffic flow of 17652 AADT one-way and overall mean percentage of large vehicles of 23.19 %. The texture data relate to Lane 1 the nearside lane and Lane 2, the middle lane of the three-lane motorway. For Lane 1, the test section of road was constructed originally of dense bitumen macadam (DBM) laid on 11th October 1970. On the 27th August 2004 the DBM was replaced with heavy duty macadam (HDM) between chainage 0 m and 600 m. This surface was replaced again on the 1st October 2016 as part of a resurfacing of the lane between chainage 0 m to 1500 m with a thin mastic asphalt (Manual of Contract Documents for Highway Works, 2019). Finally, on the 3rd March 2008 a thin polymer surfacing was laid between chainage 1500 m and 2000 m (Manual of Contract Documents for Highway Works, 2019). In Lane 2 the test section of road was constructed from thin surfacing (Manual of Contract Documents for Highway Works, 2019) laid on 27th August 2004 for chainage 0 m to 600 m, hot rolled asphalt (HRA) laid on 5th April 1998 between chainage 600 m to 1480 m, and older HRA laid on 11th October 1970 chainage 600 m to 2000 m. Road texture data for the pavement surfaces were captured using TRACS (refer to Figure 4.1b), a purpose built road surface survey vehicle (Department for Transport, 2019) over a twenty-four year period . The data were collected on behalf of Highways England as part of the annual maintenance survey of the UK Strategic Road Network, which encompasses the Class-A (Department for Transport, 2012) principal motorways and all-purpose trunk roads within England (Highways England, 2019). The TRACS vehicle was calibrated in accordance with the UK standard (Department for Transport, 2019), to safeguard the quality of data during the stages of data collection, storage and extraction for post processing. The TRACS texture data were obtained at a traffic speed 50 km/h using laser triangulating profile sensors (Zhang et al., 2018). The texture data were measured by TRACS in a 300 mm wide swath, positioned over the nearside wheel track of the lane being surveyed, collecting profiles at approximately 1 mm longitudinal intervals. The TRACS survey vehicle utilises an inertia-corrected global positioning system (GPS) data in conjunction with distance measurements, to reference the location of a texture reading to a longitudinal accuracy of ± 1 m.

4.4. Data processing method

The raw texture depth data reported by TRACS was pre-processed by Highway Agency's Machine Survey Pre-processor (MSP) software to report the SMTD (Transport Research Laboratory, 2006; Department of Transport, 2019). The MSP software prefiltered the raw texture data to remove the effect of vehicle bounce and any random noise signals. The standard deviation of the filtered texture data was then calculated for each 300 mm evaluation

length by the MSP software; before being aggregated to calculate an average texture height for all the evaluation lengths within a 10 m length. The averaged texture height was reported as the SMTD and stored within HAPMS, and essentially represents the root mean square measure of texture depth, both above and below the mean level for a 10m section. The SMTD is distinct from the mean profile depth (International Organization for Standardization, 2019), which measures the height of the highest peak above the mean level. SMTD is used in the UK for texture reporting and has been previously found to be related to MPD by the relationship:

$$MPD = 1.4 \times SMTD^{0.840} \quad \text{Equation 4.1}$$

(Transport Research Laboratory, 2006)

The SMTD data was extracted from HAPMS for the different surveys completed over the twenty-four-year period, and plotted longitudinally, in time series, in years commencing from the initial survey date for each lane. A low pass zero-phase 0.1 m^{-1} wavenumber filter (Gubbins, 2004) was then designed and applied to the SMTD data using MATLAB, to remove high wavenumber (short wavelength) noise from the longitudinal road texture signal. The filtered profiles for each lane have been presented as areal plots with the x-axis as chainage, and the y-axis as a time axis in days from the date of the first survey in the time-lapse sequence. Differencing techniques (Williams, 2012) have also been applied to the filtered SMTD data to reveal the change in road surface condition with time. The baseline SMTD data from the initial survey was removed from the later survey results to illustrate change, and cumulative change was also aggregated by finding the mean rate of change in days over each time epoch. The long-term rate of change in SMTD for the surfacing in each lane section was characterised by fitting a linear regression with a 95 % prediction interval to scatter plots of SMTD against time in days from the initial survey. Finally, wavenumber amplitude spectra were calculated using a Fast Fourier Transform designed in MATLAB (Bloomfield, 2004). The wavenumber amplitude spectra were used to characterise the dominating wavenumbers within the data. Examining the spectra, the dominating wavenumbers occurred within a band of between 0.01 m^{-1} and 0.035 m^{-1}. Consequently, a 0.01 m^{-1} to 0.03 m^{-1} band-pass wavenumber filter, with a gentle ‘roll off’ on either side was applied to the filtered SMTD data. This second filter attenuated the high and low wavenumber signals within the SMTD data. The results for each survey date were plotted longitudinally, in time series, in years commencing from the initial survey date.

4.5. Validating results and discussion

4.5.1 Filtered road texture time series data

The processed SMTD data were validated against maintenance records held in HAPMS for the two lanes. Figure 4.2a shows the SMTD for the different surveys completed over the twenty-four-year period, for which Lane 1 have been plotted in time series (years) from the initial survey date of the 1st April 1995 (refer to Figure 4.2b). The low pass zero-phase 0.1 m^{-1} wavenumber filtered SMTD data are shown in Figure 4.3 and Figure 4.4 for Lane 1 and Lane 2 respectively. Plotted in time series (days) the data for Lane 1 clearly delineates the construction joints at chainage 600 m (refer Figure 4.1d) and chainage 1500 m (refer to Figure 4.1c). Furthermore, the change in colour of Section 1 from broadly keppel and yellow colour tones to blue just before 4000 days (refer to Figure 4.3 (i)), and just after 8000 days (refer to Figure 4.3 (ii)) indicates there has been a marked change in road surfacing. This matches the HAPMS construction records for Lane 1, that confirm a heavy-duty macadam was laid on the 27th August 2004 and a thin mastic asphalt on the 1st October 2006. The change to thin mastic asphalt just after 8000 days is again evident in the colour sequencing extending into Section 2. Similarly, for Section 3 there is a change in colour tones between typically cyan shades to deep blue at a time epoch 5000 days. This is again validated by the HAPMS construction records, which record that a thin polymer surfacing was laid at this location on the 3rd March 2008. Universally, the spatially plotted filtered SMTD data was shown 'roughing-up' or having increased texture depth through the lifetime of each surface, with plot colours progressing to become more yellow with time prior to resurfacing. A general trend of increase in SMTD in this manner matches the recent findings of Plati and Pomoni (2019).

Correspondingly, for Lane 2 of the M6 motorway, the low pass zero-phase 0.1 m^{-1} wavenumber filtered SMTD data clearly indicate that the road texture is increasing in roughness with the passage of time for Section 1 and Section 2. Section 1 demonstrates a typical increase in road texture from 1.5 mm to 2 mm, and Section 2, 2.0 mm to 2.5 mm respectively. In a similar manner Section 3 (refer to Figure 4.4) of Lane 2 demonstrates some increase in roughness from the 2000 days epoch, starting at approximately chainage 1900 m, with road texture increasing from typically 1.6 mm to 1.9 mm. The spatially represented data depict the construction joints at chainage 600 m and chainage 1480 m shown in Figure 4.1 (c) and (d). Additionally, the change in colour of Section 1 (refer to Figure 4.4) of the road, from predominately turquoise (representing road texture of 2 mm) to blue (representing road texture of 1.2 mm) between the zero and 500 days epoch, indicates that there has been a change in road surfacing between the first survey and the second survey on 11th June 2005 (refer to Figure 4.4 (i)). This is consistent with both the construction records for this section of the road

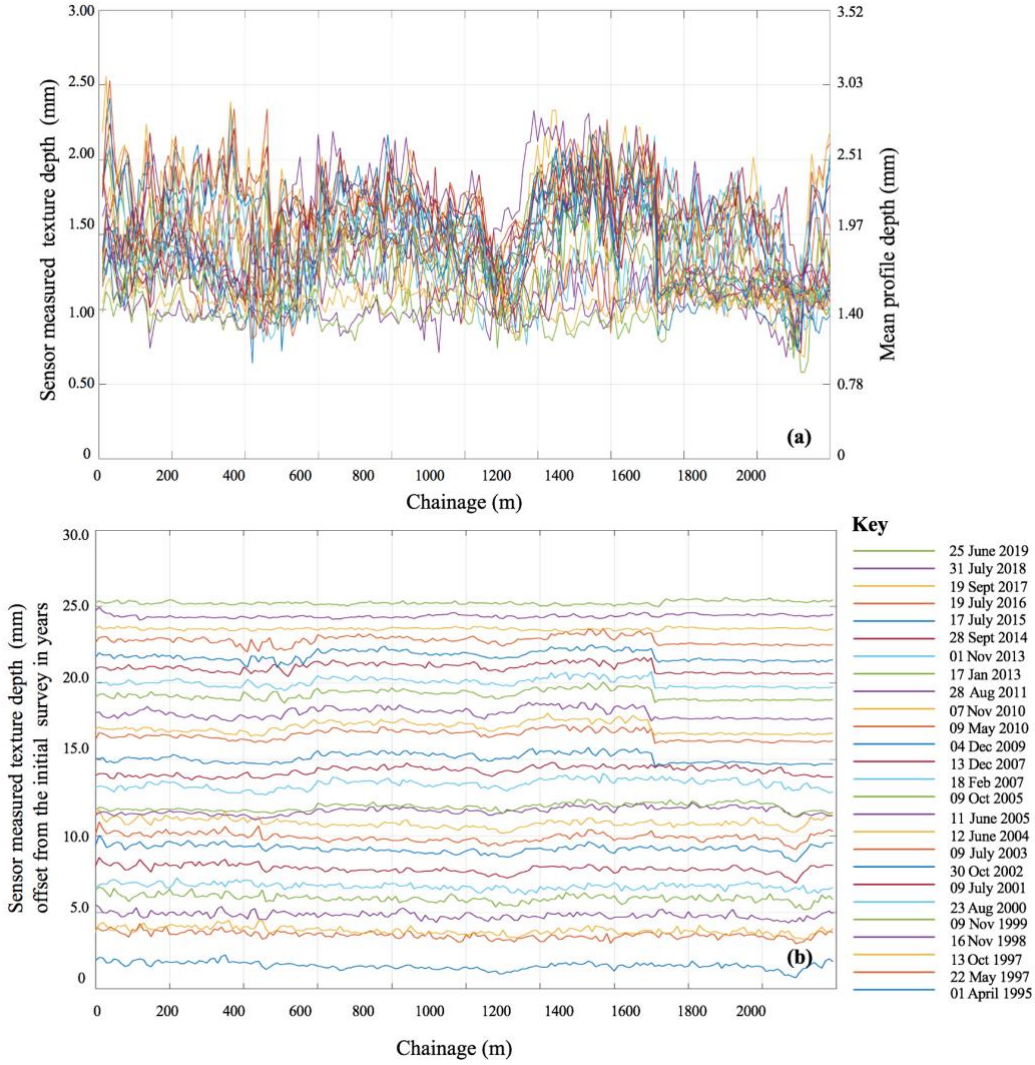

Figure 4.2. Raw Data: (a) Sensor measured texture depth data for Lane 1 of the northbound route of the M6 motorway in Cumbria, UK. (b) Sensor measured texture depth data represented spatially, in time series, in years.

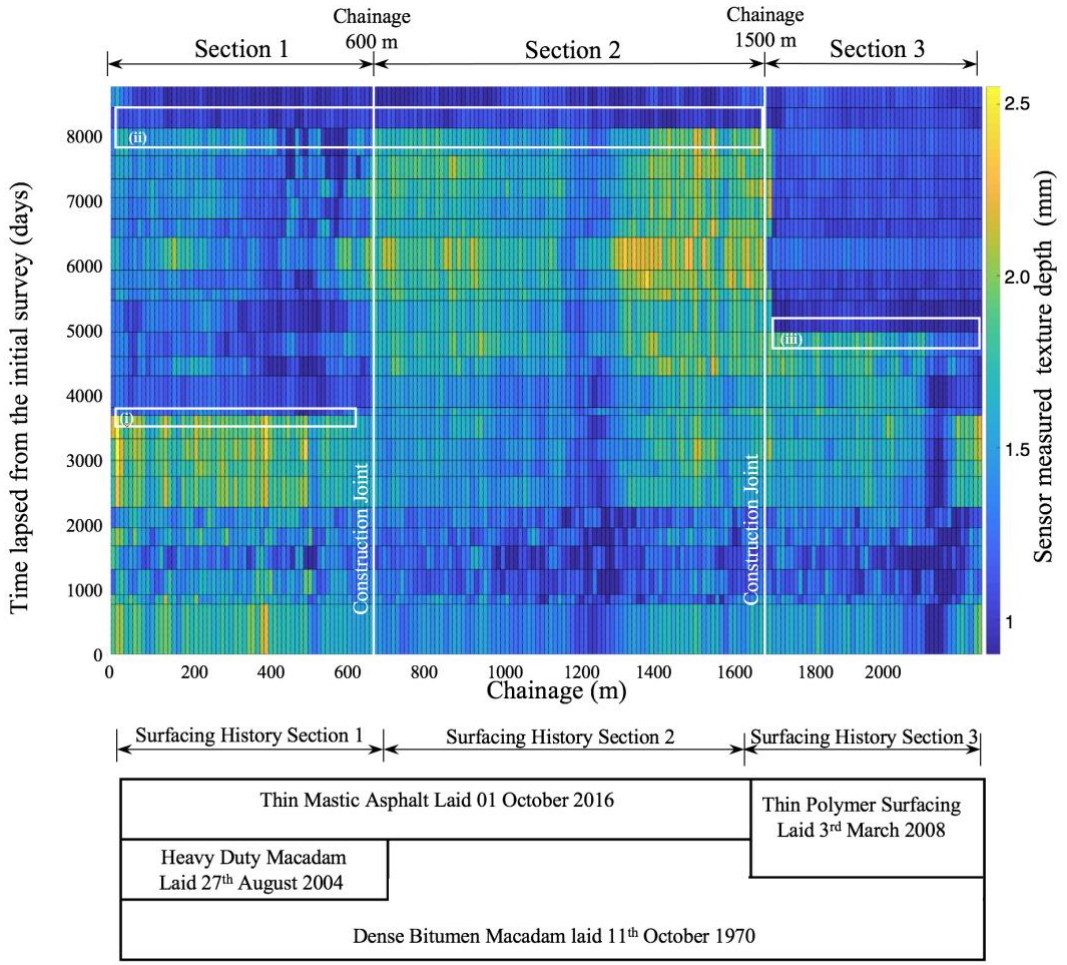

Figure 4.3. 0.1 m^{-1} Wavenumber Filtered Time Series Sensor Measured Texture Data Lane 1: (i) indicates a change in road surfacing after the 12th June 2004 survey date. (ii) indicates a change in road surfacing after the 19th July 2016 survey date. (ii) indicates a change in road surfacing after the 13th December 2007 survey date.

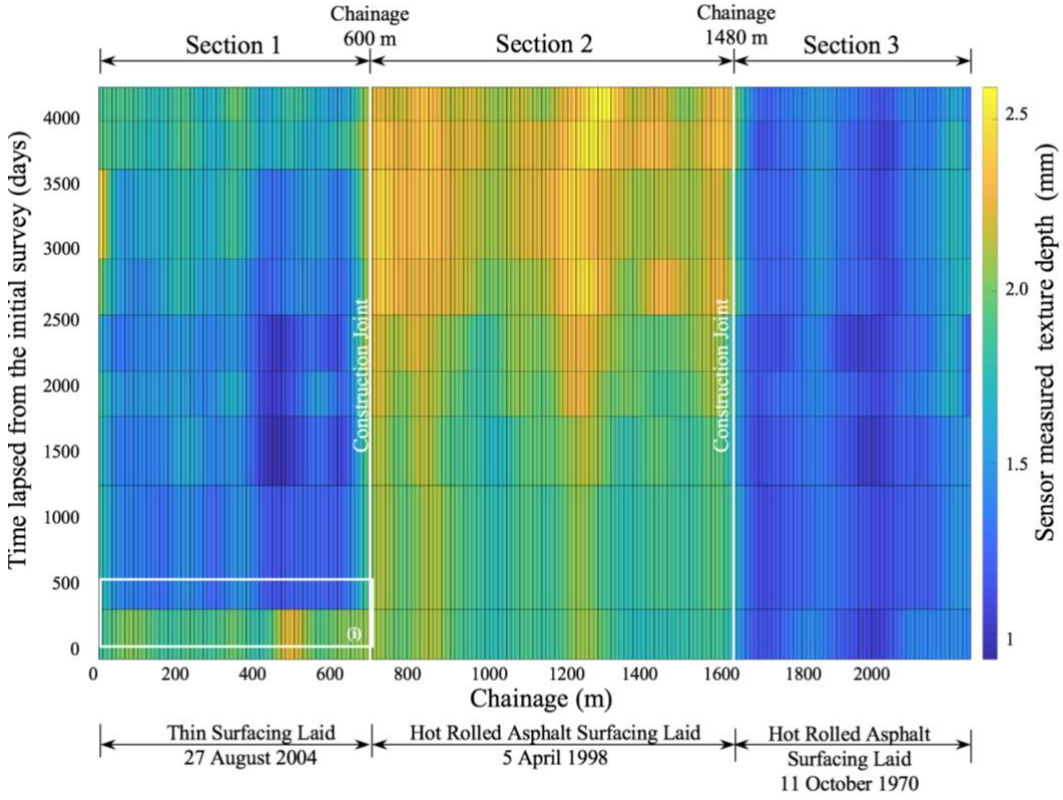

Figure 4.4. 0.1 m^{-1} Wavenumber Filtered Time Series Sensor Measured Texture Data for Lane 2. (i) indicates a change in road surfacing after the first survey date 12th June 2004.

that state a thin surfacing was laid on the 27th August 2004, and the localised patch repairs to the highway surface found in this location (refer to Figure 4.1d). Section 3 of the lane (refer to Figure 4.4) does not appear to have experienced as much road texture wear as the Section 1 or 2. Again, this matches the road conditions found in the field, with the HRA road surface after the construction joint at chainage 1480 m laid at a different date to the HRA between chainage 600m and 1480m (refer to Figure 4.1 (c)). The HRA between chainage 600m and 1480m forms a climbing gradient section of the motorway, ascending uphill towards the summit of a fell in Cumbria. The uphill section of the motorway receives slower moving traffic, as trucks and articulated vehicles climb to the fell crest, and consequently the HRA road surface is likely to experience sustain greater loading with the probable result of an increased rate of texture change (refer to Figure 4.4b). The SMTD of the HRA between chainage 600 m and 1480 m (Section 2) is reported as being deeper, typically 2 mm to 2.5 mm, than the adjacent Section 3 comprised of HRA, where SMTD is typically between 1 mm and 1.5 mm (refer to Figure 4.3). The increase in the SMTD within Section 2 of the study length might indicate a condition failure of the surface, fretting for example may increase texture depth if gaps left by the lost aggregates form a higher overall texture than with the stones present. Finally, the difference in texture between Section 2 and 3 might be attributed to variability in the bitumen penetration index or binder mix between the two road sections (Wu et al., 2012). The bitumen binder mix influences pavement stiffness and can harden with exposure to oxygen and different temperature effects, contributing to variability in the deterioration of the pavement (Visscher and Vanelstraete, 2017). Overall, the results demonstrate that it is possible for the filtered SMTD time series to be plotted spatially and used effectively to visually observe segments of a road surface which are changing at different rates. Within Section 2 of the Lane 2 the changing SMTD appears as yellow bands, which widen progressively with the passage of time. This advance presents the potential for future research to explore the use of visual recognition software to identify ‘change traces’ and establish if they coincide with areas of poor pavement condition in order to improve pavement management systems.

4.5.2 Road texture change data

The mean cumulative change of SMTD for all the sections of the 2 km study length are shown on Figure 4.5b for Lane 1 and Figure 4.6b Lane 2. The mean cumulative change has been plotted spatially against the time lapsed from the initial survey, in days for each lane. The plots reveal the changes in surfacing that have occurred in each lane through time and the location of the construction joints. The figures confirm that the new analysis method make it possible to track the change in SMTD over time, generating useful monitoring data for pavement management systems and underpinning highway maintenance decisions. A long-

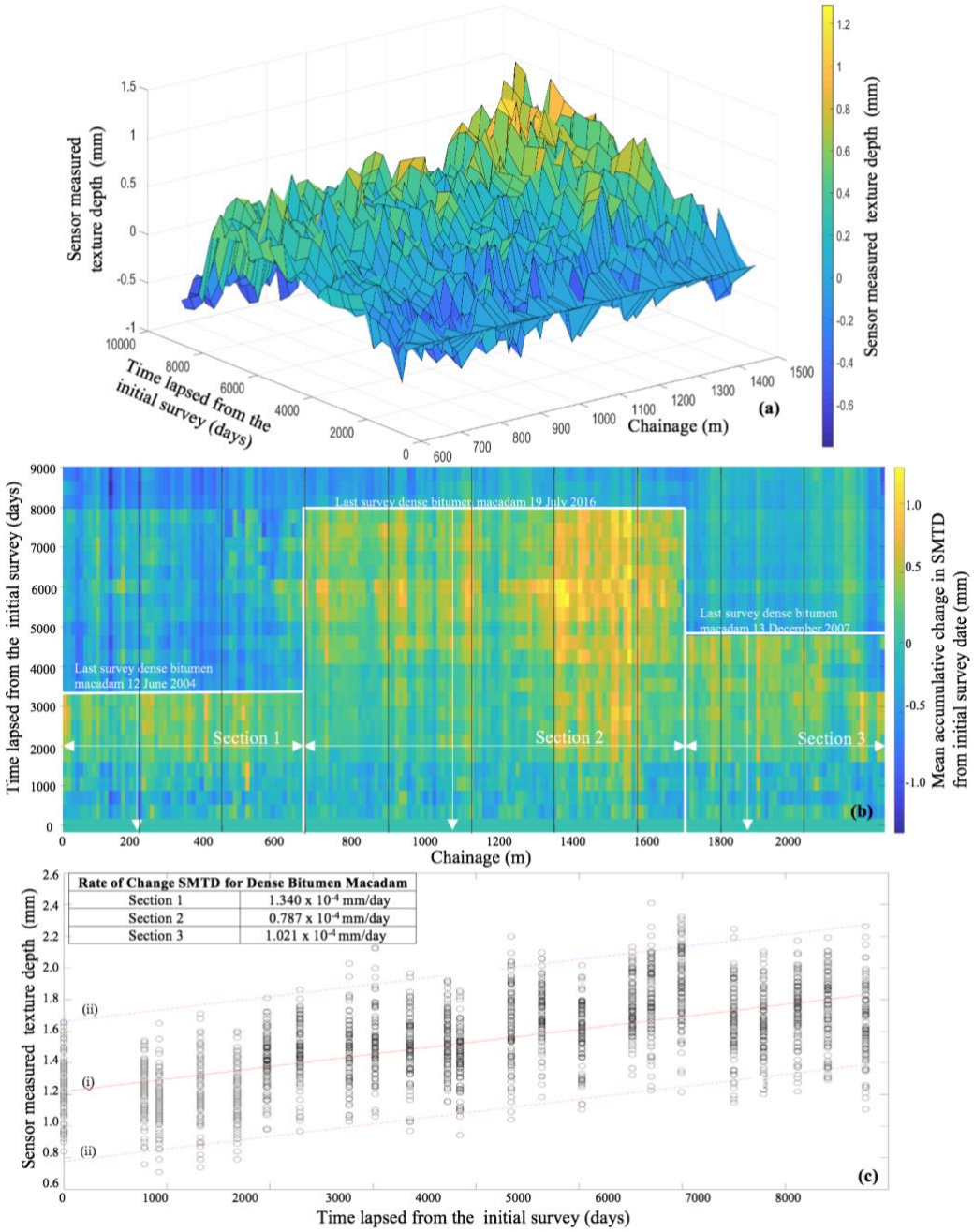

Figure 4.5. Lane 1 Rate of Change of Road Texture with Time: (a) A difference plot of the sensor measured texture depth data for Section 2 of Lane 1. (b) Mean cumulative change in sensor measured texture depth for Lane 1. (c) The change in sensor measured texture depth with time for Section 2 of Lane 1. (i) A linear regression line illustrates the rate of change in sensor measured texture depth. ii) The 95 percent prediction interval.

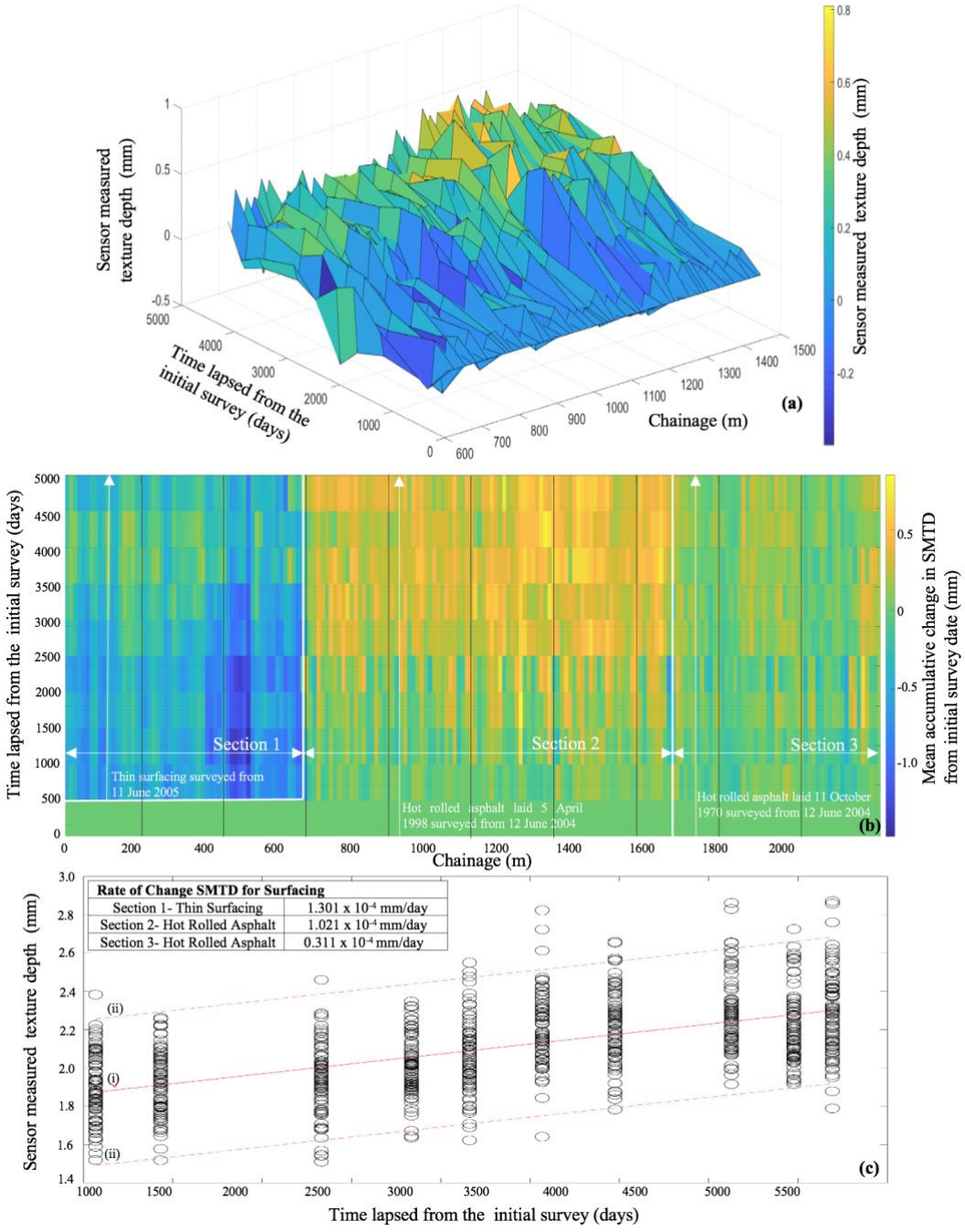

Figure 4.6. Lane 2 Rate of Change of Road Texture with Time: (a) A difference plot of the sensor measured texture depth data for Section 2 of Lane 2. (b) Mean cumulative change in sensor measured texture for Lane 2. (c) The change in sensor measured texture depth with time for Section 2 of Lane 2 (i) A linear regression line illustrates the rate of change in sensor measured texture depth. (ii) The 95 percent prediction interval.

term rate of change for each section of lane has been characterised by fitting a linear regression with 95 % prediction interval to scatter plots of SMTD against time in days from the initial survey (refer to Figure 4.5c and 4.6c). The long-term rate of change is distinct from the evolution of surface texture, characterised spatially on the 0.1 m^{-1} wavenumber filtered times series SMTD data plots (refer to Figure 4.3 and Figure 4.4). In Lane 2 the thin surfacing of Section 1 demonstrates the most rapid rate of long-term change at 1.301 x 10^{-4} mm/day, this might be expected because thin surfacing represents a surface rejuvenation technique and is known by road managers to have a shorter service life. In Lane 2 the HRA in Section 2 is changing at 1.021 x 10^{-4} mm/day, a long-term rate 328% faster than Section 3 at 0.311 x 10^{-4} mm/day over the same time period of 4122 days. Section 2 is an uphill climbing section and is likely to experience sustained greater loading from slower climbing vehicles leading to increased change. Interestingly, in Lane 1 the long-term rate of change for the DBM in the uphill climbing section of Section 2 is 0.787 x 10^{-4} mm/day, and in contrast to Lane 2, is less than Section 3 at 1.021 x 10^{-4} mm/day. However, the long-term rate of change for Section 2 is influenced by the time epoch for section. The DBM remained in-situ as a highway surfacing for 7780 days from the first survey in Section 2, 67 % longer than the DBM surfacing in Section 3 which was replaced after 4639 days. Assessed over the same 4639 day epoch, the long-term rate of change of Section 2 is 1.063 x 10^{-4} mm/day, which is 4 % faster than Section 3, suggesting that that uphill and downhill sections of DBM were wearing at largely the same rate. The DBM in Section 2 Lane 1 is also changing more slowly than the HRA in the same section in Lane 2. The DBM is in the nearside land of the motorway, which is generally accepted to receive a higher proportion of slow-moving heavy vehicles. The slower rate of wear might indicate that the negative texture of the DBM is more favourable to climbing sections of road than HRA long-term, but further research of surfacing of comparable age, over the same epoch would be required at a number of sites to establish if this is the case. Being able to categorise a linear rate of change has unlocked the potential to develop a method for forecasting the future long-term rate of change of SMTD by extrapolation, for highway surfaces at discrete lane locations upon a road network. Thus, enabling legacy data collected annually for 7000 km of the UK Strategic Road Network, relating to SMTD, to be used in predictive planning of texture depth thresholds for essential road repair (Design Manual for Roads and Bridges, 2008; and 2015). Further developing, this method would need to take account of potentially non-linear variables influencing future road conditions such as traffic volumes and weather patterns. Additionally, the long-term rate of change of SMTD might feasibly be adapted to estimate skid resistance in the manner of Plati and Pomoni (2019), were available data enables the minimum cumulative traffic threshold to be established.

4.5.3 Road spectra analysis data

A difference plot of the SMTD data for Section 2 of Lane 1 and Lane 2 (refer to Figure 4.5a and 5.6a) confirms the findings from the filtered time series SMTD data and mean cumulative SMTD change graph , further illustrating the change in road surface condition with time. It is evident that the SMTD becomes rougher with time, and that wavenumber signal also grows larger. Additionally, there is a clear periodicity to the wavenumber signal, represented by the regular sinusoidal signal of the road texture. Greater SMTD change occurs at the peaks of the sinusoidal wave as opposed to the troughs. The amplitude of the periodicity changes at chainage 600 m and 1480 m suggesting that the spaced changes in pavement texture might be triggered as a moving vehicle's suspension passes across a construction joint. Wavenumber amplitude spectra of the SMTD data calculated using a Fast Fourier Transform characterises the periodicity of the sinusoidal wavenumber signal observed in the difference plot (refer to Figure 4.7 (a)). The wavenumber spectra have three clear bimodal shape peaks occurring between wavenumber 0.01 m^{-1} to 0.035 m^{-1} respectively, demonstrating that the signal is dominated by wavelengths within this wavenumber banding. Accordingly, a 0.01 m^{-1} to 0.03 m^{-1} band-pass wavenumber filter was applied to the SMTD data to attenuate the high and low frequency wavenumber signals within the raw data. Figure 4.7b illustrates the band-pass filtered SMTD data for each survey represented temporally on the y-axis, in time series, in years commencing from the initial survey date of the 12th June 2004. The filtered data have a periodicity extending systematically through the eleven years of survey data analysed. The invariant nature of the periodicity through time suggests that the unevenness might be constructed into the road (possibly as a consequence of the use of highway paving plant), or perhaps imprinted during its early history after construction.

The periodicity is associated with a wavelength typically of between 33 m and 62 m, which represent the location of the two highest peaks (Peak A and Peak B, Figure 4.7a) of the spectral analysis at wavenumbers of 0.0163 m^{-1} and 0.0305 m^{-1}. It is known that the suspension systems of heavy vehicles such as a buses and trucks apply a cyclic loading to a pavement surface via the tyre-road interaction. The suspension system of a large vehicle such as a bus, can be simplified to a spring-mass-dashpot model and for a bus has previously been shown to have a resonance frequency of around 0.5 Hz (Sekuic and Dedovic, 2011). At this resonance, the tyres of a vehicle travelling at a speed of 96.56 km/h would apply a cyclic load to a pavement surface with a wavelength of 53.6 m. On climbing sections of motorway, heavy vehicles such as trucks or buses tend to travel more slowly, and this would shorten the distance between the application of each tyre load; for example, at 72.42 km/h a truck or bus with a suspension system operating at 0.5 Hz would apply a load every 40 m. As the periodicity observed at the study site was banded with wavelength between 33 m to 62 m, a plausible causation theory is

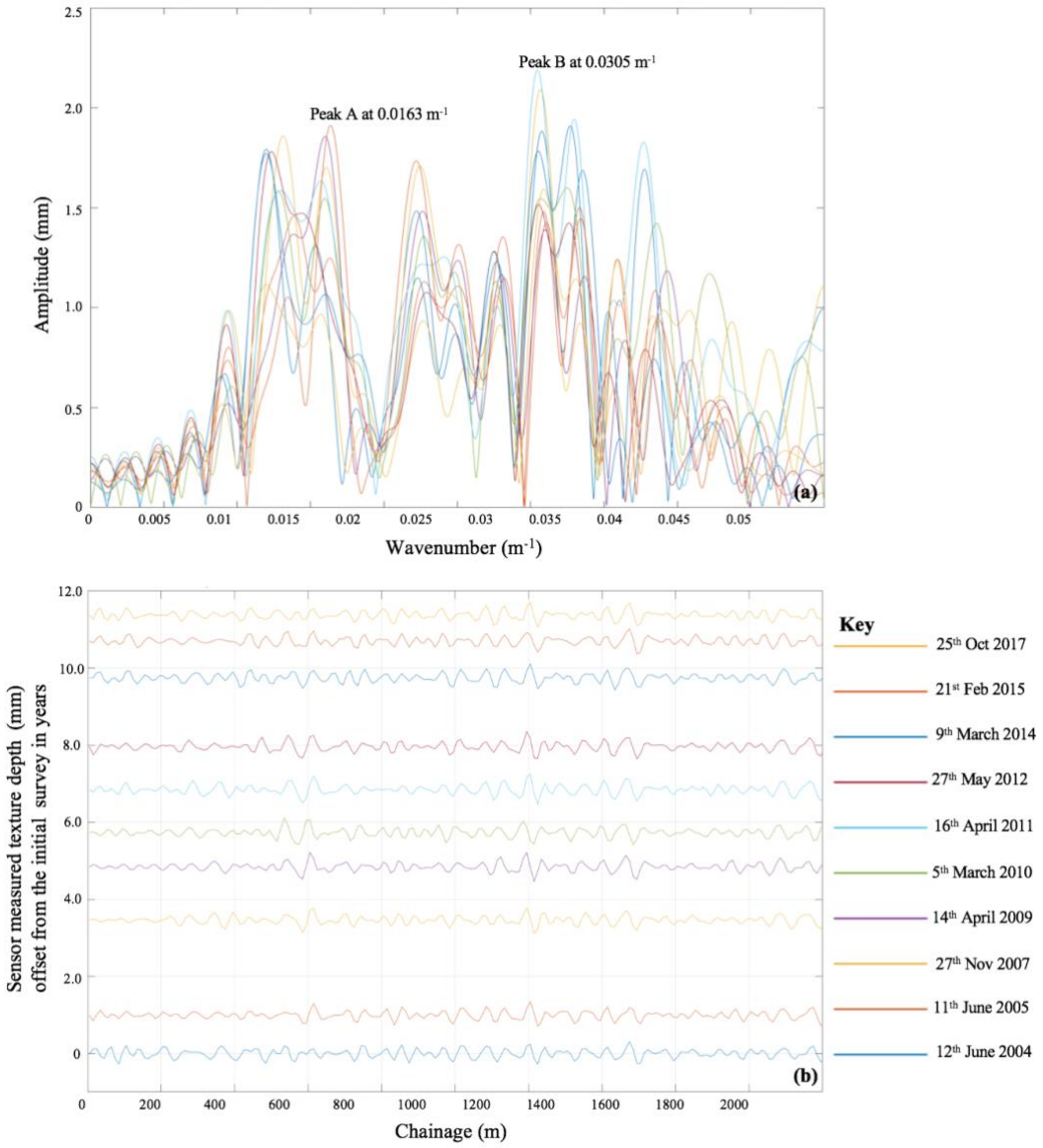

Figure 4.7. Spectra Analysis and Band Pass Filtered Data: (a) A 0.1 m^{-1} wavenumber low pass 1D spectral analysis of the sensor measured texture depth data for Section 3 Lane 2 (b) A 0.01 m^{-1} to 0.03 m^{-1} band pass wavenumber filter with a gentle 'roll off' on either side has been applied to the sensor measure texture depth data for Lane 2.

that the cyclic loading of heavy vehicle suspension systems has imprinted the undulating wavelengths into the road surface early in the road's life. Imprinting may have arisen through a process of the intermittent-localised compaction of the lower pavement layers or the pavement surface when the bitumen matrix becomes marginally softer in the warmth of the summer. The periodic features observed are systematically well-organised, meaning that the heavy vehicles such as trucks or buses would have to be in phase with each other when driving along the pavement surface, which is what would be expected. Synchronisation of traffic flow is a recognised phenomenon (Kerner, 2018) and in phase movement of vehicle suspension in traffic flow could be triggered by an irregularity such as a bump or more likely a construction joint within the road. Indeed, Figure 4.7b shows a step in the periodicity features occurring at both chainage 600 m and chainage 1480 m, which coincide with known construction joints for Lane 2. Conceivably, the construction joints act as triggers at consistent points on the route, exciting high amplitude resonances within the suspension systems of the travelling vehicles and leading them to move up and down in phase with each other. Subsequent change in the pavement surface through compaction arising from the cyclic tyre load, would reinforce the resonant excitation of the heavy vehicle and thus maintain them in phase with one another. The proposed influence of the cyclic tyre loading action of the heavy vehicles to the pavement is supported by Figure 4.5a and Figure 4.6a which shows change of SMTD generally coinciding with the peaks of the periodicity features, and this change being amplified with time suggesting consistent and progressive tyre-pavement interaction at these locations.

The influence of trafficking on the development of SMTD upon a road surface is further illustrated by comparing the wavenumber amplitude spectra for Section 2 of Lane 1 and Lane 2 (refer to Figure 4.8a and 4.8b respectively). Lane 1 clearly contains more signal frequencies than Lane 2 demonstrating a greater mix of vehicle loading conditions in the more congested nearside lane of the motorway, arising from cars and heavy goods vehicles travelling at different speeds. The amplitude of the wavenumber spectra signal rises steeply at 0.01^{-1} m delineating the start of the dominance of wavelengths at 100 m. Cars have been shown to have a resonance frequency of between 1 to 2 Hz (Barbosa, 2012). A car travelling at 144.84 km/h, a typical speeding velocity for a performance vehicle in the UK, with a median frequency of 1.4 Hz, will have a wavelength of 100 m. Figure 4.8a has three dominant peaks; Peak A at 0.0167 m^{-1} and Peak B at 0.0208 m^{-1} correspond to wavelengths of 60 m and 48.2 m respectively. These signals might be introduced to the SMTD as discussed before by a heavy vehicle with a resonance frequency of 0.5 Hz travelling between 86.76 km/h and 108 km/h. The Peak C at 0.0274 m^{-1} matches a wavelength of 36.4 m and equates to a car travelling at 131 km/hr again with a resonance frequency of 1.4 Hz. The comparison of wavenumber amplitude spectra reinforces the potential effect of cyclic tyre load action on the highway

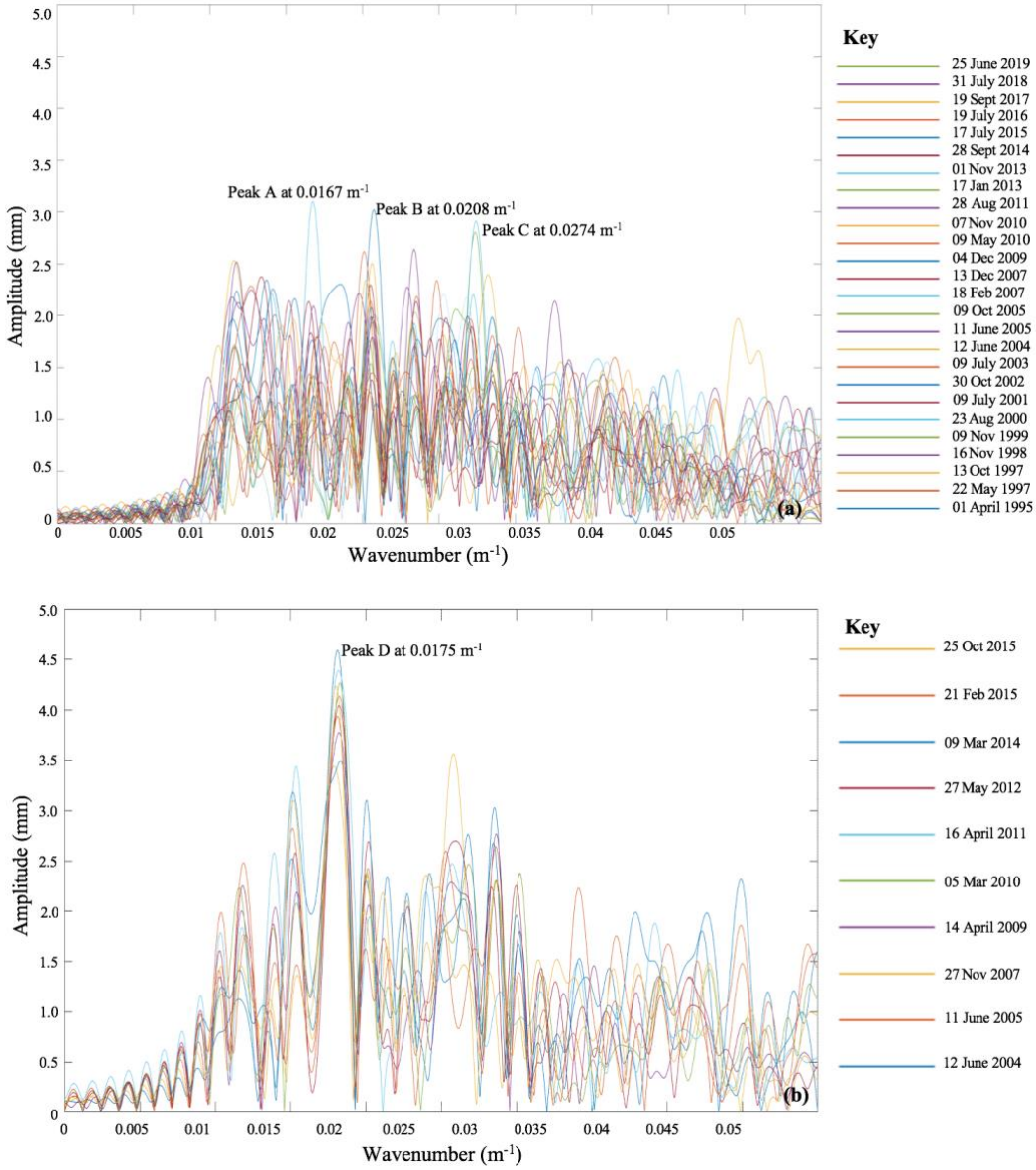

Figure 4.8. Comparison of Spectra Analysis Data for Section 2 of Lane 1 and Lane 2: (a) A 0.1 m^{-1} wavenumber low pass 1D spectral analysis of the sensor measured texture depth data for Section 2 Lane 1. (b) A 0.1 m^{-1} wavenumber low pass 1D spectral analysis of the sensor measured texture depth data for Section 2 Lane 2.

surface by different vehicle types. The influence of cyclic tyre load action from the initial findings of this studying characterising dominant wavelengths and discovering a periodicity in SMTD, suggest that further research in this field is warranted. If vehicle suspension systems are found to influence texture evolution through cyclic tyre loading, then this will have implications for the future design of highway pavements.

4.6. Conclusion

In conclusion, the paper has provided rare and a valuable long-term study of SMTD. A new computational process has been developed and applied to reveal a number of key and important trends influencing long term change in pavement texture as follows:

- It is possible for wavenumber filtered SMTD time series time-lapse data to be used to visually observe discrete segments of a road surface which are changing with time.

- Change 'traces' are evident within the wavenumber filtered SMTD time series. This presents the potential for further research to use visual recognition software to identify change 'traces' in order to locate areas of poor pavement condition.

- The study presents a viable method to track the rate of change of SMTD over time, generating essential monitoring data for pavement management systems and highway maintenance decisions.

- The long-term rate of change in SMTD could be used to predict the useful working life of a pavement surface and to predict when maintenance or preventative interventions will be necessary.

- At unevenness scale a periodicity is observable in the data systematically through time, suggesting that unevenness might be imprinted into a road surface during construction or early in its life.

- A plausible theoretical cause of the observed unevenness periodicity is that it is 'imprinted' in the early life of the pavement. 'Imprinting' may occur as a consequence of cyclic tyre loading applied by the suspension systems of heavy vehicles.

- Construction joints in pavement surfaces, in combination with vehicle travel speeds, have the potential to trigger periodically spaced change in pavement texture.

Chapter 5.0: Published Paper 3 – Seasonal signals observed in non-contact long-term road texture measurements.

5.1. Abstract

Texture is required on road pavements for safe vehicle braking and manoeuvres. This paper provides a unique analysis of long-term texture obtained using TRACS (TRAffic Speed Condition Survey) data from fourteen sites, located along a north to south transect spanning the longest highway in the UK. 19 years of Sensor Measured Texture Depth (SMTD) data have been analysed using spatial filtering techniques and compared with meteorological and traffic datasets. The results for hot rolled asphalt (HRA) surfaces reveal that changes to SMTD follow a linearly increasing trend with time. The 'rate of change' is influenced by the order of magnitude of annual average daily traffic (AADT), when factored for the percentage of heavy goods vehicles. This linear trend is disrupted by environmental parameters such as rainfall events and seasonal conditioning. In the summer this signal is evident as a transient peak in the 'rate of change' of texture greater than 0.04 mm, and in the winter as a reduction. The transient changes in texture corresponded to above average rainfall occurring in the week prior to SMTD measurement. The signal observed demonstrates an inverse pattern to the classically understood seasonal variation of skid resistance in the UK, where values are low in the summer and high in the winter. The findings demonstrate for the first time that texture measurements experience a seasonal signal, and provide compelling evidence pointing toward surface processes (such as polishing and the wetting and drying of surface contaminants) causing changes to texture that are affecting seasonal variation in skid resistance.

5.2. Introduction

Road surface texture is fundamental to safe manoeuvres by vehicles on pavement surfaces (Meegoda and Gao, 2015). Texture has previously been defined as having four increasing scales: microtexture, macrotexture, unevenness and megatexture (International Organisation for Standardisation, 2019). Microtexture and macrotexture are known to influence skid resistance, i.e. the friction available between the tire and a road surface (Klüppel and Heinrich, 2000; Moore, 1975; Persson, 2013). Therefore, the presence of adequate pavement texture is actively monitored on highway networks by road agencies (Múčka, 2017). Unevenness, megatexture, and macrotexture are routinely monitored at traffic speed, using laser profile sensor techniques and cameras mounted on specialist vehicles (Peraka and Biligiri, 2020). Conversely, the frictional response to microtexture and macrotexture, whilst also surveyed at traffic speed using specialist vehicles, adopts techniques that make contact with a pavement in order to measure skid resistance. These contact techniques frequently make use of a fixed

slip rate of braking test wheel (Kogbara et al., 2016). Skid resistance measurements have been shown by previous researchers to be influence by a number of interrelated parameters, such as temperature, speed, presence of contaminants on the road surface, tire tread thickness and viscoelastic deformation (Kane and Edmondson, 2020, 2018). A particular problem to government authorities, road agencies, asset manager and engineers seeking to make decision on pavement surface maintenance priorities using skid resistance measurements is the phenomena of seasonal variation in skid resistance. Seasonal variation in skid resistance is the term used to describe short-term variability in skid resistance readings throughout a year (Wilson, 2013). Typically, skid resistance values are found to be lower in summer months and higher in winter months (Kogbara et al., 2016). This phenomena of seasonal variation in skid resistance is well reported in many countries across the world (Bijsterveld and Val, 2016; Jayawickrama and Thomas, 1998; Oh et al., 2010; Pomoni et al., 2020), and has been recognized as an issue for eight decades (Kogbara et al., 2016). Additionally, seasonal variation can lead to inter year variability in skid resistance measurement which resulted in some road agency guidance seeking to statistically adjust measurement to be in line with previous years, in order to successfully manage pavement surface assets over the longer term (Design Manual for Roads and Bridges, 2021; Múčka, 2017).

The cause of seasonal variation in skid resistance has been linked to a number of theories. One hypothesis is that skid resistance is caused by changes to surface processes (Ahammed and Tighe, 2009). In the summer months, fine dust and debris builds up on the roads, which is continually ground up under the action of tires and polishes the surface. This polishing effect is believed to lead to smoother surface and reduced skid resistance values. Conversely, in the winter fine dust is more easily expurgated from the pavement texture, resulting in coarse debris dominating the surfaces (Wilson, 2013). The presence of primarily coarse debris leads to pavement surfaces becoming rougher leading to higher skid resistance readings (Kennedy et al., 1990). Another hypothesis involves the temperature of the measuring wheel making the contact measurement for skid resistance, suggesting that the tire will be stiffer during winter months leading to higher readings (Kennedy et al., 1990). Alternatively, links have been suggested with meteorological conditions, with some researchers finding that friction readings are higher after periods of rainfall (Henry, 2000), due to the washing away of debris and contaminants from the pavement surface. Cumulative rainfall in the week preceding measurement has previously been found to be significant, with a linear trend being observed with skid resistance measurement (Bijsterveld and Val, 2016). Conversely after prolonged dry spells the same study observed a linearly decreasing trend.

The inter year deviations and seasonal variation of skid resistance has led some researchers to investigate the reliability of non-contact methods of measurement (Edmondson et al., 2019). The optimization of reliable, consistent, non-contact measurements to collect macrotexture and microtexture has been sought primarily for two reasons: 1) to model frictional skid resistance (Kane and Edmondson, 2018); and 2) to inform maintenance decisions on where texture depth has reached a minimum threshold level requiring retexturing or pavement renewal on road networks (Abbondati et al., 2021; Design Manual for Roads and Bridges, 2020). The International Roughness Index (IRI) is widely used for this purpose, with acceptable IRI threshold levels specified on a country-by-country basis for new, reconstructed and rehabilitated roads (Múčka, 2017). Recent, research has also suggested that texture readings can enhance maintenance planning by estimating long-term 'rates of change' from legacy data as a guide to predicting the future evolution of texture on pavement surfaces (Edmondson et al., 2020). Several parameters related to vehicle type and traffic flow have been proven to have an effect on the state of texture evolution. The controlling principal is the cumulative action of loads applied by the passage of different types of vehicle across a road surface in a given time period; often expressed as Equivalent Standard Axles (Bagui et al., 2013). Other factors relate to tire features, and tire inflation pressure which have been shown to influence the transverse application of load to a surface (Do et al., 2009, 2007; Vaiana et al., 2012).

An overarching aim of the research community has been understanding the correlation between frictional skid resistance and macro and microtexture measurements made in the field. Working towards this aim, recent research reported on a section of highway in Croatia, before and after a programme of renewal, found a correlation between the level of pavement macrotexture and skid resistance (Pranjić et al., 2020). Furthermore, an investigation considering eleven years of field data for a road section, found after a threshold level of cumulative traffic flow that the evolution of macrotexture increase with time whilst skid resistance decreases (Pomoni et al., 2020). However, there remains a paucity of data on the potential for seasonal signals to present in macrotexture measurements. The longest study to date considered a six-year period, however this study did not consider measurements obtained in the field from an operational live highway (Wang and Flintsch, 2007). This paper provides a unique analysis of long-term texture obtained over 19 years for fourteen sites located on the A1(M); the UK's longest north to south transecting highway. Data are obtained from operational surveys using TRACS (TRAffic Speed Condition Survey) measurements, as part of annual pavement monitoring undertaken by Highways England. Sensor Measured Texture Depth (SMTD) data are analysed using novel spatial filtering techniques and compared with

meteorological and traffic data sets to produce long term evolution trends, and first compelling evidence of seasonal conditioned events in macrotexture measurements.

5.3. Methods

5.3.1 Selecting the sites and legacy data

The study considers legacy raw texture depth data captured using TRACS, a purpose-built road survey vehicle (Department for Transport, 2019), over a 19-year period, commencing from the 11th August 1998. The data were collected on behalf of Highways England as part of the annual maintenance survey of the UK Strategic Road Network (SRA) (Highways England, 2020). The TRACS vehicle was calibrated in accordance with the UK Standard (Department for Transport, 2019), to safeguard the quality of data during the stages of data collection, storage and post processing . The TRACS texture data were obtained at a traffic speed of 50 km/h using laser triangulating profile sensors (Zhang et al., 2018). The texture data were measured by TRACS in a 300 mm wide swath, positioned over the nearside wheel track of the lane being surveyed. The vehicle has inertia-corrected global positioning system (GPS) data in conjunction with distance measurement, to reference the location of a texture reading to a longitudinal accuracy of ± 1m. Texture data were obtained for 15 sites located on the A1(M). At 659.8 km it is the longest north to south highway in the UK, connecting Edinburgh with London. Study sites were selected where long-term (typically >12 years) legacy data were available for the same surface material. Hot rolled asphalt (HRA) surfaces were selected as they have been used widely on the SRA and thereby provide the largest, longest and most representative dataset. HRA is a dense gap graded asphalt, with bitumen coated 20 mm aggregate rolled into the surface (UK Government, 2019).

Sites were selected for comparison in the North and South of England, to allow the greatest potential differences in traffic flow and meteorological conditions for study purposes. Sites were also selected at locations with traffic counters. Ten suitable sites were identified in the North of England located at approximately 20 km intervals (refer to Figure 5.1a) and four in the South of England (refer to Figure 5.1b). Fewer sites were available in the South due to frequent resurfacing, disrupting the availability of consistent long-term records for a single surface material. The A1(M) varies along its route from one to four lanes. Data for the sites were collected from the inside lane of the southbound side of the A1(M). The southbound inside lane was considered more likely to have the heaviest traffic usage being the lane favored by HGVs. The mean average length of the inside southbound lane considered at each site was 800 m. The raw texture depth data captured by TRACS for these sites were preprocessed by the Highway Agency's Machine Preprocessor and stored as SMTD in the Highways England

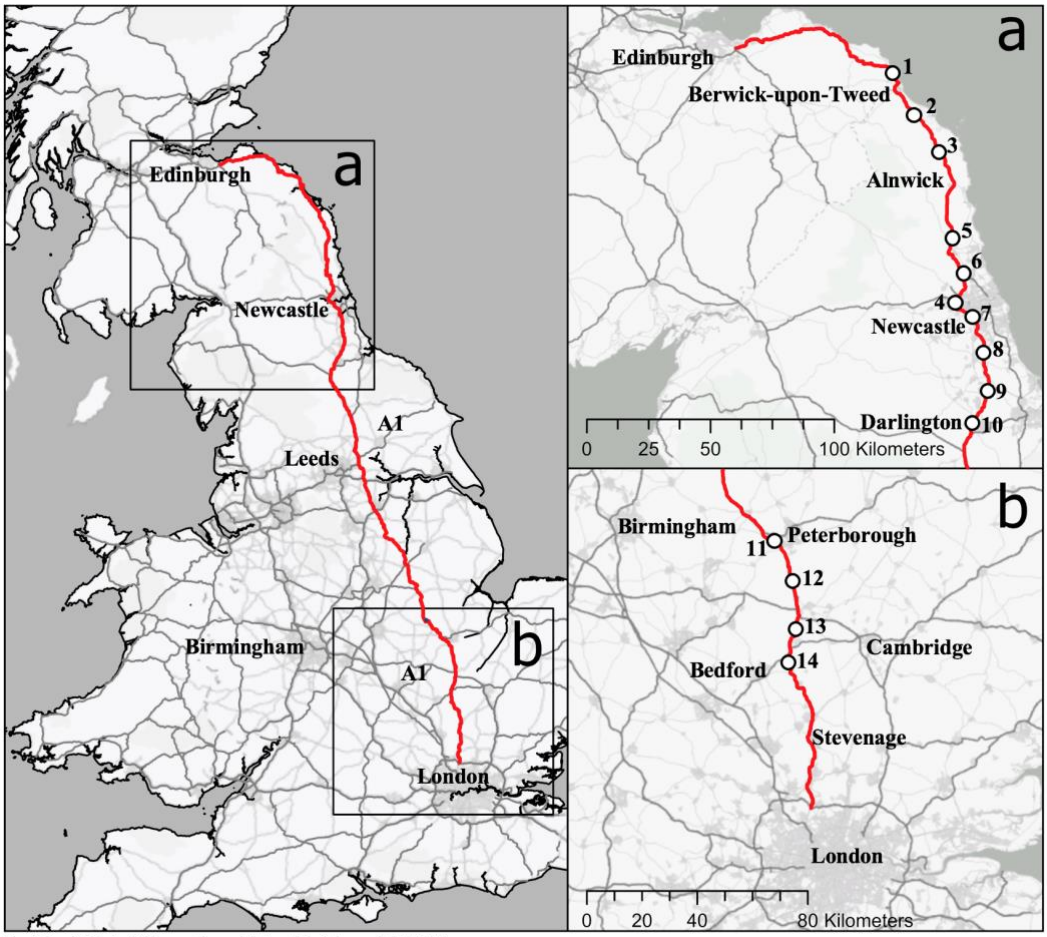

Figure 5.1. Location of the study sites on the A1 in the United Kingdom. (a) the northern sites (b) the southern sites

Pavement Management System (HAPMS) (Department for Transport, 2019), for a 300 mm evaluation length at 10 m intervals as previously described in (Edmondson et al., 2020). SMTD is used in the UK for texture reporting and has previously been found to relate to Mean Profile Depth (MPD) by the relationship (Viner et al., 2006):

$$MPD = 1.4 \times SMTD^{0.840} \qquad \text{Equation 5.1}$$

5.3.2 Data processing of the SMTD data

Once extracted from HAPMS, a 0.1 m^{-1} low pass wavenumber filter (Gubbins, 2004) was then applied to the SMTD using mathematical programming software (Mathworks, 2018) at each 10m interval to remove high wavenumber (short wavelength) noise from the longitudinal road texture signal. The mean SMTD data over the overall lane chainage considered at each TRACS epoch were then calculated and plotted for each site to show the long-term evolution of SMTD through time. The mean bias of the 5th epoch data point for each site was then calculated and removed from the filtered mean SMTD to normalize the data.

5.3.3 Comparison of SMTD with traffic Flow

The rate of change in SMTD data was compared with both Annual Average Daily Traffic (AADT) flows and HGV AADT flows; and linear best fit lines added to the plotted data. To determine the variability in these data the rate of change was characterized both for the full time period of SMTD measurement available at an individual site, and for the linear trend occurring between the pronounced 'troughs' at point (i) and (ii) on Figure 5.2 for the northern sites and point (i) and (ii) on Figure 5.3 for the southern sites.

A decadal AADT was calculated from WebTRIS Highways England Traffic (Highways England, 2020) flow data, to differentiate the traffic flow usage at the different sites on the A1(M). The data were collected using a series of fixed induction loop road sensors. The AADT flows were calculated from the latest available data (from 1st January 2010 to 31st December 2019), there was no significant fluctuation in AADT flows over this period at individual sites. Finally, the AADT flows were factored by the mean percentage of HGVs, calculated from the annual HGV percentage figures for the same period.

5.3.4 Seasonal analysis

A 7th order polynomial best fit line was applied to the filtered mean SMTD for each site to model the long-term trends of texture evolution. Lower order polynomials were tested, but the 7th order was found by observation to best represent the evolution of mean SMTD for sites. The deviations of mean SMTD from the long-term trends were then characterized. 'Troughs'

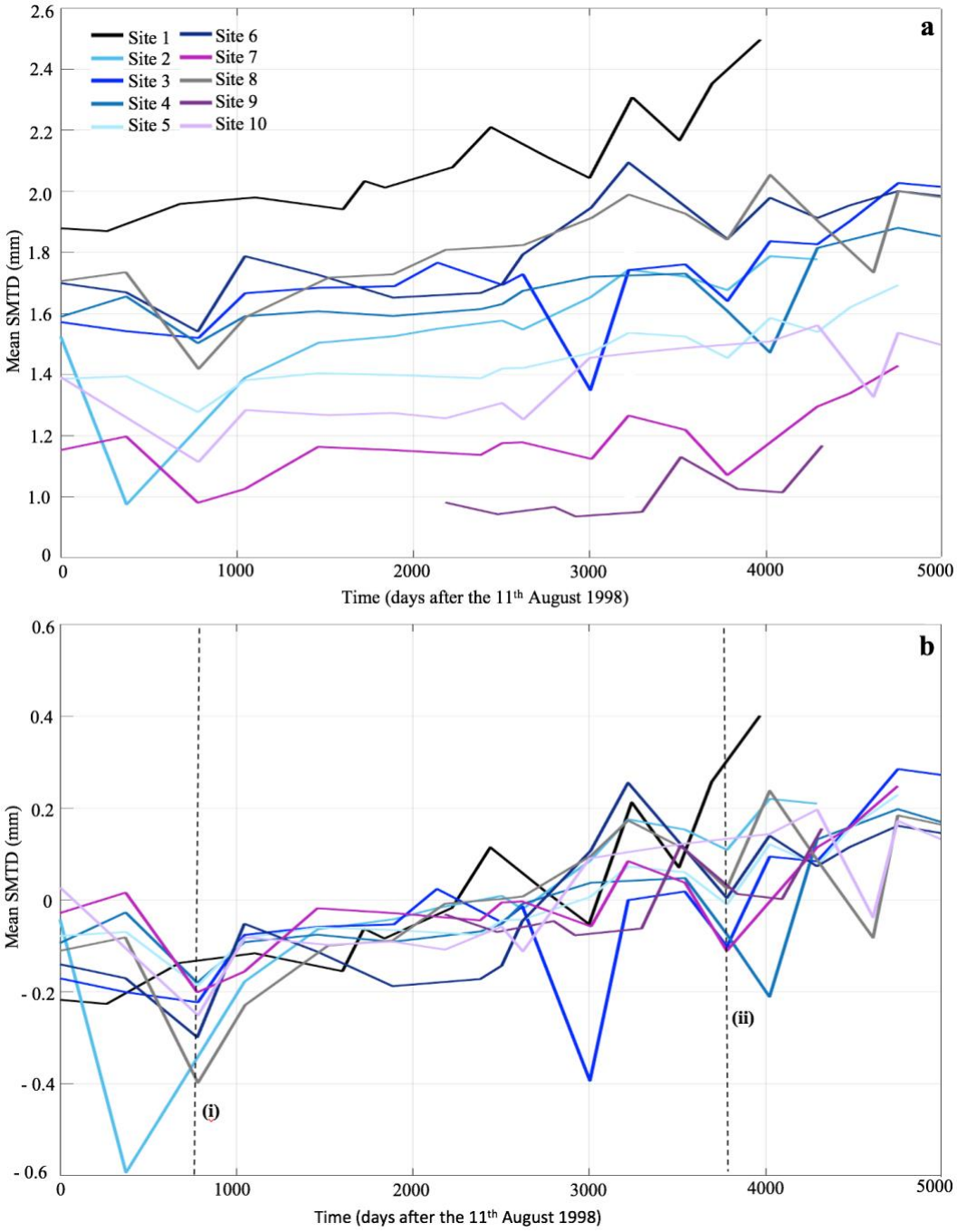

Figure 5.2. (a) Filtered mean Sensor Measured Texture Depth (SMTD) data for the northern sites on the A1. (b) Normalized mean SMTD data for the northern sites on the A1. The mean bias of the 5th data point value has been removed from the data. (i) and (ii) are 'troughs' in data coinciding with severe rainfall events.

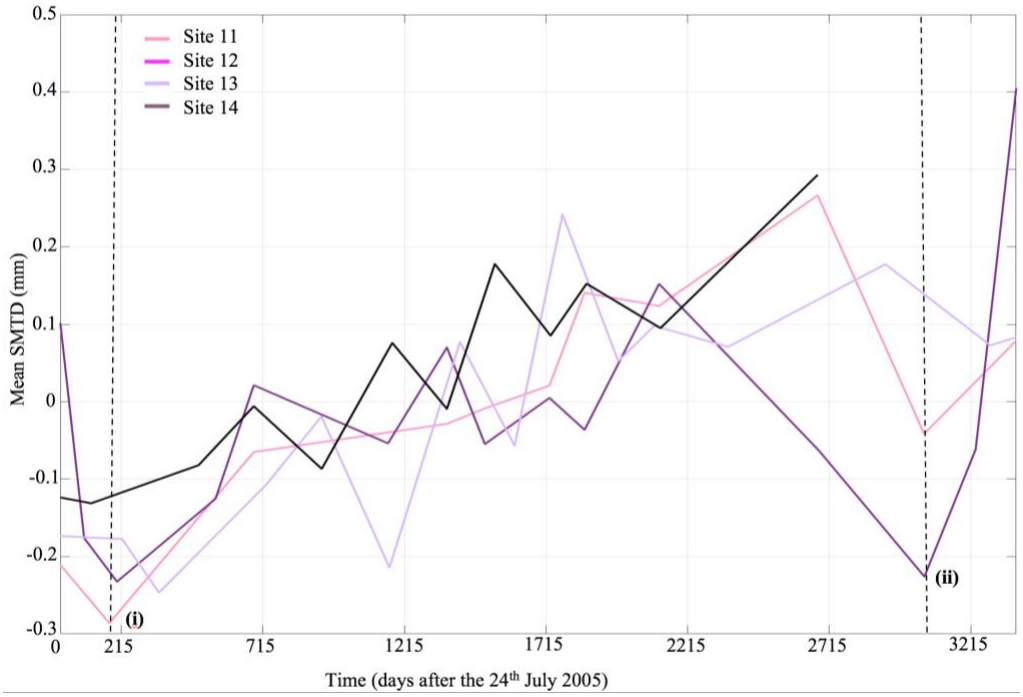

Figure 5.3. Normalized mean Sensor Measured Texture Depth (SMTD) data for the southern sites on the A1. The mean bias of the 5th data point value has been removed from the data. (i) and (ii) are 'troughs' in data coinciding with severe rainfall events.

were defined as negative deviations and ‘peaks’ positive deviations greater than 0.04 mm. Deviations less than 0.04 mm represent very minor fluctuations from the trend and were not considered significant. The sequencing of the ’peaks’ and ‘troughs’ within a year, where plotted as a day number against the magnitude of the deviation to characterize the seasonality of the deviations. Finally, the timings of the ‘peaks’ and ‘troughs’ where compared with rainfall records.

Daily rainfall records were obtained from the UK Meteorological (Met) Office (2019) MIDA UK Hourly Rainfall Data (Met Office, 2019) for the precipitation gauge nearest to each of the A1(M) sites. The rainfall data were totalled for each month and subtracted from the monthly mean for the overall study period for the northern and southern sites respectively. The resultant change in monthly rainfall from the monthly mean for the overall study period, was plotted on the same graph as the ‘peak’ and ‘trough’ deviations of mean SMTD from the long-term trend. Furthermore, the graphical markers for the ‘peaks’ and ‘troughs’ were scaled to represent the magnitude of cumulative rainfall seven days prior to the date of the SMTD measurement by TRACS.

5.4. Results

5.4.1 Changes in road texture

The filtered mean SMTD data for the A1(M) northern sites are shown on Figure 5.2. SMTD data for nine sites (Sites 1 to 8 inclusive and Site 10) were first measured on either the 11th or 12th August 1998. The initial mean SMTD measurements vary on Figure 5.2a for these sites, from 1.18 mm to 1.88 mm. The construction records available of Sites 1 to 8 indicated that these HRA pavement surfaces were first constructed at between 1976 and 1993, so the youngest pavements had been laid for a minimum of five years when they were first measured. No clear correlation was found between the dates of construction and the initial measurement of SMTD recorded in August 1998. This suggests that the evolution of pavement SMTD is influenced by site specific processes such as meteorological conditions and traffic flow.

The normalized data are shown in Figure 5.2b. For the period on the graph between 1000 days and 3500 days after the 11th August 1998, the filtered mean SMTD generally increases linearly with the passage of time for all the northern sites. A similar trend is demonstrated in the normalized filtered mean SMTD data for the four southern sites 11 to 14, shown on Figure 5.3. The period on the graph between 215 days to 2215 days after the 24th July 2004 again shows that the data like the north follows a general linear trend increasing with time. The rate of change of SMTD is steeper for southern sites than for the northern sites. The collective rate of change in the filtered mean SMTD was 2.017x10-4 mm/day for the northern sites between

1000 and 3500 days after the 11th August 1998, and 8.459x10-5 mm/day for the southern sites between 215 and 2415 days after 24th July 2005, representing a difference of 238%. The southern sites, with closer proximity to London experience much higher volumes of traffic, than the northern sites. The mean AADT flow for the collective group of southern sites is 30070 vehicles, compared to 11645 vehicles for the northern sites. The difference between the southern and northern sites is 258%, a comparable magnitude to the difference in gradient of the rate of change in filtered SMTD. Thus, suggesting that SMTD change may be influenced amongst other factors by traffic flow.

The rate of change in filtered mean SMTD compared with AADT is shown in Figure 5.4a, for the individual sites analysed. As AADT increases then the HRA pavement surfaces are experiencing a greater rate of change in SMTD. The same is also true when AADT figures are factored to take into account the mean percentage of HGVs. Figure 5.4b shows a positive trend between the rate of change in the filtered mean SMTD and the HGV AADT flow. Interestingly, the gradient of the linear best fit line on Figure 5.4a at 4.44 x 10-9 mm/AADT is twenty percent as steep as the linear best fit line for the adjusted HGV AADT values at 2.23 x 10-8 mm/AADT shown on Figure 5.4b. This suggests that HGVs are having more impact on the evolution of mean SMTD than other vehicles. This result meets expectation as HGVs have previously been attributed as the main cause of change on pavement surfaces due to heavier axle loading and tire features (Bagui et al., 2013; Do et al., 2009; Vaiana et al., 2012).

5.4.2 Seasonal trends in road texture

The general linear trend in the normalized filtered mean SMTD is interrupted on Figure 5.2a at (i) and (ii), with a drop or 'trough' occurring of approximately 0.2 mm . When these time series were investigated it was found they coincided with periods of intense precipitation. Point (i) for example occurs in autumn 2000, at the time the wettest recorded since 1766 on the England and Wales Precipitation Series (Simpson and Jones, 2012) experiencing 503 mm of precipitation, which was 196% of the 1961 to 1990 autumn average. Similar behaviour was observed for the southern sites, for example point (ii) on Figure 5.3 shows a drop or 'trough' in the mean filtered SMTD data, on the 30th November 2013. The winter of 2013 was again exceptionally wet, at the time the third wettest since 1766 (Simpson and Jones, 2012), with Central and Southern England experiencing 250% of the 1981 to 2010 winter average. The general linear evolution of filtered mean SMTD for the HRA surfaces studied was found to be repeatedly disrupted by extreme precipitation events. Other meteorological triggers were investigated including ground surface temperature, minimum and maximum ambient temperature, and number of frost days, but no clear correlation with the transient drop or 'troughs' in the mean SMTD was established.

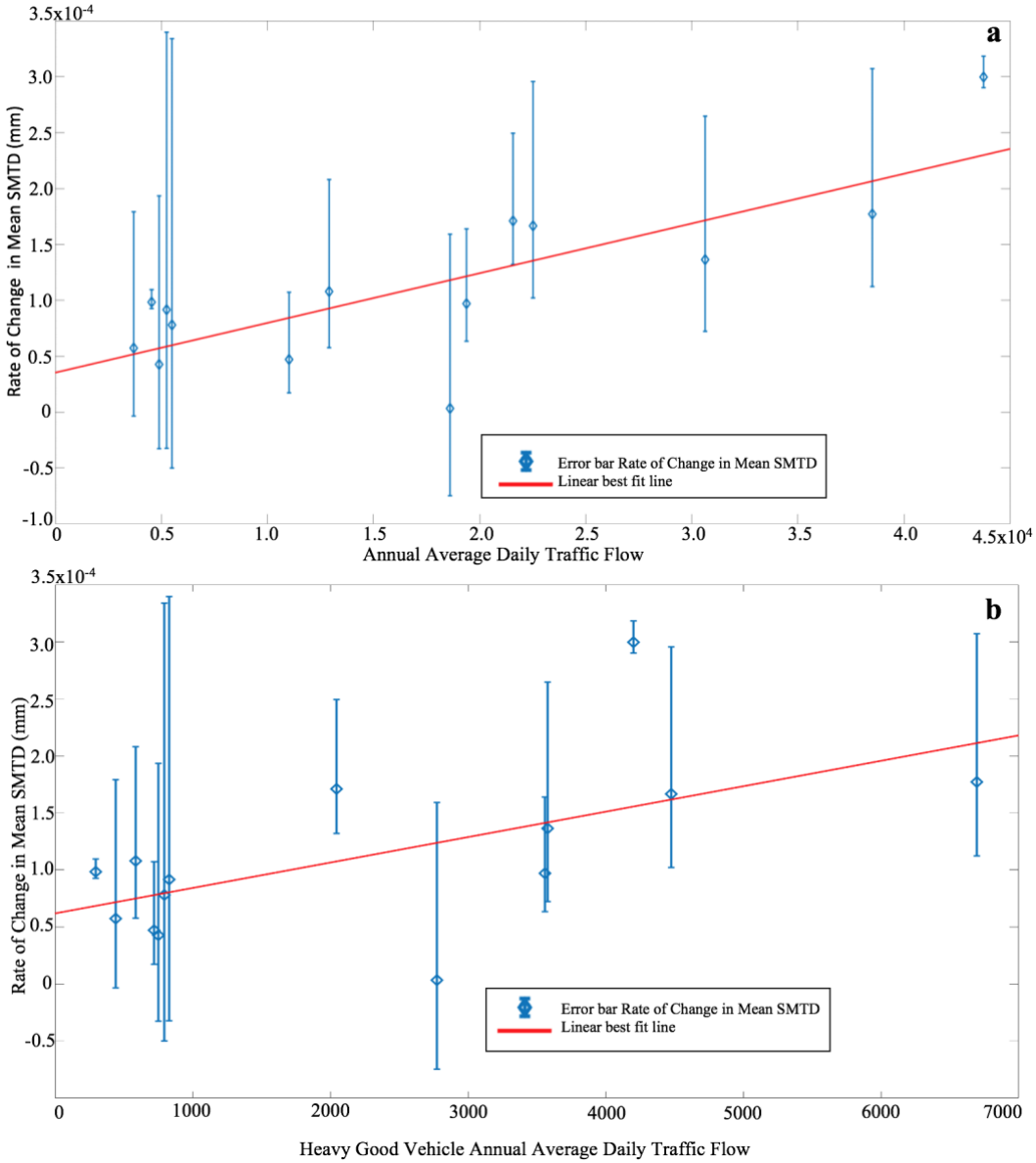

Figure 5.4. (a) Rate of change in mean Sensor Measured Texture Depth (SMTD) data compared with annual average daily traffic flow (AADT). (b) Rate of change in mean SMTD compared with heavy good vehicle (HGV) AADT. The results reveal a linear trend between SMTD and increasing AADT and HGV AADT flow.

A detailed study was made of the 'peaks' and 'troughs' occurring in the filtered mean SMTD data for each of the sites, within the northern and southern groups. It was found that the long-term trends in filtered mean SMTD against time in days could be modelled as a 7th order polynomial for all the sites. The 7th order polynomial was found to represent the long-term trend, from which the 'peaks' and 'troughs' can be detected. Figure 5.5 shows as an example, the 7th order polynomial best fit line for Site 3 (one of the northern sites, Figure 5.1a) as a black dashed line and the filtered mean SMTD as a red line. The deviations in filtered mean SMTD from the 7th order polynomial trend are presented as red crosses for 'troughs' and blue crosses for 'peaks', for negative and positive deviations greater than 0.04 mm respectively. Deviations less than ±0.04 mm are not considered significant (presented as green crosses in Figure 5.5). The same order polynomial arising for all the sites modelled, indicates that the rate of change in filtered mean SMTD with time follows a trend, and the trend is influenced by site specific conditions as the polynomial is a of a higher order.

The timing of the 'peak' and 'trough' deviations from the filtered mean SMTD for the northern sites are plotted according to seasonal periods in Figure 5.5. It was found that the 'peaks' shown as blue circles on the Figure 5.5, generally occur in the summer period characterized as the 1st April through to the 30th September. Conversely 'troughs' shown as red diamonds in Figure 5.5, generally occur in the winter period, characterized as the 1st October to the 31st March. The clustering in Figure 5.6 indicates a seasonal signal in the deviations in filtered mean SMTD data from the long-term trends. Moreover, the surface processes governing this signal is likely to vary from the summer to the winter period, as clear contrasting patterns are discernible in the data.

The surface processes with the potential to contribute to the seasonal signal are examined in the discussion section of this paper. These processes dominate when above average precipitation occurs close to (within 7 days of) the collection dates for the SMTD data. Figures 5.7 and 5.8 plot for the northern and southern sites respectively, the 'peaks' and 'troughs' in filtered mean SMTD against the preceding (seven days) rainfall. The blue shaded bands on the plots represent the winter months of October to March and the change in monthly rainfall from the mean over the study period (August 1999 – July 2016) are provided for context. The seasonal bias in the positioning of the peaks and troughs is evident, with the negative deviation ('toughs') from the filtered mean long-term SMTD trend predominantly occurring in the winter months, and the short-term positive deviations ('peaks') occurring in the summer months.

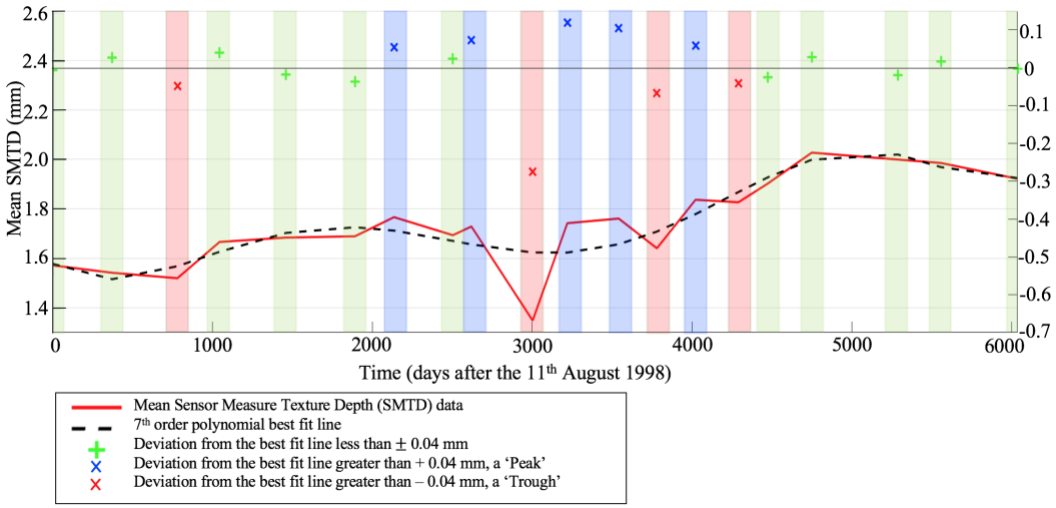

Figure 5.5. Mean Sensor Measured Texture Depth (SMTD) data compared with a 7th order polynomial best fit line for Site 3 on the A1. The deviations of mean SMTD from the best fit line are presented as red crosses ('troughs') or blue crosses ('peaks') for negative and positive deviations greater than 0.04mm respectively. Deviations less than ± 0.04mm are not consider significant and are presented as a green cross.

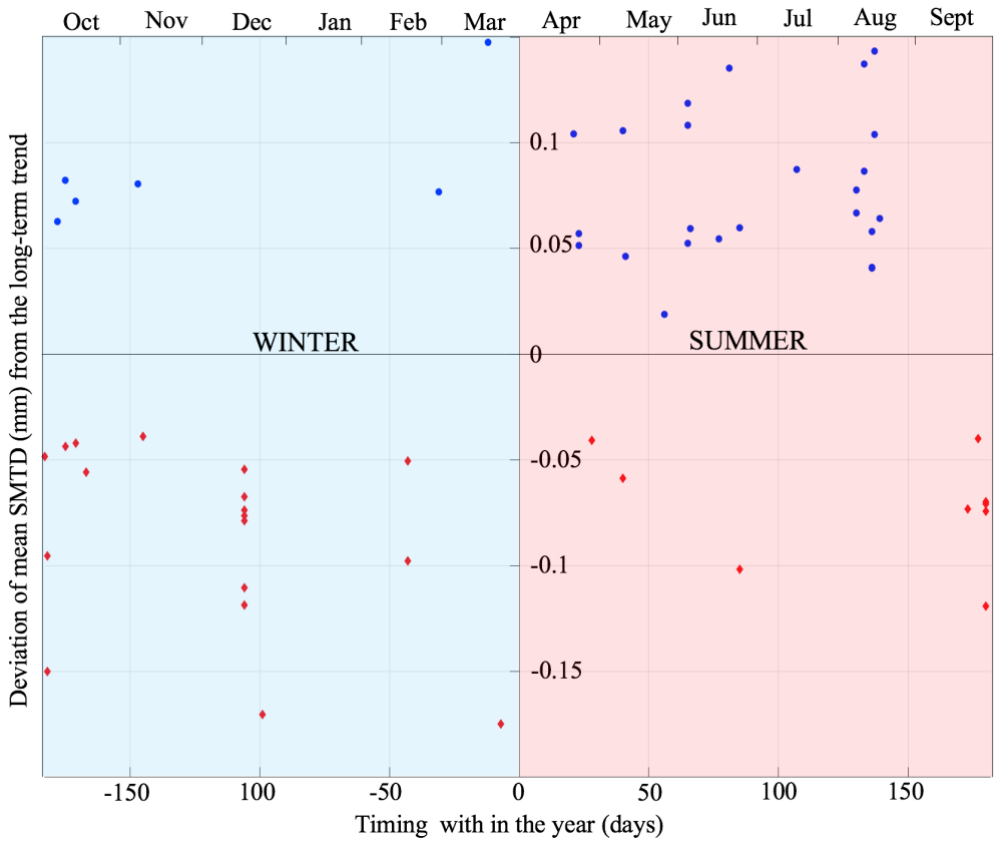

Figure 5.6. The graph plots the seasonal timing of the deviation in 'peaks' and 'troughs' from the 7th order polynomial trend for the northern sites of the A1.

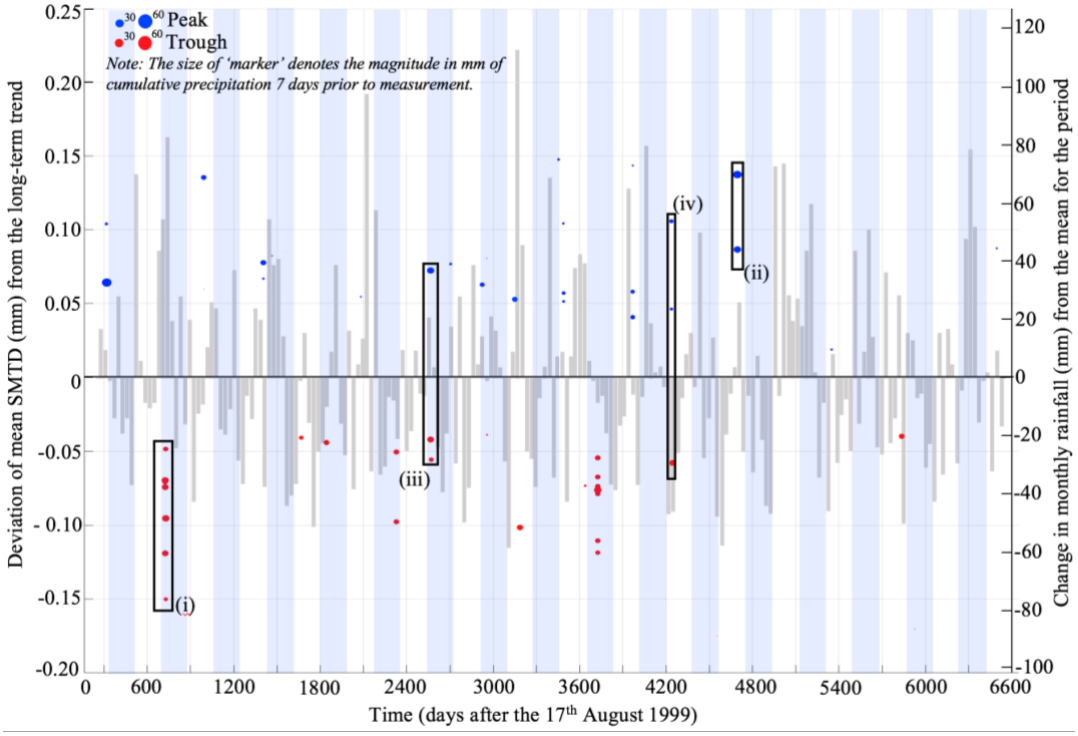

Figure 5.7. The graph plots change from mean monthly rainfall for the period 17th August 1999 to 17th July 2016, against the 'peaks' and 'troughs' in the deviation of mean SMTD for the northern sites on the A1. The blue shading bands represents the winter months of October to March inclusively. The 'troughs' in rate of change in SMTD typically occur in the winter months and the 'peaks' occur in summer months (often across multiple sites (i) and (ii) respectively). However, the pattern is disrupted by a coincidence of above average rainfall with collection dates (see for example anomalous peaks and troughs (iii) and (iv)).

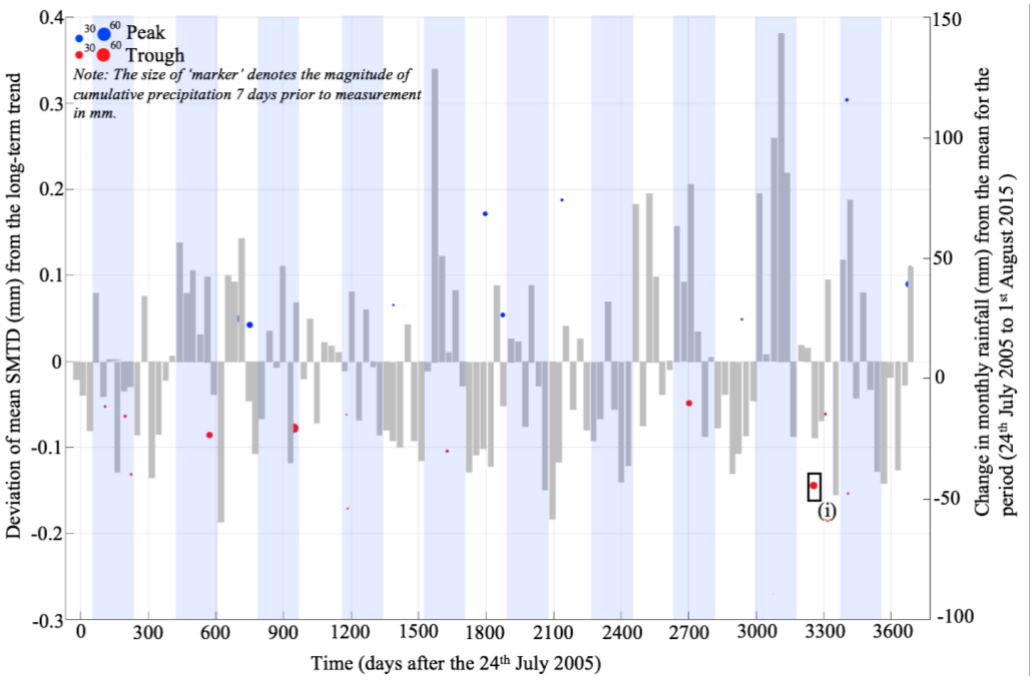

Figure 5.8. The graph plots change from mean monthly rainfall, against the 'peaks' and 'troughs' in the deviation of mean SMTD for the southern sites on the A1. The blue shading bands represents the winter months of October to March inclusively. The 'troughs' in rate of change in SMTD typically occur in the winter months and the 'peaks' occur in summer months. However, the pattern is disrupted by a coincidence of above average rainfall with collection dates (see for example anomalous peaks and troughs (i).

There is evidence of ‘toughs’ or ‘peaks’ occurring at multiple sites at similar times (see for example Figure 5.7 (i) and (ii)). On Figure 5.7 at point (i), ‘troughs’ in the signal were observed at six independent sites (Sites 2, 4, 5, 6, 7 and 10) over five days between 28th September 2000 and 2nd October 2000. These sites are located at intervals of approximately 20 km over a 154 km stretch of the A1(M). This consistency across multiple sites is occasionally complicated by the close occurrence of ‘peaks’ and ‘troughs’ at different sites. On Figure 5.7 at point (iii) one ‘peak’ and two ‘troughs’ occur in October 2005 a winter period. Furthermore, at point (iv) on Figure 5.7 two ‘peaks’ and one ‘trough’ occur in the summer period of May 2010. Upon investigation the ‘peaks’ and ‘troughs’ for both time series considered occurred within five days of two days of heavy precipitation. These data suggest a bias towards the observed seasonal pattern (with more ‘peaks’ occurring in the summer, and more ‘troughs’ in the winter), and points also to the potential for site-specific responses potentially influenced by interruptive events such as the presence of a surface covering of mud . The hypothesis that precipitation is occasionally a trigger for transient change in SMTD data with local road surface conditions governing, is reinforced by the data presented in Figure 5.8 (see point (i)), where a ‘trough’ occurs on the 30th May 2014 early within the summer period for a southern site. The winter of 2013/2014 was recorded as being particularly wet across south-east England, being at the time the wettest since 1766 (Met Office, n.d.). In the month of May 2014, 83.5 mm of precipitation fell. In the week prior to the SMTD reading being taken on the 30th May 2021, 57% or 47.6 mm of this precipitation was recorded. This intense period of precipitation occurred after a dry spell of seven days. The data indicate that ‘peaks’ and ‘troughs’ occur where there has been above average precipitation for several days within the week prior to a measurement being taken, suggesting that processes occurring on the HRA pavement surface are temporarily interrupted by surface processes such as precipitation. Furthermore ‘peaks’ and ‘troughs’ generally present with a seasonal signal, potentially conditioned by local, site specific controls

5.5. Discussion

To summarize the trends observed in data from the study results and to advocate the surface processes that might be driving these we present Figure 5.9 our conceptual model. The governing trends of long-term change to texture on HRA pavement surfaces is shown as thick black line on Figure 5.9, at an angle of (∅). This illustrated that uninfluenced by exceptionally high precipitation, the rate of change in filtered mean SMTD was found to continue to increase linearly with time, at a gradient (∅) that was correlated with the magnitude of AADT for the sites considered. Furthermore, the observed steepening of the angle (∅) when AADT is adjusted for the percentage of HGVs is expected because the heavier axle loading and tire

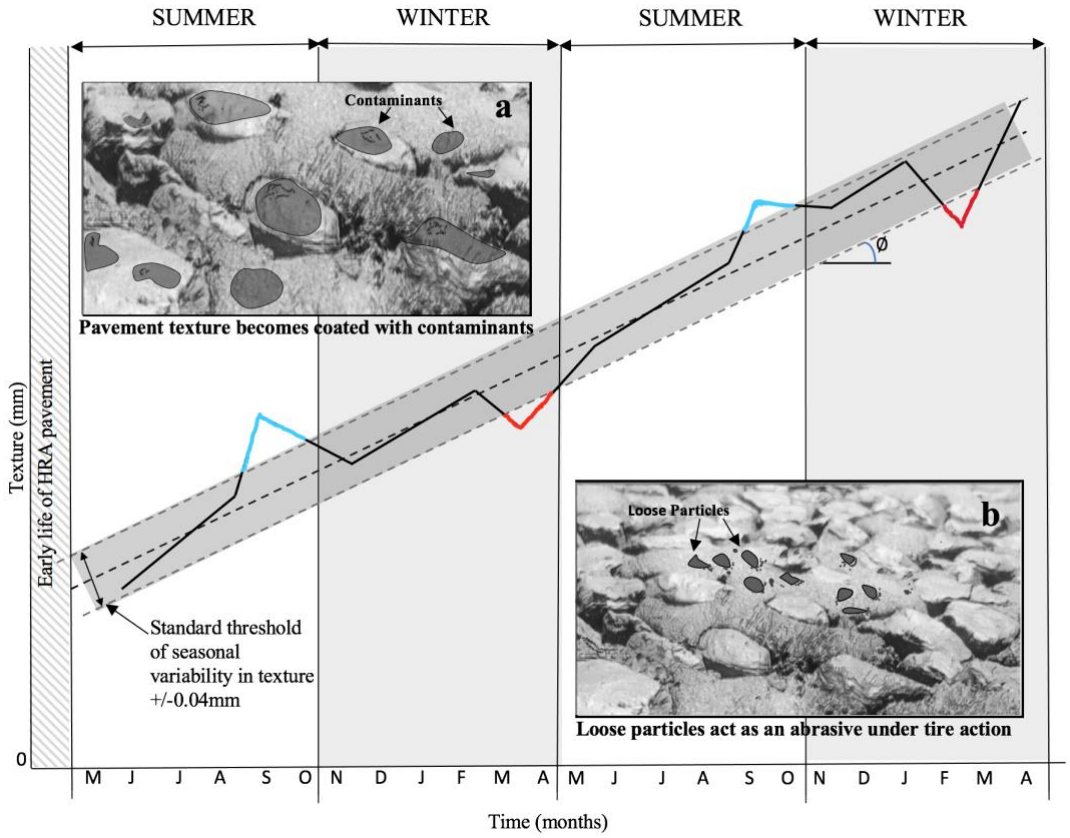

Figure 5.9. The governing trends of long-term change to pavement texture on Hot Rolled Asphalt (HRA) pavement surface. (a) During the summer season pavement texture can become coated with contaminants such as the residue of rubber or rubber particles from vehicle tires, oils or auto lubricants. (b) During the winter season frost shattering in pavement microcracks, leads to loose particles, which can act as an abrasive under tires, polishing the pavement surface

types associated with commercial vehicles cause more impact on macrotexture polishing than other types of road vehicles (Bagui et al., 2013; Do et al., 2007; Vaiana et al., 2012). These observed long-term linearly increasing trends do not consider the very 'early life' of the HRA pavement (represented on Figure 5.9 conceptually as a grey hatched vertical band), a period likely to be governed by other processes, such as the stripping of bitumen bloomed on a newly laid surface (Kane et al., 2012).

The presentation on the conceptual model (refer to Figure 5.9) of a long-term increase in filtered mean SMTD data with time, at a gradient (Ø) correlated with AADT, is a finding aligned with other studies. Pomoni et al (Pomoni et al., 2020) tracked change on a hot mix asphalt surface using cumulative traffic data and observed an increase in macrotexture on pavement surfaces after a threshold level of cumulative traffic had been achieved in the life of the pavement. Prior to the threshold, during the early life of the pavement the change in surface texture was shown to behave differently. Generally, Pomoni et al (2020) observed a decreasing trend with some fluctuations in texture results attributed to short-term variations arising from changes in the asphalt surface due to processes influenced by conditions of the area, for example the influence of dust and rain.

Similar minor annual variability was found in the long-term data considered during this study, characterized as change in filtered mean SMTD values less than ±0.04 mm. These are presented on the conceptual model (Figure 5.9) as the area within the linear grey band. Changes less than 0.04 mm in SMTD are thought to represent surface processes occurring in the winter and summer. Previous researchers have presented hypotheses over these governing processes, the most plausible from the results studied are again presented conceptually on Figure 5. 9. Box (a) on Figure 5.9 illustrates that in the summer pavement texture can becomes coated with residual rubber, rubber particles, oils and lubricants (Gobmann et al., 2021; Kogbara et al., 2016) . Furthermore, sunny days with air temperatures of 20°C or above can generate road surface temperatures of the order of 50°C as dark asphalt surfaces absorb heat. This has been shown to be sufficient to cause unmodified binders present in a road to become sticky in places with the potential to smut and cover part of the pavement surface in localized areas (Kodippily et al., 2012).

Box (b) on Figure 5.9 illustrated that in the winter at temperatures below 0°C water present in small voids in the pavement aggregate can freeze. The resulting nine percent volumetric expansion in this water can cause fragments of aggregate to break away from the pavement surface, a process known as frost shattering. This can lead to loose aggregate on the pavement surface, which can act as an abrasive under tires polishing the pavement surface [11]. The

potential for voids is increased by embrittlement in asphalt pavements caused by the aging of the SARA (Saturate, Aromatic, Resin and Asphaltene) components of the bitumen binder through oxidization under ultra-violet radiation and hydrological erosion (Eberhardsteiner et al., 2015). Embrittlement of the binder leads to the development of micro-cracks into which water can infiltrate and freeze. These theoretical seasonal surface phenomena are widely accepted, but much research is still required to monitor them practically in the field.

It is discernible from the results of the study undertaken that whilst within the threshold of ±0.04 mm these surface processes are 'in balance'. However, disruptions are observed arising from notable precipitation events, causing the development of 'peaks' in the deviation of filtered mean SMTD from long term trends during summer months and 'troughs' in the winter months. Figure 5.9 illustrates the 'peaks' occurring in the summer as blue shading on the black texture evolution line, and similarly the 'troughs' occurring in the winter as red shading.

The link between above average precipitation events and transient changes in SMTD suggests that a washing effect may be occurring on the HRA pavement surface. In the summer months the disruptive precipitation events are potentially removing any oil, lubricants, rubber or rubber particle contaminants present either on the surface of the HRA aggregate or within the voids, causing an increase in the SMTD measurements. In the summer these contaminants are likely to be drier and therefore more likely to be expelled from the pavement macrotexture in an emulsion. In the winter it its theorized that due to the quantity of abrasive material and also sand from road salting activities present on the surface, that polishing of the HRA aggregate governs. It has been suggested by other researchers that whether a surface becomes more polished or whether it becomes rougher is a function of the minerology and polish stone values of the aggregate and of the nature of dust/detritus finding its way onto the pavement surface (Kogbara et al., 2016). However, it is clear from the data presented here that negative deviations from filtered mean SMTD from the long-term trend are typically occurring after above average precipitation in the winter. It is therefore postulated that either dust, debris, and sand from salting on the surface are being 'redistributed' within the negative texture of the HRA pavement; or that the contaminants in the winter are more likely to be miscible on the surface and less susceptible to washing. Ultimately, little is known about the characteristics of precipitation needed to effectively clear or clean a highway surface or the wetting and drying processes occurring and interacting with surface contaminants (Kogbara et al., 2016).

It is clear that rainfall is acting to disrupt the SMTD. The findings presented here demonstrate for the first time that the disruption has a seasonal pattern. Interestingly this pattern follows an inverse trend to the classically understood pattern of seasonal variation in skid resistance

in the UK, where skid resistance is thought to be lower in the summer and higher in the winter. As skid resistance is measured as a frictional response to pavement texture, this suggests that processes on pavement surfaces are influencing seasonal variation in skid resistance; along with the other recognized parameters such as speed, temperature, tire tread thickness and viscoelastic deformation. An inverse relationship between texture and skid resistance has been observed by others (Pomoni et al., 2020) when considering the long-term pavement texture evolution with cumulative traffic. Furthermore, recent studies seeking to determine a percentile dry skid resistance based on wet period measurement, noticed the same percentile occurring with different traffic and precipitation intensity, concluding that this pointed to the potential for asphalt pavement surfaces to be influencing seasonal variation (Plati et al., 2020). Certainly, the summer 'peak' signals were observed during the months of April to September, which broadly match the seasonal summer period of low skid resistance measurement in the UK (Design Manual for Roads and Bridges, 2021). Further study of the seasonal signal observed in the SMTD will be required to ascertain the contribution of surface processes to seasonal variations of skid resistance. Such research will require measuring in a controlled manner: skid resistance, macrotexture depth, environmental conditions and monitoring at the macroscale the wetting and drying processes of contaminants on the surface of the pavement. These findings demonstrate that texture measurements experience a seasonal signal and point to a requirement for measuring equipment to be modified to clean pavement surface of detritus prior to readings being taken to achieve more accurate and representative measurement of SMTD

5.6. Conclusion

An investigation of the long-term evolution of SMTD for HRA surfaces was undertaken for fourteen sites located on the north to south transect of the A1(M) in the UK and compared with traffic flow and meteorological dataset for 19 years. Sensor Measured Texture Depth (SMTD) data were analysed using novel spatial filtering techniques. The long-term evolution of SMTD for HRA surfaces, when seasonal signals are discounted in the 'rate of change', follow a linearly increasing trend at a gradient ($\emptyset$) correlated to the order of magnitude of the AADT. The results also demonstrate for the first time a seasonal signal in SMTD measurements corresponding with above average precipitation occurring within the week prior to the SMTD measurement being taken. The pattern observed demonstrates positive deviation from the long-term evolution of filtered mean SMTD in the summer and negative deviations in the winter. The results indicated that processes occurring on the surface of the HRA pavement are influenced by seasonal conditioning.

The study results are presented as a new conceptual model summarizing the governing trends of long-term change on Hot Rolled Asphalt pavement surfaces. The conceptual model considers new theories of the surface processes driving the detected patterns related to the wetting and drying of surface contaminants. In the summer, the build-up of surface contaminants (such as rubber, rubber particles, oils and lubricants) are likely to be drier and are believed to be washed away with rainfall more easily from the pavement texture in an emulsion. In the winter, it is postulated that either dust, debris, and sand from salting on the surface are being 'redistributed' within the negative texture of the HRA pavement; or that the contaminants in the winter are more likely to be miscible on the surface and less susceptible to washing. The pattern observed is inverse to the behaviour of seasonal variation in skid resistance because skid resistance is measured as a friction response to texture. However, further research is required to confirm conclusively the link between the two phenomena. Such research will require measuring in a controlled manner: skid resistance, macrotexture depth, environmental conditions and monitoring at the macroscale throughout the wetting and drying processes of contaminants on the surface of the pavement.

The results presented suggest that more accurate reading of pavement texture might be obtained by cleaning the surface of debris/contaminant prior to measurement being performed. Although this may not be practical at road network scale, more frequent texture surveys synergized with more focused and constrained weather monitoring will do much to improve the understanding of surface processes on the evolution of texture.

Chapter 6.0 : Published Paper 4 – Skid resistance: understanding the role of road texture scales using a signal decomposition technique and a friction model.

6.1. Abstract

Skid resistance markedly depends upon road surface characteristics, particularly the texture. Texture can be considered to be composed of a range of different scales each of which contributes differently to the generation of adequate friction at the tyre-road interface in wet conditions. This work aims to contribute to understanding the role of these different scales. The method adopted deploys a signal processing technique, termed Empirical Mode Decomposition, to decompose the road surface texture into a set of component profiles of different wavelengths. The Dynamic Friction Model, a computational friction model already validated on real road surfaces, is then used to determine the relative effect of partially recomposed profiles and associated components on skid resistance. The results demonstrate the importance of not only "small-scale" and "large-scale" textures but also their spatial arrangement and shape. Indeed, on wet road surfaces, "small-scale-texture" was found to be key to achieving good skid resistance at low speeds, whilst "large-scale-texture" was found to be crucial to maintaining it with increasing speed. But furthermore, the distribution of the summits of the large-scale-textures was established as being able to compensate for a lack of small-scale-texture. Conversely, the reverse was established as also being true, with the small sharp local summits of small-scale-texture being found to compensate for a lack of large-scale-texture. Even though it should be noted that this random distribution and the pointed shape of the summits may also be an inconvenience with respect to other surface properties such as noise and rolling resistance.

6.2. Introduction

Adequate skid resistance is key to the safe transit of vehicles upon roads. It describes the contribution that the road makes to tyre/road friction. The textures of these road surfaces and in particular the scales termed "Macrotexture" and "Microtexture" (International Standards Organisation, 2002) remain the principal parameters governing skid resistance. Macrotexture refers to the texture of wavelengths of between 0.5 and 50 mm and amplitudes of between 0.2 and 10 mm. The Macrotexture is mainly dictated by among others the shape, size, and gradation of the aggregates in the pavements and is widely accepted as making the main contribution to water drainage out of the tyre-road contact patch. Microtexture refers to the texture of smaller wavelengths of between 0 and 0.5 mm and of amplitudes of between 0 and 0.2 mm. Microtexture is mainly dictated by among others the micro-asperities upon the

surface of the aggregates, and is known to break any residual water film in the tyre-road contact patch to restore partially a direct contact between the tyre and road surfaces.

Within this paper, instead of precisely defining texture scales as ‘Microtexture’ and ‘Macrotexture’, ‘Small-Scale-Texture’(SST) and ‘Large-Scale-Texture’ (LST) will be adopted. These definitions are dictated by the texture decomposition method adopted in this work, that decomposes the road surface texture to naturally inherent and not pre-defined different scales. LST is defined as the texture wavelengths and amplitudes equivalent to the size of road surface aggregates. Similarly, SST is defined as the texture wavelengths and amplitudes equivalent to the size of the roughness present upon the surface of these aggregates. Instead of the common 0.5 mm corresponding to the lower microtexture wavelengths, the lower limit of the SST is set to 0.87 mm due to the resolution of the used profilometer to capture the topography of the surface in this work that is equal to 0.87 mm (Refer to Section 6.4 and the reference : American Society for Testing and Materials, 2015, 2011) However, to not forget the contribution of the wavelengths from 0.5 to 0.87 mm, a local friction coefficient is introduced in the calculations (Refer to Equation 6.2 and the reference: Kane et al., 2019; Kane and Cerezo, 2015).

In view of the importance of these two texture scales for skid resistance in wet conditions, as specified above, their presence on road surfaces is ensured by specifying the components and the design of the pavement before construction. SST is provided by aggregates selected on the capacity to stay unpolished when subjected to the traffic. The mineralogical composition, of aggregates comprised primarily of hard quartz mineral particles cemented together with a softer mineral matrix, like Greywacke aggregate, maintain long term adequate SST as a consequence of the differential wear and debonding of individual particles under traffic (Kane et al., 2013; Rezaei et al., 2009). LST depends upon the shape, size, and gradation of the coarse aggregates, with coarse aggregates dominating LST when they are closely packed (Hall et al., 2009).

To determine the role of these texture scales, many investigations have been already undertaken. Sabey’s experimental tests showed in the 1950s that in wet conditions at low speeds, that higher LST and SST benefit skid resistance (Sabey, 1958). At higher speeds, lowering LST leads to a reduction in available skid resistance. The effect of both these texture scales on speed-dependent wet skid resistance has been repeatedly confirmed and empirically modelled (Fwa, 2017; Leu and Henry, 1983). As an example, one can consider the International Friction Index (IFI) and the Penn State model derived from statistical fittings of measured skid resistance data (American Society for Testing and Materials, 1998;

Kulakowski, 1991). These models represent the graphical curve of skid resistance versus speed by means of equations with two parameters. The first parameter, the intercept, occurring at zero vehicle speed is related to SST, whilst the second parameter describes the shape of the curve and is related to the LST. However, even if these studies allowed a better understanding of the role of the texture scales, they completely ignored the effect of their spatial distribution.

To go further in the understanding of the texture scales' effects, mathematical methods of signal decomposition like Fractals, Fourier, Wavelet Transforms have been explored, considering the road surface texture. Attempts, to couple models to surface textures approximated from their fractal's parameters, have been undertaken to correlate skid resistance to texture (Heinrich, 1997; Rado, 1996; Villani et al., 2011). Villani et al. calculated the hysteresis contribution to friction by means of an analytical model of a sliding elastomer passing over a road surface with a texture described from its fractal dimension. But, despite the significant advances in friction modeling, no conclusion has been drawn about the role of the different texture scales and their spatial distribution.

Recently, Kane et al. found a statistical correlation to skid resistance (Kane et al., 2015) after calculating a set of texture parameters from amplitudes and frequencies using functions derived from an Empirical Mode Decomposition (EMD) (Cho, 2010; Huang and Pan, 2006). Furthermore, Kane et al. developed and validated a computational model the 'Dynamic Friction Model' (DFM) to predict the skid resistance of roads using topographies (Kane et al., 2019; Kane and Cerezo, 2015) Based on the above two studies by synergizing the EMD and DFM, the present work tries to contribute to the effort of identifying the role of SST and LST on skid resistance in wet conditions. The method adopted will be based on the different steps:

- The extraction of the inherent road surface basic profiles of different wavelengths from the original road surface profile using the EMD,

- The recombination of these basic profiles to produce a set of new profiles of different levels of SST and LST,

- And the use of the DFM on these new profiles to determine the relative effect of SST and LST.

6.3. Revisiting the DFM

The basic equations of the DFM derive from balancing the forces acting at the contact point between the road and a moving rubber element (Equation 6.1 & Figure 6.1) [Kane et al., 2017].

$$\overrightarrow{F_{ij}} + \overrightarrow{T_{ij}} + \overrightarrow{R_{ij}} + \overrightarrow{FR_{ij}} = \vec{0} \qquad \text{Equation 6.1}$$

Where, $\overrightarrow{F_{ij}}$ is the force applied by the rubber element on the road surface. The force, it is calculated using a "Kelvin-Voigt" model, where K is the spring's elastic modulus and *C* is the dashpot's viscosity. $\overrightarrow{F_{ij}}$is balanced by the load through the integrated respective components of the contact pressure p_{ij}.

$$F_{ij}(t) = l \times dx \times p_{ij}(t) \text{ with } p_{ij}(t) = Ku_{ij}(t) + C\frac{du_{ij}(t)}{dt} \text{ and } u_{ij}(t) = \delta(t) - h_i + z_j$$

With, t representing the time and $u_{ij}(t)$ the displacement of the rubber i^{th} element contacting j^{th} element on the road at time *t*. $\delta(t)$ is the solid displacement of the pad at *t*. h_i represents the pad geometry. z_j is the height of the j^{th} point of the road profile. $\overrightarrow{T_{ij}}$ is the traction force. $\overrightarrow{R_{ij}}$ is the surface reaction force. $\overrightarrow{FR_{ij}}$ is a local friction force. $FR_{ij} = \mu_{\boldsymbol{loc}} R_{ij}$ when the element is moving on a "pseudo smooth inclined plane" with angle α_j and where $\mu_{\boldsymbol{loc}}$ represents a local friction coefficient. The projection of Equation 6.1 in local contact coordinates, onto global contact coordinate's axes *x* and *z*, coupled with the condition that $FR_{ij} = \mu_{loc} R_{ij}$ leads to:

$$T_{ij}(t) = F_{ij}(t)\frac{sin(\alpha_j) + \mu_{loc}\, cos(\alpha_j)}{cos(\alpha_j) - \mu_{loc}\, sin(\alpha_j)} \qquad \text{Equation 6.2}$$

When an element is not in contact with the road surface, its contact pressure is nil, and the rubber element is subjected to a relaxation phase. Its position on the Z-axis is then determined by solving Equation 6.3:

$$Ku_{ij}(t) + C\frac{du_{ij}(t)}{dt} = 0 \qquad \text{Equation 6.3}$$

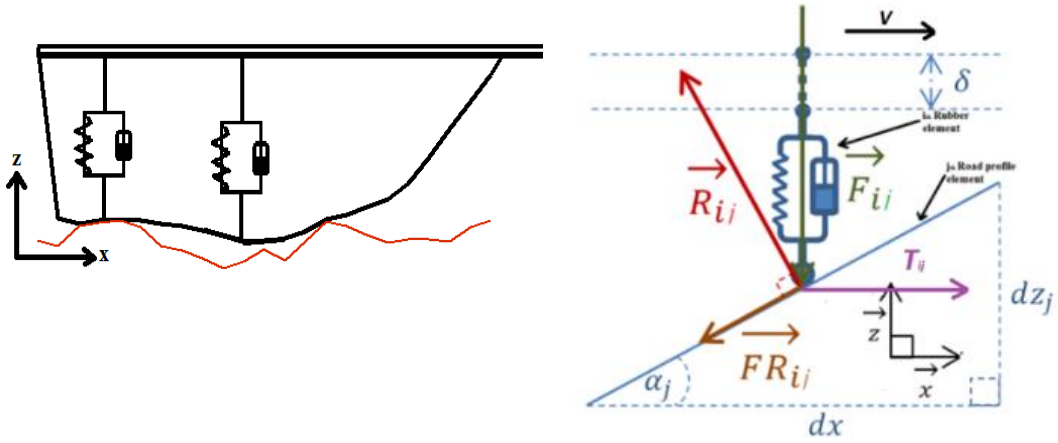

Figure 6.1. Forces acting in the contact point between a rubber element and a road profile

At any time, the load W applied on the pad must be balanced by the sum of the normal contact pressures:

$$W = \sum_i^N F_{ij}(t) \qquad \text{Equation 6.4}$$

Where *N* is the number of discrete elements of the rubber pad. Accordingly, the global skid resistance $\mu_j(t)$ can then be calculated using the following formula:

$$\mu_j(t) = \frac{\sum_i^N T_{ij}(t)}{W} \qquad \text{Equation 6.5}$$

At this stage, the only unknown factors are those relating to $F_{ij}(t)$, representing the contact force applied by the rubber elements on the road surface. To obtain the calculation details of these dynamic viscoelastic contact forces, the reader is advised to refer to the following publication: (Kane et al., 2019; Kane and Cerezo, 2015)

To take into account the water in the contact patch, a simplification is adopted. The contact geometry is approached as an equivalent hydrodynamic bearing. The equivalent geometry of that hydrodynamic bearing is estimated from the water thickness at the surface and the "opening spaces" available in the contact. At each calculation iteration, its load capacity is estimated and subtracted to the normal load. The reader is advised to refer to Kane's publication (Kane et al., 2019) to get the details.

$$W_h = \frac{\alpha 6 \eta V^{\beta} l L^2}{H_{out}^2 (a-1)^2} \left[log(a) - 2\frac{a-1}{a+1} \right] \qquad \text{Equation 6.6}$$

Where, $a = \frac{H_{in}}{H_{out}}$, with H_{out} and H_{in} are respectively the outlet and inlet water thicknesses of the simplified hydrodynamic bearing. η is the water viscosity. *L* and *l* are the lengths and the width of the bearing, in this case, the rubber pad. α and β are two empirical coefficients (10^5 and 1.75 respectively) added to adjust the load-bearing capacity of the hydrodynamic bearing component.

To learn more about the formalism details and the validation with field data of the DFM, the readers are advised to refer to the publications Kane et al. 2017 and 2018 on the references list.

6.4. Selecting the tested surfaces

The specified test surfaces represent a range of different morphologies to cover a broad combination of both SST and LST (Figure 6.2). They are composed of an artificial surface and a set of selected surfaces located on the 'French Institute of Science and Technology for Transport, Developments and Networks' (Ifsttar) test track, located near Nantes in France:

The artificial surface is fabricated by sticking rounded and sandblasted aggregates onto a plate. This surface is considered as "Analytical Surface" because of the clarity of the LST and SST, corresponding respectively to the average size of the rounded aggregates and the impacts left by the sandblasting procedure.

The other surfaces are selected from the Ifsttar test track to cover a broad combination of LST and SST. These "Test-Track Surfaces" feature some surfaces with "extreme" textural characteristics, i.e., a smooth resin finish, calcined bauxite, painted surfaces, etc. Other track test sections are representative of actual pavements laid on the national highways like Porous Asphalt, Very Thin Asphalt Concrete, etc.

6.5. Capturing texture and skid resistance of the tested surface

To capture the original profiles of the selected surfaces and to measure their skid resistance, the Circular Track Meter (CTM) and the Dynamic Friction Tester (DFT) devices are used respectively Figure 6.3 (American Society for Testing and Materials, 2019).

The DFT is equipped with three rubber pads attached to a disc. During the measurement process, driven by a motor, the disc in the "up" position (without contacting the road surface) is accelerated to reach the target speed imposed by the operator. When the required speed is reached, water is sprayed onto the tested surface via a pipe system. The motor then shuts down and the pads are brought into contact with the surface and slide across it. Consequently, the speed of the pads decreases before achieving a total stop due to the friction generated in the pad/road contact patch. The CTM is complementary to the DFT as all texture measurements can be done along the same tracks where DFT measures are done. It measures texture profiles along a circle using a laser mounted upon a rotating arm. The obtained profile is composed of 1024 points scaled at 0.87 mm, meaning a total profile length of 892 mm.

Analytical Surface

Test track surfaces

Figure 6.2. Analytical Surface and test track surfaces

DFT CTM

Figure 6.3. Side (Up) and bottom (Down) views of the DFT (Left) and the CTM (Right)

6.6. Decomposing the surface profiles and creating the new profiles

6.6.1 Texture decomposition

The decomposition procedure applied to derive the fundamental IMF of the profiles follows the EMD methodology (Equation 6.8). The details of that method can be found in Huang's or Kane's publications (Huang and Pan, 2006; Kane et al., 2015).

$$Z(x) = r_n(x) + \sum_{j=1}^{n} C_j(x) \qquad \text{Equation 6.7}$$

Where, x represents the distance in the texture profile, $Z(x)$ is the height of a point located at distance x in the profile, $C_j(x)$ is the j^{th} Intrinsic Mode Function (IMF), "n" is the total number of IMF and $r_n(x)$ is the residue obtained after the decomposition.

Figure 6.4 displays the original profile of the Analytical Surface captured using the CTM profilometer. On that profile, the LST (corresponding to the size of the aggregate) and the SST (corresponding to the roughness created by the sandblasting process) are easily distinguishable. Figure 6.5 displays the IMF of the original profile of the Analytical Surface after applying the EMD procedure:

- IMF 1 captures the smallest intrinsic wavelengths of the original profile. It is assumed to correspond to its SST.

- The IMFs 2 to 5 capture the larger wavelengths of the original profile. It is assumed to correspond to the different scales of the LST of the surface.

- The rest of the IMF, from sixth to ninth, embed larger wavelengths above the LST. These correspond to the undulation and the global slope of the original profile and have no influence on the skid resistance.

Reversely, by summing all the nine profiles, the original profile can be reconstructed.

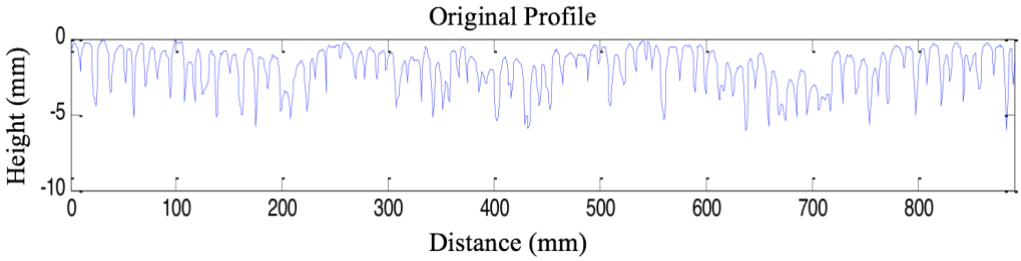

Figure 6.4. Original profile of the analytical surface captured using the CTM

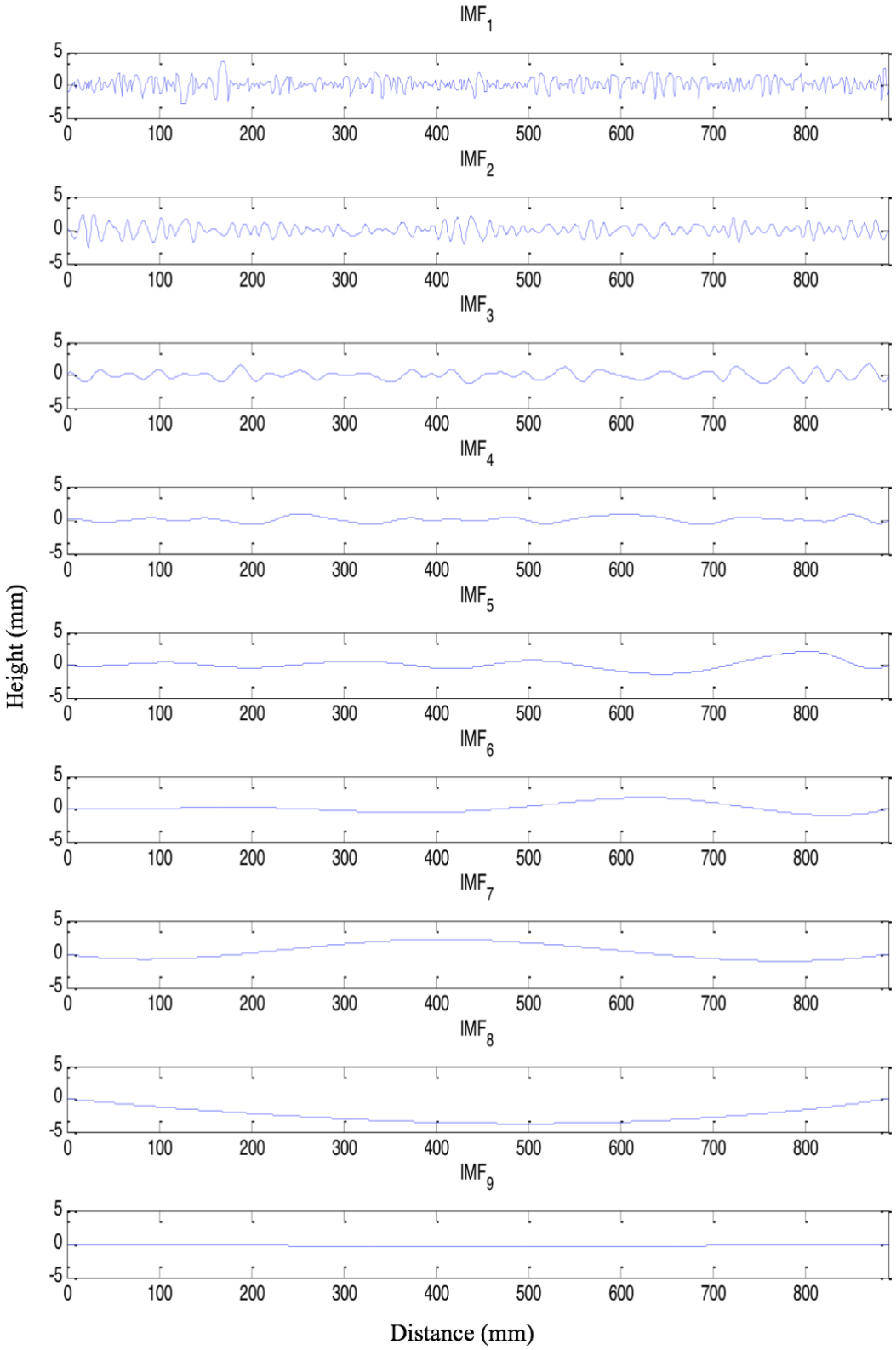

Figure 6.5. The nine embedded Intrinsic Mode Functions (IMF) of the Analytical Surface

6.6.2 Creation of the new profiles

The new profiles to be analyzed are constructed as follows (refer to Figure 6.6):

- The IFMs 1 to 5 are combined to raise a new profile named “Profile 0”. This Profile 0 consists of the SST and LST of the original profile (without the IMFs 6 to 9 that embed the undulation and the slope of the surface).

- IMF 1 is removed from the Profile 0 to derive a profile without SST. This new profile is named “Profile 1”. So, this Profile 1 embeds only LST.

- Then, IMF 2 is removed from the Profile 1 to obtain a second even smoother LST profile compared to Profile 1.

Figure 6.6 displays the three newly created profiles (Profiles 0 to 2). It can be seen from that figure that Profile 0 is very similar to the original profile.

6.7 Analysis procedure

The overall analysis procedure for each surface is as follows (refer to Figure 6.7):

- The DFT measures the experimental skid resistance on that real (physical) surface,

- The CTM captures the original profile of that real surface,

- This captured profile gives rise to Profiles 0, 1 and 2 after decomposition and re-composition,

- The DFM (the model) predicts the skid resistance on Profile 0,

- The skid resistance measured by the DFT and the skid resistance predicted by the DFM on Profile 0 (which is roughly the equivalent of the original profile captured with the CTM, but without the undulation and general slope) are compared, this to validate the DFM.

- Once the DFM has been validated, it can be now used to predict the skid resistance that Profiles 1 and 2 would display.

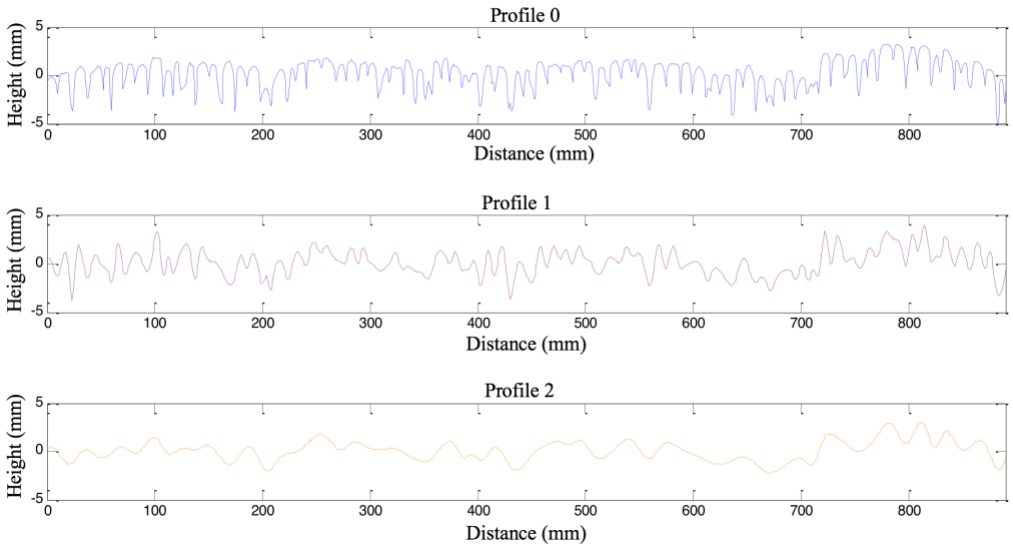

Figure 6.6. The nine embedded Intrinsic Mode Functions (IMF) of the Analytical Surface

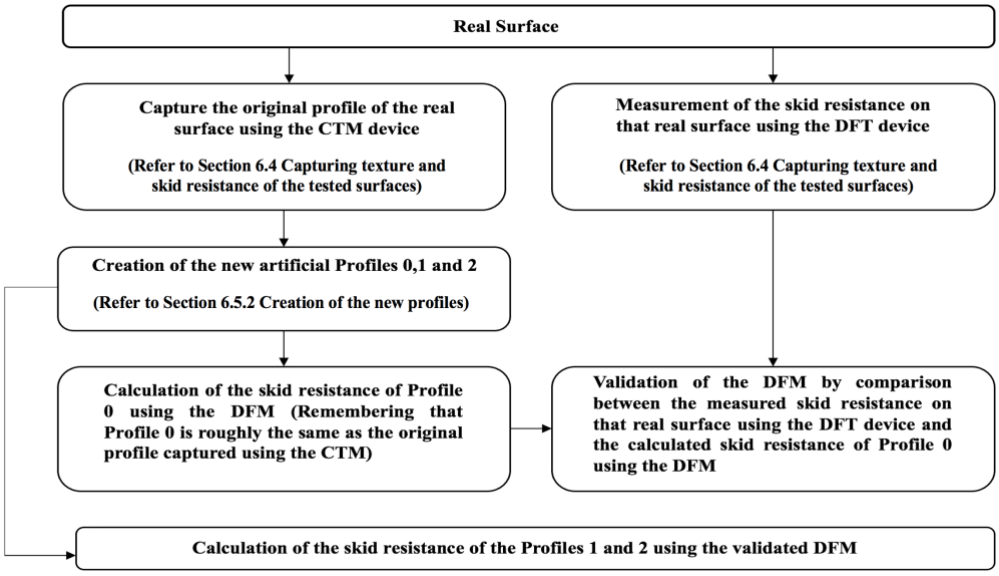

Figure 6.7. The overall analysis procedure followed for each surface

The DFM is then applied successively to Profiles 0, 1 and 2 at different speeds to calculate the skid resistance. Table 6.1 displays the inputs used to run the model. These values are related to the DFT (characteristics of the measuring rubber pad, operating conditions) and wetting water (Kane et al., 2019).

For all the surfaces studied, the local friction coefficient μ_{loc} is introduced to take into account the wavelength smaller than 0.87 mm (Equation 6.2). The μ_{loc} is arbitrary set to 0.2 because this value allows the best correspondence of simulations versus experiments skid resistance values of the Analytical Surface. However, maintaining this value equal for all tested surfaces means that the contribution of the wavelengths of the texture lower than the CTM resolution (0.87 mm) is the same for all tested surfaces. This is not necessarily true and may explain the difference between some predicted and experimental results. Indeed, the contribution at these wavelengths lower than the CTM resolution will depend on microtexture and thereby consequently on the type of aggregate (Do et al., 2007; Forster, 1989; Tourenq and Fourmaintraux, 1971).

6.8 Results and discussion

6.8.1 Analytical surface

Figure 6.8 displays the estimated skid resistance with the DFM for Profiles 0, 1 and 2 (respectively in blue diamonds, purple triangles, and yellow crosses) of the Analytical Surface at speeds 0 to 100 km/h and the measured skid resistance using the DFT at 20, 40 and 60 kmh^{-1} (the red squares). Profiles 0 and 1 derived from the Analytical Surface display the same skid resistance behaviour whatever the speed. This similarity is unexpected as IMF 1 is subtracted from the Profile 0 to create the Profile 1. So normally the latter has less SST and consequently, to be in accordance with the Horn and Buhlmann's and Sabey's observations (Horne and Buhlmann, 1983), the skid resistance estimated with the Profile 1 would be shifted down compared to the skid resistance estimated with the Profile 0 at low speeds (but both would maintain roughly the same slope with increasing speed, as both profiles embed roughly the same LST).

The analysis of the height distributions of the Profile 0 reveals that the local summits can be almost connected by a flat surface (transduced by a negative skewness of -0.72) whereas, for the Profile 1, it would be connected by a very irregular surface (an almost nil skewness -0.01) (Figure 6.9). As a result, is likely that the rubber pad will encounter more obstacles when it slides over the Profile 1 rather than Profile 0, which tends to generate friction and thus to compensate for the absence of SST. So, if the presence of SST has a positive impact on skid

K	C	dx	W	h	l	L	H_{in}	η
spring's elastic modulus **N/m^3**	dashpot's viscosity **$N.s/m^3$**	measuring the resolution of the profiles **mm**	applied load on the rubber **N**	the thickness of the rubber pad **mm**	width of the rubber **mm**	length of the rubber **mm**	Water thickness **mm**	Dynamic viscosity **Pa.s**
$1.4.10^8$	10^2	0.87	11.8	6	16	20	10^{-3}	10^{-3}

Table 6.1. The DFM input parameters

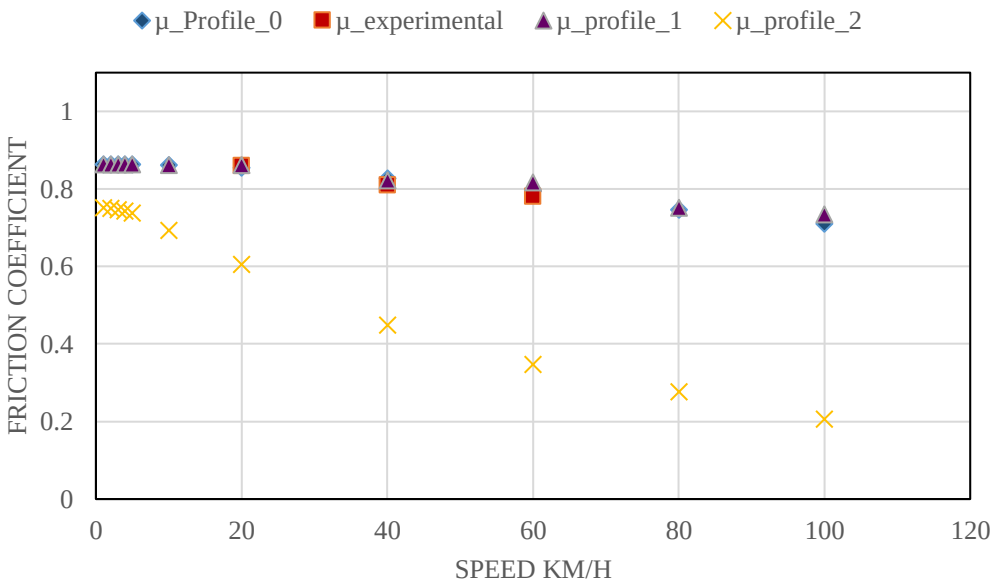

Figure 6.8. The Analytical Surface – DFM and DFT friction coefficients of Profiles 0, 1 and 2 versus speed

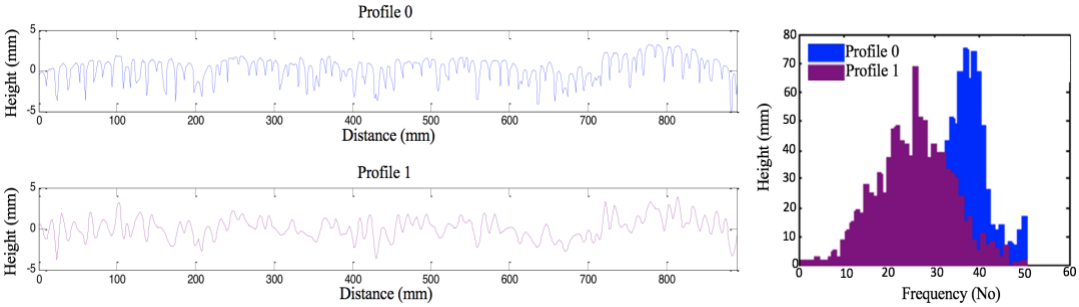

Figure 6.9. The Profiles 0 and 1 derived from the Analytical Surface (on the left) and their height distributions (on the right).

resistance, the irregular distribution of the local summits of the LST is also beneficial and can even compensate for a lack of SST. The Profile 2 derived from the Analytical Surface displays lower skid resistance but close to the Profile 1 one at low speed. Indeed, even though both profiles display irregularities of their local summit heights, the Profile 1 embeds more SST than the Profile 2 (Figure 6.10). With increased speed, the skid resistance drops continuously for Profile 2, this because of its low LST. This behavior is in accordance with some of the works exposed in the introduction section of this paper (Sabey, IFI, Penn State model…) with the SST governing skid resistance at low speeds, and the gradient with increasing speed being governed by the LST.

6.8.2 Analysis of the test-track surfaces

To confirm whether the above observations completed on the Analytical Surface, apply to real road surfaces representative of European highway networks, some surfaces selected from the Ifsttar test track are analyzed: a Very Thin Asphalt Concrete 0/6 (VTAC 0/6), a Porous Asphalt 0/6 (PA 0/6), Dense Asphalt Concrete 0/10 (DAC 0/10), a Painted Flexible Asphalt, a Calcined Bauxite Surface Dressing, and a smooth Epoxy Resin (ER).

6.8.2.1 The asphalt concretes

The three asphalt surfacing (VTAC, PA, and DAC) are similar in terms of texture, embedding the same mean level of both SST and LST. For each of these surfaces, the global shape of their derived three Profiles 0 to 2 display similar LST (contrary to the Profiles 1 and 2 derived from the Analytical Surface) but different SST (refer to Figures 6.11, and Figures 6.14 and 6.15 of the Paper 4 - Appendix).

For these three surfaces, the DFM predicts relatively well the skid resistance measured with the DFT. This is most likely explained by the probable use of the same aggregate type to build these three surfaces, meaning that the contribution of the SST below the CTM resolution is the same and well reflected by the adhesion coefficient set as 0.2 for all the three surfaces within the DFM simulations.

Additionally, for each of the three surfaces, the skid resistance estimated with the DFM of the Profiles 0, 1 and 2 follow the same trend with increasing speeds but are just shifted downward between ones and others. The highest skid resistance at low speed is achieved for Profile 0 with respect to Profile 2 which has the highest SST. This behaviour is again in accordance with the expectations and agreeing with some of the works exposed in the introduction section

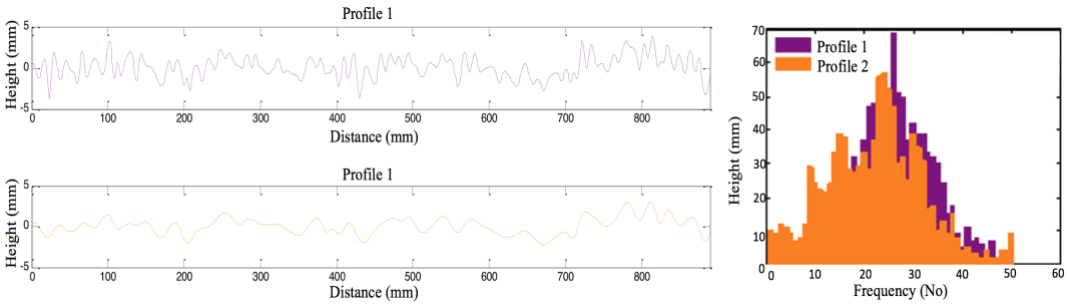

Figure 6.10. The Profiles 1 and 2 derived from the Analytical Surface (on the left) and their height distributions (on the right)

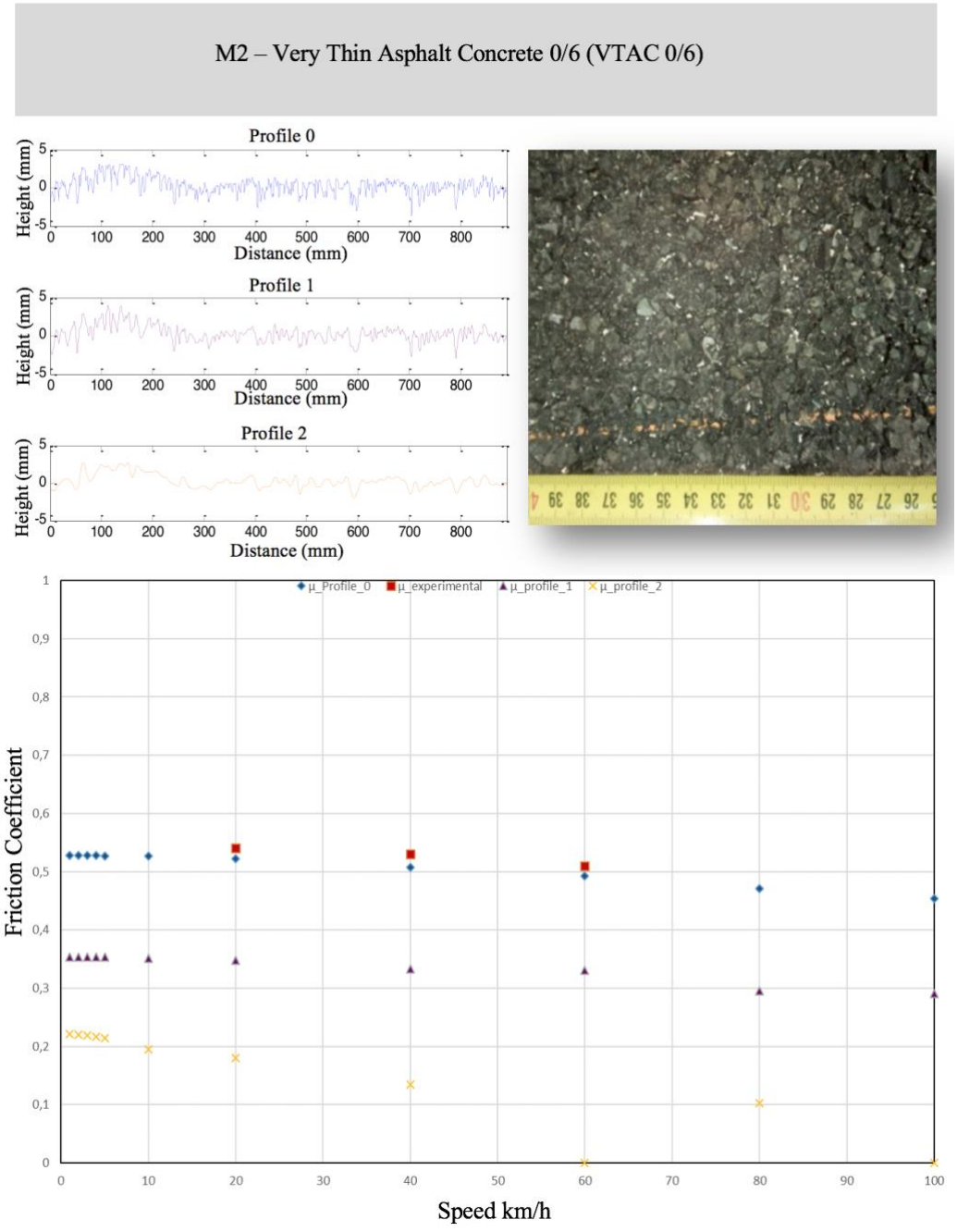

Figure 6.11. The Very Thin Asphalt Concrete Surface. Up-left: Newly constructed profiles. Up-right: Picture of the surface. Bottom: DFM and DFT Skid resistance of Profiles 0, 1 and 2 versus speed.

of this paper (Sabey, IFI, Penn State model…) which state that the skid resistance at low speed is governed by the SST, and the shape of the curve against speed is related to the LST.

6.8.2.2 The painted flexible asphalt and the smooth epoxy resin

These two surfaces have the particularity of displaying very low SST and LST, possibly even nil for the smooth Epoxy Resin. For the Epoxy Resin, the Profiles 0 to 2 are similar and even all smooth. For the Painted Flexible Asphalt, the Profiles 0 to 2 have similar LST, but differences residing in the presence or not of SST (refer to Figures 6.12 and Figure 6.16 in the Appendix).

For these two surfaces, the DFM predicts relatively low skid resistance (with some instability in the calculations) which is in accordance with the DFT measurements, but not as precise as for the Asphalt Concrete surfaces. This may again be explained by the use of the same value for the adhesion coefficient, with 0.2 being adopted for all surfaces to proceed to the DFM simulations, a value that may be different in reality for each surface.

Again, for both surfaces, the DFM predictions of the skid resistance for the Profiles 0, 1 and 2 follow the same trend, starting with a low skid resistance at low speed and ending with almost nil value at higher speeds. This behavior is again in accordance with the expectations, low SST means low skid resistance at low speed and low LST leads to the high negative slope of the skid resistance curve against speed.

6.7.2.3 The calcined bauxite colgrip

This material is known to provide a high grip surface. The surface is built using sharp calcined bauxite particles of very small size, resulting in good SST, but a mean (or even weak) LST. The three Profiles 0 to 2 derived from this surface are similar in LST: being low but very sharp (conical) shape at their tops of the indentors (refer to Figure 6.13). For the SST, the ranking is from Profile 0 (very high) to Profile 2 (very low), which was logically expected.

The DFM skid resistance predictions are relatively low in comparison to the DFT measurements. Again, this may be explained by the adhesion coefficient value being set to 0.2 for DFM simulations, whereas this value should be higher for such a micro-rough surface.

The DFM predictions of the skid resistance for the Profiles 0, 1 and 2 follow the same trend with increasing speeds, but Profiles 1 and 2 are shifted significantly downwards compared to Profile 0. The skid resistance of these three profiles does not display a high negative slope despite their low LST. This behavior is unexpected (in accordance with the works exposed in

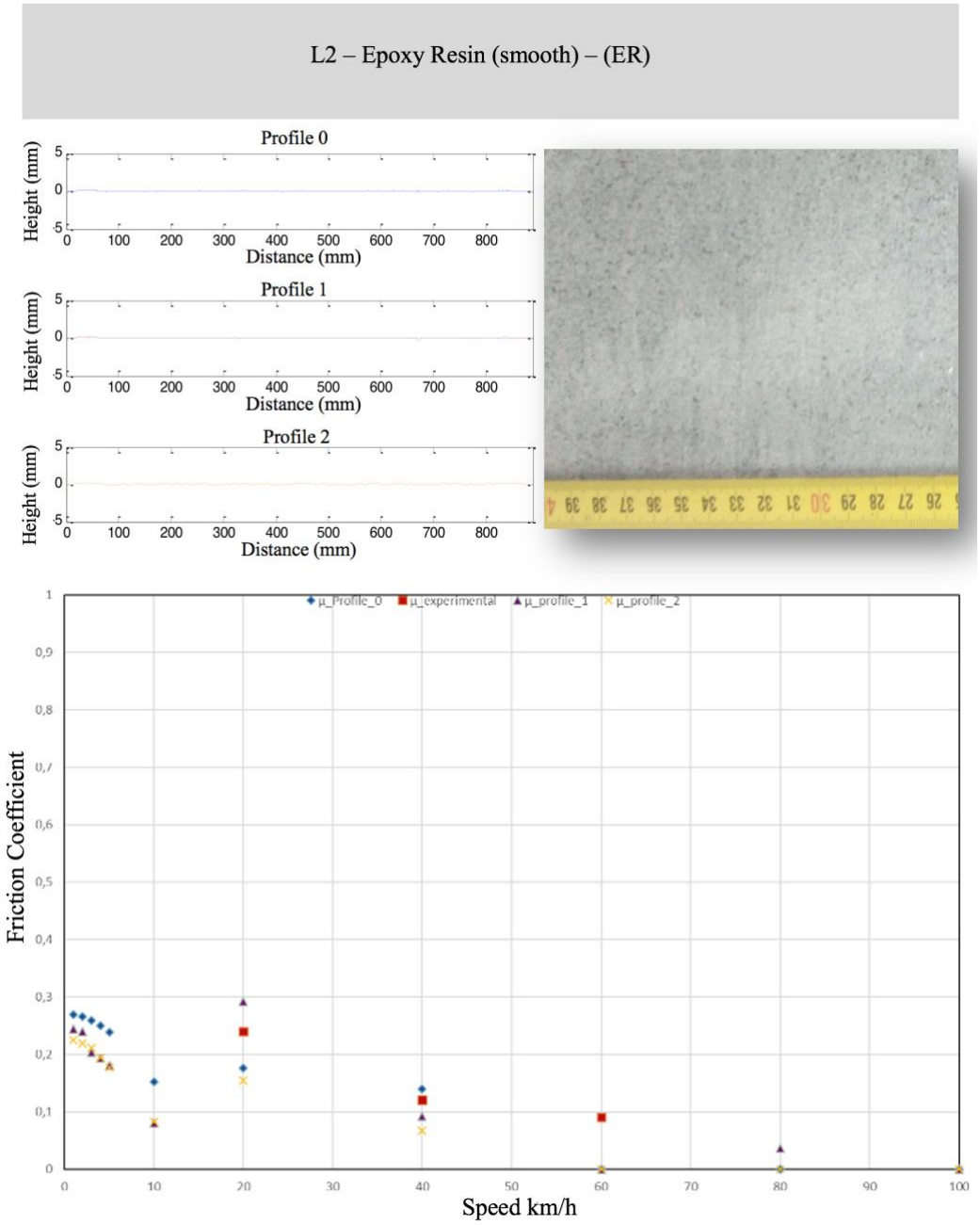

Figure 6.12. The Epoxy Resin (smooth) Surface. Up-left: Newly constructed profiles. Up-right: picture of the surface. Bottom: DFM and DFT Skid resistance of Profiles 0, 1 and 2 versus speed

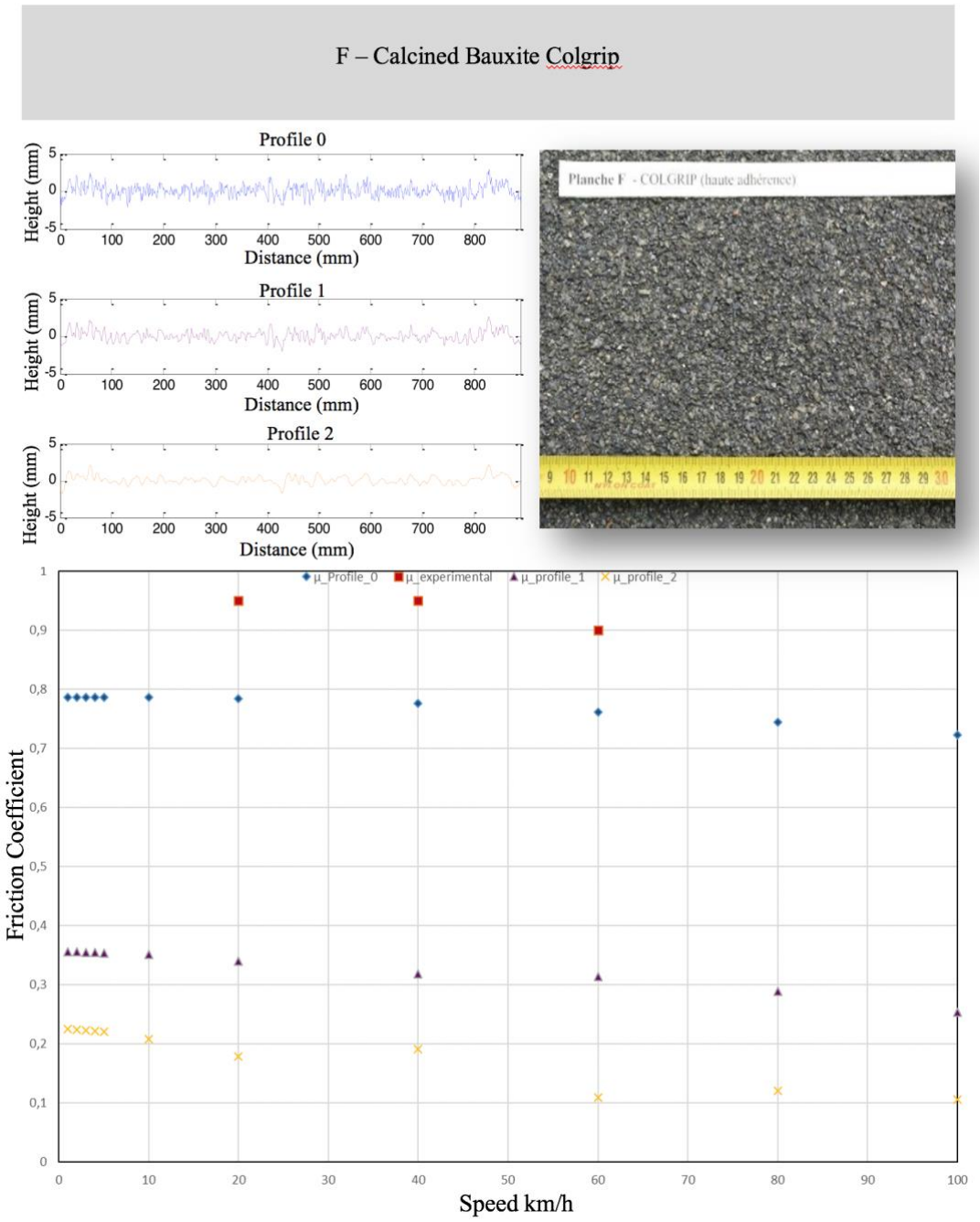

Figure 6.13. The Calcined Bauxite Colgrip Surface. Up-left: Newly constructed profiles. Up-right: picture of the surface. Bottom: DFM and DFT Skid resistance of Profiles 0, 1 and 2 versus speed

the introduction which state that the skid resistance at low vehicle speed is governed by the SST and the shape of the curve against speed is related to the LST).

The low slope of the skid resistance curve is probably due to the pronounced conicity of the indentors despite the low level of LST. This observation rejoins Forster's who claimed that the most correlated aggregate characteristic to skid resistance is its shape (Forster, 1981). This means that if the presence of LST is good when the speed increases, the shape of local summits of the SST can be beneficial and can even compensate for the lack of LST.

Even though it should be noted that this random distribution and the pointed shape of the summits may also be an inconvenience with respect to other surface properties such as noise and/or rolling resistance.

6.8 Conclusion

This paper aimed to contribute to identifying the role of road surface SST and LST on wet skid resistance. To achieve this, the EMD used to first smoothen at different degrees the textures of selected surfaces and second to apply the DFM on these newly created surfaces to predict their wet skid resistance at different speeds. The results of these simulations showed the importance of both texture scales, but also reveal that the spatial arrangements and shapes of them are just as important. Indeed, on wet road surfaces,

- the SST is key to achieving good skid resistance at low speeds and
- the LST is crucial to maintaining it when the speed increases.
- Also, if the presence of SST is important to improve skid resistance, the distribution of the summits of the LST is also beneficial and can even compensate for the lack of SST.
- And finally, if the presence of LST is important for the maintenance of skid resistance when the speed increases, the shape of local summits of the SST may be also important and can even compensate for the lack of LST.

Even though it should be noted that this random distribution and the pointed shape of the summits may also be an inconvenience with respect to other surface properties such as noise and rolling resistance.

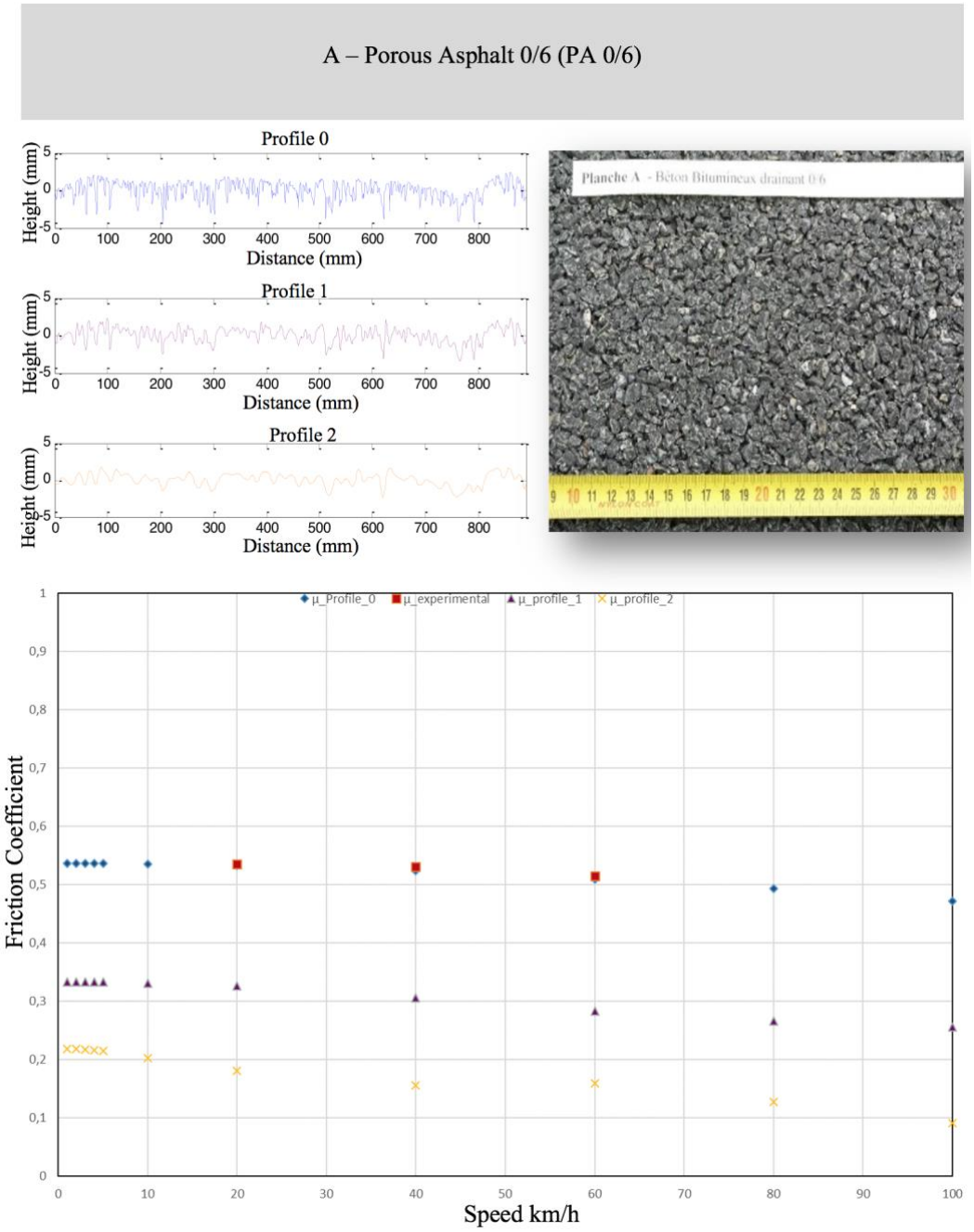

Figure 6.14. The Very Porous Asphalt Surface. Up-left: Newly constructed profiles, Up-right: picture of the surface, Bottom: DFM and DFT Skid resistance of Profiles 0, 1 and 2 versus speed

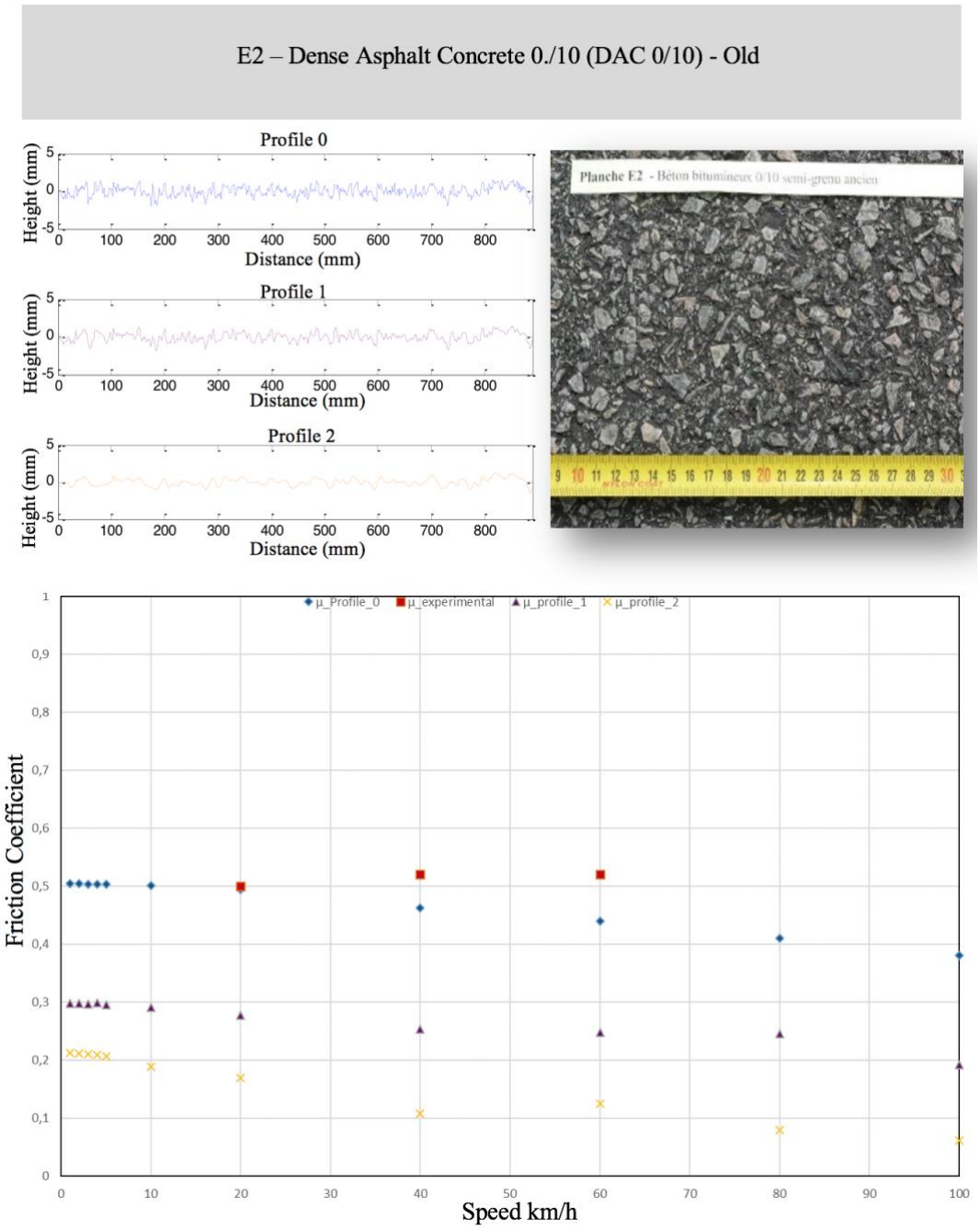

Figure 6.15. The Dense Asphalt Concrete Surface. Up-left: Newly constructed profiles. Up-right: picture of the surface. Bottom: DFM and DFT Skid resistance of Profiles 0, 1 and 2 versus speed

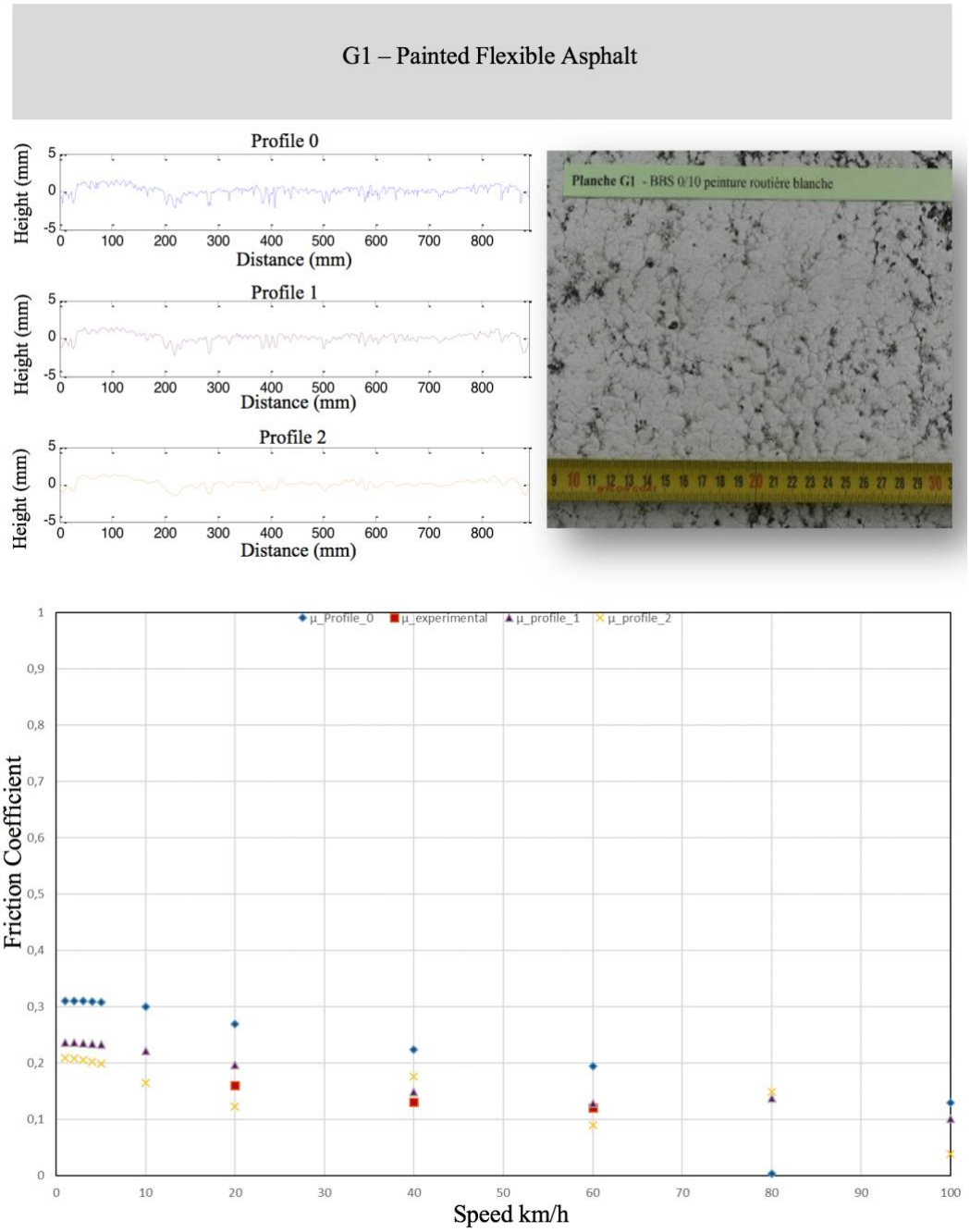

Figure 6.1. The Painted Flexible Asphalt Surface. Up-left: Newly constructed profiles, Up-right: picture of the surface. Bottom: DFM and DFT Skid resistance of Profiles 0, 1 and 2 versus speed

7.0 Discussion

7.1 Introduction.

This thesis investigates the evolution of macrotexture on asphalt pavements using non-contact field techniques. In *Chapter 3* three non-contact measurement techniques: a 3D smart laser profile scanner; Structure from Motion (SfM) photogrammetry and; Terrestrial Laser Scanning (TLS) for characterising and monitoring pavement macrotexture in the field were evaluated. The discussion in Section 7.2 will provide a scarce comparison of the respective accuracy of these wider scale techniques, when used to spatially measure macrotexture with areal parameters. The findings consider the sensitivity of functional areal parameters to resolution, filtering and sample size. Within *Chapter 4* a new data analysis approach utilising time series data with spectral analysis and spatial filtering procedures, was presented to determine long term rates of change in road surface macrotexture. Section 7.3 will discuss the outcome of the application of these new methods to visualise temporal and spatial change, for twenty-four years of legacy SMTD data acquired for a 2 km stretch of the M6 motorway in Cumbria. *Chapter 5* applied the new methods to a wider study of fourteen sites located on a north to south transect spanning the longest highway in the UK. Section 7.4 will compare the resulting macrotexture evolution trends to meteorological and traffic datasets, establishing for the first time that SMTD measurements experience a seasonal signal. Thus, providing compelling evidence pointing toward surface processes (such as polishing and the wetting and drying of surface contaminants), causing changes to texture that are affecting seasonal variation in skid resistance. *Chapter 6* considers the role of asphalt texture scales on the development of skid resistance. Section 7.5 will discuss the importance of the spatial arrangement and shape of 'small-scale-texture' (SST) and 'large-scale-texture' (LST) on skid resistance. Finally, Section 7.6 will provide a useful synopsis of the main points covered within this discussion.

7.2 Measuring the surface macrotexture of asphalt pavements using non-contact techniques.

Three non-contact measurement techniques: a 3D smart laser profile scanner; Structure from Motion (SfM) photogrammetry and; Terrestrial Laser Scanning (TLS) were used to capture pavement texture for different asphalt road surfaces and point clouds generated from the data. Resolution governs the level of identifiable detail in a point cloud. The Nyquist-Shannon (Shannon, 1998) sampling theorem is a useful rule to apply to point cloud resolution. It states that the minimum size of a features should be twice that of the sampling interval. Macrotexture represents pavement texture components with wavelengths from 0.5 mm to 50 mm and amplitude of 0.1 mm to 20 mm, formed by the shape, size and gradation of road aggregates

on a pavement surface (International Standards Organisation, 2009). This means that the minimum required sampling interval, or distance between points within a cloud is 0.25 mm to adequately sample for macrotexture. In practice, the minimum Nyquist wavelengths measured by the techniques was observed to vary for the different asphalt samples, possibly because the techniques are sensitive to pavement surface albedo, environmental conditions, and edge effects. Given technique sensitivity to these conditions, oversampling to ensure a sufficiently fine Nyquist wavelength is recommended. The minimum measured wavelength for the 3D Smart Laser Profile Sensor meant the technique was unable to measure a small part of the lower range of macrotexture between 0.5 and 1 mm. This was comparable to the spatial sampling of the prototype test rig of Wang et al. (2012) which also employed a laser utilising triangulation. The SfM and TLS techniques were able to measure the full range of macrotexture wavelengths and demonstrated the potential to also measure some part of microtexture below 0.5 mm. However, as consequence of angular resolution, which causes the elongation of the laser beam as the angle of incidence with a surface increases, the Nyquist wavelength for a TLS instrument increases with distance from the laser source. Therefore, the optimal location to acquire TLS data with an 'off-the-shelf scanner', is within a narrow cone of incidence directly in line with the laser source, with data captured using an inverted head tripod set-up. This means that several static TLS point cloud surveys would need to be registered together to acquire long sections of road, or an effective TLS instrument arrangement developed to be mounted in some manner upon a vehicle.

As contact friction devices are known to be susceptible to seasonal variation and machine operating conditions such as load, speed slip ratio and the composition of rubber (Dunford, 2013), using reliable non-contact texture data to analytically model a relationship with friction is desirable. In 2012, Part 2 of ISO 25178 covering the definitions areal parameters (International Organisation of Standardisation, 2012) to characterise textured surfaces was published. Limited research has been undertaken studying the application of areal parameters to characterise road texture on live networks, in order to establish empirical, statistical or analytical modelled relationship with contact friction.

Kogbara et al. (2008) found that frictional resistance is sensitive to the density of the peaks within the macrotexture of a highway (areal parameter S_{pc}), and to the pointiness or arithmetic curvature of the same peaks (areal parameter S_{pc}) characterising the shape and size of road aggregate. The authors suggest sensitivity arises as sharp peaks and edges on a road pavement surface, assist in breaking through the lubricating water film between the tyre and the pavement. The Kogbara et al. (2008) study proposed a statistical relationship between areal parameters derived from filtered close range photogrammetry data and skid resistance, but did

not specifically consider the sensitivity of area parameters to technique resolution, filtering or sample size.

The work undertaken in this thesis demonstrates that unfiltered S_{pd} and S_{pc} are sensitive to resolution, incurring order of magnitude differences between the techniques and surfaces considered. The variability of the parameters limits the potential to adopt unfiltered data in 'universal' across technique parametric comparison studies with friction. The application of a 2D low pass a 0.1 mm^{-1} wavenumber filter improved agreement, particular between the 3D smart profiler and SfM, for the S_{pd} and S_{pc} parameters. Notwithstanding, optimising such filters consistently across a range of non-contact techniques and asphalt surfaces is needed to achieve a 'universal' correlation between areal parameters and to model relationships with skid resistance. Importantly, the work completed in this thesis indicates that filtering can improve spatial agreement, but at the cost of vertical measurement, a factor that should be considered by researchers seeking correlations between non-contact texture measurements and skid resistance. S_q represent the root mean square of surface departures, and like linked parameters S_p and S_v (maximum peak and pit height) is equivalent to MTD. The value for S_q, S_p and S_v, demonstrated greater agreement between the SfM and 3D Smart Laser Profile techniques. It was found that SfM photogrammetry successfully provides an alternative method to the 3D Smart Laser Profile Sensor to capture vertical pavement measurements. Yet, with filtering S_q, S_p and S_v, experienced magnification at a range of four to ten times for the two techniques. Findings thereby suggest that filters should be applied only to the spatial parameters such as S_{pd} and S_{pc}. Moreover, higher resolution does not always equate to greater accuracy. S_q, S_p and S_v, obtained from the higher resolution TLS unfiltered data contained significant inaccuracies. The inaccuracies occur largely due to 'noise' generated by edge effects and 'specular flares' (Boehler et al., 2003) within the scanned point cloud data. Post-filtering the TLS technique did offer the best balance between the vertical and spatial areal functions, fundamentally because it enables oversampling of the surfaces, with correspondingly the shortest Nyquist wavelength. However, the improved filtered data still did not result in sufficiently accurate measurements for either S_q or S_{pc}.

S_{pd}, previously identified by Kogbara et al. (2008) to correlate with frictional resistance, was found in the research concluded within this thesis to be sensitive to sample size. The S_{pd} parameter representing the number of peaks in a unit area, demonstrated the greatest variability across seventy-two different 150 mm x 150 mm samples considered for a 1.8 m x 0.9 m HRA surface in comparison with other areal parameters (S_p, S_{sk}, S_q, S_v, and S_{pc}). The variability of S_{pd} values, means one 150 mm x 150 mm sample of the HRA is unlikely to be representative of the whole pavement surface, presenting validity difficulties to researcher like

Kogbara et al. (2008) using 'spot' sand patch size samples to explore correlations between S_{pd} and friction. Moreover, the susceptibility of individual areal parameters used to characterise friction (S_p, S_v, S_{pd} and S_{pc}) to change in sample size, was investigated by this thesis and optimal sample sizes suggested. For S_{pd} the optimum sample size for the HRA surface was found to be 1050 mm x 1050mm. For the vertical macrotexture parameters, the optimum sample size was found to be 750 mm x 750 mm for S_v , 1050 mm x 1200 mm for S_p, and 1050 mm x 1650 mm for S_q. For S_{pc} mean curvature of peaks, the optimum sample size was discovered to be 450 mm x 450 mm for the HRA surface. S_{pc} was found to have the smallest sample size of all the parameters considered perhaps reflecting its general lack of heterogeneity. Overall reviewing the optimal sample size, suggests that a suitable sample size of 1050 mm x 1200mm is appropriate to characterise HRA; this being established from the maximum size of the individual parameters.

7.3 Methods to determine the evolution of asphalt pavement macrotexture.

A new data analysis approach utilising time series data with spectral analysis and spatial filtering procedures, was applied to legacy SMTD data obtained for a 2 km stretch of the M6 motorway in Cumbria between 1995 to 2019. The SMTD data related to Lane 1 the nearside lane and Lane 2, the middle lane of the three-lane motorway. For Lane 1, the test section of road was constructed originally of dense bitumen macadam (DBM) laid on 11th October 1970. On the 27th August 2004 the DBM was replaced with heavy duty macadam (HDM) between chainage 0 m and 600 m. This surface was replaced again on the 1st October 2016 as part of a resurfacing of the lane between chainage 0 m to 1500 m with a thin mastic asphalt (Manual of Contract Documents for Highway Works 2019). Finally, on the 3rd March 2008 a thin polymer surfacing was laid between chainage 1500 m and 2000 m (Manual of Contract Documents for Highway Works 2019). In Lane 2 the test section of road was constructed from thin surfacing (Manual of Contract Documents for Highway Works 2019) laid on 27th August 2004 for chainage 0 m to 600 m, hot rolled asphalt (HRA) laid on 5th April 1998 between chainage 600 m to 1480 m, and older HRA laid on 11th October 1970 chainage 600 m to 2000 m.

The new technique facilitated the visualisation of change in road surface macrotexture. Temporally, change in plot colour correctly indicated when a change in road surfacing and/or some localised patch repairs to the highway surface had occurred in agreement with construction records (described in the paragraph above). Spatially, the approached delineated the position of construction joints between the distinct surfacing materials used for the different sections of motorway lane. Universally, the spatially plotted filtered SMTD data was shown 'roughing-up' or having increased texture depth through the lifetime of each surface

material. This general trend of increase in SMTD, matches the findings of previous research undertaken by Vaiana et al. (2012) and Plati and Pomoni (2019). These studies found respectively, that subsequent to the early life of the pavement or after the achievement of a minimum cumulative traffic threshold macrotexture evolution generally increased.

The results demonstrate that it is possible for the filtered SMTD time series to be plotted spatially and used effectively to visually observe segments of a road surface which are changing at different rates. Within Section 2 of the Lane 2 the changing SMTD appears as yellow bands, which widen progressively with the passage of time. This advance presents the potential for future research to explore the use of visual recognition software to identify 'change traces', and establish if they coincide with areas of poor pavement condition in order to improve pavement management systems. A long-term rate of change for each section of motorway lane was characterised by linear regression. Being able to categorise a linear rate of change has unlocked the potential to develop a method for forecasting the future long-term rate of change of SMTD by extrapolation, for highway surfaces at discrete lane locations upon a road network. Further developing this method would need to take account of potentially non-linear variables, influencing future road conditions such as traffic volumes and weather patterns (refer to Section 7.3).

Furthermore, wavenumber amplitude spectra of the filtered SMTD data were found to have a periodicity extending systematically through time, associated with a wavelength typically of between 33 m and 62 m. The invariant nature of the periodicity suggests that the unevenness might be constructed into the road (possibly as a consequence of the use of highway paving plant), or perhaps imprinted during its early history after construction. It is known that the suspension systems of heavy vehicles such as buses and trucks apply a cyclic loading to a pavement surface via the tyre-road interaction. The suspension system of a large vehicle such as a bus, can be simplified to a spring-mass-dashpot model and for a bus has previously been shown to have a resonance frequency of around 0.5 Hz (Sekuic and Dedovic 2011). At this resonance, the tyres of a vehicle travelling at a speed of 96.56 kmh^{-1} would apply a cyclic load to a pavement surface with a wavelength of 53.6 m. On climbing sections of motorway, heavy vehicles such as trucks or buses tend to travel more slowly, and this would shorten the distance between the application of each tyre load; for example, at 72.42 km/h a truck or bus with a suspension system operating at 0.5 Hz would apply a load every 40 m. As the periodicity observed at the study site was banded with wavelength between 33 m to 62 m, a plausible causation theory is that the cyclic loading of heavy vehicle suspension systems has imprinted the undulating wavelengths into the road surface early in the road's life. Imprinting may have arisen through a process of the intermittent-localised compaction of the lower pavement layers

or the pavement surface when the bitumen matrix becomes marginally softer in the warmth of the summer. The periodic features observed are systematically well-organised, meaning that the heavy vehicles such as trucks or buses would have to be in phase with each other when driving along the pavement surface, which is what would be expected. Synchronisation of traffic flow is a recognised phenomenon (Kerner 2018) and in phase movement of vehicle suspension in traffic flow could be triggered by an irregularity such as a bump or more likely a construction joint within the road. Conceivably, construction joints act as triggers at consistent points on the route, exciting high amplitude resonances within the suspension systems of the travelling vehicles and leading them to move up and down in phase with each other. Subsequent change in the pavement surface through compaction arising from the cyclic tyre load, would reinforce the resonant excitation of the heavy vehicle and thus maintain them in phase with one another. The proposed influence of the cyclic tyre loading action of the heavy vehicles to the pavement is supported by the change of SMTD generally coinciding with the peaks of the periodicity features, and this change being amplified with time suggesting consistent and progressive tyre-pavement interaction at these locations.

7.4 The influence of environmental parameters on asphalt pavement macrotexture.

Legacy Sensor Measured Texture Depth (SMTD) data over a 19-year period, have been analysed using spatial filtering techniques and compared with meteorological and traffic datasets. The SMTD data was collected for fourteen sites located on the A1(M), the longest north to south highway in the UK, connecting Edinburgh with London. The results for HRA surfaces reveal that the 'rate of change' to SMTD uninfluenced by exceptionally high precipitation follow a linearly increasing trend with time, at a magnitude or gradient (∅) that correlates with AADT. The angle (∅) steepens when AADT is adjusted for the percentage of HGVs, as might be expected because the heavier axle loading and tyre types associated with commercial vehicles are known to cause more impact on macrotexture polishing than other types of road vehicles (Bagui et al., 2013; Do et al., 2007; Vaiana et al., 2012). The conclusion aligns with other studies, completed by Pomoni et al, (2020) who tracked changes on a hot mix asphalt surface using cumulative traffic data and observed an increase in macrotexture on pavement surfaces after a threshold level of cumulative traffic had been achieved in the life of the pavement. In the work undertaken as part of this thesis the observed long-term linearly increasing trends do not consider the very 'early life' of the HRA pavement, a period likely to be governed by other processes, such as the stripping of bitumen bloomed on a newly laid surface (Kane et al., 2012).

Pomoni et al, (2020) determined during the early life of the pavement, prior to the achievement of the cumulative traffic threshold, change in surface texture behaves differently. They

observed a decreasing trend with some fluctuations in texture attributed to short-term variations arising from changes in the asphalt surface due to processes influenced by conditions of the area, for example the influence of dust and rain. Similar minor annual variability was found in the long-term data considered during this study, characterized as change in filtered mean SMTD values less than ±0.04 mm. Changes less than 0.04 mm in SMTD are thought to represent surface processes occurring in the winter and summer. Previous researchers have presented hypotheses over these governing processes. In the summer it has been hypothesised that pavement texture can becomes coated with residual rubber, rubber particles, oils and lubricants (Gobmann et al., 2021; Kogbara et al., 2016). Furthermore, sunny days with air temperatures of 20°C or above can generate road surface temperatures of the order of 50°C as dark asphalt surfaces absorb heat. This has been shown to be sufficient to cause unmodified binders present in a road to become sticky in places with the potential to smut and cover part of the pavement surface in localized areas (Kodippily et al., 2012). Alternatively, in the winter at temperatures below 0°C water present in small voids in the pavement aggregate can freeze. The resulting nine percent volumetric expansion in this water can cause fragments of aggregate to break away from the pavement surface, a process known as frost shattering. This can lead to loose aggregate on the pavement surface, which can act as an abrasive under tyres polishing the pavement surface (Wilson, 2013). The potential for voids is increased by embrittlement in asphalt pavements caused by the aging of the SARA (Saturate, Aromatic, Resin and Asphaltene) components of the bitumen binder through oxidization under ultra-violet radiation and hydrological erosion (Eberhardsteiner et al., 2015). Embrittlement of the binder leads to the development of micro-cracks into which water can infiltrate and freeze. These theoretical seasonal surface phenomena are widely accepted, but much research is still required to monitor them practically in the field.

It is discernible from the results of the study undertaken that whilst within the threshold of ±0.04 mm these surface processes are ‘in balance’. However, disruptions are observed arising from notable precipitation events, causing the development of ‘peaks’ in the deviation of filtered mean SMTD from long term trends during summer months and ‘troughs’ in the winter months. The link between above average precipitation events and transient changes in SMTD suggests that a washing effect may be occurring on the HRA pavement surface. In the summer months the disruptive precipitation events are potentially removing any oil, lubricants, or rubber particle contaminants present either on the surface of the HRA aggregate or within the voids, causing an increase in the SMTD measurements. In the summer these contaminants are likely to be drier and therefore more likely to be expelled from the pavement macrotexture in an emulsion. In the winter it its theorized that due to the quantity of abrasive material and also sand from road salting activities present on the surface, that polishing of the HRA aggregate

governs. It has been suggested by other researchers that whether a surface becomes more polished or whether it becomes rougher is a function of the minerology and polish stone values of the aggregate and of the nature of dust/detritus finding its way onto the pavement surface (West and Ross, 1962; Kogbara et al., 2016) However, it is clear from the data studied in this thesis that negative deviations from filtered mean SMTD from the long-term trend are typically occurring after above average precipitation in the winter. It is therefore postulated that either dust, debris, and sand from salting on the surface are being 'redistributed' within the negative texture of the HRA pavement; or that the contaminants in the winter are more likely to be miscible on the surface and less susceptible to washing.

Ultimately, little is known about the characteristics of precipitation needed to effectively clear or clean a highway surface or the wetting and drying processes occurring and interacting with surface contaminants. It is clear though that rainfall is acting to disrupt the SMTD (Ongel et al., 2009). The findings presented in this thesis demonstrate for the first time that the disruption has a seasonal pattern. Interestingly this pattern follows an inverse trend to the classically understood pattern of seasonal variation in skid resistance in the UK, where skid resistance is thought to be lower in the summer and higher in the winter (Hosking and Woodford, 1975). As skid resistance is measured as a frictional response to pavement texture, this suggests that processes on pavement surfaces are influencing seasonal variation in skid resistance; along with the other recognized parameters such as speed, temperature, tire tread thickness and viscoelastic deformation. An inverse relationship between texture and skid resistance has been observed by others (Pomoni et al., 2020) when considering the long-term pavement texture evolution with cumulative traffic. Furthermore, recent studies seeking to determine a percentile dry skid resistance based on wet period measurement, noticed the same percentile occurring with different traffic and precipitation intensity, concluding that this pointed to the potential for asphalt pavement surfaces to be influencing seasonal variation (Plati et al., 2020) Certainly, the summer 'peak' signals were observed during the months of April to September, which broadly match the seasonal summer period of low skid resistance measurement in the UK (Design Manual for Roads and Bridges, 2021). Further study of the seasonal signal observed in the SMTD will be required to ascertain the contribution of surface processes to seasonal variations of skid resistance. Such research will require measuring in a controlled manner: skid resistance, macrotexture depth, environmental conditions and monitoring at the macrotexture scale the wetting and drying processes of contaminants on the surface of the pavement. These findings demonstrate that texture measurements experience a seasonal signal and point to a requirement for measuring equipment to be modified to clean pavement surface of detritus prior to readings being taken to achieve more accurate and representative measurement of SMTD.

7.5 The role of asphalt texture scales on the development of skid resistance.

A signal processing technique termed Empirical Mode Decomposition (Kane et al., 2015) was used to decompose the texture measurements of seven surfaces into a set of component profiles of different wavelengths. These different profiles were partially recomposed to derive a profile consisting of 'small-scale-texture' (SST) and 'large-scale-texture', a profile without SST, and a third profile where LST was smoothed even further. The friction on these three recomposed profiles will be calculated using the Dynamic Friction Model (Kane and Cerezo, 2015b). The outcome confirmed the findings of previous research completed to investigate the effect of SST and LST scales on speed-dependent wet skid resistance (Sabey, 1958; Leu et al., 1983; Flintsch et al, 2013; Fwa, 2017). SST was recognized to be the key to achieving good skid resistance at low speed for the surfaces sampled, whilst LST was found to be crucial to maintaining skid resistance with increasing speed, influencing the shape of the skid resistance coefficient/speed curve. Importantly, the plots of skid resistance coefficient verses speed for the 'analytical surface' constructed in the laboratory displayed the same behaviour with increasing speed for Profile 0 (profile with SST and LST) and Profile 1 (profile without SST). This was an unexpected result when compared to previous work (Horn et al, 1983; Flintsch et al, 2013) which would have suggested that the Profile 1 without SST should have had a lower initial peak value of friction coefficient. Upon examination the irregular distribution of the local summits of the LST were discovered to be able to compensate for the lack of SST. Conversely, the reverse was also established as a being true, with the small sharp local summits of SST being found to compensate for a lack of LST. This conclusion is useful to those investigating the optimisation of skid resistance for the development of texture for new pavement materials. Even though it should be noted that this random distribution and the pointed shape of the summits may also be an inconvenience with respect to other surface properties such as noise and rolling resistance

7.6 Summary.

The work undertaken in this PhD scrutinises the measurement of pavement macrotexture using non-contact techniques, and subsequently moves on to consider analysis approaches using legacy data sets to maximise knowledge of macrotexture evolution. Studies focusing on macrotexture measurement found that SfM photogrammetry successfully provides an alternative approach to capture vertical and spatial pavement measurements at an accuracy comparable to a 3D Smart Laser Profile Sensor operating on triangulation principles. TLS instrumentation operating on phased-based principles offered the highest resolution technique in terms of Nyquist sampling, but critically this was discovered not to equate to greater

accuracy. Even with filtering TLS data does not render comparable accuracy with a 3D Smart Laser Profile Sensor for spatial and vertical measurement at macrotexture scales. The TLS technique suffers from inaccuracies occurring due to 'noise' generated by edge effects and 'specular flares' (Boehler et al, 2003) within the scanned point cloud data. Researchers must select appropriate non-contact laser techniques for pavement macrotexture, and this means practically considering the response of laser light energy and pulse rate to different pavement surfaces, as well as resolution and Nyquist sampling strategies.

The scrutiny work completed established that unfiltered S_{pd} (density of peaks) and S_{pc} (the pointiness or arithmetic curvature of peaks) previously correlated to friction by Kogbara et al., (2008) are sensitive to resolution, incurring order of magnitude differences between the different techniques and surfaces considered. The variability of the S_{pd} and S_{pc} parameters limits the potential to adopt unfiltered data in 'universal' across technique parametric comparison studies with friction. The application of a 2D low pass 0.1 mm^{-1} wavenumber filter improved agreement, particular between the 3D smart profiler and SfM, for S_{pd} and S_{pc}. Notwithstanding, optimising such filters consistently across a range of non-contact techniques and asphalt surfaces is needed to achieve a 'universal' correlation between areal parameters to model relationships with skid resistance. Importantly, the work completed in this thesis indicates that filtering can improve spatial agreement, but at the cost of vertical measurement, a further factor that should be considered by researchers seeking correlations between non-contact texture measurements and skid resistance. Moreover, researchers need to consider sample size as the areal parameters used most frequently in correlations with friction (S_p, S_v, S_{pd} and S_{pc}) are susceptible to size variation. Sample size needs to be optimised for both asphalt surface and the non-contact measurement technique deployed. The work undertaken found that HRA measured using SfM requires an optimised sample size of 1050 mm and 1200 mm; an area fifty-six times bigger than that of the volumetric sand patch test.

The second aspect of the PhD work developed a new data analysis technique using spectral analysis and spatial filtering to characterise temporal and spatial change in pavement macrotexture using legacy SMTD data. The results demonstrate that it is possible for the filtered SMTD time series to be plotted spatially and used effectively to visually observe segments of a road surface which are changing at different rates. Long-term rates of change for each section of motorway lane were characterised by linear regression. The 'rate of change' was shown to be influenced by the order of magnitude of annual average daily traffic (AADT), when factored for the percentage of heavy goods vehicles. This linear trend was disrupted by environmental parameters such as rainfall events and seasonal conditioning. In the summer a 'seasonal signal' is evident as a transient peak in the 'rate of change' of texture

greater than 0.04 mm, and in the winter as a reduction. The transient changes in texture corresponded to above average rainfall occurring in the week prior to SMTD measurement. The signal observed demonstrated an inverse pattern to the classically understood seasonal variation of skid resistance in the UK, where values are low in the summer and high in the winter. The findings demonstrate for the first time that texture measurements experience a seasonal signal, and provide compelling evidence pointing toward surface processes (such as polishing and the wetting and drying of surface contaminants) causing changes to texture that are affecting seasonal variation in skid resistance.

Finally, wavenumber amplitude spectra of the filtered SMTD data were found to have a periodicity extending systematically through time. The invariant nature of the periodicity suggests that unevenness, might be constructed into the road (possibly as a consequence of the use of highway paving plant), or perhaps imprinted during its early history after construction. If vehicle suspension systems are found to influence texture evolution through cyclic tyre loading, then this will have implications for the future design of highway pavements. Additionally, those investigating the development of texture for new pavement materials to optimise skid resistance, might take advantage of irregular distribution of the local summits of LST which were discovered by this PhD to be able to compensate for a lack of SST. Conversely, the small sharp local summits of SST were found to compensate for a lack of LST.

8.0 Conclusion

8.1. Introduction

This concluding chapter will document the main findings from the thesis (Section 8.2), before detailing any inherent limitations of the work (Section 8.3). Finally, suggestions for future work, beyond the scope of this PhD will be outlined in Section 8.4.

8.2. Main findings

Objective 1: **Measure the surface macrotexture of asphalt pavements using non-contact techniques.**

The work undertaken in this PhD makes a first contribution to the establishment of reliable standardised texture measurements using point cloud derived data; to inform analytical prediction methods for tyre-pavement contact friction, without the influences of seasonal variation measuring devices and their operating conditions. Results from the analysis of the data lead to the following conclusions:

- Unfiltered close field SfM photogrammetry provides values of S_p, S_v and S_q, within an acceptable degree of tolerance to those obtained from the 3D Smart Laser Profile Sensor, so SfM photogrammetry is an effective, readily scalable alternative method to capture mean profile depth for pavement evaluation.
- The parameters S_{pc} and S_{pd}, for which previous studies have established an important correlation with pavement friction, are sensitive to technique resolution and an optimised 2D low pass wavenumber filter needs to be applied to obtain a 'universal' measurement for pavement friction assessment across non-contact techniques.
- The Nyquist wavelengths of the SfM techniques means it has the potential to measure microtexture wavelengths below 0.5mm.
- Where 150 mm x 150 mm industry sample sizes are used to determine parameters from point clouds data derived from non-contact techniques, these are not sufficient to correctly characterise functional areal parameters to describe the spatial variability of macrotexture upon a pavement. This study suggests a suitable sample size of 1050 mm x 1200mm is appropriate to characterise HRA.

Objective 2: **Develop an analysis method to determine the evolution of asphalt pavement macrotexture.**

This PhD provides a rare and valuable long-term study of SMTD. A new computational process has been developed and applied to reveal a number of key and important trends influencing long term change in pavement texture

- It is possible for wavenumber filtered SMTD time series time-lapse data to be used to visually observe discrete segments of a road surface which are changing with time.
- Change 'traces' are evident within the wavenumber filtered SMTD time series. This presents the potential for further research to use visual recognition software to identify change 'traces' in order to locate areas of poor pavement condition.
- The study presents a viable method to track the rate of change of SMTD over time, generating essential monitoring data for pavement management systems and highway maintenance decisions.
- At unevenness scale a periodicity is observable in the data systematically through time, suggesting that unevenness might be imprinted into a road surface during construction or early in its life. 'Imprinting' may occur as a consequence of cyclic tyre loading applied by the suspension systems of heavy vehicles.
- Construction joints in pavement surfaces, in combination with vehicle travel speeds, have the potential to trigger periodically spaced change in pavement texture.

Objective 3: **Determine the influence of environmental parameters on asphalt pavement macrotexture.**

SMTD data were analysed using the novel spatial filtering techniques and compared with traffic flow and meteorological datasets for fourteen sites located on the north to south transect of the A1 (M) in the UK. The long-term evolution of SMTD for HRA surfaces, when seasonal signals were discounted in the 'rate of change', was determined to follow a linearly increasing trend at a gradient ($\emptyset$) correlated to the order of magnitude of the AADT. The results also demonstrate for the first time a seasonal signal in SMTD measurements corresponding with above average precipitation occurring within the week prior to the SMTD measurement being taken. The pattern observed demonstrates positive deviation from the long-term evolution of filtered mean SMTD in the summer and negative deviations in the winter. The results indicated that processes occurring on the surface of the HRA pavement are influenced by seasonal conditioning.

The study results are presented as a new conceptual model summarizing the governing trends of long-term change on Hot Rolled Asphalt pavement surfaces. The conceptual model considers new theories of the surface processes driving the detected patterns related to the

wetting and drying of surface contaminants. In the summer, the build-up of surface contaminants (such as rubber particles, oils and lubricants) are likely to be drier and are believed to be washed away with rainfall more easily from the pavement texture in an emulsion. In the winter, it is postulated that either dust, debris, and sand from salting on the surface are being 'redistributed' within the negative texture of the HRA pavement; or that the contaminants in the winter are more likely to be miscible on the surface and less susceptible to washing. The pattern observed is inverse to the behaviour of seasonal variation in skid resistance because skid resistance is measured as a frictional response to texture. However, further research is required to confirm conclusively the link between the two phenomena.

The results presented suggest that more accurate readings of pavement texture might be obtained by cleaning the surface of debris/contaminant prior to measurement being performed. Although this may not be practical at road network scale, more frequent texture surveys synergized with more focused and constrained weather monitoring will do much to improve the understanding of surface processes on the evolution of texture.

Objective 4: **Determine the role of asphalt textures scales on the development of skid resistance.**

This PhD has made a contribution to identifying the role of road surface SST and LST on wet skid resistance. A signal processing technique termed Empirical Mode Decomposition (Kane et al., 2015) was used to decompose the texture measurements of six surfaces into a set of component profiles of different wavelengths. These different profiles were partially recomposed to derive a profile consisting of 'small-scale-texture' (SST) and 'large-scale-texture' (LST), a profile without SST, and a third profile where LST was smoothed even further. The friction on these three recomposed surfaces will be calculated using the Dynamic Friction Model (Kane and Cerezo, 2015). The results of these simulations reveal the importance of both texture scales, but also more importantly that the spatial arrangements and shapes of these scales are just as important. Indeed, on wet road surfaces, the SST is key to achieving good skid resistance at low speeds, and LST is crucial to maintaining it when the speed increases. Moreover, the distribution of the summits of the LST is also beneficial and can even compensate for the lack of SST, alternatively the shape of local summits of the SST may also be important and can compensate for lack of LST at increasing vehicle speed.

8.3 Limitations of this research

All attempts have been made to minimise limitations where possible during the course of this PhD. The legacy SMTD data used in the macrotexture evolution studies were for HRA pavements, and it would be appropriate to consider too, other types of surfacing; for example, thin surfacing often used as a 'sealing' material to prolong pavement life in the UK. Furthermore, weather data were obtained from UK Meteorological (Met) Office (Met Office, 2019) and traffic count data from WebTRIS Highways England Traffic (Highways England, 2020) databases. It would be helpful to confirm conclusively the link between pavement surface process and seasonal variation in skid resistance, to measure in a controlled manner at a site: skid resistance, macrotexture depth, environmental conditions and monitoring at the macroscale the wetting and drying processes of contaminants on the surface of a pavement. Finally, this PhD has principally considered – macrotexture. It is recognised that pavement performance is related to other texture scales, and in particular, microtexture which also influences (amongst other factors) skid resistance warrants more investigation too.

8.4 Suggestions for further work

As a direct result of the outcomes of the research undertaken a number of suggestions can be made for future work:

i. The capacity of non-contact SfM techniques to capture microtexture wavelengths below 0.5 mm warrants further exploration.

ii. Selecting non-contact techniques to characterise the spatial variability of pavement surface textures using areal parameters requires the optimisation of sample sizes. More research is required to determine optimal sample sizes for a full range of pavement surfaces, embedding many combinations of microtexture and macrotexture scales.

iii. Legacy wavenumber filtered SMTD data plotted in time series revealed, changes in pavement surface condition. This presents the potential to develop visual recognition software to automatically identify changes, in order to locate areas of pavement in poor condition on road networks.

iv. The use of legacy long-term rate of change in SMTD data to predict the useful working life and/or maintenance interventions for different pavement surfacing materials is worthy of further study.

v. The source of periodicity occurring at unevenness scale observed systematically through time in the 1D spectral analysis of wavenumber filter SMTD data requires scrutiny.

vi. The seasonal signal revealed in the filtered mean SMTD measurements indicates that surface processes on HRA pavements are influenced by seasonal conditions. To confirm if this is the case a more granular study of SMTD data is required. This would necessitate collecting SMTD data in a controlled manner for a pavement surface on a weekly basis, along with monitoring environmental conditions and the wetting and drying processes of contaminants at macrotexture scale.

Although all six of these suggestions are important, the last point provides the greatest scope for further work. The seasonal signals observed in the SMTD data following an above average precipitation event (occurring within the week prior to measurement), were found to cause an increase above the long-term evolution of filtered mean SMTD where an event occurred in the summer, and similarly a decrease in the winter. The pattern exhibited is the inverse to the recognised behaviour of seasonal variation in skid resistance within the United Kingdom. This poses the potential for some interconnection between the phenomena, as skid resistance being measured as a frictional response to texture, will theoretically be opposite. Although, it is recognised that skid resistance is known to be influenced by a number of other factors including temperature, speed, tyre tread thickness and viscoelastic deformation.

If seasonal signals in pavement surface processes are confirmed, then the next step must be to investigate a link with skid resistance. Seasonal variation in skid resistance is known to lead to inter year variability in skid resistance. This presents problems of reliability and consistency over the long-term for road agencies, using skid resistance data to confirm that there is adequate texture on pavement surfaces for vehicle safety. Road agencies typically statistically adjust measurements to be in line with previous years, in order to successfully manage pavement surface assets over time. Establishing and successfully quantifying the contribution of pavement surface processes in seasonal variation of skid resistance, is likely to be a research pursuit of many years. However, theoretically if achieved this would enable texture measurement collected from clean benchmark pavement reference surfaces, located at points on a road network, to be used in calculations to determine and remove that aspect of seasonal variation of skid resistance relating to surface processes.

REFERENCES

Abbondati, F., Biancardo, S.A., Veropalumbo, R., Dell'Acqua, G., 2021. Surface monitoring of road pavements using mobile crowdsensing technology. *Measurement* 171, 108763. https://doi.org/10.1016/j.measurement.2020.108763

Abe, H., Atinori, T., Henry, J.J., Wambold, J.C., 2001. Measurement of Pavement Macrotexture with Circular Texture Meter. *Transport Research Record: Journal of the Transport Research Board* 1764, 201–209 https://doi.org/10.3141/1764-21

Abellán, A., Jaboyedoff, M., Oppikofer, T., Vilaplana, J.M., 2009. Detection of millimetric deformation using a terrestrial laser scanner: experiment and application to a rockfall event. *Nat. Hazards Earth Syst.* Sci. 9, 365–372. https://doi.org/10.5194/nhess-9-365-2009

Ahammed, M.A., Tighe, S.L., 2009. Early-Life, Long-Term, and Seasonal Variations in Skid Resistance in Flexible and Rigid Pavements. *Transp. Res. Rec. J. Transp. Res. Board* 2094, 112–120. https://doi.org/10.3141/2094-12

Ahammed P. Eng., M.A., Tighe, S.L., 2010. Effect of Short-term and Long-term Weather on Pavement Surface Friction. International Journal of Pavement Research and Technology 3. [Online] Available at https://trid.trb.org/view/1083701 (accessed 24th November 2021)

Aktaş, B., Gransberg, D.D., Riemer, C., Pittenger, D., 2011. Comparative Analysis of Macrotexture Measurement Tests for Pavement Preservation Treatments. *Transportation Research Record* 2209, 34–40. https://doi.org/10.3141/2209-05

Alamdarlo, M.N., Hesami, S., 2018. Optimization of the photometric stereo method for measuring pavement texture properties. *Measurement* 127, 406–413. https://doi.org/10.1016/j.measurement.2018.05.109

American Society for Testing and Materials, 2019. ASTM E1911-19 - Standard Test Method for Measuring Surface Frictional Properties Using the Dynamic Friction Tester. https://doi.org/10.1520/E1911-19

American Society for Testing and Materials , 2018. Test Method for Measuring Surface Frictional Properties Using the British Pendulum Tester (No. ASTM E303-93). ASTM International, West Conshohocken, PA, USA. https://doi.org/10.1520/E0303-93R18

American Society for Testing and Materials, 2015. ASTM E965-15 : Standard Test Method for Measuring Pavement Macrotexture Depth Using a Volumetric Technique. https://doi.org/10.1520/ E0965-15R19

American Society for Testing and Materials, 2015. Standard Practice for Calculating Pavement Macrotexture Mean Profile Depth (No. ASTM E1845). ASTM International. https://doi.org/10.1520/E1845-15

American Society for Testing and Materials, 2015. ASTM E1960-15 - Standard Practice for Calculating International Friction Index of a Pavement Surface. https://doi.org/10.1520/E1960-07R15

American Society for Testing and Materials, 2011. ASTM E1960-07(2011) - Standard Practice for Calculating International Friction Index of a Pavement Surface. https://doi.org/10.1520/ E1960-07R11

American Society for Testing and Materials, 2001. Specification for Hot-Mixed, Hot-Laid Bituminous Paving Mixtures (No. ASTM D3515-01). ASTM International, West Conshohocken, PA, USA. https://doi.org/10.1520/D3515-01

American Society for Testing and Materials, 1998. ASTM E1960-98 - Standard Practice for Calculating International Friction Index of a Pavement Surface. https://doi.org/10.1520/E1960-98

Araujo, V.M.C., Bessa, I.S., Castelo Branco, V.T.F., 2015. Measuring skid resistance of hot mix asphalt using the aggregate image measurement system (AIMS). *Constr. Build. Mater*. 98, 476–481. https://doi.org/10.1016/j.conbuildmat.2015.08.117

ASTM International, 2019. Test Method for Measuring Pavement Macrotexture Properties Using the Circular Track Meter. ASTM International. https://doi.org/10.1520/E2157-15R19

ASTM International, 2019. Test Method for Measuring Pavement Texture Drainage Using an Outflow Meter (No. ASTM E2380). ASTM International, West Conshohocken, PA, USA. https://doi.org/10.1520/E2380_E2380M-15R19

ASTM International, 2015. ASTM E1926-08: 2015. Standard practice for computing International Roughness Index of roads from longitudinal profile measurements, West Conshohocken [Online] Available from: https://www.astm.org/Standards/E1926 (accessed 18th August 2019).

ASTM International, 2015. Test Method for Measuring Pavement Macrotexture Properties Using the Circular Track Meter (No. ASTM E2157-01). ASTM International, West Conshohocken, PA, USA. https://doi.org/10.1520/E2157-01

Bagui, S., Das, A., Bapanapalli, C., 2013. Controlling Vehicle Overloading in BOT Projects. *Procedia - Soc. Behav*. Sci. 104, 962–971. https://doi.org/10.1016/j.sbspro.2013.11.191

Baltsavias, E.P., 1999. Airborne laser scanning: basic relations and formulas. *ISPRS Journal of Photogrammetry and Remote Sensing* 54, 199–214. https://doi.org/10.1016/S0924-2716(99)00015-5

Balzani, M., Pellegrinelli, A., Perfetti, N., Uccelli, F., 2001. A terrestrial 3D laser scanner: accuracy tests, in: Undefined. Presented at the Proceedings 18th International Symposium CIPA, Schweizerbart and Borntraeger, Potsdam, Germany. [Online] Available at: https://www.semanticscholar.org/paper/A-terrestrial-3D-laser-scanner%3A-

accuracy-tests-Balzani-Pellegrinelli/ac67ce2ef53cad4f8dadb8d25a19df36fcd8467f (accessed 12th November 2021)

Bazlamit, S.M., Reza, F., 2005. Changes in Asphalt Pavement Friction Components and Adjustment of Skid Number for Temperature. *Journal of Transportation Engineering* 131, 470–476. https://doi.org/10.1061/(ASCE)0733-947X(2005)131:6(470)

Bay, H., Ess, A., Tuytelaars, T., Van Gool, L., 2008. Speeded-Up Robust Features (SURF). *Computer Vision and Image Understanding* 110, 346–359 https://doi.org/10.1016/j.cviu.2007.09.014

Barbosa, R.S, 2012. Vehicle vibration response subjected to longwave measured pavement irregularity. *Journal of Mechanical Engineering and Automation*, 2 (2), 17–24. doi:10.5923/j.jmea.20120202.04

Becerik-Gerber, B., Jazizadeh, F., Kavulya, G., Calis, G., 2011. Assessment of target types and layouts in 3D laser scanning for registration accuracy. Automation in Construction 20, 649–658. https://doi.org/10.1016/j.autcon.2010.12.008

Bijsterveld, W., Val, M.A., 2016. Towards quantification of seasonal variations in skid resistance measurements. *Road Mater. Pavement Des.* 17, 477–486. https://doi.org/10.1080/14680629.2015.1090909

Bird, G., Scott, W.J.O., 1936. Studies in road friction. Road surface resistance to skidding (Road Research Technical Paper No. 1). Department of Scientific and Industrial Research, London.

BituChem, n.d. How long does a road surface last? Bituchem. [Online] Available from: https://www.bituchem.com/knowledge-hub/how-long-does-a-road-surface-last/ (accessed 18th November 2021).

Boehler, W., Bordas Vincent, M., Marbs, A., 2003. Investigating Laser Scannar Accuracy. Presented at the XIXth CIPA Symposium, Antalya, Turkey. [Online] https://www.cipaheritagedocumentation (accessed 11th November 2021)

Bloomfield, P., 2004. Fourier Analysis of Time Series: An Introduction, 2nd ed. Wiley-InterScience, New York. ISBN: 9780471722236

Blunt, L., Jiang, X., Leach, R., Harris, P., Scott, P., 2008. The development of user-friendly software measurement standards for surface topography software assessment. *Wear*, 10th International Conference on Metrology and Properties of Engineering Surfaces 264, 389–393. https://doi.org/10.1016/j.wear.2006.08.044

Boscaino, G., Praticò, F., 2001. A classification of surface texture indices of pavement surfaces. Bull LaborPonts Chaussees 234, 17-34

Bose, T., Meyer, F., 2003. Digital Signal and Image Processing. New Jersey, United States. John Wiley and Sons, ISBN 0471452300

British Standard Institute, 2011. BS EN 13036-4:2011 - Road and airfield surface characteristics. Test methods . Method for measurement of slip/skid resistance of a surface: The pendulum test. The British Standards Institute, London.

British Standard Institute, 2010. BS EN 13036-1:2010 - Road and airfield surface characteristics. Test methods. Measurement of pavement surface macrotexture depth using a volumetric patch technique. The British Standards Institute, London.

British Standard Institute, 2006. BS 7941-1:2006 - Methods for measuring the skid resistance of pavement surfaces. Sideway-force coefficient routine investigation machine. British Standards Institute, London. ISBN: 0580332101

British Standard Institute, 2000. BS 7941-2:2000 - Methods for measuring the skid resistance of pavement surfaces. Test method for measurement of surface skid resistance using the GripTester braked wheel fixed slip device. British Standards Institute, London.

Čelko, J., Kováč, M., Kotek, P., 2016. Analysis of the Pavement Surface Texture by 3D Scanner. Transportation Research Procedia, Transport Research Arena TRA2016 14, 2994–3003. https://doi.org/10.1016/j.trpro.2016.05.434

Cho, C., 2010. Application of Hilbert Huang Transformation to Analyze Pavement Texture-Friction Relationship. Pennsylvania State University, USA.

Creaform, n.d. HandyScan 3d, The truly portable metrology grade 3D-Scannar.

Cunto, F.J.C., and Branco, V.T.F.C, 2016. Influence of Skid Resistance in Microscopic Simulate Traffic Conflict. In: *17th International Conference Road Safety on Five Continents Conference*, 17th–19th May 2016 Rio de Janeiro, Brazil [Online] Available from: http://vti.diva-portal.org/smash/get/diva2:926094/FULLTEXT01.pdf.

Deng, Q., Zhan, Y., Liu, C., Qiu, Y., Zhang, A., 2021. Multiscale power spectrum analysis of 3D surface texture for prediction of asphalt pavement friction. *Construction and Building Materials* 293, 123506. https://doi.org/10.1016/j.conbuildmat.2021.123506

De Mauro, A., Greco, M., Grimaldi, M., 2016. A formal definition of Big Data based on its essential features. *Library Review* 65, 122–135. https://doi.org/10.1108/LR-06-2015-0061

Department for Transport. 2012. Guidance on Road Classification and Primary Route Network. Great Britain. London, [Online] Available from: https://www.geoplace.co.uk/documents/10181/87438/Guidance+on+Road+Classification+and+the+Primary+Route+Network/b7144810-af9a-41a1-a4cf-0f9c6de015d4 (accessed 10th May 2020).

Department for Transport. 2019. Technical Note: Version 1.4, 03.10.19. Road Condition and Maintenance Data. Great Britain. London, [Online] Available from: https://assets.publishing.service.gov.uk/government/uploads/system/uploads/attachment_data/file/775107/road-conditions-technote.pdf (accessed 11th August 2019).

Design Manual for Roads and Bridges, 2021. CS 228 - Skidding resistance. Norwich: The Stationary Office, Office of Public Sector Information. [Online] Available from: https://www.standardsforhighways.co.uk/prod/attachments/50d43081-9726-41e8-9835-9cd55760ad9e?inline=true (accessed 19th August 2021)

Design Manual for Roads and Bridges, 2020. CS 229 - Data for pavement assessment. Norwich: The Stationary Office, Office of Public Sector Information. [Online] Available from: https://www.standardsforhighways.co.uk/prod/attachments/2e9e1b1c-528a-4b7d-bea8-d1c49a3caded?inline=true (accessed 19th August 2021)

Design Manual for Roads and Bridges. 2008. HD29/08: Volume 7, Section 3, Part 2: Data for Pavement Assessment. Norwich: The Stationary Office, Office of Public Sector Information. [Online] Available from: http://www.standardsforhighways.co.uk/ha/standards/dmrb/vol7/section3/hd2908.pdf (accessed 11th August 2019).

Design Manual for Roads and Bridges, 2015. HD28/15:Skid Resistance. The Stationary Office, Office of Public Sector Information, Norwich.

Digital Surf, n.d. MountainsMap® Premium. Digit. Surf. [Online] https://www.digitalsurf.com/profilometry/mountainsmap-premium/ (accessed 9th August 2021).

Do, M.-T., Cerezo, V., 2015. Road surface texture and skid resistance. *Surf. Topogr. Metrol.* Prop. 3, 1–16. https://doi.org/10.1088/2051-672X/3/4/043001

Do, M.-T., Tang, Z., Kane, M., Larrard, F. de, 2009. Evolution of road-surface skid-resistance and texture due to polishing. *Wear* 5–6, 574–577. https://doi.org/10.1016/j.wear.2008.04.060

Do, M.-T., Tang, Z., Kane, M., de Larrard, F., 2007. Pavement polishing—Development of a dedicated laboratory test and its correlation with road results. *Wear*, 16th International Conference on Wear of Materials 263, 36–42

Do, M.-T., 2005. Relationship between microtexture and skid resistance. *Bulletin des Laboratoires des Ponts et Chaussees* 117–136. [ONLINE] Available from: https://www.researchgate.net/publication/289444443_Relationship_between_microtexture_and_skid_resistance (accessed 28th October 2021)

Du, Y., Qin, B., Weng, Z., Wu, D., Liu, C., 2021. Promoting the pavement skid resistance estimation by extracting tire-contacted texture based on 3D surface data. Construction and Building Materials 307, 124729. https://doi.org/10.1016/j.conbuildmat.2021.124729

Dunford, A., 2013. Friction and the texture of aggregate particles used in the road surface course. http://eprints.nottingham.ac.uk/13412/ (accessed 30th July 2021).

Dunford, A., 2008. PRJ PPR315 Measuring skid resistance without contact, Transport Research Laboratory - Publication Index | NBS. The Transport Research Laboratory, Wokingham, UK.

Dunford, A., Leach, R., 2013. Road surfaces, in: The Characterisation of Areal Surface Texture. Springer, Teddington, pp. 337–348. ISBN 9783642364570

Eberhardsteiner, L., Füssl, J., Hofko, B., Handle, F., Hospodka, M., Blab, R., Grothe, H., 2015. Towards a microstructural model of bitumen ageing behaviour. *Int. J. Pavement Eng*. 16, 939–949. https://doi.org/10.1080/10298436.2014.993192

Ech, M., Morel, S., Yotte, S., Breysse, D., Pouteau, B., 2009. An Original Evaluation of the Wearing Course Macrotexture Evolution using the Abbot Curve. *Road Materials and Pavement Design* 10, 471–494. https://doi.org/10.1080/14680629.2009.9690210

Ech, M., Yotte, S., Morel, S., Breysse, D., Pouteau, B., 2012. Qualification of wearing course material surface evolution after durability test. *Construction and Building Materials* 35, 313–320. https://doi.org/10.1016/j.conbuildmat.2012.02.081

Ech, M., Yotte, S., Morel, S., Breysse, D., Pouteau, B., 2007. Laboratory evaluation of pavement macrotexture durability. *Revue Européenne de Génie Civil* 11, 643–662. https://doi.org/10.1080/17747120.2007.9692949

Edjeou, W., Cerezo, V., Zahouani, H., Salvatore, F., 2020. Multiscale analyses of pavement texture during polishing. *Surf. Topogr.: Metrol. Prop*. 8, 024008. https://doi.org/10.1088/2051-672X/ab8f1b

Edmondson, V., Ardill, O., Martin, J., Lim, M., Kane, M., Woodward, J., 2020. Quantifying long-term rates of texture change on road networks. *Int. J. Pavement Eng*. 0, 1–13. https://doi.org/10.1080/10298436.2020.1830283

Edmondson, V., Woodward, J., Lim, M., Kane, M., Martin, J., Shyha, I., 2019. Improved non-contact 3D field and processing techniques to achieve macrotexture characterisation of pavements. *Constr. Build. Mater*. 227, 116693. https://doi.org/10.1016/j.conbuildmat.2019.116693

Ejsmont, J., et al., 2017. Road texture influence on tyre rolling resistance. *Road Materials and Pavement Design*, 18 (1), 181–198. doi:10.1080/14680629.2016.1160835.

Emerald Insight, 1998. Triangular and CCD technology boost displacement sensor capability. *Sensor Review* 18. https://doi.org/10.1108/sr.1998.08718baf.002

Ergun, M., Iyinam, S., Iyinam, A.F., 2005. Prediction of Road Surface Friction Coefficient Using Only Macro- and Microtexture Measurements. Journal of Transportation Engineering 131, 311–319. https://doi.org/10.1061/(ASCE)0733-947X(2005)131:4(311)

European Collaborative Project. 2014. Tomorrow's Road Infrastructure Monitoring and Management- Final Summary Report. Sweden: European Collaborative Project, FP7-285119 (7th RTD Framework Programme) [Online]. Available from:

https://trimis.ec.europa.eu/sites/default/files/project/documents/9751/final1-trimm-d5-3-finalreport2014-to-print.pdf (accessed 13th August 2019).

European Committee for Standardisation. 2017. prEN 13036-5: Road and airfield surface characteristics – Test methods: Part 5: Determination of longitudinal unevenness indices. Brussels: Comite Europeen de Normalisation. [Online] Available from: https://infostore.saiglobal.com/en-gb/Standards/PREN-13036-5-DRAFT-2017-342626_SAIG_CEN_CEN_784565/ (accessed 11th August 2019).

European Standards, 2014. UNE EN 12697-49:2014 Bituminous mixtures - Test methods for hot mix asphalt - Part 49: Determination of friction after polishing (No. UNE EN 12697-49:2014). Germany. [Online] Available from: https://www.en-standard.eu/une-en-12697-49-2014-bituminous-mixtures-test-methods-for-hot-mix-asphalt-part-49-determination-of-friction-after-polishing/ (accessed 16th November 2021)

Fan, L., Smethurst, J.A., Atkinson, P.M., Powrie, W., 2015. Error in target-based georeferencing and registration in terrestrial laser scanning. *Computers & Geosciences* 83, 54–64. https://doi.org/10.1016/j.cageo.2015.06.021

FARO, 2021. User Manuals for the Focus3D X 330 or 330 HDR. FARO Technologies Incorporated. [Online] Available from: https://knowledge.faro.com/Hardware/3D_Scanners/Focus/User_Manuals_for_the_Focus3D_X_330_or_330_HDR (accessed 11th November 2021)

Findlay Irvine, 2002. Road base GripTester Survey Software for Roads User Manual. Findlay Irvine Limited, Penicuik, Scotland. [Online] Available from: http://www.findlayirvine.com/downloads_admin/skid_resistance_downloads/griptester_mk2/highways/GripTester%20MK2%20Highways%20Data%20Sheet.pdf (accessed 17th November 2021)

Flintsch, G.W., de León, E., McGhee, K.K., AI-Qadi, I.L., 2013. Pavement Surface Macrotexture Measurement and Applications. *Transp. Res. Rec*. 1860, 168–177. https://doi.org/10.3141/1860-19

Flintsch, G.W., Leon, I.E., Saleh, M., McGhee, K.K., 2008. Area-based macrotexture measurements using stereo vision. Presented at the 6th Symposium on Pavement Surface Characterisation, Portoroz, Slovenia. [Online] Available from: https://www.researchgate.net/publication/275334661_Area_based_macrotexture_measurements_using_stereo_vision (accessed 28th October 2021)

Forster, S.W., 1989. Pavement Microtexture and Its Relation to Friction. *Transp. Res. Rec*. 1215, 151–164.

Forster, S.W., 1981. Aggregate microtexture: profile measurement and related frictional levels. U.S. Dept. of Transportation, Federal Highway Administration, Offices of

Research & Development, Materials Division ; National Technical Information Service Washington, D.C.; Springfield, Va

FSV-Austrian Transport Research Association. 2008. COST 354 Performance Indicators for Road Pavements – Final Report. Vennia: Austria, ISBN 978-3-200-01238-7 [Online] Available from: http://cost354.zag.si/fileadmin/cost354/1fr/COST354_FinalReport_05062008.pdf (accessed 9th January 2020).

Furukawa, Y., Ponce, J., 2010. Accurate, Dense, and Robust Multiview Stereopsis. *IEEE Trans. Pattern Anal. Mach. Intell.* 32, 1362–1376. https://doi.org/10.1109/TPAMI.2009.161

Fwa, T.F., 2017. Skid resistance determination for pavement management and wet-weather road safety. *Int. J. Transp. Sci. Technol.*, Safer Road Infrastructure and Operation Management 6, 217–227. https://doi.org/10.1016/j.ijtst.2017.08.001

Gao, L., Liu, M., Wang, Z., Xie, J., Jia, S., 2019. Correction of texture depth of porous asphalt pavement based on CT scanning technique. *Constr. Build. Mater*. 200, 514–520. https://doi.org/10.1016/j.conbuildmat.2018.12.154

Gardziejczyk, W., 2014. Influence of Road Pavement Macrotexture on Tyre/Road Noise of Vehicles. *The Baltic Journal of Road and Bridge Engineering* 9, 180–190. https://doi.org/10.3846/bjrbe.2014.23

Gendy, A.E., Shalaby, A., 2007. Mean Profile Depth of Pavement Surface Macrotexture Using Photometric Stereo Techniques. *Journal of Transportation Engineering* 133, 433–440. https://doi.org/10.1061/(ASCE)0733-947X(2007)133:7(433)

Girardeau-Montaut, D., n.d. CloudCompare 3D point cloud and mesh processing software - Open Source project. http://www.danielgm.net/cc/ (accessed 1st August 2021).

Gobmann, I., Halbach, M., Scholz-Bottcher, B., 2021. Car and truck tire wear particles in complex environmental samples - A quantitative comparison with “traditional” microplastic polymer mass loads. *Sci. Total Environ*. https://doi.org/10.1016/j.scitotenv.2021.145667

Gothie, M., Colombrita, R., Moliteo, G., 2004. Macrotexture measurement with many methods and devices; single irregularities influence on the megatexture indicators. Presented at the Symposium on Pavement Surface Characteristics [of Roads and Airports], 5th, 2004, Toronto, Ontario, Canada. [Online] https://trid.trb.org/view/1157355 (accessed 10th November 2021)

Green, E.H., 1973. Black deposits on motorways (TRRL Supplementary Report No. 74). Transport and Road Research Laboratory, Crowthorne, Berkshire, UK.

Gubbins, D., 2004. Time series analysis and inverse theory for Geophysicists. Cambridge University Press, Cambridge. ISBN: 0521819652

Guo, F., Pei, J., Zhang, J., Li, R., Zhou, B., Chen, Z., 2021. Study on the skid resistance of asphalt pavement: A state-of-the-art review and future prospective. Construction and Building Materials 303, 124411. https://doi.org/10.1016/j.conbuildmat.2021.124411

Hall, J.W., Smith, K.L., Titus-Glover, L., Wambold, J.C., Yager, T.J., Rado, Z., 2009. Guide for Pavement Friction. The National Academies Press. https://doi.org/10.17226/23038

Harwood, D.W., Blackburn, R.R., Kulakowski, B.T., Kibler, D.F., 1987. Wet Weather Exposure Measures. Final Report [Online] Available from: https://trid.trb.org/view/280063 (accessed 29th November 2021)

Heritage, G., Large, A. (Eds.), 2009. Laser Scanning for the Environmental Sciences. Wiley-Blackwell, Chichester, West Sussex. ISBN 9781405157179

Herbert, D., Khoudeir, M., Do, M.-T., 2007. Rough surfaces and relief extraction by generalised Lambertain's Photometric Model. Presented at the 2007 IEEE International Conference on Signal Processing and Communications, Dubai, United Arab Emirates. ISBN: 1424412366

Henry, J.J., 2000. Evaluation of Pavement Friction Characteristics. *Transportation Research Board*, Washington DC, USA. ISBN: 9780309068741

Highways England, 2020. Highways England - WebTRIS - Map View [WWW Document]. URL https://webtris.highwaysengland.co.uk/ (accessed 5.28.21).

Highways England. 2019. Network Management [Online] Available from: https://assets.publishing.service.gov.uk/government/uploads/system/uploads/attachment_data/file/800964/Network_management.pdf (accessed 11th August 2019).

Hong, S.J., Park, S.W., and Lee, S.W, 2018. Tire-pavement noise prediction using pavement texture. KSCE *Journal of Civil Engineering*, 22 (9), 3358–3362. doi:10.1007/s12205-018-9501-3

Hosking, J.R., Woodford, G.C., 1976. Measurement of Skidding Resistance Part II . Factors Affecting the Slipperiness of a Road Surface. *Transp. Road Res. Lab*. TRRL 1–10.

Hu, L., Yun, D., Liu, Z., Du, S., Zhang, Z., Bao, Y., 2016. Effect of three-dimensional macrotexture characteristics on dynamic frictional coefficient of asphalt pavement surface. *Constr. Build. Mater*. 126, 720–729. https://doi.org/10.1016/j.conbuildmat.2016.09.088

International Organisation for Standardisation, 2019. ISO 13473-1:2019 Characterisation of pavement texture by the use of surface profiles - Part 1: determination of mean profile depth. International Organisation for Standardisation, Geneva, Switzerland. [Online] Available from: https://www.iso.org/cms/render/live/en/sites/isoorg/contents/data/standard/04/51/45111.html (accessed 1st August 2021)

International Organisation for Standardisation. 2016. ISO 8608: 2016 Mechanical Vibration – Road Surface Profiles – Reporting of Measured Data, Geneva, Switzerland: International Organization for Standardization [Online] Available from: https://www.iso.org/standard/71202.html (accessed 11th August 2019).

International Organisation of Standardisation, 2012. ISO 25178-2:2012 Geometrical product specification (GPS) - Surface texture: areal part 1: terms, definitions and surface texture parameters. International Standards Organisation, 2019. [Online] Available from: https://www.iso.org/cms/render/live/en/sites/isoorg/contents/data/standard/04/27/42785.html (accessed 1st August 2021)

International Organisation of Standardisation, 2009. ISO 13473-5:2009, Characterization of pavement texture by use of surface profiles — Part 5: Determination of megatexture. [Online] Available from: https://www.iso.org/obp/ui/#iso:std:iso:13473:-5:ed-1:v1:en (accessed 30th August 2021)

International Organisation of Standardisation, 2002. ISO 13473-2: 2002 Characterization of pavement texture by use of surface profiles — Part 2: Terminology and basic requirements related to pavement texture profile analysis [Online] Available from: https://www.iso.org/obp/ui/#iso:std:iso:13473:-2:ed-1:v1:en (accessed 17th September 2021)

International Organisation of Standardisation, 1997. ISO 4287:1997. International Organisation for Standardisation, Geneva, Switzerland. [Online] Available from: https://www.iso.org/cms/render/live/en/sites/isoorg/contents/data/standard/01/01/10132.html (accessed 1st August 2021)

International Organisation for Standardisation, 1996. ISO 4288:1996 Geometrical Product Specifications (GPS)- Surface texture: Profile method - Rules and procedures for the assessment of surface texture. International Organisation for Standardisation, Geneva, Switzerland. [Online] Available from: https://www.iso.org/cms/render/live/en/sites/isoorg/contents/data/standard/00/20/2096.html (accessed 1st August 2021)

IWS Messtechnik, n.d. ELAtexture 3.0. Pavement Texture Depth Measurement. Celle, Germany. [Online] http://www.abmbv.nl/files/iws_elatextur_en.pdf (accessed 21st October 2021)

Jayawickrama, P.W., Thomas, B., 1998. Correction of Field Skid Measurements for Seasonal Variations in Texas. *Transportation Research Record* 1639, 147–154. https://doi.org/10.3141/1639-16

James, M.R., Robson, S., 2014. Mitigating systematic error in topographic models derived from UAV and ground-based image networks. *Earth Surface Processes and Landforms* 39, 1413–1420. https://doi.org/10.1002/esp.3609

James, M.R., Robson, S., 2012. Straightforward reconstruction of 3D surfaces and topography with a camera: Accuracy and geoscience application. J. *Geophys. Res. Earth Surf.* 117, 1–17. https://doi.org/10.1029/2011JF002289

Jayawickrama, P.W., Thomas, B., 1998. Correction of Field Skid Measurements for Seasonal Variations in Texas. *Transp. Res. Rec. J. Transp. Res. Board* 1639, 147–154. https://doi.org/10.3141/1639-16

Kane, M., Artamendi, I., Scarpas, T., 2013. Long-term skid resistance of asphalt surfacings: Correlation between Wehner–Schulze friction values and the mineralogical composition of the aggregates. *Wear* 303, 235–243. https://doi.org/10.1016/j.wear.2013.03.022

Kane, M., Cerezo, V., 2015. A contribution to tire/road friction modeling_ From a simplified dynamic frictional contact model to a "Dynamic Friction Tester" model *Wear* 324–343, 163–171. https://doi.org/10.1016/j.wear.2015.08.007

Kane, M., Do, M.-T., Cerezo, V., Rado, Z., Khelifi, C., 2019. Contribution to pavement friction modelling: an introduction of the wetting effect. *Int. J. Pavement Eng*. 20, 965–976. https://doi.org/10.1080/10298436.2017.1369776

Kane, M., Edmondson, V., 2018. Modelling the bitumen scour effect: Enhancement of a dynamic friction model to predict the skid resistance of rubber upon asphalt pavement surfaces subjected to wear by traffic polishing. *Wear* 400–401, 100–110. https://doi.org/10.1016/j.wear.2017.12.013

Kane, M., Edmondson, V., 2020. Tire/road friction prediction: introduction a simplified numerical tool based on contact modelling. *Veh. Syst. Dyn*. 0, 1–20. https://doi.org/10.1080/00423114.2020.1832696

Kane, M., Rado, Z., Timmons, A., 2015. Exploring the texture–friction relationship: from texture empirical decomposition to pavement friction. *Int. J. Pavement Eng.* 16, 919–928. https://doi.org/10.1080/10298436.2014.972956

Kane, M., Zhao, D., Chailleux, E., Delarrard, F., Do, M., 2013. Development of an accelerated pavement test reproducing the effect of natural ageing on skid resistance. *Road Materials and Pavement Design* 14, 126–140. https://doi.org/10.1080/14680629.2012.749804

Kane, M., Zhao, D., De-Larrard, F., Do, M.-T., 2012. Laboratory evaluation of aggregate polishing as a function of load and velocity. Application to the prediction of damages on skid resistance of road surfaces due to trucks and passenger cars. *Road Mater. Pavement Des.* 13, 312–326. https://doi.org/10.1080/14680629.2011.649424

Karami, E., Prasad, S., Shehata, M., 2015. Image Matching Using SIFT, SURF, BRIEF and ORB: Performance Comparison for Distorted Images. Presented at the Newfoundland Electrical and Computer Engineering Conference, St John's, Canada. [Online] Available from: https://arxiv.org/pdf/1710.02726.pdf (accessed 16th December 2021)

Kennedy, C.K., Young, A.E., Butler, I.C., 1990. Measurement of Skidding Resistance and Surface Texture and the Use of Results in the United Kingdom, in: *Surface Characteristics of Roadways: International Research and Technologies*. ASTM International, West Conshohocken, PA, USA, p. 87.

Kerner, B.S, 2018. Autonomous driving in framework of three-phase traffic theory. In: *The 7th International Workshop on Agent-based Mobility, Traffic and Transportation Models, Methodologies and Applications* (ABMTRANS-2018), Procedia Computer Science 130, 785–790. https://doi.org/10.1016/j.procs.2018.04.136

Khasawneh, M.A., Laing, R.Y., 2012. Temperature effects on the frictional properties of HMA at different polishing stages. *Jordan J. Civ. Eng*. 6, 39–53.

Khasawneh, M., Samadi, M., and Zelelew, H., 2016. Investigation of the factors influencing wavelet-based macrotexture values for HMA pavements. *Road Materials and Pavement Design*, 17 (3), 779–791. doi:10.1080/14680629.2015.1120229.

Kiwa, nd. Road Testing - Kiwa KOAC [Online] Available from: https://www.kiwa.com/nl/en/markets/construction-and-infrastructure/infrastructure/services/road-testing/ (accessed 11th October 2021).

Klüppel, M., Heinrich, G., 2001. Rubber Friction on Self-Affine Road Tracks. *Rubber Chem. Technol*. 73, 578–606. https://doi.org/10.5254/1.3547607

Kodippily, S., Henning, T.F.P., Ingham, J.M., 2012. Detecting Flushing of Thin-Sprayed Seal Pavements Using Pavement Management Data. *J. Transp. Eng*. 138, 665–673. https://doi.org/10.1061/(ASCE)TE.1943-5436.0000354

Kogbara, R.B., Masad, E.A., Kassem, E., Scarpas, A. (Tom), Anupam, K., 2016. A state-of-the-art review of parameters influencing measurement and modeling of skid resistance of asphalt pavements. *Constr. Build. Mater*. 114, 602–617. https://doi.org/10.1016/j.conbuildmat.2016.04.002

Kogbara, R.B., Masad, E.A., Woodward, D., Millar, P., 2018. Relating surface texture parameters from close range photogrammetry to Grip-Tester pavement friction measurements. *Constr. Build. Mater*. 166, 227–240. https://doi.org/10.1016/j.conbuildmat.2018.01.102

KPR, n.d. Highway Services - Outflow Meter. [Online] Available from: http://www.kprcompany.com/highway-services (accessed on the 1st November 2021).

Kulakowski, B.T., 1991. Mathematical model of skid resistance as a function of speed. *Transp. Res. Rec*. 26–33 [Online] Available from: https://onlinepubs.trb.org/Onlinepubs/trr/1991/1311/1311-005.pdf (accessed 15th August 2021)

Kummer, H.W., 1966. Unified Theory of Rubber and Tire Friction. (No. PB184487). Pennsylvania State Univ., University Park. Coll. of Engineering [Online] Available at:

https://ntrl.ntis.gov/NTRL/dashboard/searchResults/titleDetail/PB184487.xhtml (accessed 1st December 2021)

Leach, R. (Ed.), 2013. Characterisation of Areal Surface Texture. Springer, London. ISBN: 9783642364570

Leu, M.C., Henry, J.J., 1983. Prediction of Skid Resistance as a Function of Speed From Pavement Texture Measurements. Transp. Res. Rec. 7.

Li, S., Noureldin, S., Zhu, K., Jiang, Y., 2012. Pavement Surface Microtexture: Testing, Characterization, and Frictional Interpretation. *Pavement Perform. Curr. Trends Adv. Chall*. https://doi.org/10.1520/STP104426

Lichti, D., Stewart, M., Tsakiri, M., Snow, A., 2000. Calibration and testing of a terrestrial laser scanner. International Archives of Photogrammetry and Remote Sensing 33, 485–492. [Online] Available at: https://www.semanticscholar.org/paper/CALIBRATION-AND-TESTING-OF-A-TERRESTRIAL-LASER-Lichti-Stewart/d3930a682708ac6e63e617cf9efa9738c16c4017 (accessed 12th November 2021)

Lichti, D.D., Jamtsho, S., 2006. Angular resolution of terrestrial laser scanners. *The Photogrammetric Record* 21, 141–160. https://doi.org/10.1111/j.1477-9730.2006.00367.x

LMI Technologies, 2021. Gocator Firmware 4.6, The Latest Features and Tools. https://lmi3d.com/firmware/ (accessed 1st August 2021).

LMI Technologies, n.d. LMI Gocator 2300. STEMMER IMAGING. [Online] https://www.stemmer-imaging.com/en-gb/products/series/lmi-gocator-2300-series/ (accessed 1st August 2021).

Loprencipe, G., Zoccalli, P., and Cantisani, G, 2019. Effects of vehicular speed on the assessment of pavement road roughness. *Applied Science*, 9 (1783), 1–18. doi:10.3390/app9091783.

Lowe, D.G., 2004. Distinctive Image Features from Scale-Invariant Keypoints. International *Journal of Computer Vision* 60, 91–110. https://doi.org/10.1023/B:VISI.0000029664.99615.94

Mathworks, 2018. Matlab Version. The MathWorks Inc, United Kingdom.

Manual of Contract Documents for Highway Works. 2019. Volume 1, Series 900, Clause 942: Specification for highway Works. Norwich: The Stationary Office, Office of Public Sector Information. [Online] Available from: http://www.standardsforhighways.co.uk/ha/standards/mchw/vol1/pdfs/2989369_MCHW_Vol1_Series_900_v2.pdf (accessed 11th August 2019).

Matthews, R., n.d. How do they paint white lines on roads so accurately? BBC Science Focus Magazine. [Online] Available from: https://www.sciencefocus.com/science/how-do-they-paint-white-lines-on-roads-so-accurately/ (accessed 13th November 2021)

Masad, E., et al., 2009. Prediction asphalt mixture skid resistance based on aggregate characteristics. Texas: Department of Transportation and Federal Highway Administration. [Online] Available from: https://static.tti.tamu.edu/tti.tamu.edu/documents/0-5627-1.pdf (accessed 20th May 2020).

Mauro, A.D., Greco, M., and Grimaldi, M, 2016. A Formal Definition of Big data based on its essential features. *Library Review*, 65 (3), 122–135. doi:10.1108/LR-06-2015-0061.

McGhee, K.K., Flintsch, G.W., 2003. Final Report High-Speed Texture Measurement of Pavements (No. VTRC 03-R9). Charlottesville, Virginia.

McQuaid, G., Millar, P., Woodward, D., 2015. Use of 3D modeling to assess pothole growth. Presented at the 6th International Conference on Bituminous Mixtures and Pavements, Taylor and Francis Group, Thessaloniki, Greece, pp. 161–166. https://doi.org/10.1201/B18538-26

Meegoda, J.N., and Gao, S, 2015. Evaluation of pavement skid resistance using high speed textile measurements. *Journal of Traffic and Transportation*, 2 (6), 382–390. doi:10.1016/j.jtte.2015.09.001.

Met Office, 2019. MIDAS Open: UK hourly weather observation data, v201901. https://doi.org/10.5285/C58C1AF69B9745FDA4CDF487A9547185

Met Office, n.d. Weather and climate change Met Off. https://www.metoffice.gov.uk/ (accessed 28th May 2021)

Micheletti, N., Chandler, J.H., Lane, S.N., 2015. BRITISH SOCIETY FOR GEOMORPHOLOGY. *Geomorphol. Tech*. Chapter 2.2, 12.

Millar, P., Woodward, D., 2011. Non contact assessment of highway surface vulnerability to water induced damage. *International Journal of Pavements* 10, 39–49. ISSN:16762797

Millar, P., Woodward, D., Woodside OBE, A., 2009. Use of close-range terrestrial photogrammetry to assess accelerated wear of asphalt concrete surface course mixes, in: 6th International Conference on Maintenance and Rehabilitation of Pavements and Technological Control. Turin, pp. 734–740. [Online] Available from: https://trid.trb.org/view/899182 (accessed 30th October 2021)

Moore, D.F., 1975. THE FRICTION OF PNEUMATIC TYRES. Elsevier, New York. ISBN: 9780444413239

Mucka, P, 2017. International roughness index specifications around the world. *Road Materials and Pavement Designs*, 18 (4), 929–965.doi:10.1080/14680629.2016.1197144.

Mucka, P, 2018. Simulated road profiles according to ISO 8608 in vibration analysis. *Journal of Testing and Evaluation*, 46 (1), 405–418. doi:10.1520/JTE20160265.

National Highways, 2021. Manual of contract documents for highway works. Volume 2 Notes for guidance on the specification for highway works. Series NG 900. Road Pavements - Bituminous Bound Materials (No. Series NG900). [Online] https://www.standardsforhighways.co.uk/ha/standards/mchw/ (accessed 15th November 2021)

Nippo Sangyo Co. Ltd, n.d. Product Guide Circular Track Meter [Online] Available from: http://www.nippou.com/en/products/ct.html (accessed on 1st November 2021).

O'Brien, J. P., and Haddock, J. E, 2009. Frictional resistance of aggregates for hot-mix asphalt pavements (Final Report (FHWA/IN/JTRP-2004/23)). Joint Transportation Research Programme (JTRP) and Purdue University, Indiana Department of Transportation https://doi.org/10.5703/1288284314215.

Oh, S.M., Madanat, S.M., Ragland, D.R., Chan, C.-Y., 2010. Evaluation of Traffic and Environment Effects on Skid Resistance in California 12

Oliver, J.W.H., Tredrea, P.F., Pratt, D.N., 1988. Seasonal variation of skid resistance in Australia. Austrailian Road Research Board 37. [online] Available at: https://trid.trb.org/view/257181 (accessed 24th November 2021)

Ongel, A., Lu, Q., Harvey, J., 2009. Frictional properties of asphalt concrete mixes. *Proceedings of the Institution of Civil Engineers - Transport* 162, 19–26. https://doi.org/10.1680/tran.2009.162.1.19

Organization for Economic Co-operation and Development. 2001. Asset Management for the Roads Sector Transport. Paris: France, OCED Publication Service [Online] Available from: https://www.itf-oecd.org/sites/default/files/docs/01assete.pdf (accessed 9th January 2020).

Peraka, N.S.P., Biligiri, K.P., 2020. Pavement asset management systems and technologies: A review. *Autom. Constr*. 119, 103336

Persson, B.N.J., 2001. Sliding Friction: Physical Principles and Applications *(Nanoscience and Technology)*. Springer-Verlag, Berlin. ISBN: 9783662042830

PIARC, 1987. Report of the committee on surface charterisation, in: *Permanent International Association of Road Congress (PIARC) XVIIIth World Road Congress, Brussels*. [Online] https://www.piarc.org/en/activities/World-Road-Congresses-World-Road-Association/Congress-Proceedings/Brussels-1987/technical-committee-report.htm (accessed 30th July 2021).

Plati, C., Georgouli, K., Loizos, A., 2014. Utilising the seasonal variations of skid resistance to plan preventative maintenance, in: Losa, M., Papagiannakis, T. (Eds.), *Sustainability,*

Eco-Efficiency, and Conservation in Transportation Infrastructure Asset Management. CRC Press, London, pp. 509–518. https://doi.org/10.1201/b16730

Plati, C., and Pomoni, M, 2019. Impact of traffic Volume on pavement macrotexture and skid resistance long-term performance. *Journal of Transportation Research Board*, 2763 (2), 314–322. doi:10.1177/0361198118821343

Pomoni, M., Plati, C., Loizos, A., Yannis, G., 2020. Investigation of pavement skid resistance and macrotexture on a long-term basis. *Int. J. Pavement Eng*. 1–10. https://doi.org/10.1080/10298436.2020.1788029

Pranjić, I., Deluka-Tibljaš, A., Cuculić, M., Šurdonja, S., 2020. Influence of pavement surface macrotexture on pavement skid resistance. *Transp. Res. Procedia*, Transport Infrastructure and systems in a changing world. Towards a more sustainable, reliable and smarter mobility. TIS Roma 2019 Conference Proceedings 45, 747–754. https://doi.org/10.1016/j.trpro.2020.02.102

Praticò, F.G., Astolfi, A., 2017. A new and simplified approach to assess the pavement surface micro- and macrotexture. *Constr. Build. Mater*. 148, 476–483. https://doi.org/10.1016/j.conbuildmat.2017.05.050

Prowell, B.D., Hanson, D.I., 2005. Evaluation of Circular Texture Meter for Measuring Surface Texture of Pavements. *Transp. Res. Rec*. 1929, 88–96. https://doi.org/10.1177/0361198105192900111

Rado, Z., Kane, M., 2014. An initial attempt to develop an empirical relation between texture and pavement friction using the HHT approach. Wear 309, 233–246. https://doi.org/10.1016/j.wear.2013.11.015

Rado, Z., 1996. Fractal characterisation of road surface textures for analysis of friction. Presented at the International Symposium on Pavement Surface Characteristics, 1996, Christchurch, New Zealand, *Transport Research Board*, New Zealand, pp. 101–33 ISBN: 9780869107119

Ragland, D. R., Mi Oh, S., and Chan, C.Y, 2010. Evaluation of Traffic and Environment Effects on Skid Resistance and Safety Performance of Rubberized Open-Grade Asphalt Concrete. Research Report: UCB-ITS-PRR-2010-14. California PATH Program, Institute of Transportation Studies, University of California, Berkley, CA [Online] Available from: https://safetrec.berkeley.edu/sites/default/files/publications/evaluation_of_traffic_and_enviornment_effects.pdf (accessed 10th May 2020).

Rainsford, S., and Parkman, C., ND. Predicting texture deficiency in pavement management. NWH NZ Ltd: Transit New Zealand [Online] Available from: http://saferroadsconference.com/wp-content/uploads/2016/05/5-PARKMAN-C-Predicting-textureFP.pdf (accessed 7th January 2020).

Reshetyuk, Y., 2006. Investigation and calibration of pulsed time-of-flight terrestrial laser scanners (Licentiate thesis in Geodesy). Royal Institute of Technology, Stockholm. [Online] Available at: https://www.diva-portal.org/smash/get/diva2:10841/fulltext01.pdf (accessed 12th November 2021)

Rezaei, A., Masad, E., Chowdhury, A., Harris, P., 2009. Predicting Asphalt Mixture Skid Resistance by Aggregate Characteristics and Gradation. *Transp. Res. Rec. J. Transp. Res. Board* 2104. https://doi.org/10.3141/2104-03

Roads UK Road Board, 2009. SCANNER survey for Local Roads. User Guide and Specification Volume 5: Technical Requirements for SCANNER Parameters and Accreditation. [Online] Available from: https://www.ciht.org.uk/media/11987/scanner_specification_volume_5_october_2009.pdf (accessed on 17th September 2021)

Roe, P., Hartshorne, S., 1998. TRL The Polished Stone Value of aggregates and in-service skidding resistance. The Transport Research Laboratory, p. 28. [Online] Available from: https://trl.co.uk/publications/trl322 (accessed 30th July 2021)

Roe, P.G., Webster, D.C., West, G., 1991. The relation between the surface texture of roads and accidents. Transport and Road Research Laboratory. [Online] Available at: https://trid.trb.org/view.aspx?id=1174885 (accessed 15th November 2021)

Rublee, E., Rabaud, V., Konolige, K., Bradski, G., 2011. ORB: An efficient alternative to SIFT or SURF. Presented at the 2011 International Conference on Computer Vision, IEEE, Barcelona, Spain. https://doi.org/10.1109/ICCV.2011.6126544

Runkle, S.N., Mahone, D.C., 1980. Variation in skid resistance over time (No. VHTRC 80-R33). Virginia Highway and Transportation Research Council, Charlottesville, Virginia. [Online] Available from: https://rosap.ntl.bts.gov/view/dot/18882 (accessed 24th November 2021)

Sabey, B.E., Luton, G.N., 1967. Measurement of road surface texture using photogrammetry (Road Research Laboratory No. LR57). Crowthorne, UK.

Sabey, B.E., 1958. Pressure Distributions beneath Spherical and Conical Shapes pressed into a Rubber Plane, and their Bearing on Coefficients of Friction under Wet Conditions. *Proc. Phys. Soc*. 71, 979–988. https://doi.org/10.1088/0370-1328/71/6/311

Sanders, P.D., McRobbie, S., Gopaldas, J., Viner, H.E., 2015. Published Project Report PPR771. Development of a reference surface for the assessment of pavement skid resistance measurement devices. Transport Research Laboratory, Crowthorne.

Sayers, M.W., Gillespie, T.D., and Paterson, W.D.O, 1986. Technical Paper Number 46: Guidelines for conducting and calibrating road roughness measurements, Washington DC, The World Bank (1986) [Online] Available from:

https://deepblue.lib.umich.edu/bitstream/handle/2027.42/3133/72764.pdf (accessed 18th August 2019).

Sekuic, D., and Dedovic, V, 2011. The effects of stiffness and damping on the suspension system elements on the optimisation of the vibrational behaviour of a bus. *International Journal of Traffic and Transportation Engineering*, 1 (4), 231–244. [Online] Available from: https://trid.trb.org/view.aspx?id=1127006 (accessed 13th January 2020)

Sengoz, B., Topal, A., Tanyel, S., 2012. Comparison of pavement surface texture determination by sand patch test and 3D laser scanning. *Periodica Polytechnica Civil Engineering* 56, 73–78. https://doi.org/10.3311/pp.ci.2012-1.08

Serway, R.A., Jewett, J.W., 2006. Principles of Physics, 4th ed. Thomas Brooks/Cole, Belmont, CA, USA. ISBN: 0534496059

Shannon, C.E., 1998. Communication In The Presence Of Noise. *Proceedings of the IEEE* 86, 447–457. https://doi.org/10.1109/JPROC.1998.659497

Shalaby, A., El Gendy, A., 2010. Digital image analysis: Current practice of pavement texture measurement 2, 1313–1321.

Simpson, I.R., Jones, P.D., 2012. Updated precipitation series for the UK derived from Met Office gridded data. Int. J. Climatol. 32, 2271–2282. https://doi.org/10.1002/joc.3397

Smith, K.L., Wambold, J.C., Yager, T.J., Rado, Z., 2009. Guide for Pavement Friction: Final Report for the National Cooperative Highway Research Program. Transport Research Board of the National Academies, Washington DC.

Smith, R.H., 2008. Analysing Friction in the Design of Rubber Products and their Paired Surfaces. CRC Press (Taylor and Francis Group), Boca Raton, Florida. ISBN: 9780849381379

Specht, L.P., Khatchatourian, O., Santos, R.T. dos, 2013. Measurement of pavement macrotexture through digital image processing. *Acta Scientiarum. Technology* 35, 31–38. https://doi.org/10.4025/actascitechnol.v35i1.12808

Thomas, T.R., 2009. Kenneth J. Stout 1941–2006: A memorial. *Wear, Metrology and Properties of Engineering Surfaces* 266, 490–497. https://doi.org/10.1016/j.wear.2008.04.053

Tourenq, C., Fourmaintraux, D., 1971. Propriétés des granulats et glissance routières. Bull. Liaison Lab. Ponts Chaussées 51, 61–69.

Transport Research Board. 2016. HCM6-16 Highway Capacity Manual A guide for Multimodal Mobility Analysis. 6th ed. USA: Transport Research Board. ISBN-10 0309369975.

Transport Research Laboratory. 2006. TRL Published Project Report PPR148: Surface Texture Measurement on Local Roads, Crowthorne: TRL. [Online] Available from https://trl.co.uk/reports/PPR148 (accessed 11th August 2019).

UK Government. 2019. Highways England's Pavement Management System Network Layer [Online] Available from https://data.gov.uk/dataset/2b0dd22d-213e-4f5b-99da-8b5ec409112c/highways-england-pavement-management-system-network-layer (Accessed 10th May 2020).

UK Government, 2019. Manual of Contract Documents for Highway Works. Volume 1 Specification for Highway Works.

Ueckermann, A., Wang, D., Oeser, M., Steinauer, B., 2015. Calculation of skid resistance from texture measurements. J. *Traffic Transp. Eng. Engl*. Ed., Special Issue: Functional Pavement Materials and Characterization 2, 3–16. https://doi.org/10.1016/j.jtte.2015.01.001

Ullman, S., 1979. The interpretation of structure from motion. Proceedings of the Royal Society of London. Series B. Biological Sciences. https://doi.org/10.1098/rspb.1979.0006

Vaiana, R., Capiluppi, G.F., Gallelli, V., Iuele, T., Minani, V., 2012. Pavement Surface Performances Evolution: an Experimental Application. *Procedia - Soc. Behav. Sci*. 53, 1149–1160. https://doi.org/10.1016/j.sbspro.2012.09.964

VicRoads, 2002. Performance levels for surface texture (Technical Note 59). Australia. [Online] Available at: https://www.google.com/search?q=Performance+levels+for+surface+texture+(Technical+Note+59).+Australia.&oq=Performance+levels+for+surface+texture+(Technical+Note+59).+Australia.&aqs=chrome..69i57.500j0j7&sourceid=chrome&ie=UTF-8 (accessed 16th November 2021)

Villani, M.M., Artamendi, I., Kane, M., Scarpas, A. (Tom), 2011. Contribution of Hysteresis Component of Tire Rubber Friction on Stone Surfaces. *Transp. Res. Rec*. 2227, 153–162. https://doi.org/10.3141/2227-17

Viner, H., Abbott, P., Dunford, A., Dhillon, N., Parsley, L., Read, C., 2006. Surface texture measurement on local roads. Publ. Proj. Rep. PPR148 [Online] Available at: https://trid.trb.org/view/795321 (accessed 28th May 2021)

Viner, H., Burton, D., 2021. Updating Texture Depth Policy, IAT Technical Event Presentation Videos. [Online] Available at: https://www.instituteofasphalt.org/index.php?id=video_list (accessed 12th November 2021)

Visscher, J., and Vanelstraete, A, 2017. Ravelling by traffic: performance testing and field validation. *International Journal of Pavement Research and Technology*, 10 (1), 54–61. doi:10.1016/j.ijprt.2016.12.004

Wang, W., Qiu, S., Wang, S., Wang, P., Zhang, J., 2018. Investigation of seasonal variations of Beijing pavement condition data using unevenly spaced dynamic panel data model.

International Journal of Pavement Engineering 19, 851–856. https://doi.org/10.1080/10298436.2016.1213590

Wang, W., Yan, X., Huang, H., Chu, X., Abdel-Aty, M., 2011. Design and verification of a laser based device for pavement macrotexture measurement. *Transp. Res. Part C Emerg. Technol.* 19, 682–694. https://doi.org/10.1016/j.trc.2010.12.001

Wang, H., Flintsch, G.W., 2007. Investigation of Short- and Long-Term Variations of Pavement Surface Characteristics at the Virginia Smart Road. Presented at the Transportation Research Board 86th Annual MeetingTransportation Research Board 21 to 25 January 2007, Washington DC, USA.

Wang, W., Yan, X., Huang, H., Chu, X., Abdel-Aty, M., 2011. Design and verification of a laser based device for pavement macrotexture measurement. Transportation Research Part C: Emerging Technologies 19, 682–694. https://doi.org/10.1016/j.trc.2010.12.001

West, N.W., Ross, T.F., 1962. Polishing of the Road Surface in New South Wales. Proceedings of the Australian Road Research Board 1. [Online] Available from: https://trid.trb.org/view/1209161 (accessed 29th November 2021)

Williams, R.D., 2012. Chapter 2, Section 3.2 DEMS of Difference. In *Geomorphology Techniques*, [Online] Available from: https://www.geomorphology.org.uk/sites/default/files/geom_tech_chapters/2.3.2_DEMsOfDifference.pdf.

Wilson, D.J., 2013. The effect of rainfall and contaminants on road pavement skid resistance. New Zealand Transport Agency, New Zealand ISBN: 9780478407240

Woodward, D., Millar, P., McQuaid, G., 2014. Use of 3D modelling techniques to better understand road surface textures. Presented at the 4th International Safer Roads Conference, Cheltenham, UK, p. 12. [Online] Available at: https://saferroadsconference.com/wp-content/uploads/2016/05/Tuesday-am-MA-5-Woodward_David_144_V1_2014312-Use-of-3D-modelling-techniques-to-better-understand-road-surface-textures.pdf (accessed on 30th October 2021)

Woodward, D., Woodside, A., Ellis, R., Phillips, P., Walsh, I., Sinhal, R., 2008. The effect of aggregate type and size on the performance of thin surfacing materials: International Conference Managing Road and Runway Surfaces to improve safety. Presented at the International Conference Managing Road and Runway Surfaces to Improve Safety, SaferRoads, Cheltenham, UK. [Online] Available at: http://www.saferroads.org.uk/2008papers.asp#anc10 (accessed 17th October 2021)

Woodward, D., Woodside, A., Jellie, J., 2003. Predicting the early life skid resistance of asphalt surfacings: Performance testing and evaluation of bituminous materials PTEBM'03, in: Part l Presented at the Performing testing and evaluation of bituminous materials, RILEM Publications, Zurich, Switzerland, pp. 198–204. [Online] Available at:

https://pure.ulster.ac.uk/en/publications/predicting-the-early-life-skid-resistance-of-asphalt-surfacings-3 (17th November 2021)

Wu, S., et al., 2012. Rheological properties for aged bitumen containing ultraviolate light resistant materials. *Construction and Building Materials*, 33, 133–138. doi:10.1016/j.conbuildmat.2012.01.019

Yaacob, H., Hassan, N.A., Hainin, M.R., Rosli, M.F., 2014. Comparison of Sand Patch Test and Multi Laser Profiler in Pavement Surface Measurement. *J. Teknol*. 70. https://doi.org/10.11113/jt.v70.3497

Z Corporation, 2007. Z Corp introduces ZScanner 800 handheld 3D scanner. automation.com. [Online] https://www.automation.com/en-us/products/product19/z-corp-introduces-zscanner-800-handheld-3d-scanner (accessed 1st August 2021).

Xin, Q., Qian, Z., Miao, Y., Meng, L., Wang, L., 2017. Three-dimensional characterisation of asphalt pavement macrotexture using laser scanner and micro element. *Road Materials and Pavement Design* 18, 190–199. https://doi.org/10.1080/14680629.2017.1329874

Yu, M., You, Z., Wu, G., Kong, L., Liu, C., Gao, J., 2020. Measurement and modeling of skid resistance of asphalt pavement: A review. *Construction and Building Materials* 260, 119878. https://doi.org/10.1016/j.conbuildmat.2020.119878

Zhang, D., Zou, Q., Lin, H., Xu, X., He, L., Gui, R., Li, Q., 2018. Automatic pavement defect detection using 3D laser profiling technology. *Autom. Constr*. 96, 350–365. https://doi.org/10.1016/j.autcon.2018.09.019

Zhang, X., Liu, T., Liu, C., Chen, Z., 2014. Research on skid resistance of asphalt pavement based on three-dimensional laser-scanning technology and pressure-sensitive film. *Constr. Build. Mater*. 69, 49–59. https://doi.org/10.1016/j.conbuildmat.2014.07.015

Zou, Y., Yang, G., Huang, W., Lu, Y., Qiu, Y., Wang, K.C.P., 2021. Study of Pavement Micro- and Macro-Texture Evolution Due to Traffic Polishing Using 3D Areal Parameters. Materials 14, 5769. https://doi.org/10.3390/ma14195769